PHOTOELECTROCATALYTIC PURIFICATION OF WATER USING SPRAY DEPOSITED ZINC OXIDE THIN FILMS

A THESIS SUBMITTED TO

SHIVAJI UNIVERSITY, KOLHAPUR

FOR THE DEGREE OF

DOCTOR OF PHILOSOPHY

IN

PHYSICS

UNDER THE FACULTY OF

SCIENCE

BY

Mr. R.T. SAPKAL

M.Sc., M.Phil.

UNDER THE GUIDANCE OF

Prof.(DR.) C. H. BHOSALE

M.Sc., Ph.D.

ELECTROCHEMICAL MATERIALS LABORATORY, DEPARTMENT OF PHYSICS, SHIVAJI UNIVERSITY, KOLHAPUR - 416 004, INDIA

2012

DECLARATION

I hereby declare that, the thesis entitled, "**PHOTOELECTROCATALYTIC PURIFICATION OF WATER USING SPRAY DEPOSITED ZINC OXIDE THIN FILMS**" completed and written by me has not formed earlier the basis for the award of any degree or similar title of this or any other university or examining body. Further, I declare that I have not violated any of the provisions under Copyright and Piracy / Cyber / IPR Act amended from time to time.

Place: Kolhapur   Research Student,

Date:

(Mr. R. T. Sapkal)

CERTIFICATE

This is to certify that the thesis entitled, "**PHOTOELECTROCATALYTIC PURIFICATION OF WATER USING SPRAY DEPOSITED ZINC OXIDE THIN FILMS",** being submitted herewith for the award of the Degree of **Doctor of Philosophy** in **Physics** under the Faculty of **Science** of Shivaji University, Kolhapur is the result of the original research work completed by **Mr. R.T. Sapkal** under my supervision and guidance and to the best of my knowledge and belief, the work embodied in this thesis has not formed earlier the basis for the award of any degree or similar title of this or any other University or examining body.

Place: Kolhapur
Date:

Research Guide
(Dr. C.H. Bhosale, Professor and Head)

Forwarded through Head of the Department, Physics,

CONTENTS

1.1 General

Water is one of the world's most important resources for all human life, as with all animals and plant life on the planet. Civilization would be impossible without steady supply of fresh and pure water and it has been considered a plentiful natural resource because the sensitive hydrosphere covers about 71% of the Earth's surface. Its total water content is distributed among the main components of the atmosphere, biosphere, oceans and continents. However, 97% of the Earth's water is salty ocean water, which is unusable for most human activities. Much of the remaining 3% of the total global water resource, 2% is locked away in glaciers and icebergs and only 1% is thought to be easily accessible surface water located in biomass, rivers, lakes, soil moisture and distributed in the atmosphere as water vapor[1].

In the process of rapid development of science and technology, the demand for pure water is increasing to serve multifarious purposes in different types of industries. Human water consumption raised six fold in the past century, double the rate of population growth. In addition, the increasing population of the world is also escalating the requirements of pure water for drinking and household purposes. The high population density and the level of industrialization have triggered the hydrosphere to be polluted with inorganic and organic matter at an increasing rate. Moreover, to fulfill growing demand of food supply for increasing population of the world, a lot of pesticides, herbicides are used in agricultural purposes, which also cause the scarcity of clean water. Besides this, ground water has also been found contaminated in some parts of the world with some toxic metal ions both for natural and anthropogenic reasons. Therefore, specified quality of water for industrial use, household activities and drinking purpose is of great concern for the whole community of the world. More importantly, environmental regulation is also becoming stringent day by day to keep environment friendlier for human beings. To overcome the water pollution problems and to meet stringent environmental regulations, scientists and researchers have been focusing on the development of new and improvement of existing water purification processes. On the other hand, awareness has also been increased about water pollution all over the world and people have also started to realize that water is no longer an unlimited resource [2].

Biodegradation, adsorption in activated carbon, air stripping, incineration, ion-exchange, coagulation-precipitation, membrane separation, thermal and catalytic

1

oxidation, oxidation by permanganate, chlorine, ozone and hydrogen peroxide are widely used conventional water treatment processes for organic and microbial pollutants containing water. Each process has some shortcomings and to overcome this, researchers are looking for some new technologies. Photoelectro catalysis on ZnO represents a promising alternative technology for degradation of organic pollutants and inactivation of microorganisms in water [3].

Heterogeneous photocatalysis has become an increasingly viable technology in environmental remediation. Photocatalytic degradation utilizing zinc oxide (ZnO) and titanium dioxide (TiO_2) as photocatalyst has several advantages with comparison to traditional water purifications and wastewater treatment methods. Complete destruction of most contaminants without the hassle of disposing spent catalyst/adsorbent is one of them. Photocatalysis also runs at room temperature and pressure and the photocatalyst is stable with high efficiency when activated using ultraviolet light ($\lambda < 380$ nm). Many catalysts, like ZnO, TiO_2, ZrO_2, WO_3, SrO_2, Fe_2O_3, Nb_2O_5, CeO_2, CdS and ZnS have been attempted for the photocatalytic degradation of a wide variety of environmental contaminants [4]. Metal chalcogenides possess narrower band gaps, which make them sensitive to visible irradiation; however, they are subject to photocorrosion.

The photocatalysts effectiveness for oxidation of organic compounds in water treatment is dependent on the oxidation potential of the valance band (VB) and the reduction potential of the conduction band (CB). Fig. 1.1 shows the relative positions of the surface bands of the common semiconductors at pH 7 [5]. It can be seen that the CB of ZnO is sufficiently negative for the reduction of O_2, while the VB is sufficiently positive for the oxidation of OH$^\bullet$ making it an excellent semiconductor for oxidation of organic compounds in water.

The reduction potentials of TiO_2, $SrTiO_3$, WO_3 and ZnS could also be used for the photocatalytic oxidation of organic pollutants; however, it is often found that TiO_2 is the most efficient semiconductor for the treatment of water containing organic pollutants and microorganisms [6-7]. ZnO is a possible alternative as it has similar band gap energy; however, it has been reported to be unstable upon irradiation [8].

This chapter encompasses the theoretical aspects of various experimental techniques, which are employed to characterize structural, morphological, optical,

photoelectrochemical and photoelectrocatalytic properties of thin films apart from literature survey of ZnO, Ag:ZnO, Au:ZnO and ZnO/TiO_2 thin films.
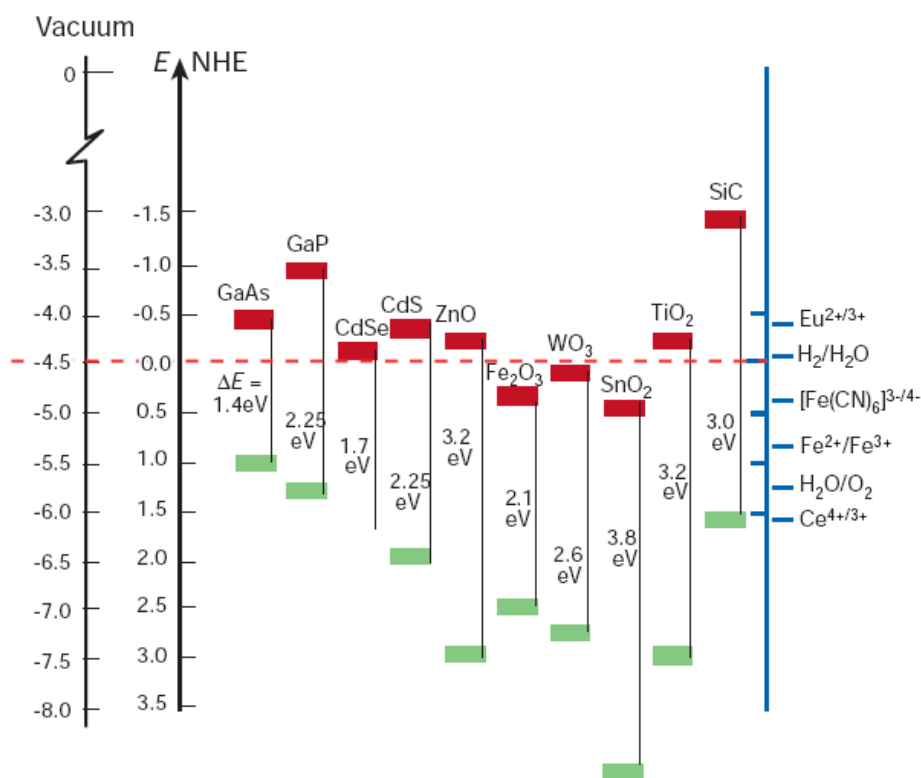
Fig. 1.1 Energy-level diagram for various semiconductors indicating the energy positions of valence band and conduction band edges in aqueous media at pH 7.0.

1.2 Literature survey on photoelectrochemical purification of water using oxide semiconductors

1.2.1 Zinc oxide (ZnO)

Zinc oxide is an n – type wide band gap (> 3 eV) semiconductor, which may be considered candidate for photocatalytic application, due to its high photosensitivity and non – toxicity [9]. ZnO nanoparticles have been used for photocatalytic degradation of pollutants and antibacterial treatment. Antibacterial agents are of relevance to a number of industrial sectors including environmental, food, synthetic textile, packaging, healthcare, medical, construction and decoration [10-11]. The antibacterial activity of ZnO powder and nanoparticles against various bacteria has been extensively investigated by Yang et.al [12]. Concerning the mechanism for antibacterial property of

ZnO nanostructures, the oxidative stress mechanism leading to membrane damage has been demonstrated for *E.coli* [13-15].

Organic antibacterial materials are often less stable particularly at high temperature and pressure compared to inorganic antibacterial agents [16]. As a consequence, inorganic materials such as metal and metal oxides have attracted lot of attention over the past decade due to their ability to withstand harsh process conditions [17]. ZnO nanoparticles and nanostructures exhibit strong antibacterial activity [18]. ZnO has also been shown to behave differently towards microorganism from other metal oxides such as TiO_2, SiO_2, MgO and CaO. There are relatively few reports on the interaction between ZnO nanoparticles and bacterial cells [19]. There are limited investigations on antibacterial activity of supported ZnO nanostructures coatings [20].

Recently, bacterial activity of ZnO nanorod arrays fabricated by a hydrothermal method was also reported. Most applications of ZnO photocatalysis have been concentrated on suspension of ZnO particles in a solution [21-28]. However, the use of ZnO catalytic slurries suffers limitations related to the filtering of particles. This requires either long time sedimentation or centrifugation process [29]. Thus there has been much interest in developing various supported ZnO nanostructured thin films for photocatalytic process. However, very few researchers have paid attention to use ZnO thin films as antimicrobial coatings. Xihong Li et.al [30] developed ZnO-coated poly (vinyl chloride) (PVC) packing film and tested its antibacterial property against the food pathogenic bacteria like *E. coli*, *Staphylococcus aureus* and fungi like *Aspergillus flavus* and *Penicillium citrinum.* The ZnO /PU (polyurethane) films and coats were fabricated by Li et.al [31] using solution casting and evaporation and tested their mechanical strength and antibacterial activity for *E.coli.* A layer of zinc oxide (ZnO) micro-grid was deposited on the surface of ZnO film using DC reactive magnetron sputtering and micro-sphere lithography on glass substrates and studied photocatalytic degradation experiments on methylene blue [32]. Textile effluent with diverse composition was effectively treated using hydrothermally synthesized ZnO [33].

Heterogeneous photo catalysis by semiconductor through particulate systems has become an exciting and rapidly growing area of research in the last few years [34]. Lan et.al reported the photoinduced hydrogen elimination reaction in phenol and the electronic ground state has been investigated by time-dependent quantum wave-packet

4

calculations. [35]. Want et.al studied quinine methide intermediates and have been investigated in organic photochemistry [36]. Shin et.al discovered the photodecomposition on the photochemistry of riboflavin [37]. Joshi et al. synthesized degradation of o-nitro phenol that has been studied in the presence of semiconducting oxide [38]. Ameta et.al studied the photoelectro chemical study of picric acid by using ZnO [39]. The photocatalytic degradation of 2,4-dinitrophenol over ZnO was carried out in the presence of light and probable mechanism for this process has been proposed [40]. Photocatalytic removal of p-nitrophenol has been carried out in the presence of ZnO by using a batch reactor with a UV-C lamp (15 W) [41]. There have been up-to-date, however, only few reports on the photocatalytic properties of nanostructured ZnO thin films [42-46]. Highly oriented ZnO nanowires were obtained via aqueous solution growth on seeded corning substrates and exhibit an outstanding photocatalytic activity, degrading stearic acid by almost 93 % in 30 min [47].

Though the method involving suspension of ZnO nanoparticles as photocatalyst is emerging as one of the best methods for destruction of contaminants, it possesses two major drawbacks: (a) the separation of ZnO nanoparticles after the treatment to the water and (b) the low quantum efficiency of these processes. Moreover, in case of powdered photocatalysts, long settlement times are required and have difficulty of their separation from pure water or alternatively fine filters have to be used [48]. Very little work has been done on photocatalysis of organic impurities in water using oxide semiconductor thin films using electrical bias, which can boost the photocatalytic activity.

Grätzel for the first time reported that when an electroactive species is present in the electrolyte the charge transfer can take place directly across the semiconductor-solution interface [49]. The photoelectrochemical effect by application of a bias to a ZnO film is illustrated in detail by Butterfield et al. [50]. A little progress has been made thereafter on photocatalysis of pollutants in water using electrical bias. Few researchers described the photoelectrochemical properties of such ZnO films [51-52].

Recombination of photogenerated holes and electrons inside the semiconductor particles is responsible for the relatively low quantum yield of photocatalytic degradation. Two different types of photoreactors are generally employed in photodegradation studies, containing either mixed aqueous slurries or immobilized layers of the ZnO photocatalyst. Good mass transport characteristics are the great

advantage of the slurries. However, the catalyst requires long settlement times to be separated from the purified water or alternatively, fine filters have to be employed. Therefore, attention turned recently to immobilize photocatalysts [53].

Recently, M. Neumann-Spallart has given an overview of the photoelectrocatalytic process in which it has been showed that photocatalytic performance can be boosted considerably using electrical bias, while considering the rectifying nature of semiconductor oxide/ aqueous electrolyte junctions [54]. Many other authors reported that imposed bias on the decomposition of organics leads to the positive effect [55-56].

1.2.2   Ag doped zinc oxide (Ag: ZnO)

Photocatalytic degradation of organic pollutants in water and air using semiconductors, such as TiO_2 and ZnO, has attracted extensive attention in the past two decades. Previous studies have proved that such semiconductors can degrade most kinds of persistent organic pollutants, such as detergents, dyes, pesticides and volatile organic compounds, under UV-irradiation. However, the fast recombination rate of the photogenerated electron/hole pairs hinders the commercialization of this technology [57]. It is of great interest to improve the photocatalytic activity of semiconductors for the degradation of organic compounds in water. It is anticipated that ZnO would become an excellent photocatalyst if the photocorrosion could be greatly suppressed. Several methods have been developed to improve its photostability, including surface organic coating of ZnO and surface modification by doping. The modification of ZnO with nobal metals has attracted significant attension especially in photocatalysis. Ag:ZnO films successfully fabricated by spray pyrolysis technique [58]. Kim et al. investigated effect of annealing temperature on structural, electrical and optical proprperties of Ag:ZnO films[59]. Many groups have fabricated p- type ZnO with group V dopant [60]. The effect of different doping elements auch as Cu, Fe, Sn and Ag on ZnO thin film microstructure was investigated [61]. The Ag nanocluster doped ZnO thin films have been prepared on fused substrate and studed photovolyaic effect [62]. Jeong et al. well documented metal doped ZnO films and twisted their crystallinity transmitance and band gap [63]. It has been demonstrated that the UV emission of ZnO films can be enhanced significantly via - doping [64]. The influence of oxygen / argon ratio on structural, electrial and optical properties of ZnO : Ag films have been investigated [65]. Ag doped ZnO thin films exibit various electrical and   optical

properties depending upon the deposition temperature [66]. The group I element is a candidate aceptor for ZnO, substituting for Zn [67]. Infact silver ions also have novel effects on the photoactivity of semiconductor photocatalysis [68]. Ag doping in ZnO could improve the photocatalytic degradation activity of ZnO [69]. Silver atoms could be incorporated into the lattice of ZnO as substitution for Zn atom, sites [70].Thus it is necessary to investigate effect of doping Ag into ZnO systematicaly.

Highly active silver-modified ZnO has been prepared and the effect of silver modification was studied. The photocatalytic activity of these materials was studied by analyzing the degradation of an organic dye, rhodamine 6G (R6G) and it is found that 3 mol % silver-modified ZnO at 400 °C shows approximately four times higher rate of degradation than that of unmodified ZnO and a three times higher rate than that of commercial TiO_2 photocatalyst Degussa P-25. The sensitizing property of the dye and electron scavenging ability of silver together constitute to the interfacial charge transfer process in a such way to utilize the photoexcited electrons [71]. Doping ZnO with Ag sharpens the band gap absorption, leads to surface plasmon resonance, suppresses the blue emission, enhances the near band gap emission, increases the charge transfer resistance and improves the antibacterial activity [72]. Ag/ZnO nanocatalysts with excellent photocatalytic performance were successfully prepared using a simple solvothermal method, which has shown that photocatalytic degradation of (Methyl Orange) MO can be readily performed in the presence of Ag/ZnO in an aqueous suspension system, leading to the complete degradation of MO [73]. Nanocrystalline Ag-doped ZnO powders were synthesized directly from an aqueous solution of zinc acetate dihydrate and silver which increases of the photocatalytic efficiency for degrading methylene blue increases with the Ag loading up to 1.0 mol %, while the best of the antibacterial activity against *Staphylococcus aureus* was found at 0.5–0.8 mol % of Ag [74]. It was shown that the catalytic behavior of Ag/ZnO nanoparticles in the visible-light range is notably improved through the Ag deposition onto ZnO nanoparticles by the method of laser-induction with a maximum effectiveness of 92% degradation of MB [75].

1.2.3 Au doped zinc oxide (Au: ZnO)

Zinc oxide appears as a very promising photocatalyst for degradation of organic solutes in aqueous systems, it seems to be a suitable alternative to TiO_2 since its photodegradation mechanism has been proven to be similar to that of TiO_2. However,

the photocatalytic efficiency of ZnO is always affected by the quick recombination of the photo excited electrons and holes [76]. To retard the recombination of the excited electrons and holes, one possible strategy is to dope ZnO with certain metal such as Ag, Pt, Au, Cu, N, Mn, etc [77 - 84]. The excited electrons in ZnO are supposed to transfer to the metal if the interface between ZnO and metal is optimized and the work function of the metal is greater than that of ZnO [85]. The electron transfer will greatly suppress the electron–hole recombination and then improve the catalytic efficiency of ZnO. Until now, many kinds of noble metals have been combined with semiconductors, such as Ag–ZnO core-rods [86], Au-TiN [87], ZnO–Au core–shell [88], Au-doped iron oxide thin films [89], Au-doped mesostructured SnO_2 [90] and ZnO– Au thin films [91-96]. To date, synthesis of optimized catalytic efficiency has been attempted by several research groups. However, the ZnO–Au thin films obtained in these previous works are not well designed for photocatalysis but for chemical sensors. For instance, Sarkar et al. reported, the photo-dependent excitonic mechanism and the charge migration kinetics in a colloidal ZnO–Au system and demonstrated that excited ZnO nanoparticles (NPs) resonantly transfer visible optical radiation to the Au NPs and the quenching of defect-mediated visible emission depends solely on the excitation level of the semiconductor [97]. Thin films of $Au:TiO_2$ on glass substrates have been prepared by simple sol–gel dip coating method. $Au:TiO_2$ photocatalytic activity was improved by 2–2.3 times than undoped TiO_2 [98]. The presence of the Au buffer layer in R-F magnetron sputtered WO_3 thin films improves photodegradation of methylene blue. Due to plasmon resonance Au nanoparticles the absorption edge shifted to longer wavelength and increased the film surface roughness [99].

Semiconductor photocatalyst generates electron and hole pair (e^--h^+) upon irradiation of light energy that could be utilized in initiating oxidation and reduction reactions of the pesticide, respectively[100]. Guillard et al. [101] reported that the number of photons striking the photocatalyst actually controls the rate of reaction which is an indication that the reaction takes place only on the adsorbed phase of the semiconductor particle. Surface morphology, namely, the particle size and shape is a very important parameter influencing the performance of photocatalyst in photocatalytic oxidation [102-106].

Nanosized Gold particle possesses many excellent properties, such as easy reductive preparation, water solubility, high chemical stability and significant

biocompatibility [107]. Surface plasmon resonance absorption is a unique property of gold which is the ability of showing a strong absorption band in the visible region when the frequency of the electromagnetic field is resonant with the coherent electron motion [108]. The prospect of developing new multifunctional nanocomposites of metal gold hybridized with inorganic components has become of great importance [108-109]. Bimetallic colloids are interesting from a number of perspectives, such as their unique electronic, catalytic and optical properties [110-113].

The photochemical sterilization of water in which microbial cells could be inactivated using heterogeneous photocatalysis. *Shigella flexneri*, *Listeria monocytogenes*, *Vibrio parahaemolyticus*, *Staphylococcus aureus*, *Streptococcus pyogenes,* and *Acinetobacter baumannii,* were killed by visible-light-illuminated nitrogen-doped TiO_2 substrates than by pure TiO_2 substrates [114]. The antibacterial activity of suspensions of ZnO nanofluids against (*E. coli*) has been evaluated by estimating the reduction ratio of the bacteria treated with ZnO. Survival ratio of bacteria decreases with increasing the concentrations of ZnO nanofluids and time [115]. ZnO have notable bactericidal activity against a biofilm of *S.epidermidis* when back-illuminated with a UVA light source in an aqueous environment [116]. In accordance with Ruffolo [117], the nanopowered ZnO and $ZnTiO_3$ seems to show an antifungal activity and used for antimicrobial stone coating. Ag/ZnO nanocomposites have potential applications in inhibition both gram-negative and gram-positive bacteria [118]. To overcome quick electron- hole recombination, one efficient way is to deposit noble metals, such as gold [119-122], platinum [123-124], silver [125–126] and palladium [127], on the semiconductors. Then the photogenerated electrons in the conduction band of the semiconductor can be transferred to metal deposits due to the Schottky barrier formed at the metal–semiconductor interface [128], while the holes can remain on the semiconductor surfaces. Thus the noble metal can act as electron sinks, facilitating the charge separation and improving the photocatalytic efficiency.

1.2.4 Stratified layer of ZnO and TiO_2

Some reports have highlighted that ZnO exhibits better efficiency than TiO_2 for removing organic compounds in water and photo-electric conversion [130-131]. However, ZnO undergoes photo-corrosion under UV light illumination, which results decrease in photocatalytic activity [132]. There are several ways to enhance photocatalytic ability, one is the modification in shape, size and surface properties of

ZnO, second way is to increase wavelength response range and third way is to dope metals, non-metals and rare earth elements in host lattice [132-135]. The coupling of two semiconductors provides a novel approach to the enhancement in photocatalytic activity. Recent, studies have shown that binary oxides viz. TiO_2/SnO_2, TiO_2/ZrO_2, TiO_2/MoO_3, TiO_2/CdS, TiO_2/Fe_2O_3, TiO_2/WO_3, CdS/ZnO, CdS/AgI, ZnO/ZnS, $Fe_2O_3/ZnO/TiO_2$ and Fe_2O_3/TiO_2 etc. can provide a more efficient charge separation, increased lifetime of charge carriers and enhanced interfacial charge transfer to absorbed substrates [136-143].

The use of catalyst as slurry, after photocatalytic degradation, has been a problem of leaching and separation of photocatalysts from the degraded reaction mixture. This needs either long time sedimentation or centrifugation. Hence, many researchers have decided to study the feasibility of photocatalyst on inert surfaces like glass, polythene fibers and cement surface [144-145]. The photo stability is much better for microscale ZnO than nano scale ZnO due to its better crystallinity and lower defects. Also photo stability of the microscale ZnO is greatly improved by the surface modification of ZnO with a small amount of TiO_2 [146-147]. ZnO/TiO_2 semiconductor photocatalyst may increase the photocatalytic efficiency by increasing the charge separation and extending the photo-responding range. It is expected that, use of ZnO/TiO_2 binary oxide is not only to obtain higher efficiency but also to avoid the photo-corrosion of ZnO.

1.3 Characterization techniques

1.3.1 Photoelectrochemical (PEC) technique

PEC is a new, reliable and unique technique in thin film technology, which has proven to be the best tool for optimization of preparative and post preparative parameters of the semiconducting electrodes prepared by any deposition technique. A PEC cell consists of photoelectrode on conducting substrate, suitable electrolyte and counter electrode, is illuminated with light of an appropriate energy. For optimization of preparative parameters, the values of short circuit current (I_{sc}) and open circuit voltage (V_{oc}) are plotted against desired preparative parameter. The values of I_{sc} and V_{oc} go through the maximum for an optimized value of the desired parameter. It has been observed that values of optimized preparative parameters obtained by PEC technique match well with the optimized values obtained by other techniques. The technique can be used for optimization of preparative parameters of any physical or chemical

methods where PEC can be used also to check the type of conductivity exhibited by semiconductor electrode thin films [148]. In a spray pyrolysis technique, one can optimize preparative parameters such as substrate temperature, concentration of solution and quantity of solution etc. by using PEC technique.

1.3.2 X-ray Diffraction (XRD)

The X-ray diffraction (XRD) is well-known technique for characterization of bulk and thin film samples. It is used to determine the crystal structure of materials. A sample is exposed to X-rays, which diffracts off the atomic planes of the crystal structure. Constructive interference occurs when the atomic spacing is an integer multiple of the X-ray wavelength, resulting in a characteristic diffraction peak. By moving the detector and source across a range of different angles with respect to the sample, a diffraction pattern can be obtained. This diffraction pattern is characteristic of a material and the crystalline phases that are present in the sample. The structural identification and determination of lattice parameters are based on the interpretation of X-ray diffraction patterns.

The phenomenon of X-ray diffraction consists of reflection of X-rays from the different crystallographic planes of material and Bragg's law governs it,

$$2d_{hkl}Sin\theta = n\lambda \tag{1.1}$$

where, d_{hkl} = lattice spacing for (hkl) plane, λ = wavelength of monochromatic X-rays, n = order of diffraction (n =1) and θ = glancing or diffraction angle.

Klug and Alexander [149] have given detailed treatments of X-ray diffraction analysis. The Debye Scherer Method [150] in conjunction with diffractometer is most commonly used. In this Instrument, the diffracted radiation is detected by the counter tube, which moves along the angular range of reflections. An inbuilt program on a computer system processes the observed intensities. A diffraction pattern consisting of d values of existing atomic planes in the sample and corresponding reflected intensities is made available. From this X-ray diffraction data following structural characterization can be carried out.

Identification of Phases can be done in a following way: The observed d- values are compared with standard d- values from JCPDS diffraction pattern file, for the same material synthesized by standard chemical methods. This analysis reveals the different phases present in the sample and Miller indices of the atomic planes. The lattice parameters a, b and c for the unit cell of the phase present are then calculated using

11

equations given by Kenon [151]. The proportional amount of phases present can be determined from total intensities. The composition of the film sample, if it is a binary system, can be determined from the lattice parameters using Vagard's law [152]. Absence of reflection peaks indicates amorphous nature of the sample. A single reflection peak indicates an epitaxial growth, while many reflection peaks indicate heteroepitaxial (polycrystalline) growth.

In case of a polycrystalline sample having large number of grains, the average grain size is determined from Scherer's formula [153].

$$D = \frac{0.9\lambda}{\beta \cos\theta} \tag{1.2}$$

where, λ = wavelength of X- rays, θ = Bragg's angle and β = full width at half maxima (FWHM) (in radian) of the peak intensity

1.3.3 Thickness measurement by Interferometric method:

The determination of film thickness is of critical importance for the quantitative evaluation of certain parameters. The film thickness can be measured using several methods like multiple beam interferometry, film thickness probe coupled with optical microscope, interference fringe patterns, Talystep and optical Nano scope, surface profiler, weight difference method, etc.

Interferometric method:

Large band gap oxide thin films show a pronounced interference maxima and minima in the spectral transmission. This is due to the interference between the waves reflected from film surface and the substrate surface. The interference peaks can be used as a tool to determine the film thickness. The oscillations after the edge are caused by the electron, which can be viewed as a wave, being scattered by the neighboring atoms causing constructive and destructive interference between the propagated and reflected waves. Fitting the observed transmittance data with the calculated one given by Eq. (1.6), the thickness of the film can be estimated, [154]

$$T = \frac{t_1^2 t_2^2}{\left(1 + 2r_1 r_2 \cos 2\delta_1 + r_1^2 r_2^2\right)} \times \frac{n_2}{n_0} \tag{1.3}$$

where

$$r_1 = \frac{n_0 - n_1}{n_0 + n_1}, \quad r_2 = \frac{n_1 - n_2}{n_1 + n_2},$$

$$t_1 = \frac{2n_0}{n_0 + n_1}, \quad t_2 = \frac{2n_1}{n_1 + n_2} \quad and \quad \delta = \frac{2\pi n_1 d}{\lambda}$$

n_0, n_1 and n_2 are respectively refractive indices of air, ZnO and glass, d the film thickness and λ the wavelength of incident electromagnetic radiation.

1.3.4 Scanning Electron Microscopy (SEM) and Energy Dispersive Analysis by X-ray (EDAX)

Scanning electron microscopy (SEM) is a convenient and versatile tool for studying the surface morphology of the bulk and thin samples. It provides the information about the surface or near the surface region.
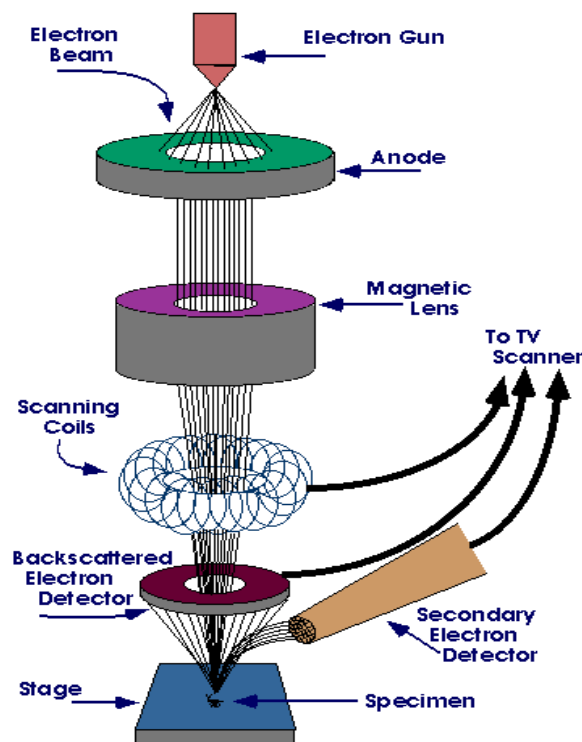
Fig.1.2 Schematic ray diagram of scanning electron microscope 6360

Fig. 1.3 shows the photograph and schematic diagram of SEM model 6360. It consists of a cavity surrounded by large electromagnetic lenses. The electron gun is the source of electron beam. The beam after passing through the cavity falls on the sample, which knocks out secondary electrons (Auger electrons), which are detected by a detector. All SEM instruments have facilities for detecting secondary and backscattered electrons. The secondary electrons are orbital electrons knocked out of the sample atoms by collisions with the incident electrons of energy less than 50eV. These

secondary electrons are generated from the specimen depth of about 50 to 100 nanometers. The region from which they originate is little larger than the beam diameter. The typical resolution may be of 3 nm.

The number of secondary electrons per incident electrons varies with specimen tilt, hence for topographic examination; the specimen is generally tilted at 10-20° towards the detector. The detector counts the number of secondary electrons produced at each spot on the surface. The amplified current from the detector gives magnified surface topology. These surface features can be used to determine grain structure, texture and grain size. When higher energy electrons (greater than 50 eV) penetrate into the bulk of the specimen, some undergo Rutherford Back Scattering (RBS) from the atoms from the sample and thus provide information about bulk.

Energy Dispersive Analysis by X-ray (EDAX)

A metal target in an X-ray tube when bombarded with electrons of sufficiently high energy, emit characteristic X-rays. This is the basis of Energy Dispersive X- ray Spectroscopy, a powerful method of chemical analysis of the sample. The EDAX facility is coupled with SEM.

The emitted X-rays from the sample bombarded by high-energy electron beam are analyzed in an X-ray spectrometer and the elements present in the sample are qualitatively identified by their characteristic wavelengths. Quantitative estimation is also possible by measuring relative intensities in the X-ray spectra. For compositions greater than or about 1 % and elements separated by few atomic numbers, EDAX is very useful because the intensities are increased by about 100-fold [155]. Due to limitations of resolution overlapping of lines from nearby elements may occur. The specimen must be either electrically conducting or made so by evaporating a metallic layer on it.

1.3.5 UV-Vis spectroscopy

The equilibrium charge carrier distribution in any material (conductor, semiconductor or insulator) can be disturbed by its exposure with electromagnetic radiation of suitable energy. The photons incident on any material may be reflected (R), transmitted (*T*) or absorbed (*A*). The quantity of radiation of wavelength λ absorbed by a material slab of thickness t is measured in terms of optical density (αt). Assuming negligible reflection (R=0), the energy absorbed can be given by Lambert's equation,

$$I = I_0 \exp(-\alpha t) \qquad (1.4)$$

where I and I_o are incident and transmitted intensities respectively.

In other words, optical absorption coefficient of films is evaluated from transmittance as [156].

$$T = A \exp(-\alpha t) \qquad (1.5)$$

where T is transmittance, t is film thickness, A is a coefficient related to the refractive index, which is nearly equal to unity at the absorption edges and α is the absorption coefficient.

A photon absorption by a material is characterized by means of electron transition between energy states or bands according to quantum rules. An ideal semiconductor, at moderate temperature has small number of holes in the valance band electrons in the conduction band. Absorption of photons of sufficient energy tends to transfer the electrons from valance band to conduction band giving absorption maxima. Thus, the optical absorption spectrum of a pure semiconductor exhibits a fundamental absorption edge at a certain incident photon energy, which can be attributed to the excitation of electrons from valence to conduction band separated by energy equal to the band gap energy (E_g)

The photon energy dependence at the absorption edge is given by [157],

$$(\alpha h \nu) = B(h \nu - E_g)^n \qquad (1.6)$$

where hν is the incident photon energy, B the edge width parameter and n an exponent that determines the type of electronic transition causing absorption, which is 1/2, 3/2, 2, 3 for direct allowed, direct forbidden, indirect allowed and indirect forbidden transitions, respectively. Band gap energy of the films can be obtained by extrapolating the linear region of the plots $(\alpha h \nu)^n$ to zero absorption coefficient i.e. at $\alpha=0$.

1.3.6 Fourier Transform Infrared Spectroscopy (FTIR)

A variety of IR techniques have been used in order to get information on the surface chemistry of different solids. With respect to the characterization of metal oxides two techniques are largely used, namely the transmission/absorption and diffuse reflection techniques. The infrared spectroscopy is the method of qualitative analysis of organic material and it has broad application in inorganic substances as well. The molecular vibrations in the sample can be detected by the vibration spectroscopy.

The roots of the vibrational spectrometry are strengthened by the discovery of inelastic scattering of the photons also known as "Raman effect" in 1928 by Raman and Krishnan [158].
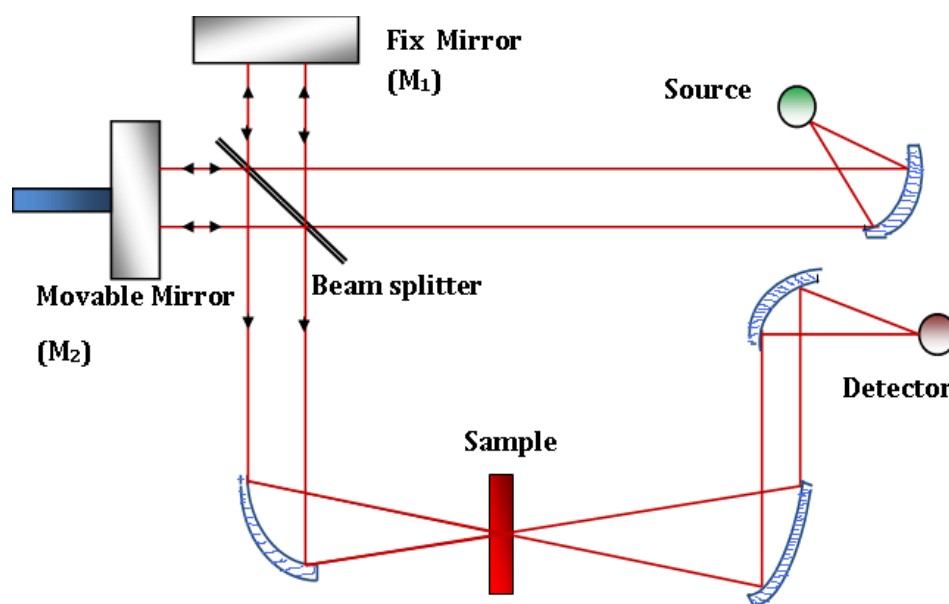
Fig. 1.3 Scamitic of FTIR Spectrometer

It is well known that, IR encompasses a spectral region from red end of visible spectrum (12,500cm^{-1}, 0.8 mm) to the microwave 10 cm^{-1}, 1000 mm)in the electromagnetic spectrum.

However, based upon applications and instrumentation involved, it is divided in to near (12,500 to 4000 cm^{-1}), mid-IR (4000 to 400 cm^{-1}) and far-IR (400 to 10 cm^{-1}). It is found that most of the fundamental molecular vibrations occur in mid-IR region. Modern Fourier transform IR spectrometers are superior to that of dispersive IR spectrometers on several counts. Due to these advantages the measurements of transmission, reflection or even emission spectra has become significantly faster and even with higher sensitivity than ever before. FTIR spectrometers are based upon Michelson interferometer. Figure 1.4 shows schematic of the spectrometer. A typical spectrometer mainly consists of components like (a) radiation source, which is always Nernst filament (ZrO$_2$ + Y$_2$O$_3$) or Globar (SiC). (b) optical path and monochromator, in which the beam is guided and focused by the mirrors aluminized or silverized on their surfaces. (c) detectors, which detects the heat radiations .

To obtain an IR absorption spectrum, one mirror of the interferometer moves to generate interference in the radiations reaching the detector. However as all

wavelengths are passing through the interferometer, interferogram is a complex pattern. In these experiments the absorption/transmission spectrum as function of wavenumber (cm^{-1}) is obtained from the Fourier transform of the interferogram, which is the function of the mirror movement. Interestingly, this design doesn't have the reference cell which is generally used in the dispersive IR instrument, so a reference spectrum is recorded and stored in the memory to subtract from the sample spectrum.

1.3.7 High pressure liquid chromatography (HPLC)

High pressure liquid chromatography (HPLC) is basically a highly improved form of column chromatography. Instead of a solvent being allowed to drip through a column under gravity, it is forced through under high pressures of up to 400 atmospheres. It also allows you to use a very much smaller particle size for the column packing material which gives a much greater surface area for interactions between stationary phase and molecules flowing past it. This allows a much better separation of the components of the mixture. The other major improvement over column chromatography concerns the detection methods which can be used. These methods are highly automated and extremely sensitive [159].

The column and the solvent

Confusingly, there are two variants in use in HPLC depending on the relative polarity of the solvent and the stationary phase.

Normal phase HPLC

This is essentially just the same thin layer chromatography or column chromatography. Although it is described as "normal", it isn't the most commonly used form of HPLC.

The column is filled with tiny silica particles and the solvent is non-polar - hexane, for example. A typical column has an internal diameter of 4.6 mm (and may be less than that) and a length of 150 to 250 mm. Polar compounds in the mixture being passed through the column will stick longer to the polar silica than non-polar compounds will. The non-polar ones will therefore pass more quickly through the column.

Reversed phase HPLC

In this case, the column size is the same, but the silica is modified to make it non-polar by attaching long hydrocarbon chains to its surface - typically with either 8 or 18

carbon atoms in them. A polar solvent is used - for example, a mixture of water and an alcohol such as methanol.

In this case, there will be a strong attraction between the polar solvent and polar molecules in the mixture being passed through the column. There won't be as much attraction between the hydrocarbon chains attached to the silica (the stationary phase) and the polar molecules in the solution. Polar molecules in the mixture will therefore spend most of their time moving with the solvent.

Non-polar compounds in the mixture will tend to form attractions with the hydrocarbon groups because of van der Waals dispersion forces. They will also be less soluble in the solvent because of the need to break hydrogen bonds as they squeeze in between the water or methanol molecules, for example. They therefore spend less time in solution in the solvent and this will slow them down on their way through the column.That means that now it is the polar molecules that will travel through the column more quickly. Reversed phase HPLC is the most commonly used form of HPLC.

Retention time

The time taken for a particular compound to travel through the column to the detector is known as its retention time. This time is measured from the time at which the sample is injected to the point at which the display shows a maximum peak height for that compound.

Different compounds have different retention times. For a particular compound, the retention time will vary depending on:

- The pressure used (because that affects the flow rate of the solvent)
- The nature of the stationary phase (not only what material it is made of, but also particle size)
- The exact composition of the solvent
- The temperature of the column

That means that conditions have to be carefully controlled if you are using retention times as a way of identifying compounds.

The detector

There are several ways of detecting when a substance has passed through the column. A common method which is easy to explain uses ultra-violet absorption. Many organic compounds absorb UV light of various wavelengths. If you have a beam of UV light shining through the stream of liquid coming out of the column and a UV detector

on the opposite side of the stream, you can get a direct reading of how much of the light is absorbed. The amount of light absorbed will depend on the amount of a particular compound that is passing through the beam at the time.
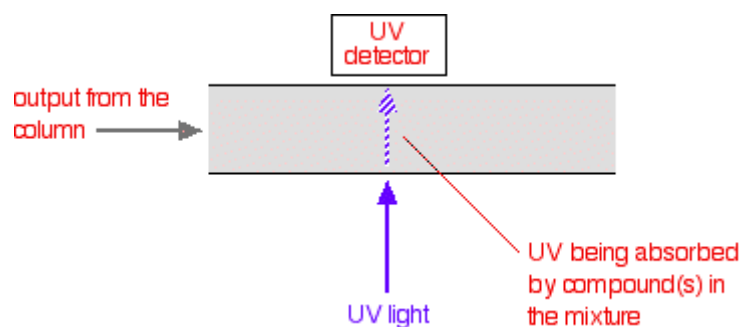
Figure1.4 Scamatics of UV absotption by sample and UV dectector

Methanol, for example, absorbs at wavelengths below 205 nm and water below 190 nm. If you were using a methanol-water mixture as the solvent, you would therefore have to use a wavelength greater than 205 nm to avoid false readings from the solvent [160].

1.3.8 Gas chromatography mass spectrometry (GC-MS)

Gas chromatography mass spectrometry (GC-MS) is an instrumental technique, comprising a gas chromatograph (GC) coupled to a mass spectrometer (MS), by which complex mixtures of chemicals may be separated, identfied and quantified [161]. This makes it ideal for the analysis of the hundreds of relatively low molecular weight compounds found in environmental materials. In order for a compound to be analysed by GC-MS it must be sufficiently volatile and thermally stable. In addition, functionalised compounds may require chemical modification (derivatization), prior to analysis, to eliminate undesirable adsorption effects that would otherwise affect the quality of the data obtained. Samples are usually analyzed as organic solutions consequently materials of interest (e.g. soils, sediments, tissues etc.) need to be solvent extracted and the extract subjected to various 'wet chemical' techniques before GC-MS analysis is possible [162].

The sample solution is injected into the GC inlet where it is vaporized and swept onto a chromatographic column by the carrier gas (usually helium). The sample flows through the column and the compounds comprising the mixture of interest are separated by virtue of their relative interaction with the coating of the column (stationary phase) and the carrier gas (mobile phase). The latter part of the column

passes through a heated transfer line and ends at the entrance to ion source (Fig. 1.6) where compounds eluting from the column are converted to ions.
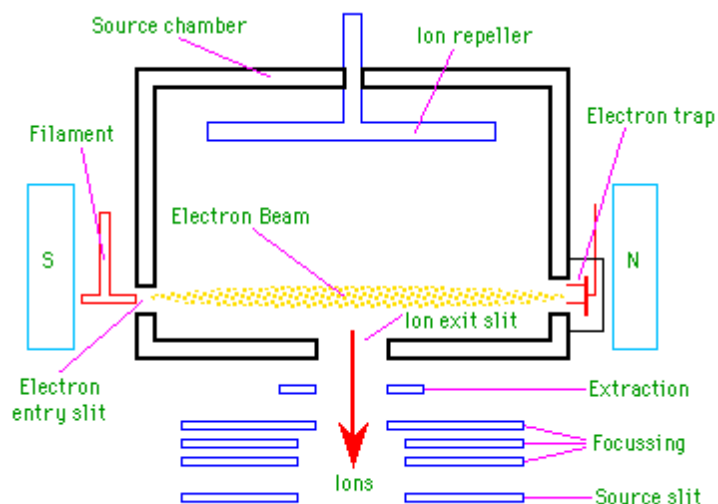
Figure 1.6 Scamatics of Gas chromatography mass spectrometry (GC-MS)

Two potential methods exist for ion production. The most frequently used method is electron ionization (EI) and the occasionally used alternative is chemical ionization (CI). For EI a beam of electrons ionize the sample molecules resulting in the loss of one electron. A molecule with one electron missing is called the molecular ion and is represented by M+. (a radical cation). When the resulting peak from this ion is seen in a mass spectrum, it gives the molecular weight of the compound. Due to the large amount of energy imparted to the molecular ion it usually fragments producing further smaller ions with characteristic relative abundances that provide a 'fingerprint' for that molecular structure. This information may be then used to identify compounds of interest and help elucidate the structure of unknown components of mixtures. CI begins with the ionization of methane (or another suitable gas), creating a radical which in turn will ionize the sample molecule to produce [M+H]+ molecular ions. CI is a less energetic way of ionizing a molecule hence less fragmentation occurs with CI than with EI, hence CI yields less information about the detailed structure of the molecule, but does yield the molecular ion; sometimes the molecular ion cannot be detected using EI, hence the two methods complement one another. Once ionized a small positive is used to repel the ions out of the ionization chamber.

The next component is a mass analyzer (filter), which separates the positively charged ions according to various mass related properties depending upon the analyzer

used. Several types of analyzer exist: quadrupoles, ion traps, magnetic sector, time-of-flight, radio frequency, cyclotron resonance and focusing to name a few. The most common are quadrupoles and ion traps. After the ions are separated they enter a detector the output from which is amplified to boost the signal. The detector sends information to a computer that records all of the data produced, converts the electrical impulses into visual displays and hard copy displays. In addtion, the computer also controls the operation of the mass spectrometer.

1.3.9 Chemical Oxygen Demand (COD) analysis

An organic contaminants, including solvents, electrical insulators, lubricants, herbicides, fungicides and pesticides, can accumulate in aquatic environments and cause toxic effects on aquatic life and increase health risks of drinking water. These chemicals are at very low concentrations in the natural environment and they are typically introduced to surface waters as waste from human activities. If effluent with high COD/BOD levels is discharged into a stream or river, it will accelerate bacterial growth in the river and consume the oxygen levels in the river. The oxygen may diminish to levels that are lethal for most fish and many aquatic insects. As the river re-aerates due to atmospheric mixing and as algal photosynthesis adds oxygen to the water, the oxygen levels will slowly increase downstream.

Reduction in chemical oxygen demand (COD) was also studied in the same sample. The chloride interference was removed by using $HgSO_4$; the mix-ture of diluted sample (before and after treatment) and $K_2Cr_2O_7$ was refluxed (acidic condition and Ag_2SO_4 as catalyst) in a reflux flask equipped with condenser on a hot plate for 3h. The refluxed sample was titrated against ferrous ammonium sulfate (FAS) as titrant. The NB medium was used as blank and similar condition was used for test [163]

Procedure for COD as follows

1   Take 20 ml of samples in 250 ml COD flask

2   If the sample is expected to have COD more than 50 mg/lit add 10 ml of 0.0025 potassium dichromate solution. The extreme care was taken in case of low COD sample

3   Add a pinch of Ag_2SO_4 and $HgSO_4$. If sample contains chloride in higher amount then $HgSO_4$ added in the ratio of 10:1 to the chlorides.

4   Add 30 ml of sulfuric acid

5   Reflex at 140 ^0C for 2 hrs in dissector

6   Add 2-3 drops of ferroin indicator mix thoroughly and titrate with 0.1 N ferrous ammonium sulphate

7   Run a blank with distilled water using sample quality of the chemicals

Finally COD was calculated by using following formula:

COD (mg/l) = (A − B) × normality × 1000 × 8 / volume of sample (mL)

where A is the ml of FAS was used for blank, B is the ml of FAS was used for test sample, N is the normality of FAS and 8 is the milliequivalent weight of oxygen.

1.3.10 Biological Oxygen Demand (BOD) analysis

Biological oxygene demand (BOD) is the measure of the degradable organic material present in a water sample and can be defined as the amount oxygen required by microorganisms under aerobic condition. The principle of the method involves measuring the difference of the oxygen concentration between the sample and after incubation after 5 days at 20 ^{0}C.

Procedure

1. Prepare dilution water in glass container by bubbling air in distilled water for about 30 min.

2. Add 1 ml of each phosphate buffer, magnesium sulphate, calcium chloride, ferric chloride solution for each liter of dilution water and mix thoroughly .

3. Neutralize sample to P ^{H} around 7.0 using 1 N NaOH and H_2SO_4.

4. Keep 1 set og BOD bottle in BOD incubator at 20^0 C for 5 days and determine DO contain in the sample bottle after completion of 5 days incubation

   Finally BOD was calculated by using following formula:

   BOD (mg/l) = (D_0 – D_5) × dilution factor

   Where , D_0 is initial DO in the sample and D_5 is DO after 5 days.

BOD of the sample was determined by measuring the dissolved oxygen levels of the control samples (uninoculated solution of dyes) and test samples (the solution of dyes inoculated with organism) before and after incubation for 5 days (APHA, 1995). Winkler's iodometric method was used for this estimation (APHA, 1995) and furthermore, BOD was calculated [163]

1.3.11 Bacterial count by serial dilution method

There are different methods to determine the number of micro-organisms that are present in a given population. This can be accomplished by using the spectrophotometer to measure the optical density of the population, by directly counting the microorganisms using a haemocytometer, or by serial diluting the bacteria and plating the diluted bacteria on media that supports the growth of the micro-organisms [164-165]. The latter method is somewhat more time consuming, but provides statistically accurate and repeatable results. This method is also the ideal method for enumerating microorganisms in a given population because it only identifies the living organisms in that population. To this end make serial dilutions of a solution containing an unknown number of bacteria, plate these bacteria and determine the total number of bacteria in the original solution by counting the number of colony forming units and comparing them to the dilution factor. Each colony forming unit represents a bacterium that was present in the diluted sample. The numbers of colony forming units (CFU's) are divided by the product of the dilution factor and the volume of the plated diluted suspension to determine the number of bacteria per mL that were present in the original

To calculate the number of bacteria per mL of diluted sample one should use the following equation:

CFU/ml = Plate Count / (Volume plated (mL) x total dilution used)

1.4 Statement of the problem

The available fresh water is not always clean as it may contain natural toxic impurities or be contaminated by human activities. Hence appropriate water treatment systems have to be provided urgently to save lives. Advanced Oxidation Process (AOP) is modern chemical method for the treatment of water containing non- biodegradable / toxic substances and to decontaminated drinking water. With classical water treatment techniques such as flocculation, precipitation, adsorption on granular activated carbon, air stripping, reverse osmosis or combustion, pollutants are only transferred from one phase to another. Whereas AOPs degrade the organic pollutants in water with byproducts carbon dioxide and water. For disinfection of water AOPs are an alternative to conventional chlorination process, which leads to generate of toxic chlorinated byproducts in the presence of natural organic matter.

Among AOPs, heterogeneous photocatalysis seems to be an attractive method as it has been successfully employed for the degradation of various organic pollutants, including dyes and microorganisms. Heterogeneous photocatalysis is a process in which a combination of photochemistry and catalysis is operable and implies that light and catalyst are necessary to bring out a chemical reaction. The reason for the increased interest for the photocatalytic method is that the process use atmospheric oxygen as the oxidant and it can be carried out under ambient conditions. Among many oxide semiconductors, zinc oxide appears as a very promising photocatalyst for degradation of organic solutes in aqueous systems. Zinc oxide can be prepared by variety of techniques such as hydrothermal, sol–gel, RF magnetron sputtering, chemical vapor deposition, thermal vaporization, laser ablation,by E-beam evaporation, ion beam assisted deposition and spray pyrolysis [166-174]. Among these spray pyrolysis technique (SPT) is easy and economic, to deposit zinc oxide thin films. Zinc acetate precursor is used to deposit zinc oxide thin films by SPT. Preparative parameters such as, substrate temperature, solution concentration and quantity of spraying solution will be optimized to get good quality zinc oxide thin films. The prepared films will be characterized by PEC, XRD, SEM, EDAX and UV-vis spectroscopy characterization techniques.

Silver and gold deposited zinc oxide films will be prepared to enhance photocatalytic inactivation of bacteria. The optimized stratified layer of TiO_2 will be given on zinc oxide thin films to improve its performance in photocatalytic process. The films prepared at optimized conditions of temperatures, concentrations will be used in specially designed photoelectrochemical detoxification reactor. This rector requires films of the size (10 X 10 X 1.5 cm^2). The prepared ZnO, Ag:ZnO , Au:ZnO and ZnO/TiO_2 films will be used to degrade Methylene blue (BM), textile effluent and inactivation bacteria such as *E.coli*, *Bacillus, Salmonella, Staphylococcus* etc.

References:

[1]   World Health Organization (WHO), Guidelines for drinking water quality, Vol. 3.Surveillance and Control of Community Supplies, 2nd ed, World health organization, Geneva, 1997].

[2]   A. Badis, F.Z. Ferradji, A. Boucherit, D. Fodil, H. Boutoumi, Desalination, 259 (2010) 216

[3]   K. Tanaka, K. Padermpole, T. Hisanaga, Water Res. 34 (2000) 327

[4]   M.A. Fox, M.T. Dulay, Chem. Rev. 93 (1993) 341

[5]   A. Hagfeldt, M. Grätzel, Chem. Rev. 95 (1995) 49

[6]   A. Mills, S.J. Le Hunte, J. Photochem. Photobiol. Chem.: A, 108 (1997) 1

[7]   M.R. Hoffmann, S.T. Martin, W. Choi, D.W. Bahnemann, Chem. Rev. 95 (1995) 69

[8]   H. Yoneyama, Crit. Rev. Solid State Mater. Sci. 18 (1993) 69

[9]   N. Daneshvar, M. Rabbani, N. Modirshahla, M.A. Behnajady, J. Photochem. Photobiol. Chem. :A, 168, (2004) 39

[10]   O. Akhavan, M. Mehrabian, K. Mirabbaszadeh, R. Azimirad, J. Phys. D: Appl. Phys. 42 (2009) 225305.

[11]   J. J. Vora, S. K. Chauhan, K. C. Parmar, S. B. Vasava, S. Sharma, L. S. Bhutadyua, E-J. Chemistry, 6(2) (2009) 531

[12]   L. Yang, J. Mao, X. Zhang, T. Xue, T. Hou, L. Wang, M. Tu, Naoscience; 11 (2006) 44.

[13]   W. Lu, G. Liu, S. Gao, S. Xing, J. Wang, Nanotechnology, 19 (2008) 445711.

[14]   C. Sirtori, P. K. Altvater, A. M. de Freitas, P. G. Peralta-Zamora, J. Hazard. Materials:B, 129 (2006) 110.

[15]   L. Zhang, Y. Jiang, Y. Ding, N. Daskalakis, L. Jeuken, M. Povey, A. J. O'Neill, D. W. York, J. Nanopart. Res., 12 (2010)1625.

[16]   J. Sawai, J. Migrobiol. Methods, 54 (2003) 177.

[17]   L. Zhang, Y. Jiang, Y. Ding, M. Povey, D. York, J. Nanoparticle Res., 9 (2007) 479.

[18]   N. Padmavathy, R. Vijayaraghavan, Sci. Technol. Adv. Mater., 9 (2008) 035004

[19]   P. J. Moos, K.Chung, D. Woessner, M. Honeggar, N. S. Cutler, J.M. Veranth, Chem. Res. Toxicol., 23(2010) 733.

[20]   A. A. Aal, S. A. Mahmoud, A. K. Aboul-Gheit, Nanoscale. Res. Lett., 4 (2009) 627.

[21]   T. Jin, D. Sun, J. Y. Su, H. Zhang, H. J. Sue, J. food science, 74 (2009) 1.

[22] Q. Li, S. Mahendra, D.Y. Lyon, L. Brunet, M. V. Liga, D. Li, P. J. J. Alvarez, Water Res., 42 (2008) 4591.

[23] D. Yan, G. Yin, Z. Huang, M. Yang, X. Liao, Y. Kang, Y. Yao, B. Hao, D. Han, J. Phys. Chem.: B, 113 (2009) 6047.

[24] E. S. Jang, J. H. Won, S. J. Hwang, J. H.C, Adv. Mater., 18 (2006) 3309.

[25] C. Chen, J. Liu, P. Liu, B. Yu, Adv. Chem. Engg. and Sci., 1 (2011) 9.

[26] A. A. Ashkarran, A. I. zad, S. M. Mahdavi, M. M. Ahadian, Appl. Phys., 100 (2010) 1097.

[27] U. I. Gaya, A. H. Abdullah, Z. Zainal, M. Z. Hussein, Int. J. Chem., 2 (2010) 1.

[28] F. Peng, H. Zhu, H. Wang, H. Yu, Korean J. Chem. Eng., 24 (2007) 1022.

[29] P. J. A. Borm, W. Kreyling J. Nanosci. Nanotechnol., 4 (2004) 521

[30] X. Li, Y. Xing, Y. Jiang, Y. Ding, W. Li, International Journal of Food Science and Technology 44 (2009) 2161.

[31] J.H. Li , R.Y. Honga, M.Y. Li, H. Z. Li, Y. Zhengd, J. Dinge, Prog.Orga. Coat., 64 (2009) 504.

[32] L. Chunzhi, W. Wang, J. Zhang, H. Zhu, W. Zhang, T. Wang, Front. Environ. Sci. Engin. China 3 (2009) 289.

[33] K. Byrappa, A.K. Subramani, S. Ananda, K .M. Lokanatha rai, R .Dinesh, M. Yoshimura, Bull. Mater. Sci., 25 (2006) 433.

[34] O. Heintz, D. Robert, J. V. Weber, J. Photo. Chem. Photobiol. :A, 135 (2000) 77.

[35] Z. Lan , W. Domcke, V. A. L. Vallet, S. Mahapatra, J. Chem. Phys., 122 (2005)24315.

[36] P. Want , D. W. Brousmiche, C. Z. Chen, C. J. Sobolewski , M. Lukeman, M. Xu, Pure Appl.Chem., 73 (2001) 529.

[37] C. T. Shin, C. A. Sciarrone Dische, J. Pharm. Sci., 59 (2006) 297.

[38] J. D. Joshi, J. J. Vora, S. Sharma, C. Patel, A. Patel, Ultra Science, 1(2004) 123.

[39] S.C. Ameta, J. J. Vora, S. Sharma, A. Patel, C. Patel, Metal-Organic, Nano-Metal Chemistry, 35(2005)433.

[40] J. J. Vora, S. K. Chauhan, K.C.Parmar, S.B.Vasava, S. Sharma, L.S.Bhutadiya, E-J. Chem., 6(2)(2009) 531.

[41] N. Modirshahla, M.A. Behnajady, O. Jangi, R. Mohammad, Iran. J. Chem. Chem. Eng., 28 (2009) 49.

[42] J. L. Yang, S.J. An, W.I. Park, G.C. Yi, W. Choi, Adv. Mater., 16 (2004) 1661.

[43] F. Xu, Z.-Y. Yuan, G.-H. Du, T.-Z. Ren, C. Bouvy, M. Halasa, B.-L. Su, Nanotechnology, 17 (2006) 588.

[44] F. Xu, G.-H. Du, M. Halasa, B.-L. Su, Chem. Phys. Lett., 426 (2006) 129.

[45] B. Pal, M. Sharon, Mater. Chem. Phys., 76 (2002)82.

[46] F. Peng, H. Wang, H. Yu, S. Chen, Mater. Res. Bull., 41 (2006) 2123.

[47] G. Kenanakisa, Z. Giannakoudakis, D. Vernardou, C. Savvakis, N. Katsarakis, Catalysis Today, 151 (2010) 34.

[48] J. Krysa, G. Waldner, H. Mestakova, J. Jirkovsky, G. Grabner, Appl. Catal. B: Environ., 64 (2006) 290.

[49] M. Grätzel, Heterogeneous photochemical electron transfer, CRC Press, 1989.

[50] I. M. Butterfield, P.A. Christensen, A. Hamnett, K.E. Shaw, G.M. Walker, S.A. Walker, J. Appl. Electrochem., 27 (1997) 385.

[51] L. Kavan, M. Grätzel, Electrochim. Acta., 40 (1995) 643.

[52] Y. Hamasaki, S. Ohkubo, K. Murakami, H. Sei, G. Nogami, J. Electrochem. Soc., 141 (1994) 660.

[53] I. M. Butterfield, P.A. Christensen, A. Hamnett, K.E. Shaw, G.M. Walker, S.A. Walker, J. Appl. Electrochem., 27 (1997) 385.

[54] Michael Neumann-Spallart, Electrochimia Acta., 61 (2007) 806.

[55] J.K.N. Mbindyo, M.F. Ahmadi, J.F. Rusling, J. Electrochem. Soc., 144 (1997) 3153.

[56] P. Fernández-Ibáñez, S. Malato, O. Enea, Catal. Today, 54 (1999) 329.

[57] W. Xie, Y. Li, W. Sun, J. Huang, H. Xie, X. Zhao, J. Photochem. Photobiol. A: Chemi., 216 (2010) 149–155.

[58] B. D. Ahn, H. S. Kang, J. H. Kim, G. H. Kim, H. W. Chang, S. Yeol, J. Appl. Phys., 100 (2006) 09370.

[59] D.H. Kim, M.A. Anderson, Environ. Sci. Tech., 28 (1994) 479.

[60] Z. Yan, Y. Ma, P. Deng, Z. Yu, C. Liu, Z. Song, App. Surf. Sci., 256 (2010) 2289.

[61] V. S. Khomchenko, V. I. Kushnirenko, V. P. Papusha, A. K. Savin, O. S. Lytvyn, Semiconductors, 44 (2010) 685.

[62] W.Liu, Physica: B, 404 (2009) 15550.

[63] S.H. Jeong, D.G. Yoo, D.Y. Kim, N.E. Lee, J.H. Boo, Thin Solid Films, 516 (2008) 6598.

[64] H. Xuie, X.L. Xu, Y. Chen, G.H. Zhang, S.Y. Ma, App. Sur. Sci., 255 (2008) 1806.

[65] R. Deng, B. Yao, Y.F. Li, T. Yang, B.H. Li, Z.Z. Zhang, C.X. Shan, J.Y. Zhang, D.Z. Shen, J. Crystal Growth, 312 (2010) 1813.

[66] D.R. Sahu , Microelectronics Journal, 38 (2007) 1252.

[67] L.J. Sun, J. Hu, H.Y. He, X.P. Wu, X.Q. Xu, B.X. Lin, Z.X. Fu, B.C. Pan, Solid State Communications, 149 (2009) 1663.

[68] J. Wang, X.M. Fan, K. Tian, Z.W. Zhou , Y. Wang, App. Sur. Sci., 257 (2011) 7763.

[69] R. Wang, J.H. Xin, Y. Yang, H. Liu, L. Xu, J. Hu , App. Sur. Sci., 227(2004) 312.

[70] R. S. Zeferino, M.B. Flores, U. Pal , J. Appl. Phys., 109 (2011) 014308.

[71] R. Georgekutty, M.K. Seery, S. C. Pillai, J. Phys. Chem.:C, 112(2008) 13563.

[72] C. Karunakaran, V. Rajeswari, P. Gomathisankar, Superlattices and Microstructures, 50 (2011) 234.

[73] Tianwen Chen, Yuanhui Zheng, Jin-Ming Lin, Guonan Chena, J Am Soc Mass Spectrom, 19 (2008) 997.

[74] P. Amornpitoksuk, S. Suwanboon, S. Sangkanu, A. Sukhoom , N. Muensit, J. Baltrusaitis, Powder Technology, 219 (2012) 158.

[75] T. Whang, M. Hsieh, H. Chen, Appl. Sur. Sci., 258 (2012) 2796.

[76] C. Hariharan , Appl. Catal. A, 304 (2006)55.

[77] F. R. Fan, Y. Ding, D. Y. Liu, Z. Q. Tian, Z. L. Wang, J. Am. Chem. Soc., 131 (2009)12036.

[78] J. Yuan, E. Shi, G. Choo, X. Tang, Y. Sheng, J. Ding, J. Xue, Nanotechnology, 21(2010) 185606.

[79] K. K. Haldar, T. Sen, A. Patra, J. Phys. Chem. C, 112(2008)11650.

[80] R. Mohan, K. Krishnamoorthy, S. Kim, Solid State Communications, 152 (2012)375.

[81] T. Xu, L. Zhang, H. Cheng, Y. Zhu, Appl. Catal. B: Environ., 101 (2011) 382.

[82] Z. Li, S. Sun, X. Xu, B. Zheng, A.Meng, Catalysis Communications, 12 (2011) 890.

[83] B. Donkova, D. Dimitrov, M. Kostadinov, E. Mitkova, D. Mehandjiev, Mater. Chem. Phy., 123 (2010) 563.

[84] J. Gao, X. Luan, J. Wang, B. Wang, K. Li, Y. Li, P. Kang, G. Han, Desalination, 268 (2011) 68.

[85] Y. S. Yoon, S. H. Jee, N. Kakati, J. Maiti, D-J. Kim, S. H. Lee, H. H. Yoon, Cer. Int., 38 (2012) S653.

[86]   M. J. Height, S. E. Pratsinis, O. Mekasuwandumrong, P. Praserthdam, Catal. B, 63(2006) 305.

[87]   N. Yuan-Yuan, C. Wang, L.Yu, Chin. Phys. Lett., 27 (2010) 056802.

[88]   G. Neri, A. Bonavita, S. Galvagno, Y. X. Li, K. Galatsis, W. Wlodarski, Thin Films, IEEE Sen. J., 3 (2003)

[89]   N. S. Ramgir, Y.K. Hwang, S. H. Jhung, H.-K. Kim, J.-S. Hwang, I.S. Mulla, J.S. Chang, App. Sur. Sci.,252 (2006) 4298.

[90]   E. D. Gaspera, Karg, M., Baldauf, J., Jasieniak, J., Maggioni, G., Martucci, A.M. Guglielmi, G. Perotto, S. Agnoli, G. Granozzi, M.L. Post, A. Langmuir, 27 (2011) 13739.

[91]   D. A.Wilson, M. Baietto, Sensors , 11(201)11105.

[92]   G. Socol, E. Axente, C. Ristoscu, F. Sima, A. Popescu, N. Stefan, I. N. Mihailescua, L. Escoubas, J. Ferreira, S. Bakalova, A. Szekeres, J. Appl. Phy. 102 (2007) 083103.

[93]   X.-H. Wang, J. Shi, S. Dai, Y. Yang, Thin Solid Films, 429 (2003) 102.

[94]   N. Hongsith, C. Viriyaworasakul, P. Mangkorntong, N. Mangkorntong, S. Choopun, 34 (2008) 823.

[95]   C. Wongchoosuk, S. Choopun, A. Tuantranont, T. Kerdcharoen, Mater. Res. Inno. 13 (2009)185.

[96]   N. L. Hung, H. Kim, S. K. Hong, D. Kim, Sen. and Act. B, 151(2010) 127.

[97]   S. Sarkar, A. Makhal, T. Bora, S. Baruah, J. Dutta, S. Kumar Pal, Phys. Chem. Chem. Phys., 13 (2011)12488.

[98]   R.S. Sonawane, M.K. Dongare, J. Mol. Catal. A: Chem., 243 (2006) 68.

[99]   H. W. Choia, E. J. Kimb, S. H. Hahna, Chem. Eng.J., 161(2010)285.

[100] S. Palomba, L. Novotny, R.E. Palmer, Opt. Commu., 281 (2008) 480.

[101] C. Guillard, H. Lachheb, A. Houas, M. Ksibi, E. Elaloui, J. M. Herrmann, J. Photochem. Photobio. Chem:A, 158 (2003) 27.

[102   K. Kogo, H. Yoneyama, H. Tamura, J. Phy. Chem., 84 (1980) 1705.

[103] Zhao, X. Yang, Building and Environ., 38 (2003)645.

[104] F. Zang, J. Zhao, T. Shen , App. Catal. B, 5(1998)147.

[105] G. Rothenberger, J. Moser, M. Gr¨atzel, N. Serpone, D. K. Sharma, J. Amer. Chem. Soci., 107 (1985) 8054.

[106] H. Tributsch, N. Serpone, E. Pelizzeti, Wiley, New York, NY, USA, 1989.

[107] M. C. Daniel, D. Astruc, Chemical Reviews, 104 (2004) 293.

[108] C. F. Bohren, D. R. Huffman, Wiley, New York, NY, USA, 1983.

[109] J. L. Lyon, D. A. Fleming, M. B. Stone, P. Schiffer, M. E. Williams, Nano Letters, 4(2004)719.

[110] S. J. Cho, J. C. Idrobo, J. Olamit, K. Liu, N. D. Browning, S. M. Kauzlarich, Chem. Mater., 17(2005) 3181.

[111] D. Caruntu, B. L. Cushing, G. Caruntu, C. J. O'Connor, Chem. Mater., 17(2005) 3398.

[112] Y. H. Chen, U. Nickel, J. Chem. Society, Faraday Transactions, 89(1993) 2479.

[113] N. Aihara, K. Torigoe, K. Esumi, Langmuir,14 (1998) 4945.

[114] M. Michaelis, A. Henglein, P. Mulvaney, J. Phy. Chem., 98 (1994) 6212.

[115] M. Muneer, M. Qamar, D. Bahnemann, J. Envir. Manag., 80(2006) 99.

[116] M. S. Wong, W. C. Chu, D. S. Sun, H. S. Huang, J. H. Chen, P. J. Tsai, N. T. Lin, M. S. Yu, S. F. Hsu, S. L. Wang, H. H. Chang, Appl. Environ. Microbiol.,72 (2006) 6111.

[117] R. Jalal, E. K. Goharshadia, M. Abareshia, M. Moosavic, A. Yousefid, P. Nancarrowe, Mater. Chem. Phy., 121 (2010) 198.

[118] J. P. Mosnier, R. J O'Haire, E.McGlynn, M.O. Henry, S. J. Mc Donnell, M. A. Boyle, K. G. McGuigan, Sci. Technol. Adv. Mater. 10 (2009) 045003.

[119] L. Russa, M. Malagodi, C. Oliviero Rossi, A.M. Palermo, G.M. Crisci, Appl. Phys.: A, 100 (2010) 829.

[120] W. Lu, G. Liu, S. Gao, S. Xing, J. Wang, Nanotechnology, 19 (2008) 445711.

[121] H. Fu, T. Xu, S. Zhu, Y. Zhu, Environ. Sci. Technol.,42 (2008) 8064.

[122] C. Ye, Y. Bando, G. Shen, D. Golberg, J. Phys. Chem.: B, 110 (2006)15146.

[123] T. Pradeep, Anshup, Thin Solid Films, 517 (2009) 6441.

[124] P. Pawinrat, O. Mekasuwandumrong, J. Panpranot, Catal. Commun.,10 (2009) 1380.

[125] H. Zeng, P. Liu, W. Cai, S. Yang, X. Xu, J, Phys. Chem.: C, 112 (2008) 19620.

[126] V. M. Djinovic, L. T. Mancic, G. A. Bogdanovic, P. J .Vulic, G. del Rosario, T. J. Sabo, O. B. Milosevic , J. Mater. Res., 20 (2005)102.

[127] R. Georgekutty, M.K. Seer, S. C. Pillai, J. Phys. Chem.: C, 112 (2008) 13563.

[128] H. Zeng, W. Cai, P. Liu, X. Xu, H. Zhou, C. Klingshirn, H. Kalt, ACS. Nano, 2 (2008) 1661.

[129] J. Zhong, J. Li, X.y. He, J. Zeng, Y. Lu, W.Hu, K. Lin, Current Appl. Phy. 12 (2012) 998.

[130] S.Cho, J.W. Jang, J. Kim, J.S. Lee, W. Choi, K.H. Lee, Langmuir 27 (2011) 10243.

[131] C. Wang, X. Wang, B.Q. Xu, J. Zhao, B. Mai, P. Peng, G. Sheng, J. Fu, J. Photochem. Photobiol. A: Chem., 168 (2004) 47.

[132] J. Iran, Chem. Soc. 6 (2009) 570.

[133] G. Kenanakis, Z. Giannakoudakis, D. Vernardou, C. Savvakis, N. Katsarakis, Catal. Today 151 (2010) 34.

[134] V.V. Shvalagin, A.L. Stroyuk, S. Ya. Kuchmii, Theoretical and Experimental Chemistry, 40 (2004) 6

[135] L. Zhang, H. Cheng, R. Zong, Y. Zhu, J. Phys. Chem. C, 113 (2009) 2368.

[136] N.V. Kaneva, D.T. Dimitrov, C.D. Dushkin, Appl. Surf. Sci., 257 (2011) 8113.

[137] H. Zhang, R. Zong, Y. Zho, J. Phys. Chem. C, 113 (2009) 4605.

[138] C. Wang, J. Zhao, X. Wang, B. Mai, G. Sheng P. Peng, J. Fu, Appl. Catal. B: Environ. 39 (2002) 269.

[139] D.L. Liao, C.A. Badour, B.Q. Liao, J. Photochem. Photobiol. A: Chem., 194 (2008) 11.

[140] S. Liao, D. Huang, D. Yu, Y. Su, G. Yuan, J. Photochem. Photobiol. A: Chem., 168 (2004) 7.

[141] Y. Shaogui, Q. Xie, L. Xinyong, L. Yazi, C. shuo, C. Guohu, Phys. Chem. Chem. Phys., 6 (2004) 659.

[142] R. Ali, W. Azelee, W.A. Bakar, L.K. Teck, Modern Appl. Sci. 4 (2010) 59.

[143] Q. Zhang, W. Fan, L. Gao, Appl. Catal. B: Environ. 76 (2007) 168.

[144 M.A. Aramendía, V. Borau, J.C. Colmenares, A. Marinas, J.M. Marinas, J.A. Navío, F.J. Urbano, Appl. Catal. B: Environ., 80 (2008) 88.

[145] Y. Abdollahi, A.H. Abdullah, Z. Zainal, N.A. Yusof, J. Appl. Sci. Technol. 1 (2011)

[146] B. Neppolian, H.C. Choi, S. Sakthivel, B. Arabindoo, V. Murugesan, J. Haz. Mater. B, 89 (2002) 303.

[147] Y. Li, W. Xie, X.Hu, G. Shen, X. Zhou, Y. Xiang, X. Zhao, P. Fang, Langmuir, 26 (2010) 591.

[148] V.D. Das, L. Damodare, Mater. Chem. Phys., 56 (1998) 48.

[149] H.P. Klug and H.A. Alexander; "X-ray Diffraction Procedure", 2nd Edn. Wiley VCH, New york (1974).

[150] B.D. Cullity, 'Elements of X-Ray Diffraction' 2nd Ed.; Addison Wesley Pub. Ind (1978).

[151] N.F. Kenon, 'Patterns in Crystals' John Wiley and Sons Pub., (1978).

[152] L.Vagard, Phys. 5 (1921) 17.

[153] H.H. Afify, R.S. Momtaz, W.A. Badawy, S.A. Nasser, J. Mater. Electron 2 (1991) 40.

[154] O. S. Heavens, Optical Properties of Thin Solid Films. Academic Press, New York, 1991.

[155] B.E. Stern and D. Lewis, Pitman Pub. Corp. (1971) 205.

[156] L.-J. Meng and M. P. dos Santos, Thin Solid Films 226 (1993) 22.],

[157] F. Micheltti and   P. Mark, J. Appl. Phys. Lett. 10 (1967) 136.

[158]   C.V. Raman and K.S. Krishnan, Nature, 121 (1928) 501.

[159] D. Tang, P. H. Santschi, Journal of Chromatography :A, 883 (2000) 305–309

[160] K. L. Stone, M. B. LoPresti, J. M. Crawford., R . DeAngelis, K. R. Williams, Reversed- phase HPLC separation of sub-nanomole amounts of peptides obtained from enzymatic digests in High Performance Liquid Chromatography of Peptides and Proteins: Separation, Analysis and Conformation. (ed.Mant, C.T., Hodges, R.S.) CRC Press, Boca Raton. 1991.

[161] J.W. Peeler, L. L. S, Kinnerand DeLuca,., "General Field Test Method Approval Process and Specific Application for a Direct Interface GCMS Source Test Method," Air and Waste Management Association, Nashville, TN, 96-RP132.01, June 23-28, 1996.

[162] Kinner, L.L., and Peeler, J.W., "Evaluation of HAPSITE and a Direct Interface GCMS Test Method for Measurement of Volatile Organic Compounds in Stationary Source Emissions" Prepared for Leybold Inficon Inc., July 1997.

[163] Standard Methods for the Examination of Water and Wastewater, 20th Ed. 1998. APHA, AWWA and WEF, Washington, D.C.

[164] R. Zimmermann, R. Iturriaga, J. Becker-Birck. 1978. Simultaneous determination of the total number of aquatic bacteria and the number there of involved in respiration, Appl. Environ. Microbiol. , 36 (1978) 926–935.

[165] P.G. Engelkirk, J.D. Engelkirk, Burton's Mocrobiology for the Health Science, 9th Edition, New York, London, (2011) .

[166] Y. Jin, Q. Cui, K. Wang, J. Hao, Q. Wang, and J. Zhang, J. Appl. Phys. 109, (2011) 053521

[167] B. Houng and C.J. Huang, Surf. Coat. Technol. 201(2006) 3188

[168] F. H. Wang, H. P. Chang, C. C. Tseng, C. C. Huang, and H. W.Liu, Curr. Appl. Phys.

11(2011)S12

[169] V. S. Khomchenko, T. G. Kryshtab, A. K. Savin, L. V. Zavyalova, N. N. Roshchina, V. E Rodionov, O. S. Lytvyn, V. I. Kushnirenko, V. B. Khachatryan, and J. A. Andraca-Adame, Superlattices Microstruct.,42 (2007)94

[170] D. H. Lee, K. H. Park, S. Kim, and S. Y. Lee,Thin Solid Film,520(2011)1160.

[171] W. Liu, S. Zhao, K. Zhao, W. Sun, Y. Zhou, K. Jin, H. Lu, M. He, and G. Yang , Physica B, 404 (2009)15550

[172] I. S. Kim, E. K. Jeong, D. Y. Kim, M. Kumar, S. Y. Choi, Appl. Surf. Sci., 255 (2009) 4011

[173] C. Karunakaran, V. Rajeswari, P. Gomathisankar, Superlattices Microstruct. 50 (2011) 234

[174] N. L. Tarwal and P. S. Patil, Electrochimica Acta., 56 (2011) 6510

2.1 Introduction

Photocatalytic oxidation is a process where semiconductor, upon absorption of a photons, act as catalyst producing highly reactive radicals. These are mainly hydroxyl radicals, which can oxidize organic compounds and inactivate microorganisms. Thus organic molecules/microorganisms are decomposed to form carbon dioxide, water and mineral acids as final products. A variety of organic compounds/ microorganisms can be photocatalytically oxidized and eventually mineralized according to the following general reaction [1-9]:

$$Organic\ compound\ /\ Microorganism + O_2 \rightarrow (ZnO + h\nu) \rightarrow CO_2 + H_2O + Mineral\ Acids$$
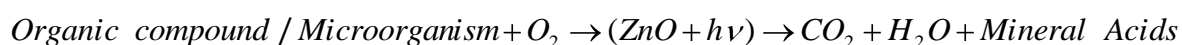
This chapter describes the theoretical aspects of various semiconductor terminologies, processes and degradation mechanisms related to purification of water.

2.2 Some important terminologies

In this section, some important terminologies are defined for the convenience to discuss experimental results.

i) Band Model

In order to describe electron transfer to or from a semiconductor, it is desirable to utilize the concept of band model. The band model of a solid stems directly from the statistic distribution of atomic energy levels. According to Pauli exclusion principle, the energy levels of identical overlapping electronic orbitals cannot be equal. Analysis shows that the discrete energy levels of the atoms forming the solid broaden when the orbitals overlap; forming bands of energy levels with about 2×10^{22} levels in each band when there is the order of 10^{22} atoms in the crystal. Bands are large number of orbitals with different energy levels. These bands are again divided into two types i.e. valence band and conduction band. The aggregate of orbitals occupied by valence electrons is called the valence band (VB) of the solid. The band associated with the first excited state, normally unoccupied by electrons, is called the conduction band (CB) of the solid. The energy gap between conduction and valence band of a solid is called the bandgap energy. One important property of semiconductor is that, when a photon of energy greater than or equal to the band gap of semiconductor is incident on it, the electron and hole pairs are generated.

ii) *Fermi level* (E$_f$)

The Fermi Level and the Fermi distribution describe the distribution of electrons and holes among the available energy levels in the solid. According to first order approximation, all the energy levels below the Fermi level are occupied by electrons, while all the energy levels above Fermi level are unoccupied by electrons. From a statistical point of view, Fermi level is the average energy of electrons and electrons moving from the solid to ions in solution originate with a free energy of E$_f$. From a chemical point of view, the Fermi level is the electrochemical potential of electrons in the solid.

iii) Photoelectrochemical (PEC) solar cell

There are several methods of collecting and converting solar energy viz. photovoltaic, photoelectrochemical, photothermal and photosynthetic. Out of these routs the photoelectrochemical system is easiest one. A PEC effect is defined as one in which irradiation of electrode/electrolyte system produce a change in electric potential (on open circuit) or in the current flowing in external circuit (under short circuit conditions) [10]

Early semiconductor electrochemistry studies [11] have shown that the distribution of potential at the semiconductor – electrolyte interface is almost similar to that at a simple p-n junction. A direct conversion of solar energy into electrical energy using a semiconductor electrolyte interface was demonstrated by Gerischer [12]. These are generally known as photoelectrochemical solar cells.

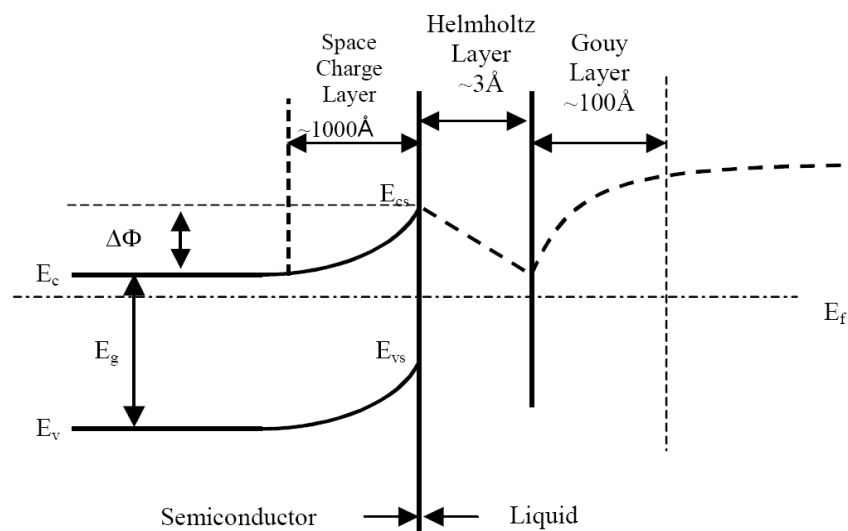### Semiconductor–electrolyte (S-E) interface

When an appropriate semiconductor is immersed in an appropriate electrolyte the excess charge residing on the electrode surface must be exactly balanced by an equal charge of opposite sign on the solution side. This can happen by charge transfer across the electrode – electrolyte system.

When semiconductors are brought into contact with liquid, due to the difference in Fermi levels of the two phases, charged planes or space charge layer almost inevitably form at the interface to reach an equilibrium. A schematic diagram of this interface is shown in Fig. 2.1.

Space charge region in the semiconductor

When a semiconductor is dipped into an electrolyte, the junction is characterized by the presence of a space charge layer in the semiconductor adjacent to the interface

with the electrolyte. For semiconductors, the chemical potential of electrons is given by the Fermi level in the semiconductor. For liquid electrolytes, the chemical potential of electrons is determined by the redox potential of redox couples present in the electrolyte. If the initial Fermi level in n-type semiconductor is above the initial Fermi level in the electrolyte, then equilibration of the two Fermi levels occurs by transfer of electrons from semiconductor to the electrolyte. This produces a positive space charge layer in the semiconductor. As a result, the conduction and valence band edges are bent upwards, establishing a potential barrier against further electron transfer into the electrolyte. A reverse effect will occurs with p-type semiconductors having an initial Fermi level below that of the redox potential.

Figure 2.1 Schematic diagram of semiconductor liquid interface

Fermi levels, $E_{f,semi}$ and $E_{f,redox}$ are at different levels resulting in electron transfer from semiconductor to electrolyte which establishes the equilibrium. This flow of electrons results in the accumulation of ions in the semiconductors to form the space charge region near the interface in the semiconductors. A strong local electric field is developed and band bending takes place. The potential drop in the semiconductor space charge layer depends on the difference between the Fermi levels of semiconductor and the redox electrolyte, if the former is free from excess charge.

Helmholtz double layer

Helmholtz double layer is a dense layer of ions stuck to the electrode. In this region, the potential varies linearly with distance. This dense layer is divided into inner and outer Helmholtz planes. The inner Helmholtz plane (IHP) is adjacent to the

electrode surface and consists of completely oriented water dipoles and specifically adsorbed (or contact-adsorbed) ions. The orientation of water dipoles depends on the specific interaction with the electrode surface as well as the electric field. Large ions with negative free energy of contact adsorption are expected to be contact-adsorbed. In aqueous system, the cations react rather strongly with the water molecule and their inner hydration sphere is retained. This limits their closest distance of approach to the electrode. They are thus separated from the electrode by approximately one or two water molecules. On the other hand, anions interact weakly with water; hence hydration sheath is not covered on them. Thus the closest distance of approach could correspond to direct contact; they can be a part of IHP. The outer Helmholtz plane (OHP) consists of solvated ions (usually cations) at the closest distance approach from the electrode interface. The OHP thus consists of partly ionized water dipole layers. Bockris et al. [13] developed a model of electrode-electrolyte interface and is shown in Fig. 2.2 (a). In absence of contact adsorbed ions the potential distribution is as shown in Fig. 2.2(b). In presence of contact adsorbed ions, it can be seen from Fig. 2.2(c) that the potential distribution changes across the double layer. OHP ($X=X_2$) is the site at which non-specifically adsorbed ions arrive to take part in the charge transfer processes.

Gouy-Chapman diffuse layer

The size of the ions forming the outer Helmholtz plane (OHP) is such that the sufficient number of them cannot neutralize the charge on the electrode. Therefore, the remaining charges are held with increasing disorder as the distance from the electrode surface increases and the electrostatic forces become weaker and dispersion by thermal motion is more effective. These less ordered charges forcing opposite to that on the electrode constitute the diffuse part of double layer. Thus all the charges, which neutralize that on the electrode, are held in a region between OHP and the bulk of the electrolyte. The additional charges required to neutralize the total charge on the electrode forms the Gouy-Chapman layer or diffuse layer.

The region of the photo-potential can now be understood by considering the changes that occur at such an interface by the absorption of band gap radiation. Irradiation of the semiconductor electrolyte interface is produces electron hole pairs, the electrons being promoted to the conduction band. The potential difference across the space charge layer causes the electrons to move towards the bulk of the semiconductor at this is downhill path for the electrons in a n-type semiconductor.
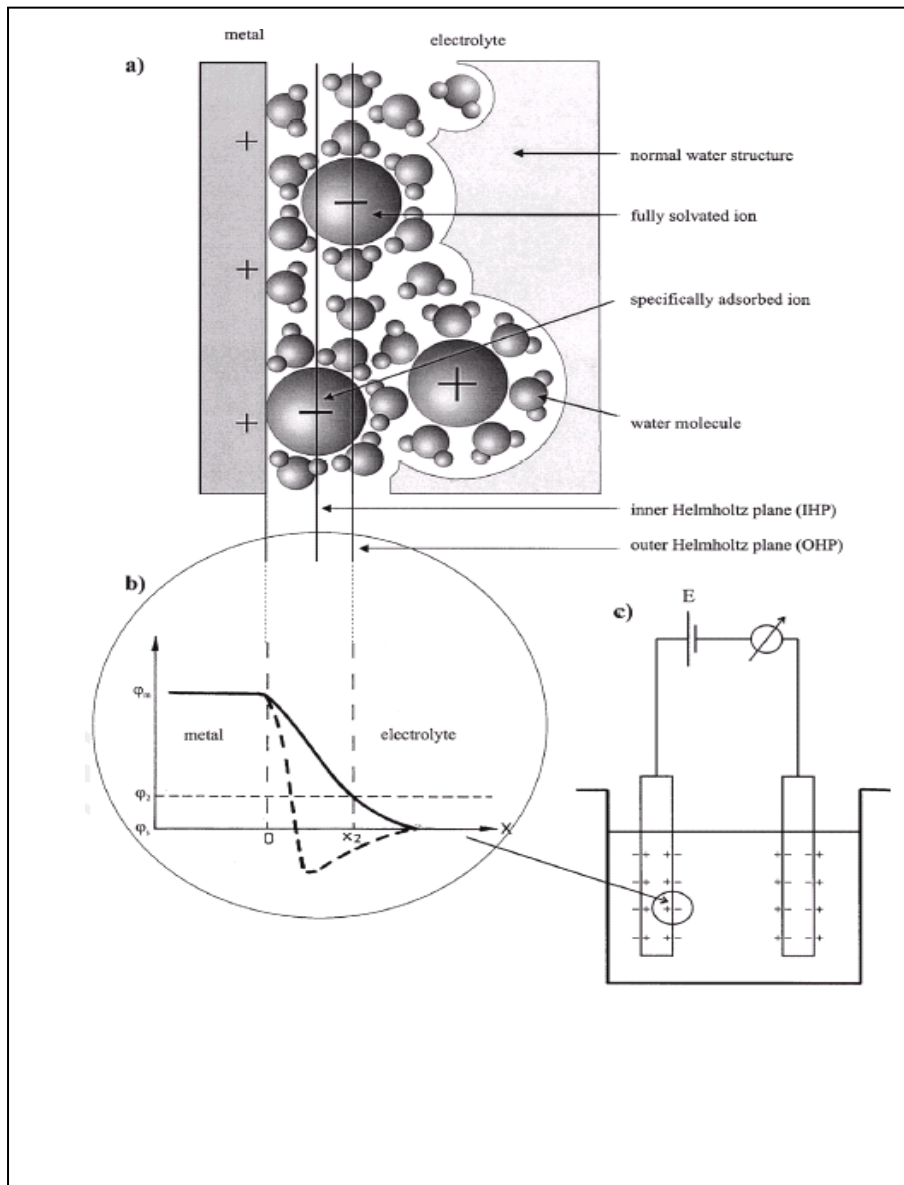
Fig. 2.2 (a) Electrode Electrolyte Interface, (b) Potential Distribution across the double layer & (c) The schematic of electrodes immersed in electrolyte.

Photoinduced charge transfer across S-E junction

The minority carriers h^+ moves towards the surface of the electrolyte. This movement of the charge carriers in the field of the space charge layer counteracts the band bending, causing as partial return to the charge carrier distribution as before band bending and is shown in Fig. 2.3.

The result is the development of a Fermi level in the semiconductor called the photon Fermi level which is no longer equal to the redox potential of the electrolyte $E_{F(Photo)}$-$E_{F(redox)}$ goes up as the photo-potential on illuminating the interface with light ($h\nu \geq Eg$). A photocurrent can now the observed by connecting the photoanode to a suitable counter electrode. The photocurrent depends on the absorption coefficient of the semiconductor, width of the space charge region, hole diffusion length, area of illuminated electrode, photon energy and radiation intensity. Under short circuit conditions the Fermi levels of the semiconductor and the potential of the redox couple of the solution are equalized and a net charge flows during the illumination.
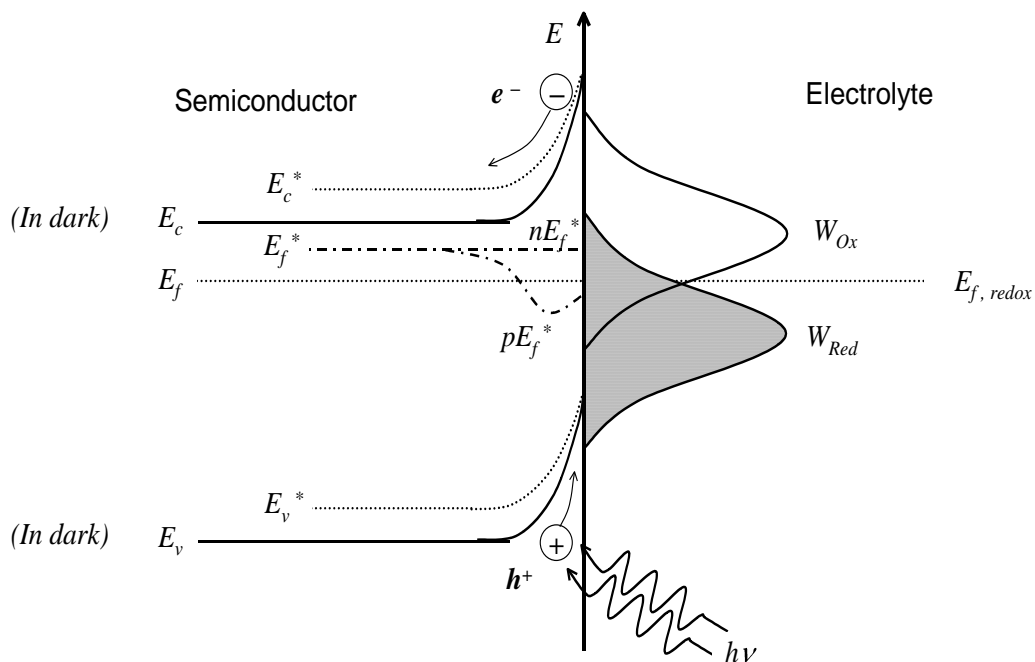
Fig. 2.3 The position of bands under illumination responsible for photo induced charge transfer

iv) Flat band potential

The Fermi level of a semiconductor can be controlled by an applied external potential bias. The flat band potential is the applied potential, when the bands of the semiconductor are flat. In other words, there is no band bending on the semiconductor side of the interface. By measuring the flat band potential, the band edge of semiconductor can be determined. For most oxide semiconductors their flat band potentials have a Nernstian-type pH dependence in aqueous media.

v) On-set potential

For a n-type semiconductor electrode, when the applied potential is below the conduction band edge (or below the flat band potential), there would be no electrons withdrawn from the semiconductor. As a result, there is no anodic current observed even if there are large amount of electrons under illumination. The on-set potential refers to the potential at which anodic photocurrent starts to be measured. In ideal cases, the on-set potential approximates the flat band potential.

2.3 Classification of photon/semiconductor systems

In semiconductors, the valence electrons have little chance of being thermally excited and only a small portion of electrons with high kinetic energy can reach the conduction band resulting in low electrical conductivity. When the two bands of a solid material are further separated to larger than 3 eV, similarly the free electron concentration is further lowered and such material is regarded as insulator. However, this definition is not rigid, since, for example ZnO is still considered to be semiconductor even though it has a band gap of 3.2 eV. Light excitation of a semiconductor promotes electrons from the valence band to the conduction band. In metals, where there is a continuum of energy states, the light generated electrons deactivates easily and the lifetime of the electron/hole pair is so short that they cannot be harvested. The existence of band gap in semiconductors prevents rapid deactivation of the excited electron/hole pairs, which can be deactivated only by recombination. This assures that an electron/hole pair lifetime is sufficiently long to participate in interfacial electron transfer [14].

Depending on the methods of harnessing the light generated electron/hole pairs and the purpose of the applications, few areas of studies have emerged from photon/semiconductor interactions. According to the types of semiconductors involved, the areas of studies can be classified in to bulk semiconductor systems and particulate semiconductor systems (Fig. 2.4). When the size of semiconductors is down to nanometer scale or sub-micrometer scale, they display a number of different properties to those of the macro-size semiconductors. The former systems are defined as *particulate* semiconductor systems and the latter are defined as bulk (thick or thin film) semiconductor systems. In history, the early research focused mainly on the bulk semiconductors. The bulk semiconductor theory has been well established and various applications have been extensively studied [15].
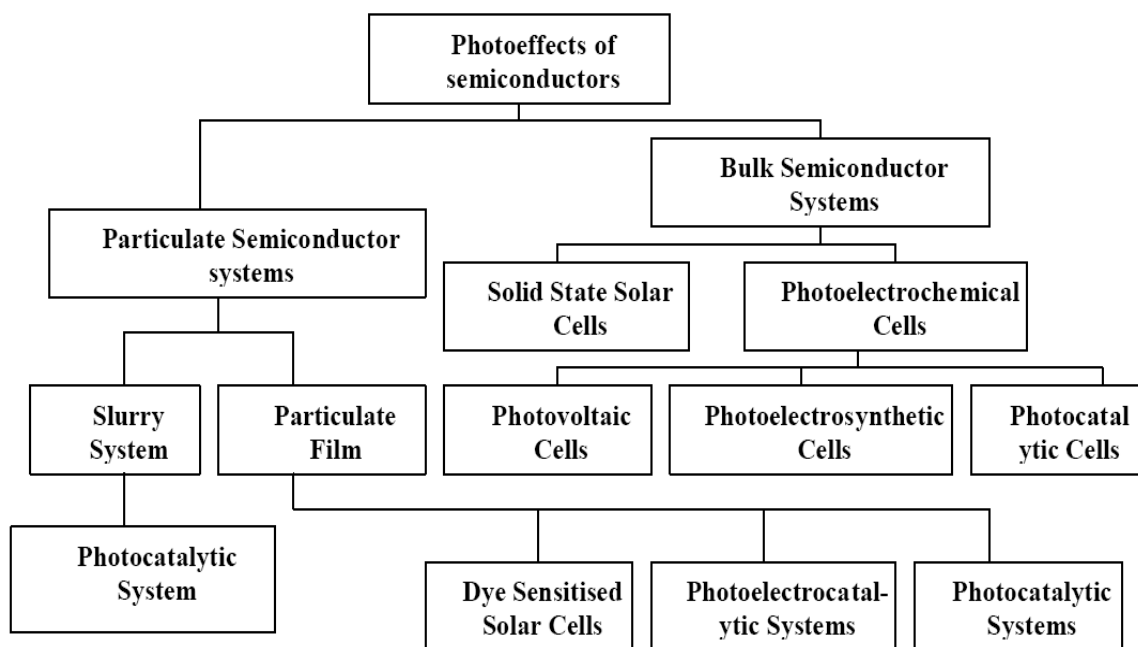
Figure 2.4 Classification of photon/semiconductor systems

The particulate semiconductors refer to semiconductor with particle sizes ranging from nanometer to sub-micrometer. The ZnO nanoparticle photocatalysis in visible light has become one of the most active research areas in the past two decades. Since the successful application of nanoparticle ZnO film electrode as photocatalyst in water purification. Moreover it can be used for the total destruction of organic compounds in wastewater [16].

2.4 Energetics and redox power of semiconductors

Semiconductor can absorbs light with energy higher than certain energy thresholds that is determined by the bandgaps (E_g) of semiconductors. Once photons are absorbed, photoelectrons and photoholes are formed. The photogenerated electrons and holes quickly relax to the bottom of the conduction band and the top of the valence band respectively by dissipating their kinetic energy. These electrons and holes can be used to drive a redox reaction. Thermodynamically, the energy level of the conduction band edge (E_{cs}) is a measure of the reduction strength of electrons in the semiconductor, whereas that of valence band edge (E_{vs}) is a measure of the oxidation power of holes in the semiconductor.

Different semiconductors possess different band edge energies. The higher the valence band edge potential, the higher oxidizing power its holes. For a semiconductor to have 'universal' photocatalytic reactivity toward different organic compounds,

thermodynamically its valence band edge must sit at a relatively high potential. Small band-gap semiconductors have a better absorption spectrum match with solar emission spectrum. From an utilization of solar energy point of view, the small band gap semiconductors would be a better choice. However, small band gap semiconductors normally do not have high valence band potential. Compounding this problem is that many semiconductors, particularly, the small band gap semiconductors suffer from serious chemical corrosion and photocorrossion when used as photocatalysts [17-18]. Therefore, the selection of semiconductor photocatalysts, depending on the application, often involves the compromise between a number of factors, such as high oxidizing power, good solar spectrum coverage and chemical/ photochemical stability.

2.5 Fundamentals of photocatalysis

Principle of photocatalysis

The band gap is characteristic for the electronic structure of a semiconductor and is defined as the energy interval (ΔE_g) between the valence band (VB) and the conduction band (CB). According to the band gap model [19], as shown in Fig 2.5, VB electrons are transferred to the CB, when the semiconductor is illuminated with photons having energy content equal to or higher than the band gap, creating electron–hole pairs (1). After migration to the semiconductor surface (2), electron–hole pairs may induce redox reactions with adsorbates having suitable redox potentials (3). From a thermodynamic point of view, VB holes can oxidize adsorbed compounds if the redox potential of the VB is more positive than that of the adsorbates. Similarly, CB electrons can reduce adsorbed species, if they have a more negative redox potential than the adsorbates. In the absence of suitable adsorbates, electron–hole pair recombination occurs with release of thermal energy and/or light (4). The rate of a photocatalytic reaction especially depends on the type of the photo catalytic semiconductor and on the light radiation that is used in its initiation [20]. Further factors that influence a photo catalytic reaction are:

- pH of the medium with which the semiconductor surface is in contact;
- Amount of the photocatalyst/area of the thin film influencing the reaction kinetics;
- Stream of photons, as oversupply of light accelerates electron–hole recombination;

- Temperature, higher temperatures cause frequent collision between the semiconductor and the substrate
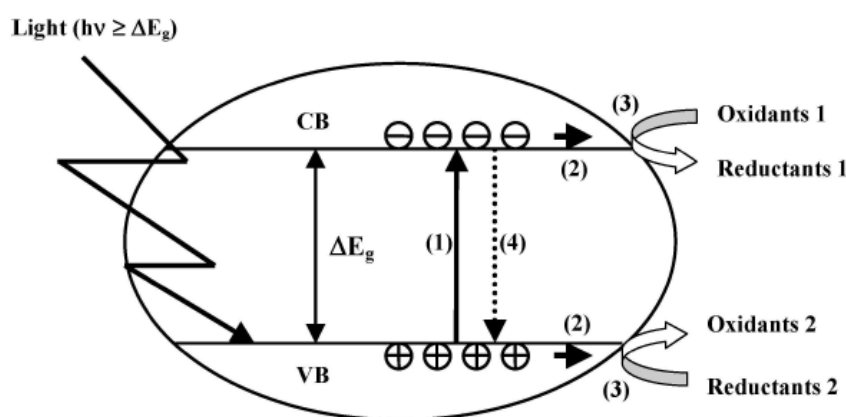
Figure 2.5 Schematic representation of the "band gap model." (1) Photo induced electron– hole pair creation; (2) charge migration to the surface; (3) redox reactions; (4)recombination. VB and CB represent valence band and conduction band, respectively.

Simply speaking, the photocatalyst is a semiconductor that on surface of which a strong oxidation occurs by the energy in light. ZnO irradiated with near ultraviolet light below $\lambda < 385$ nm, which are generated by UV-lamps and even common fluorescent lamps, free hydroxyl radicals can be generated. The oxidation can oxidize most organic and inorganic pollutants and therefore can perform functions such as anti-bacteria/anti-virus, deodorization, exhaust gases removal and self-cleaning.

Photocatalysis has great potential as an alternative water treatment method due to the possibility to remove by-product precursors. This process also ensures the public health safety of drinking water due to its ability to inactivate micro-organisms. Photocatalytic processes for water treatment are divided into two groups:

a) Homogeneous photocatalytic oxidation

In the homogeneous system, photocatalysis of either hydrogen peroxide or ozone under UV illumination supplies hydroxyl radicals. During this process continual consumption of oxidant occurs, e.g. UV/hydrogen peroxide.

**b) Heterogeneous photocatalytic oxidation**

Comparatively, in the heterogeneous process, hydroxyl radicals are produced from the redox reaction between photo-excited electrons and electron acceptors on the surface of the semiconductor photocatalyst. The process is catalytic and allows the

semiconductor to remain active for long periods of time. Therefore, heterogeneous photocatalysis is advantageous, e.g. such as UV/semiconductor photocatalysis.

2.6 Photoelectrocatalysis

Photocatalysis can be further enhanced by applying a potential to the ZnO film. This induces an electric field within the particles increasing charge separation. If one can remove the photogenerated electrons from the semiconductor particle (e.g. by application of an electric field), it is possible to increase the efficiency of oxidation at the semiconductor electrolyte interface.

Photoelectrocatalysis on ZnO represents a promising alternative technology for degradation of organic pollutants and inactivation of microorganisms in water. It is based on the photogeneration of separated electrons and positive holes. These charge carriers either recombine or move to its surface where they can react with adsorbed molecules. Positive holes typically oxidize organic compounds, inducing their oxidative degradation, while electrons mainly reduce molecular oxygen to superoxide radical anions. Recombination of photogenerated positive holes and electrons is responsible for the relatively low quantum yield of photocatalytic degradation.
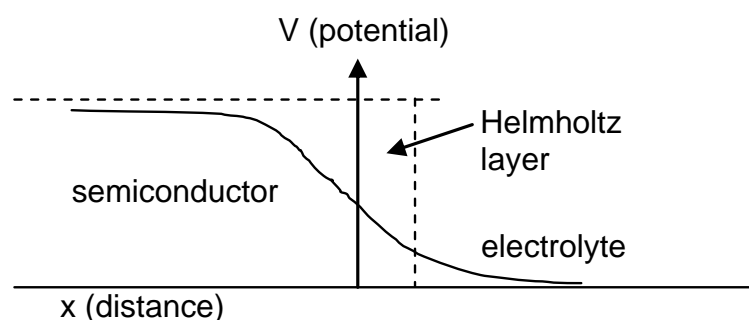

Figure 2.6 Potential distribution for a semiconductor-electrolyte interface

Upon application of an electrical bias to the ZnO film, CB electrons are removed to the back contact. This promotes charge separation and increases charge transfer through the film. As electrons are removed, hydroxyl radical production is increased therefore reducing the electrostatic repulsion of negatively charged particles. This is known as the electrical double layer effect, whereby the electrode becomes positively charged relative to the solution nearby, decreasing the local cation concentration within the Helmholtz layer. The potential varies with distance from the electrode surface and the electrolyte solution without a change in applied potential as shown in Fig. 2.6.

2. 7 Mechanism and Reaction Kinetics

2.7.1 Mechanism of photocatalysis on a ZnO thin film

ZnO is the last member of the 3d –transition metal oxide series with Zn having completely filled 3d orbitals ($3d^{10}$). The valence band of ZnO consists of only d states and the conduction band consists of s-p hybridized orbitals.   When ZnO is exposed to near UVA light, electrons in the valence band are excited to the conduction band leaving behind holes. These excited electrons in the conduction band are now in an s-p hybridized state. Thus holes are in a pure 3d state (VB) and excited electrons are in a s-p hybridized state. Hence nature of valance and conduction band is completely different, this is called dissimilar parity. Under such dissimilar parity, transition probability of electron to the valence band reduces hence reduction of e^--h^+ recombination. Such condition for the other 3d transition metal oxide members does not occur since 3d – states are present in both the valence as well as conduction bands. The photoexcited e^--h^+ pair has similar parity and hence recombination is faster. Thus TiO_2 and ZnO are only two among the 3d transition metal oxide semiconductors which remain stable on photo-oxidation [21].
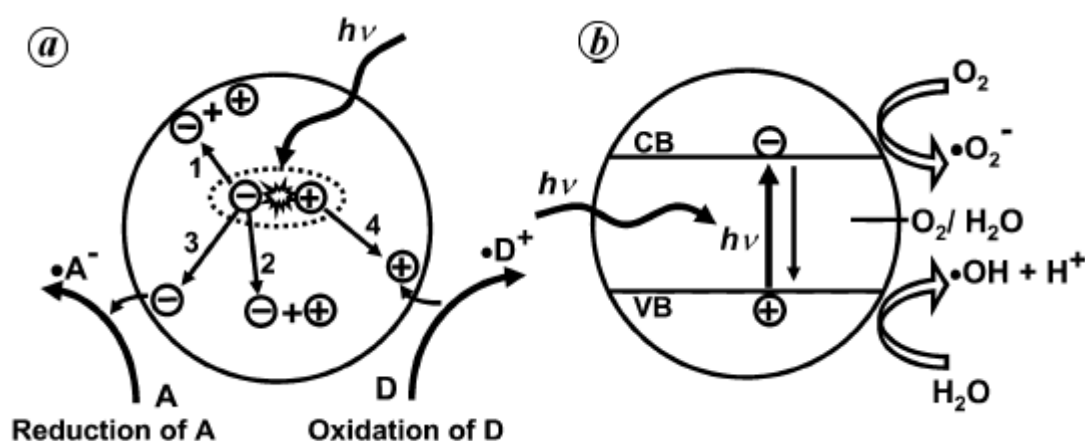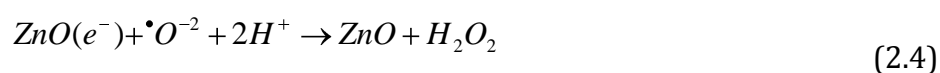

Figure 2.7 Schematic representation of some of the main processes occurring on a semiconductor particle. (a) Absorption of photon and electron–hole pair formation and migration of electron and hole: arrows marked (1) and (2) show electron–hole recombination at surface and bulk respectively, and those marked (3) reduction of acceptor and (4) oxidation of donor. (b) On absorbtion of photon of energy hn, electrons are excited from valence band (VB) to conduction band (CB). There is transfer of electron to oxygen molecule to form superoxide ion radical (·O–2) and transfer of electron from water molecule to VB hole to form hydroxyl radical (·OH)[17].
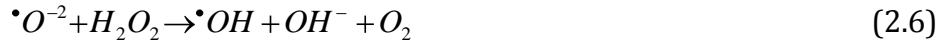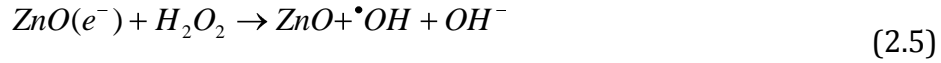
The band gap value of ZnO is 3.2 eV. Back side illumination with UVA light (λ ‹ 385 nm), will excite electrons from valence band to the conduction band, producing an e⁻-h⁺ pair. Photocatalyst is characterized by its ability to absorb simultaneously two reactants, which can be reduced and oxidized by efficiently absorbing light ($h\nu \geq E_g$) and ability to transfer electron from conduction band to the adsorbed particle (acceptor), which is governed by band gap position of the semiconductor and redox potential of the adsorbate. From the thermodynamic point of view, the redox potential of the adsorbate (acceptor) should be below the CB of the semiconductor. If the adsorbate is donor, then the potential level of the adsorbate (donor) should be above the VB position of the semiconductor in order to donate an electron to hole in the VB. The process of transfer of electron from the semiconductor to the adsorbate is called the reduction mechanism and the process of transfer of electron from the adsorbate to the semiconductor is called oxidation mechanism. Thus, the energy level at the bottom of CB determines the reduction ability of photolelctrons and the energy level at the top of VB determines the oxidation ability of photoholes. If the adsorbed couples are considered to be water and dissolved oxygen, then water gets oxidized by positive holes and it splits into •HO and H⁺. As oxygen is easily reducible, reduction of oxygen by photoelectrons of the conduction band results in generation of superoxide radical anions (•O⁻₂), which in turn reacts with H⁺ to generate •HO₂. On subsequent reaction with electron to produce hydrogen peroxide (HO⁻₂), and then with hydrogen ion, a molecule of H_2O_2 is produced [22].

Possible photocatalytic process in photodegradation phenomenon can be written as follows. Photocatalytic process begins with absorption of photon ($h\nu$)

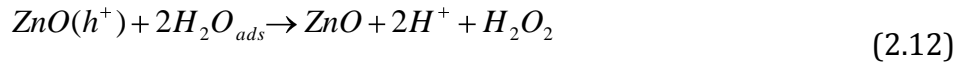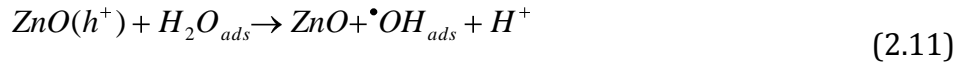$$ZnO + h\nu \rightarrow ZnO(e^- + h^+)$$

(2.2)

Reactions involving conduction band e–

$$ZnO(e^-) + O_2 \rightarrow ZnO + {}^\bullet O^{-2}$$

(2.3)

$$ZnO(e^-) + {}^\bullet O^{-2} + 2H^+ \rightarrow ZnO + H_2O_2$$

(2.4)

$$ZnO(e^-) + H_2O_2 \rightarrow ZnO + {}^\bullet OH + OH^-$$

(2.5)

$$ {}^\bullet O^{-2} + H_2O_2 \rightarrow {}^\bullet OH + OH^- + O_2 $$

(2.6)

$$ {}^\bullet O_2^- + H^+ \rightarrow ZnO + {}^\bullet HO_2 $$

(2.7)

$$ ZnO(e^-) + {}^\bullet HO_2 \rightarrow ZnO + HO_2^- $$

(2.8)

$$ HO_2^- + H^+ \rightarrow H_2O_2 $$

(2.9)

$$ 2{}^\bullet HO_2 \rightarrow O_2 + H_2O_2 $$

(2.10)

Reactions involving valence band h+

$$ ZnO(h^+) + H_2O_{ads} \rightarrow ZnO + {}^\bullet OH_{ads} + H^+ $$

(2.11)

$$ ZnO(h^+) + 2H_2O_{ads} \rightarrow ZnO + 2H^+ + H_2O_2 $$

(2.12)

$$ ZnO(h^+) + OH_{ads}^- \rightarrow ZnO + {}^\bullet OH_{ads} $$

(2.13)

Reactive oxygen species such as $H_2O_2, {}^\bullet O_2^-$ **(**ROS) and hydroxyl radicals (*OH)cause damage to various cell components leading to biocidal activity induced by photocatalysis. Subsequently, termination reactions also take place during the above process:

$$ {}^\bullet OH + H^+ + 2e^- \rightarrow H_2O $$

(2.14)

$$ \frac{1}{2}O_2 + 2H^+ + 2e^- \rightarrow H_2O $$

(2.15)
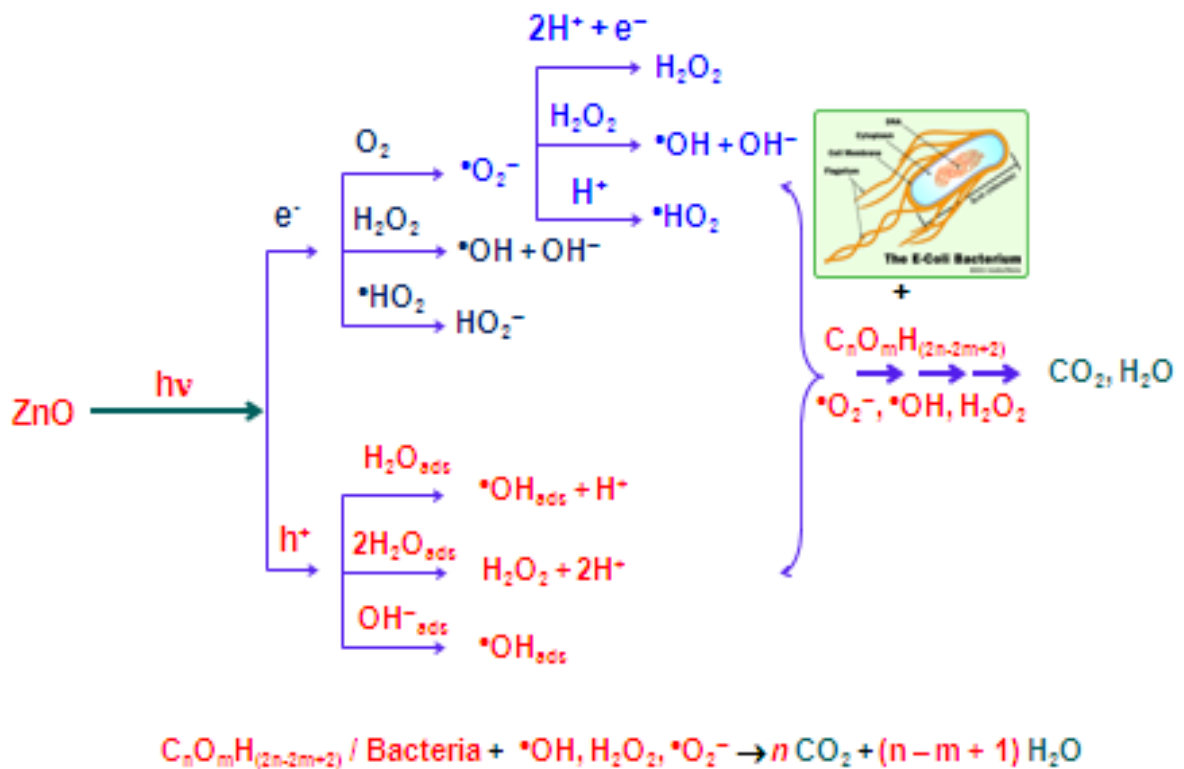
Figure 2.8 Chain of reactions involved in the production of reactive oxygen species such as H_2O_2, $^\bullet O_2^-$ and hydroxyl radical $^\bullet OH$

The hydroxyl free radical $^\bullet OH$ is highly reactive, short lived and detrimental. It can break organic host compound. The superoxide anion $^\bullet O_2^-$ is long lived and cannot destroy the bounds due to its negative charge where as hydrogen peroxide can destroy. The above chain of reaction is shown illustratively in Fig.2.8.

2.7.2 Mechanism of photoelectrocatalytic inactivation bacteria

To date, numerous studies have been carried out to demonstrate the germicidal effects of semiconductor photocatalysis [23-28]. The vast majority of thesis focus on the destruction of bacterial pathogens in particular *Escherichia coli (E.coli)*, most likely due to the fact that coliforms are traditionally used as indicators of faecal contamination in water supplies. Coliform bacteria may not necessarily cause disease, but can be indicators of pathogenic organisms that do. The latter could cause intestinal infections, dysentery, hepatitis, typhoid fever, cholera and other illnesses. Intestinal infections and dysentery are generally considered as minor health problems. They can, however, prove fatal to infants, the elderly, and those who are ill.
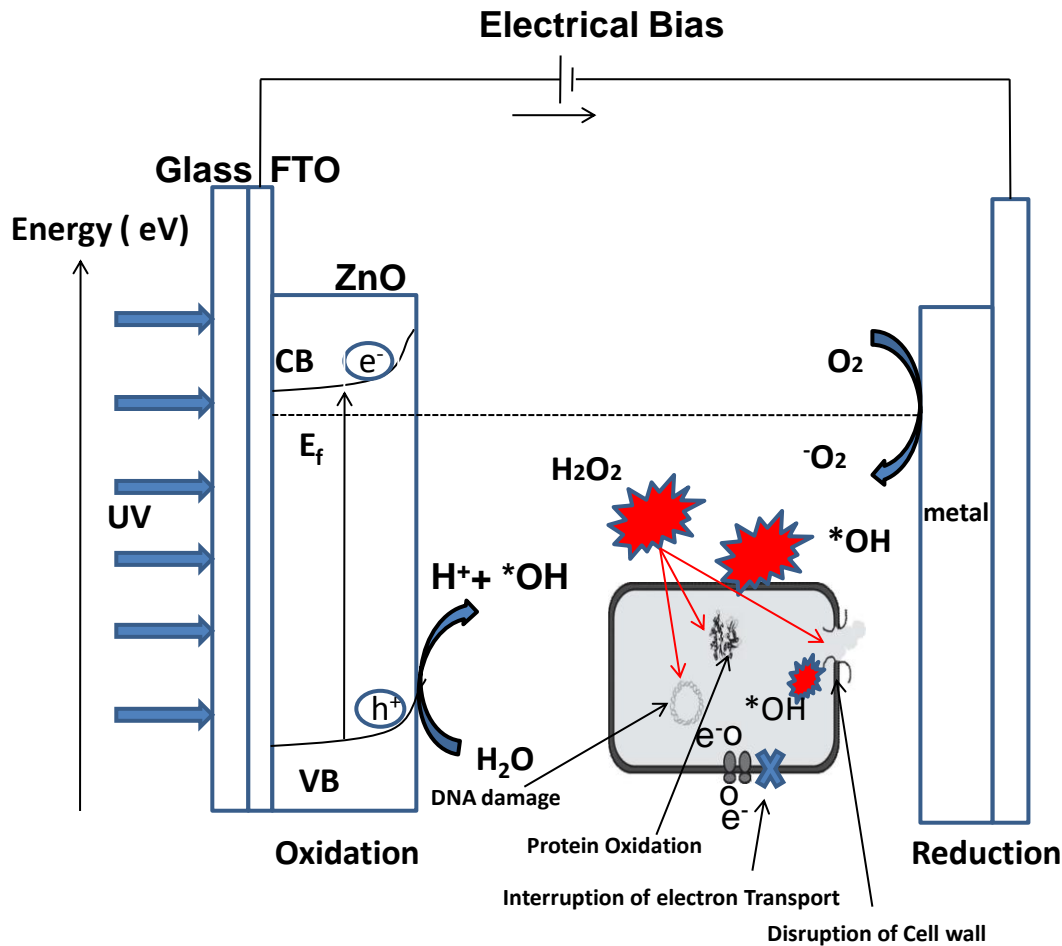
Figure 2.9 Schematics of photoelectrochemical inactivation process of bacteria
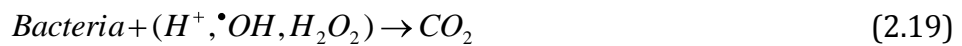
Matsunaga et al. [29] were the first to report on the "novel concept of photochemical sterilisation". They looked at the destruction of *Lactobacillus acidophilus*, *Saccharomyces cerevisiae* and *E.coli* (10^3 cells/ mL) using platinum-loaded titanium dioxide and showed that cell death occurred following incubation with TiO_2/Pt particles under metal halide lamp irradiation for 60–120 min. The several parameters affects photocatalysis process such as concentration of catalyst, UV light intensity, microbial starting concentration, temperature, pH and aeration on experimental outcome. The photocatalyst may be used in the form of an aqueous suspension or on a solid support. The schematics of photoelectrochemical inactivation of bacteria process is shown in Fig 2.9.

The hydroxyl-free radical $^\bullet$OH is highly reactive, short-lived and it can penetrate cell walls and break DNA strands. Superoxide anion $^\bullet O_2^-$ is more long-lived and cannot

penetrate the cell walls due to its negative charge whereas hydrogen peroxide (H_2O_2) can penetrate the cell walls. Superoxide anion and hydrogen peroxide are both highly reactive to biological macromolecules and also act precursors for the hydroxyl radical ($^\bullet OH$). After penetrating the cell wall, H_2O_2 gets activated by ferrous (Fe^{2+}) ion present in the cell via the Fenton reaction:

$$Fe^{2+} + H_2O_2 \rightarrow Fe^{3+} + {}^\bullet OH + OH^-$$
(2.16)

Thus, when ZnO is illuminated to produce H_2O_2, the Fenton reaction may take place in vivo and produce more hydroxyl radicals. Outside the cell wall, where both H_2O_2 and $^\bullet O^-_2$ are present, additional hydroxyl radical $\cdot OH$ is produced via and the Fenton reaction (2.16)

$$Fe^{3+} + ZnO(e^-) \rightarrow Fe^{2+} + O_2$$
(2.17)

$$Fe^{3+} + {}^\bullet O_2^- \rightarrow Fe^{2+} + O_2$$
(2.18)

$$Bacteria + (H^+, {}^\bullet OH, H_2O_2) \rightarrow CO_2$$
(2.19)

The above chemical process can be extended to any organic and bio – microorganisms, including cancer cells. The bacterial inactivation efficiency can follow first order kinetics with respect to bacterial colony count (N_t), which is shown by Eq. (2.20) [30].

$$\ln(\frac{N_t}{N_0}) = -Kt$$
(2.20)

where, N_t is the number of colony forming unit (CFU) after irradiation for t min; N_0 the number of CFU at 0 min; k the inactivation rate constant; N_t/N_0 the survival ratio. The schematic of the process of *E.coli* photokilling on semiconductor film is shown in fig. 2.10. The *E. coli* is a Gram-negative bacterium and has a membrane structure as shown in Fig. 2.11[31]. *E. coli* cells have a rod-like morphology with a length of approximately 1–3 μm and a diameter of 0.5–1 μm. The cell envelope of *E.coli* consists of an inner membrane (~ 8 nm thick), a periplasm containing the peptidoglycan (cell wall) and an outer membrane (~ 10–15 nm thick). The inner and outer membranes have a lipid bilayer structure.
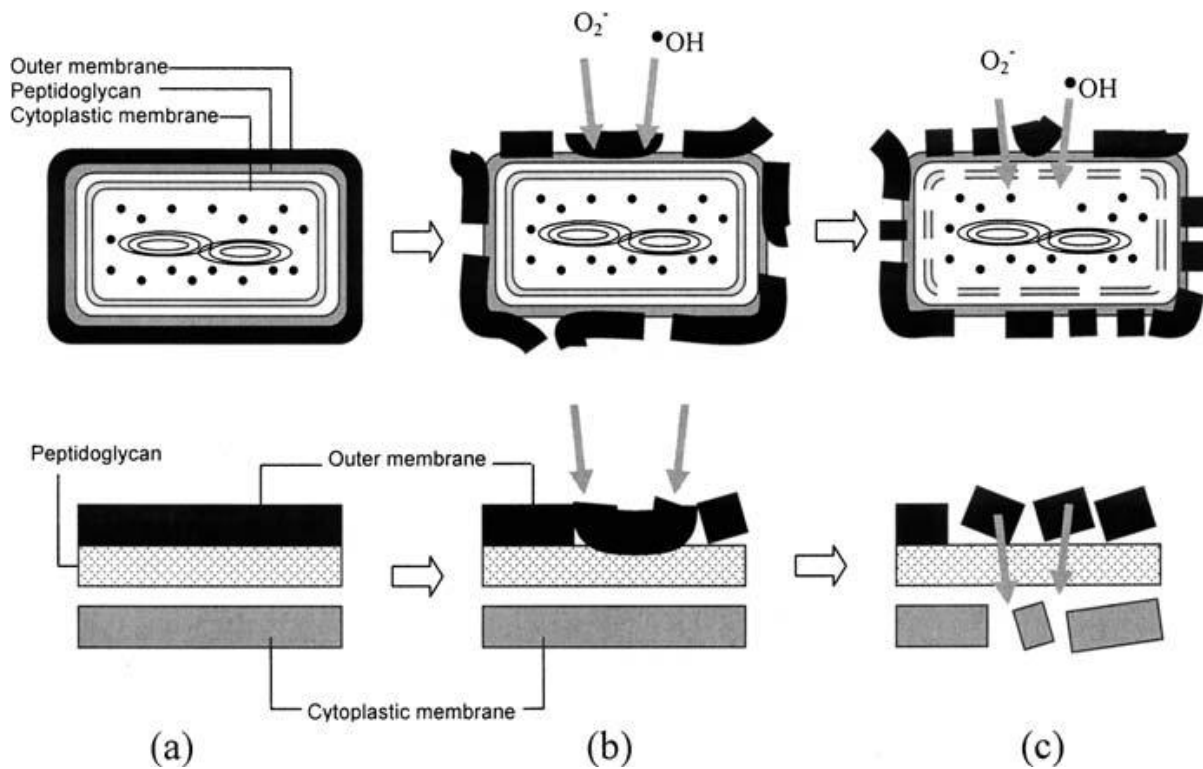
Figure 2.10 Schematic illustration (a–c) of the process of _E. coli_ photokilling on semiconductor film. In the lower row, the part of the cell envelope is magnified [18]

The outer layer of the outer membrane (OM) bilayer consists of lipopolysaccharide (LPS) and the inner layer of the OM bilayer consists of phospholipids. The OM also contains proteins such as porins that act as passive diffusion channels for hydrophilic molecules. The inner membrane consists of ~ 40% phospholipids and ~ 60% protein.
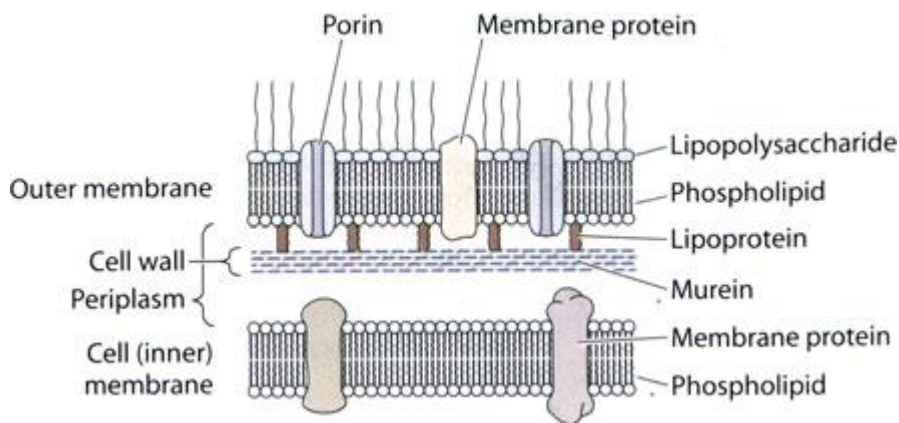
Figure 2.11 Cell envelope of gram-negative bacteria

It has become apparent that the primary target for photocatalytic attack is the cell wall. This fact goes some way towards explaining the observed differences in susceptibility of particular microbes to photocatalytic attack. The Gram positive cell wall while structurally less complex than that of the Gram negative cell wall, is surrounded a thick peptidoglycan layer and fungi, which were shown to be much less susceptible to photocatalytic attack than bacteria [32]. Once the integrity of the cell wall has been destroyed, leakage of intracellular contents takes place which ultimately results in cell death.

2.8 Parameters influencing the photocatalytic process

2.8.1 Effect of light intensity

The incident light intensity determines the rate of photoelectron and photohole generation and consequently the photoelectron/hole concentrations in an illuminated semiconductor. It influences not only the rate of photocatalytic degradation of organic matter, but also the rate of photoelectron and photohole recombination [33]. In this regard, the light intensity affects the overall quantum efficiency of photocatalytic degradation. With slurry system, at very low light intensity, photocatalytic degradation rates (or quantum efficiency) usually increase linearly with the light intensity. Nevertheless, at high light intensity, a non-linear dependence for many degradation reactions has been observed [34]. The square root dependence of the reaction rate on the light intensity is often attributed to the enhanced recombination of photoelectrons and photoholes at higher light intensities [35]. An alternative explanation attributes this to the inhibition of active surface sites and competition for photoholes by reaction intermediates [36]. The cause for this kind of rate/light intensity dependence is still unclear. Partly, it may be attributed to the way such experiments were carried out, where reduction and oxidation reaction take place on the same particles and the reduction reaction could be the control step of the overall photocatalytic process. Partly, it may be caused by the way that the photocatalytic degradation rates are expressed. In such studies, usually, the reaction rates are expressed by the disappearance rates of original substrates. Due to the uncertainty of their degradation degree and the competition for photoholes by intermediates or other photohole acceptors, only considering the part of photoholes consumed by a specific assumed reaction would be impossible to elucidate the underlining cause for this lowered quantum efficiency at

higher light intensities. Photocurrent directly reflects the photohole capture rate by various photohole acceptors including intermediates. A study of photocurrent dependence on light intensity at different potential bias would offer an insight into the reason for the lowered quantum efficiency of overall photocatalytic process at higher light intensities.

2.8.2 Effect of pH

The pH of the solution is an important parameter in the photocatalyzed degradation of organic wastes as it is known to influence the surface charge of the semiconductor thereby affecting the interfacial electron transfer and the photoredox process [37]. The effect of pH on the degradation of phenol in presence of both ZnO and TiO$_2$ reveal that, in the case of TiO$_2$, maximum degradation is observed at pH 4 and 10, with the degradation almost complete in the alkaline region. In the case of ZnO, the degradation is not varying much in the pH range of 4-7, even though in this case also, the maximum is observed in the alkaline pH range [38]. The low reactivity on ZnO, under acidic conditions can also be due to the photo-corrosion of ZnO in acidic aqueous suspensions. Significant amounts of Zn^{2+} have been detected in ZnO suspensions [39]. In this regard, the pH would greatly influence the photocatalytic oxidation kinetics of strong adsorbates.

However, at high pH, surface -OH groups on oxide semiconductors will dissociate into $-O^-$ + H$^+$. At low pH, surface -OH groups on oxide semiconductors will be protonated: -OH + H$^+$ $\rightarrow$ -OH^{2+}. At some pH in between, neither the first nor the second reaction occurs. Therefore, the surface is not charged (if no other strong electrolyte is present, whose ions may adsorb). This can be called the point of zero charge. The influence of supporting electrolyte on impurities like AO7 degradation has been noted previously and can be ascribed to pH. The point of zero charge of ZnO is reported to be 5.8 . Below this pH, ZnO is positively charged, which seems to enhance interaction with AO7 and ZnO, i.e. AO7 is adsorbed, leading to an increased probability of direct hole transfer, down to low concentrations. This directly reflects in the kinetic parameter and in the reaction decay rate.

2.8.3 Effect of initial solute concentration

Using low concentrations of pollutants is beneficial since the catalyst surface active sites may be saturated at high concentrations. According to the Langmuir-Hinshelwood reaction kinetics, for dilute solution (C$_0$ < 10^{-3} M), the reaction is of the

apparent first order, whereas the reaction is reduced to the zero order at high concentration ($C_0 > 5 \times 10^{-3}$ M) [40].

2.8.4 Effect of electrode (photocatalyst) material

The choice of electrode material is also important for its use in photodegradation of organic impurities in water. There are many ways as to how organic impurities can be removed. In most of the cases, the material is used in nanoparticulates or slurry forms. There are however, several drawbacks of these systems. Therefore, now research is moving towards using the photoelectrodes in the form of adherent thin film.

2.8.5 Effect of potential bias

There is another factor, which is responsible for facilitating the degradation reactions i.e. application of suitable potential bias to the photoelectrode. Suitable electrical bias to the photoelectrode, promotes the separation of charge carriers within the semiconductor electrode and avoids the recombination of electron-holes thereby moving the electrons towards the counter electrode. Hence, the photocatalytic action of the electrode can be boosted [41].

At a given light intensity and electrolyte composition, the photohole removal rate is constant, which is equivalent to the saturation photocurrent obtained upon illumination. At the same time, the overall photohole capture rate is also related to the removal rate of electrons, which is dependent on the applied potential bias [42]. If there is electron build-up at the surface of electrode, it will suppress the photohole capture rate and facilitate the photoelectron-hole recombination. As a result, the overall photocatalytic oxidation rate will be decreased. The applied potential bias, in effect, acts as an external force to remove the photoelectron by drawing the electron through the external circuit to the auxiliary electrode. This is, in turn, minimizes the build-up of electrons on electrode. In the low potential range, the removal rate of the available photoelectron is proportional to the electric field across the film. The degree of the electron build-up decreases with an increase in the potential bias. Therefore, the overall photocatalytic oxidation rate (photocurrent) increases with potential bias. Under these conditions, the overall process is controlled by electron migration in the semiconductor film. When the applied potential bias is sufficiently high, there is no electron build-up and the overall photocatalytic oxidation rate is solely reliant on the photohole capture rate at ZnO surface. Hence, the photohole capture rate at the electrode surface controls the overall photocatalytic oxidation process.

2.8.6 Effect of temperature

Since, photocatalysis is activated by photons; photocatalytic reactions can operate at room temperature and are relatively insensitive to temperature changes . The peer-reviewed literature reports that reaction rates are typically the highest for reactor temperatures between 20 to 80 °C, with reaction rates generally decreases for temperatures above 80 °C. Water adsorbed on the photocatalyst has been reported extensively to play a critical role in the surface-mediated photocatalytic reactions, trapping valance band holes and forming hydroxyl radicals. As reactor temperatures exceeds 80 °C and approach the boiling point of water, the loss of water on the surface may limit the photocatalytic reaction. Likewise, the surface adsorption-desorption equilibrium of target compounds and intermediates may shift towards the gas phase at elevated temperatures thereby reducing the interaction of gas molecules with photocatalytic surface. On the other hand, the change in surface coverage of the reactants and intermediates at elevated temperatures may make more surface sites available for desired reactions. Furthermore, conventional hereterogenous catalytic reactions may occur at elevated temperatures depending on the reacting species and the catalyst [43].

Thus the effect of temperature on a given photocatalytic reaction will be highly dependent on the contaminant, catalyst and other compounds present at the catalyst surface (e.g. water, intermediates or end reaction products).

2.8.7 Effect of dopant

Doping of nobel metal ions in semiconductor may lead to an enhanced efficiency of the photocatalyst [44]. The photo-physical mechanism of doped semiconductor is not fully understood. This method of improving photocatalytic activity is mainly used in aqueous media. ZnO particles can be simply substitutionally of interstially doped with different cations, can formed mixed oxides or a mixture of oxides. The dopant parameters include the concentration of dopants and the applied thermal treatment [40]. The total induced alteration of the photocatalytic activity is made up from the the sum of changes which occurs in:

i.   The light absorption capacity of the ZnO photocalyst;

ii.   Adsorption capacity of the substrate molecules at the catalysts surface;

iii.   Interfacial charge transfer rate;

iv.   Physical contact with microorganisms.

2.8.8 Effect of heterojunction (ZnO/TiO$_2$)

Photoelectrocatalytic system has received a great deal of attention due to drastically enhanced quantum efficiency. By applying external bias or by doping nobel metal ions recombination of generated electron–hole pairs is retarded. ZnO and TiO$_2$ has been widely used as photoelectrocatalyst for water and air purification because of high surface activity and absence of toxicity. However, the intrinsic semiconducting characteristics of ZnO and that of TiO$_2$ are different. The heterojunction films composed of ZnO and TiO$_2$ layers were provided to improve photoelectrocatalytic properties [45]. The heterojunction that influence the photocatalytic properties are: (a) surface recombination due to surface characteristics of each material and (b) interface recombination between TiO$_2$ and ZnO. The photocatalysis is mainly determined by the surface characteristics of the films. It is found that the surface recombination occurs more easily in ZnO. Therefore, surface recombination is fast for TiO$_2$/ZnO system, compared to ZnO/TiO$_2$ system. The photocatalytic properties for heterojunction are determined by the combination of surface and interface recombination. In addition, it is possible to increase the photocatalytic properties under applied bias. From these effects, with the ZnO film with thin TiO$_2$ layer the most organic matter and microorganisms are decomposed under applied bias.

2.9   Strategies for photocatalytic enhancement

2.9.1   Quantum efficiency and visible light absorption

Various methods and modifications are attempted to enhance the overall efficiency of the photocatalytic process. The most important modification to date is the reduction of the TiO$_2$ particle size within the nanometer range which has been shown to significantly increase its catalytic activity [46]. This is due to the higher surface-to-volume ratio, and as such, it is routine to use nanometer-sized particles. Reactor performance is enhanced by dispersing the TiO$_2$ nanoparticles in water, because of higher surface contact of the nanoparticles with the target compounds. However, the difficulty in separating unsupported particles from water for reuse is limiting commercially viable industrial reactors. Therefore, a need to employ supported catalysts is realized where a thin layer of nanometer-sized TiO$_2$ particles can be formed on a supporting surface. These can be particle or fixed supports, with the majority of research performed in the former case. TiO$_2$, for example, has been fixed onto tubes,

glass plates, fibres, membranes, or photoreactor walls [47]. However, catalytic activity approximately five to six times lower is usually seen (compared with the powdered form). This is due to reduced surface-to volume ratio (from binding with the supporting surface); catalyst agglomeration (surface clumping) during fixation; and the mass transfer limit for the organic compounds [48]. Film thickness is also of great importance: if the film is too thin, not enough light will be absorbed and if too thick, the holes are generated too deep in the catalyst layer [49]. These problems can overcome by employing a nanoporous film to ensure maximum light absorption and also by bringing the pollutant close to the film surface.

2.9.2 Sensitization of photocatalyst: composite semiconductor

In electronic applications, the exact electrical response exhibited by a metal oxide film depends strongly on composition and on microstructural characteristics, such as particle size, shape, crystallinity, and defect structure [50]. It is also well-known that intimate contacts between one nanoscale semiconducting oxide and another with different electronic properties can result in hybrid properties, including electronic rectification [51]. An additional advantage that heterostructures may have over single-component materials is the ability to shield a photochemically unstable material from the surrounding electrolyte with a corrosion-resistant outer layer allowing some narrower band gap materials to be used. There have been many reports of the improved photoelectrochemical activity that can be achieved using such coupled semiconductor systems [52-53]. In some of these studies, one semiconductor acts as a sensitizer for another, whereas in others, it is the modification of surface properties that appears to play a greater role in the enhancement of photoelectrochemical activity.

References

[1]   Y. Juan, D. Jun, Z. JinCai, M. Juan, Phys. Chem., 55 (2010)131.

[2]   Z. Meng, Z. Juan, Global Environmental Policy in Japan,12 (2008)1.

[3]   O. P. Panwar, A. Kumar, M. Paliwal, R. Ameta, C. Suresh, M. Ameta, L. Sukhadia, Bull. Catal. Soc. India, 7 (2008) 105.

[4]   Y. Abdollahi, A. H. Abdullah, Z. Zainal, N. A. Yusof, Int. J. Adv. Sci. Technol., 8(2000)135.

[5]   J. J. Vora, S. K. Chauhan, K.C.Parmar, S.B.Vasava, S. Sharma, L.S.Bhutadiya, E-J. Chem., 6(2009) 531.

[6]   S. Baruah, M. Jaisai, R. Imani, M. M. Nazhad, J. Dutta, Sci. Technol. Adv. Mater., 11 (2010) 055002.

[7]   J. A. R. Márquez, C. M. B. Rodríguez, C. M. Herrera, E. R. Rosas, O. Z. Angel, O. T. Pozos, Int. J. Electrochem. Sci., 6 (2011) 4059.

[8]   S. Baruah, S. S. Sinha, B. Ghosh, S. Kumar Pal, A. K. Raychaudhuri, J. Dutta, J. Appl.Phys., 105 (2009) 074308.

[9]   Elaziouti, N. Laouedj, B. Ahmed, Elaziouti, J. Chem. Engg. Process Technol., 2 (2011) 2 , http://dx.doi.org/4172/2157-7048.100106.

[10]   M. D. Archer, J. Appl. Electrochem., 5 (1975) 17

[11]   W. H. Brattain and C. G. B. Garret, Phys. Rev. 99 (1955) 376

[12]   H. Gerischer, J. electroanalyt. Chem., 58 (1975) 263

[13]   J.O.M. Bockris, M. A. Devanathan and K. Mullar, Proc. Roy. Soc.(Lond), 55 (1963) A274

[14]   D.F. Ollis, E. Pelizzetti, N. Serpone, Photocatalysis: Fundamentals and Applications; Wiley: New York, 1989.

[15]   S.R. Morrison, Electrochemistry at Semiconductor and Oxidized Metal Electrodes; Plenum Press: New York, 1980.

[16]   Y.V. Pleskov, Y.Y. Gurevich, Semiconductor Photoelectrochemistry; Consultants Bureau: New York, London, 1986.

[17]   P. K. J. Robertson, D.W. Bahnemann, J. M. C. Robertson, F. Wood, Hdb. Env. Chem. Vol. 2, Part M (2005): 367.

[18]   D. K. J. Dewulf, H. V. Langenhove, Critical Reviews in Environmental Science and Technology, 37 (2007) 489.

[19]   K. Koci, L. Obalova, Z. Lacny, Chemical Papers, 62 (2008)1.

[20]   S. Banerjee, J. Gopal, P. Muraleedharan, A. K. Tyagi, B. Raj, Curr. Sci., 90 (2006) 1378.

[21]   X. Domnech, J. A. Aylldn, J. Peral, ESPR - Environ Sci & Pollut. Res., 8(2001) 4.

[22]   K. Sunada, T. Watanabe, K. Hashimoto, J. Photochem. Photobiol. A: Chem., 156 (2003) 227.

[23]   M. Bekbölet, Water Sci. Techol. 35 (1997) 95.

[24]   X. Z. Li, M. Zhang, H. Chua, Water Sci. Technol., 33 (1996) 111.

[25]   N. Huang, Z. Xiao, D. Huang, C. Yuan, Supramolec. Sci., 5 (1998) 559.

[26]   G. G. Rincón, C. Pulgarin, Appl. Catal. B: Environ., 44 (2003) 263.

[27]   J. C. Ireland, P. Klostermann, E. Rice, R. Clark, Appl. Environ. Microbiol., 1(1993) 1668.

[28]   T. Matsunaga, R. Tomoda, T. Nakajima, H. Wake, FEMS. Microbiol. Lett., 29 (1985)211.

[29]   A. Pal, S.O. Pehkonen, E. L. Yu, M. B. Ray, J. Photochem. Photobiol. A: Chem., 186 (2007) 335.

[30]   M. Schaechter, J. Ingraham, F. C. Neidhardt ,(2006) Microbe. ASM Press, Washington, DC.

[31]   K. P. Kühn, I. F. Chaberny, K. Massholder, M. Stickler, V. W. Benz, H. Sonntag, L. Erdinger, Chemosphere, 53 (2003)71.

[32]   A. J. Hoffmann, G. Mills, H. Yee, M. R. Hoffmann, J. Phys. Chem., (1992) 5546.

[33]   T. Y. Wei, C. C. Wan, Ind. Eng. Chem. Res., 30 (1991) 1293.

[34]   W. J. Albery, G. T. Brown, J. R. Darwent, E. Saievar-Iranizad, J. Chem. Soc. Faraday Trans., 81 (1985) 1999.

[35]   C. Kormann, D. W. Bahnemann, M. R. Hoffmann, Environ. Sci. Technol., 25 (1991) 494.

[36]   M. C. Lu, G. D. Roam, J. N. Chen, C. P. Huang, J. Photochem. Photobiol. A: Chem., 76 (1993) 103.

[37]   K. H. Wang, Y. H. Hseih, L. J. Chen, J. Hazardous Mater., 59(1998)251.

[38]   S. P. Devipriya, S. Yesodharan, J. Environ. Biol., 31(2010) 247.

[39]   A. Mills, P. Sawunyama, J. Photochem. Photobiol. A: Chem., 84 (1994) 305.

[40]   M. N. Spallart, Electrochimia, 61 (2007) 806.

[41]   D. Jiang, H. Zhao, Z. Jia, J. Cao, R. John, J. Photochem. Photobiol. A: Chem., 144 (2001) 197.

[42]   M. Herrmann, Catalysis Today, 53 (1999) 115.

[43]   C. Wongchoosuk, S. Choopun, A. Tuantranont, T. Kerdcharoen, Materials Research Innovations, 13(2009) 185-188.

[44]   T. Santhaveesuka, D. Wongratanaphisana, S. Choopuna, Sensors and Actuators :B, 147 (2010) 502–507.

[45]   D. W. Kima, S. Leea, H. S. Jungb, J. Y. Kima, H. Shinc, K. S. Honga, Int. J. Hydro. Energy, 32 (2007) 3137.

[46]   M. S. Vohra, K. Tanaka, Environ. Sci. Technol. 2000.

[47]   A. E. Regazzoni, P. Mandelbaum, M. Matsuyoshi, S. Schiller, S.A. Bilmes, M.A. Blesa, Langmuir, 14 (1998) 868.

[48]   S. J. Hug, B. Sulzberger, Langmuir, 10 (1994) 3587.

[49]   S. Tunesi, M.A. Anderson, Langmuir, 8 (1992) 487.

[50]   T. He, Y. Ma, Y. Cao, X. Hu, H. Liu, G. Zhang, W. Yang, J. Yao, J. Phys. Chem. B ,106 (2002) 12670.

[51]   J. W. Haus, H. S. H. I. Zhou, H. Komiyama, Phys. Rev. B: Condens. Matter Mater. Phys., 47 (1993) 1359.

[52]   W. Siripala, A. Ivanovskaya, T. F. Jaramillo, S. H. Baeck, E. W. McFarland, Sol. Energy Mater. Sol. Cells, 77 (2003) 229.

[53]   L. Sheeney-Haj-Ichia, S. Pogorelova, Y. Gofer, I. Willner, Adv. Funct. Mater, 14 (2004) 416.

3.1 Introduction

Thin film technology has revolutionized in the field of optics, electronics and magnetism, considering the new and improved optics, electronics, magnetic devices and photovoltaics etc. The advantage of thin film devices are low material consumption and possible use of flexible substrates [1]. Recently considerable attention has been given for the preparation of metal oxide thin films for photovoltaic and photocatalytic applications by various techniques. Various metal oxide semiconductors such as Fe_2O_3, TiO_2, ZnO, etc. have been prepared by the spray pyrolysis technique [2-7].

This chapter deals with the basics of spray pyrolysis technique, its working, formation of thin films and factors responsible for the growth of thin films. Under thin film deposition section, procedures right from the substrate cleaning, preparation of solution and formation of different thin films such as zinc oxide (ZnO), silver doped zinc oxide (Ag:ZnO), Gold doped zinc oxide (Au:ZnO) and stratified layer of ZnO and TiO_2 is illustrated. Moreover, the design and working of a specially fabricated prototype device, known as a photoelectrochemical detoxification reactor (single cell) is discussed. This device is meant for purification of organic and microbial impurities present in water using prepared thin films.

3.2. Overview of thin film deposition techniques

Variety of techniques has been used to deposit thin films. The choice of a particular method/technique depends on factors like; 1) Material to be deposited, 2) Nature of the substrate on which the film is to be deposited, 3) Thickness of the film required, 4) Structure of the film expected and 5) Application of the thin film. The deposition method strongly affects the structural and hence physical properties; the proper choice of the method is of prime importance.

The thin film deposition can be broadly classified as physical and chemical methods. Physical methods consists vacuum evaporation and sputtering; the material to be deposited has been transferred to a gaseous state either by evaporation or an impact process and then deposited on the substrate. Under chemical methods, we have the gas phase chemical processes such as conventional chemical vapor deposition (CVD), Laser CVD, Photo CVD, Metal organo chemical vapor deposition (MOCVD) and plasma enhanced CVD. The liquid phase chemical techniques include spray pyrolysis, electrodeposition, chemical bath deposition, successive ionic layer adsorption and reaction (SILAR), anodization and liquid phase epitaxy etc.
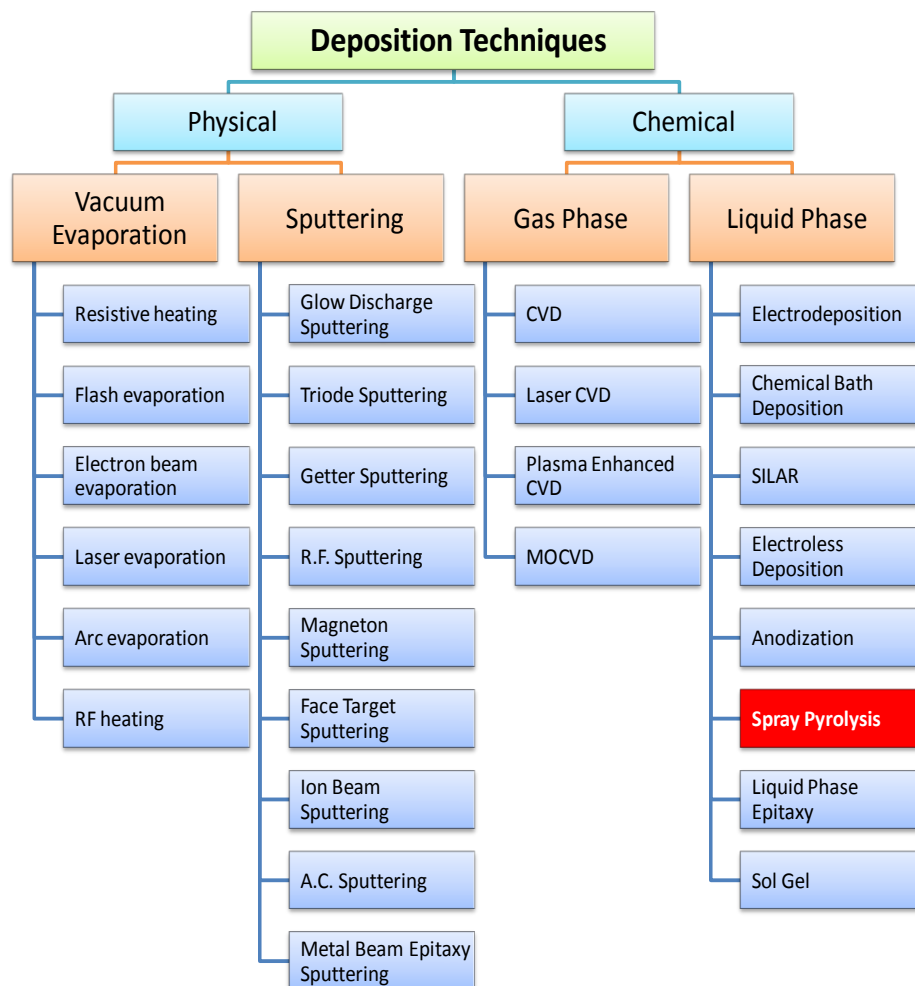
Figure 3.1 Broad classification of thin film deposition techniques

The broad classification of thin film deposition techniques is outlined in the fig. 3.1. The physical methods are plugged with certain drawbacks and difficulties. A careful and precise control of the boat temperature is an essential requirement for obtaining good stoichiometric films and to obtain the particular composition in alloy films. Chemical methods are relatively economical and easier ones as compared to physical methods. However, the chemical methods listed in fig. 3.1 have some drawbacks and advantages over the other methods. On the other hand, there is no ideal method to prepare the compounds and alloys in thin film form, which will satisfy all the requirements. Of all, spray pyrolysis is a simple and low-cost technique for the preparation of semiconductor films.

Details about various aspects of spray pyrolysis are given in review articles by many authors [8-9]. The process is particularly useful for the deposition of oxides such as ZnO, TiO_2, WO_3, etc. [10-12].

Spray pyrolysis technique involves spraying of a solution containing soluble salts of the desired compound on to preheated substrates, where the constituents react to form a chemical compound. The chemical reactants used for making solution are selected such that the products other than the desired compound are volatile at the temperature of deposition.

3.2.1 Spray pyrolysis technique (SPT)

3.2.1.1 Basics and working of spray pyrolysis technique

Among various chemical methods mentioned in the fig. 3.1, solution spraying technique is the most popular today because of its applicability to produce variety of conducting and semiconducting materials [13-14]. The basic principle involved in spray pyrolysis technique is pyrolytic decomposition of salts of a desired compound to be deposited.

Every sprayed droplet reaching on the surface of the hot substrate undergoes pyrolytic (endothermic) decomposition and forms a single crystalline or cluster of crystallites as a product. The other volatile by-products and solvents escape in the vapor phase. The substrates provide thermal energy for the thermal decomposition and subsequent recombination of the constituent species, followed by sintering and crystallization of the clusters of crystallites and thereby resulting in coherent film. The required thermal energy is different for the different materials and for the different solvents used in the spray process. The atomization of the spray solution into a spray of fine droplets also depends on the geometry of the spraying nozzle and pressure of a carrier gas.

Apart from its simplicity, spray pyrolysis technique has a number of advantages. Spray pyrolysis is a simple and low-cost technique for the preparation of semiconductor thin films. It has capability to produce large area, high quality adherent films of uniform thickness. Spray pyrolysis does not require high quality targets and /or substrates nor does it require vacuum at any stage, which is a great advantage if the technique is to be scaled up for industrial applications. The deposition rate and the thickness of the films can be easily controlled over a wide range by changing the spray parameters. A major advantage of this method is operating at moderate temperature (100–500 ^{0}C), and can produce films on less robust materials. It offers an extremely easy way to dope films with virtually any elements in any proportion, by merely, adding it in some form to the spray solution. By changing composition of the spray solution

during the spray process, it can be used to make layered films and films having composition gradients throughout the thickness.

Spray pyrolysis technique has been used to prepare thin film on a variety of substrates like glass, ceramic or metallic. Many studies have been conducted over about three decades on SPT and the mechanism of thin film formation and influence of variables on the film formation process has been comprehensively reviewed in the literature [15]. Due to the simplicity of the apparatus and the good productivity of this technique on a large scale, it offered a most attractive way for the formation of thin films of metal oxides [16-21], binary and ternary chalcogenides [22-26]. Chemical SPT has also been successfully employed for the formation of superconducting oxide films [27-28], etc. The chemical versatility of spray pyrolysis is multi component, non-oxide and composite powders synthesized as porous or nanoparticles. Therefore, spray pyrolysis process offers many opportunities to synthesize above components.

3.2.1.2 Essentials of spray pyrolysis technique

Fig. 3.2 shows the schematic diagram of the spray pyrolysis technique. It mainly consists of spray nozzle, rotor for spray nozzle, liquid level monitor, hot plate, gas regulator value and airtight fiber chamber.

a) Spray nozzle

It is made up of glass and consists of the solution tube surrounded by the glass bulb. With the application of pressure to the carrier gas, the vacuum is created at the tip of the nozzle, and the solution is automatically sucked in the solution tube and the spray starts.

b) Rotor for spray nozzle

Stepper motor-based microprocessor controller is used to control the linear simple harmonic motion of the spray nozzle over the required length of the hot plate. Hence, the to and fro motion and the speed of the spray nozzle is monitored in a controlled manner.

c) Liquid level monitor

The spray rate at a fixed air pressure depends upon the height of the solution measured with respect to the tip of the nozzle. The arrangement for the change in height of the solution forms the liquid level monitor.

d) Hot plate

The stainless steel (S. S. 304) disc (with diameter 16 cm and thickness 1.5 cm) to which 2000 W heating coil is fixed served as a hot plate. Maximum temperature of 600 ± 5 ^{0}C can be achieved with this arrangement. The chromel-alumel thermocouple is used to measure the temperature of the substrates and is fixed at the center of the front side of the S.S. plate. The temperature of the hot plate is monitored with the help of temperature controller (Aplab make Model No. 9601).
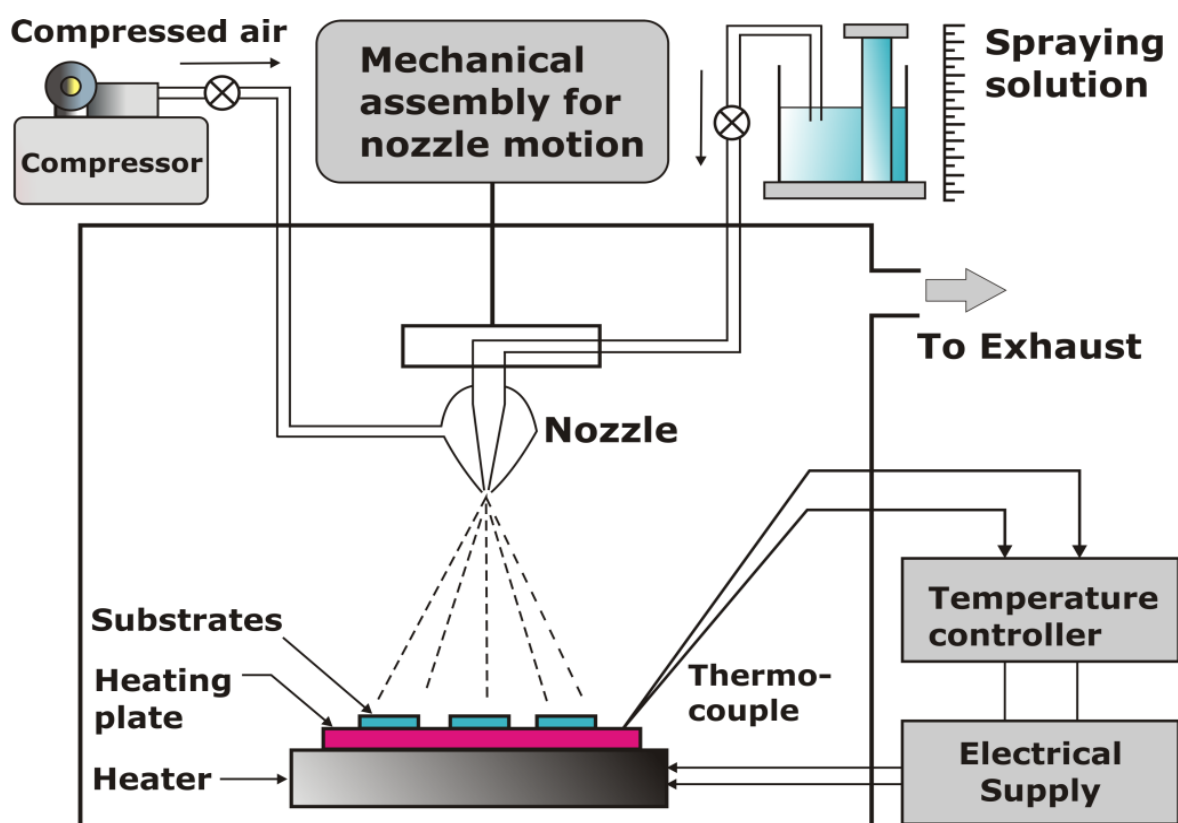
Figure 3.2 Schematic diagram of the spray pyrolysis method

e) Gas regulator valve

The gas regulator valve is used to control the pressure of the carrier gas flowing through the gas tube of the spray nozzle. A glass tube of length 25 cm and of diameter 1.5 cm is converted into gas flow meter. Since air pressure depends upon the size of the air flow meter, the air flow meter should be calibrated from nozzle to nozzle.

f) Air tight fiber chamber

Since the number of toxic gases are evolved during the thermal decomposition of sprayed solution, it is necessary to fix the spraying system inside with airtight fiber chamber. An airtight fiber chamber of the size (60 cm x 60 cm x 60 cm) was fabricated.

The fiber avoids the corrosion of the chamber. The outlet of chamber is fitted to exhaust fan to remove the gases evolved during thermal decomposition.

3.2.1.3 Mechanism of thin film formation

In spray pyrolysis, the process parameters like precursor solution, atomization of precursor solution, aerosol transport and decomposition of precursor are very important while studying the structural, optical, morphology and crystallinity of the thin films. These four process parameters are discussed in the following section.

a) Precursor solution

Precursor solution plays a vital role in the formation of thin films of various compounds. The true solutions, colloidal dispersions, emulsions, and sols can be used as aerosol precursors. Aqueous solutions are usually used due to ease of handling safety, low-cost, and availability of a wide range of water-soluble metal salts. The solute must have high solubility, which increases the yield of the process. Increasingly, alcoholic and organic solutions have been studied due to the interest in the synthesis of organic materials.

In general, metal chlorides and oxy-chlorides have the highest water solubility relative to other metal salts and are used for industrial production. The corrosive nature of the product gases at the adverse effect of residual chlorine on ceramic sintering decreases the general attractiveness of these salts for advanced ceramic solution synthesis, but the technology for handling such systems is available. Other water-soluble metal salts such as nitrates, acetates and sulfates can also introduce impurities, which may adversely affect subsequent processing, sintering or properties. The low solubility of metal acetates and high decomposition temperature of metal sulfates, limit the use of these water-soluble salts. Therefore, hybrid systems in which one of the components is added via a solution and remainder as particles have also been reported. Physical and chemical characteristics of the soluble chemical precursors strongly influence the characteristics of particles formed by spray pyrolysis.

b) Atomization of precursor solution

The critical operation of the spray pyrolysis technique is to produce uniform and fine droplets. A variety of atomization techniques have been used for solution aerosol formation, including pneumatic, ultrasonic, and electrostatics. Some of spray atomization techniques include (a) improved spray pyrohydrolysis [29], (b)

microprocessor based spray pyrolysis [30], (c) electrostatic spray pyrolysis [31], (d) corona spray pyrolysis [32], (e) ultrasonic nebulized atomization technique [33] etc. These atomizers differ in droplet size, rate of atomization and droplet velocity. The velocity of the droplet when it leaves the atomizer is very important as it determines the heating rate and the residence time of the droplet during spray pyrolysis. The size of the droplets produced with pneumatic or pressure nozzles decreases when the pressure difference across the nuclei is increased. For a specific atomizer the droplet characteristics depend on the solution density, viscosity and surface tension.

The quality of film also depends on the compressed air used to guide the solution from the nozzle. When the air pressure is more, smaller droplets are likely to form. However, this causes the substrate temperature to drop due to rapid splashing of smaller droplets. On the other hand, if the air pressure is too small, the larger droplets fall onto the substrates. Hence, it is essential to optimize the air pressure.

c) Aerosol transport

In spray pyrolysis, precursor solution is atomized through a nozzle. The nozzle converts the solution into small droplets known as aerosols. These aerosols are allowed to incident on to the preheated substrates. The pyrolytic decomposition of the aerosols depends on the substrate temperature. The formation of thin films with desired properties is possible only at optimum substrate temperature.

In an aerosol, the droplet is transported and eventually evaporates. In case dense films are desired, it is important that during transportation as many droplets as possible fly to the substrate without forming particles before reaching the surface. Krunks et al. investigated the mechanism of ZnO film growth [34]. The influence of forces, which determine both the trajectory of the droplets and evaporation, were examined and a film growth model was proposed. Gravitational, electric, thermophoretic and Stokes forces were taken into account. The thermophoretic force pushes the droplets away from a hot surface, because the gas molecules from the hotter side of the droplet rebound with higher kinetic energy than those from the cooler side. Thermophoretic forces keep most droplets away from the surface in non-electrostatic spray process. It was concluded that the film grows from the vapour of droplets passing very close to the hot substrate in a manner of chemical vapour deposition (fig. 3.3). Droplets that strike the substrate form a powdery deposit. The authors suggest that

forcing droplets closer to the substrate while avoiding actual contact would improve the efficiency of film growth.
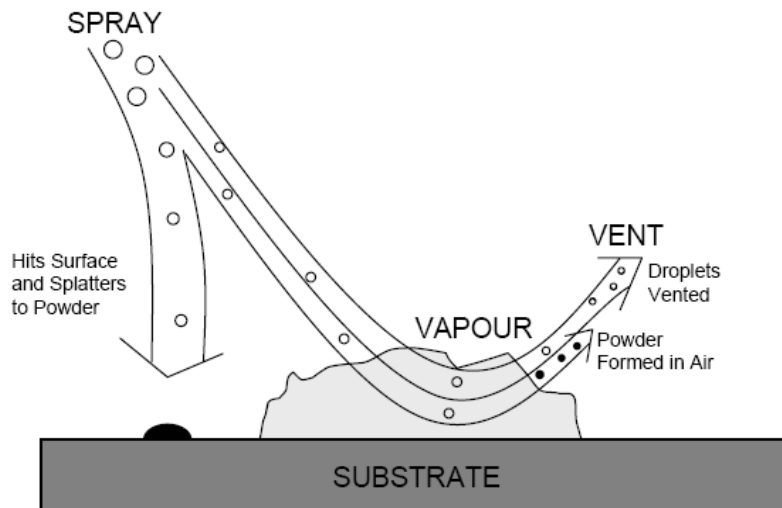
Figure 3.3 Schematic of aerosol transport

The aerosol droplets experience evaporation of the solvent during the transport to the substrate. This leads to a size reduction of the droplet and to the development of a concentration gradient within the droplet. The precursor precipitates on the surface of the droplet, when the surface concentration exceeds the solubility limit. Precipitation occurs due to rapid solvent evaporation and slow solute diffusion. This results in the formation of a porous crust and subsequently hollow particles, which are not desired in film formation because they increase the film roughness.

d) Decomposition of precursor

Many processes occur simultaneously when a droplet hits the surface of the substrate: evaporation of residual solvent, spreading of the droplet, and salt decomposition. Many models exist for the decomposition of a precursor.

Viguie and Spitz [35] classified chemical spray deposition processes according to the type of reaction. In all processes, the significant variables are the ambient temperature, carrier gas flow rate, nozzle-to-substrate distance, droplet radius, solution concentration and solution flow rate. To this list, one should add the chemical composition of the carrier gas and/or environment and most importantly, substrate temperature.

Various steps during pyrolysis of aerosols are as explained below.

A) In the first step, an aqueous precursor solution is converted into aerosols (droplets) by spray nozzle and the solvent evaporation takes place.

B) In this step, vaporization of the solvent leads to the formation of precipitate as the droplets approaches the substrate.

C) Pyrolysis of the precipitate occurs in succession before the precipitate reaches the substrate.

D) When the precipitate reaches the substrate, nucleation and the growth of metal oxide thin films on the substrate take place.

E) Finally, the growth of the nuclei leads to the formation of continuous thin layer of metal oxide.
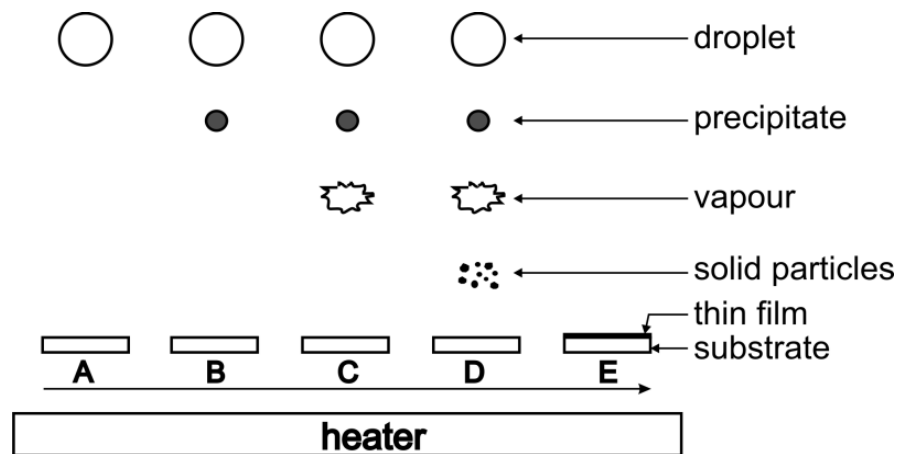
Figure 3.4 Mechanism of thin film formation by spray pyrolysis method

3.2.1.4 Factors governing the SPT

Formation of thin film using SPT depends upon a various parameters. The number of factors governing the film formation mechanism depends on,

1) The automation of the spray solution into a spray of fine droplets which depends on the geometry of the spraying nozzle and pressure of a carrier gas.

2) The properties of thin films depend upon the anion to cation ratio, spray rate, substrate temperature, ambient atmosphere, carrier gas, droplet size and also on the cooling rate after deposition.

3) The film thickness depends on the distance between the nozzle and substrate, solution concentration and quantity and substrate temperature.

4) The film formation depends upon the process of droplet landing, reaction and solvent evaporation, which are related to droplet size and its momentum.

An ideal deposition condition is that when a droplet approaches the substrate just as the solvent is completely removed. Wilhelm [36] showed that depending on droplet velocity and flow direction, a droplet would be either flattens, skip along the surface.

3.3. Thin film deposition

3.3.1. Preparation of F: SnO$_2$ thin films
3.3.1.1 Substrate cleaning

Substrate cleaning is the process of breaking the bonds between substrates and contaminants without damaging the substrates. In thin film deposition process, substrate cleaning is an important factor to get reproducible films as it affects the smoothness, uniformity, adherence and porosity of the films. The substrate cleaning process depends upon the nature of the substrate; degree of cleanliness required and nature of contaminates to be removed. The common contaminates are grease, adsorbed water, air borne dust, lint, oil particles etc. The corning glasses of dimensions 0.125 cm x 7.5 cm x 2.2 cm and 0.125 cm x 10 cm x 10 cm have been used as substrates. The following process has been adopted for cleaning the substrates.

1. The substrates were washed with detergent solution 'Labolene' and then with water.
2. These substrates were boiled in 0.1 M chromic acid for about five minutes.
3. Substrates were cleaned with distilled water.
4. These substrates were kept in NaOH solution to remove the acidic contaminations.
5. The substrates were again washed with distilled water and cleaned ultrasonically.
6. Finally, the substrates were dried in alcohol (methanol) vapors.

3.3.1.2 Preparation of solutions

First, fluorine doped tin oxide (FTO) conducting coatings were prepared onto the corning glass substrates. Initial ingredients used to deposit FTO thin films are as follows:

1. Pentahydrated stannic chloride (SnCl$_4$·5H$_2$O) (purity 99 %), supplied by sd fine chem. Mumbai.
2. Ammonium fluoride (NH$_4$F) (99%), supplied by sd fine chem. Mumbai.
3. Oxalic acid ((COOH)$_2$ × 2H$_2$O)(99 %) supplied by sd fine chem. Mumbai.
4. Propane-2-ol (Iso-propyl alcohol) (CH$_3$CHOHCH$_3$)(99 %) supplied sd fine chem. Mumbai.

A total of 50 ml of 2M stannic chloride (35.7 gm) solution was prepared in doubled distilled water and 7.14 gm of ammonium fluoride was dissolved in it. A few drops of oxalic acid were added to it to clear off some of the precipitated traces. From the above mixture, 10 ml solution was taken and 10 ml of propane-2-ol was added to it to have a total of 20 ml spraying solution.

3.3.1.3 Formation of F: SnO$_2$ thin films

The final solution was sprayed onto the corning glass substrates of size 0.125 cm × 2.5 cm × 7 cm through the specially designed glass nozzle. The compressed (2.5 kg cm^{-2}) air was used as carrier gas at a constant spray rate of 4.5 ml min^{-1}. The substrate temperature was maintained at 475 ^{0}C. The conducting films thus prepared have sheet resistance of the order of 5-15 $\Omega\,\square^{-1}$ and with transparency of 90-95 %. After optimizing all these deposition conditions, FTO films were coated on large area corning glass substrates of size 0.125 cm × 10 cm × 10 cm. These large areas FTO substrates were uniform with resistance of 5-15 $\Omega\,\square^{-1}$ at the centre and around 20-30 $\Omega\,\square^{-1}$ as we go towards its edges.

3.3.2 Preparation of ZnO thin films

3.3.2.1 Substrate cleaning

The corning glasses and conducting FTO were used as substrates for ZnO thin film deposition by spray pyrolysis technique. The similar substrate cleaning procedure (as discussed in section 3.3.1.1) was employed for cleaning corning glass substrates. Prior to using FTO as substrates for ZnO deposition, they were first etched in HCl and finally cleaned with acetone.

3.3.1.2 Preparation of solutions

Using corning glass and conducting FTO, ZnO thin films were deposited by spray pyrolysis technique. Initial ingredients used to deposit ZnO thin films are as follows:

1. Zinc Acetate (Zn(CH$_3$COO)$_2$ $\cdot$ 2H$_2$O, Molecular weight = 219.18 g mol^{-1}) (AR grade, 99 % pure) supplied by Thomas Baker Chem. Mumbai.
2. Methanol (CH$_3$OH) (99 %), supplied by Thomas Baker Chem. Mumbai
3. Acetic Acid (99 %), supplied by Thomas Baker Chem. Mumbai

The required quantity of solution of zinc acetate was prepared in double distilled water + methanol + acetic acid with volumetric ratio (25: 65: 10) respectively [37].

3.3.2.3 Formation of ZnO

The prepared precursor solution was sprayed onto the preheated corning glass and FTO coated glass substrates of size 0.125 cm × 2.5 × 7.5 cm through specially designed glass nozzle for different preparative parameters such as substrate temperature, solution concentration, quantity of solution etc. The substrate temperature was varied from 300, 350, 400 and 450 ^{0}C. The concentration of solution was varied from 0.1 to 0.4 M. The quantity of the spraying solution was varied as 50, 100, 150 and 200 ml in order to obtain films of different thickness. The compressed air (2.5 kg cm^{-2}) was used as carrier gas at a constant spray rate of 5 ml min^{-1}. For varying substrate temperature, other preparative parameters such as solution concentration (0.1M), quantity of solution (100 ml), and nozzle to substrate distance (30 cm) were kept constant for all experiments. While varying concentration, quantity of solution was kept fixed as before and kipping substrate temperature fixed at its optimized value (400 ^{0}C). Similar procedure was adopted while varying quantity of spraying solution, kipping substrate temperature (400 ^{0}C) and concentration (0.2 M) to its optimized value.

The resulting precursor solution was sprayed onto large area (100 cm^2) the FTO coated corning glass by masking ∼ 2 cm^2 area at the four corners (fig. 3.5). These four masked corners were used for making electrical contacts and application of bias. These developed large area ZnO electrodes were used in PEC detoxification reactor.

3.3.3 Preparation of Ag:ZnO thin films

3.3.3.1 Substrate cleaning

Procedure, discussed in section 3.3.2.1 was used for substrate cleaning

3.3.3.2 Preparation of solutions

Ag:ZnO thin films were deposited onto corning glass and FTO by spray pyrolysis technique. Initial ingredients used to deposit Ag:ZnO thin films are as follows:

1. Zinc Acetate (Zn(CH$_3$COO)$_2$ .2H2O, Molecular weight = 219.18 g mol^{-1}) (AR grade, 99.9% pure), supplied by Thomas Baker Chem. Mumbai

2. Methanol (CH$_3$OH) (99.9%), supplied by Thomas Baker Chem. Mumbai

3. Acetic Acid (99 %), supplied by Thomas Baker Chem. Mumbai

4. Silver Nitrate (AgNO$_3$),(99 %), supplied by Thomas Baker Chem. Mumbai
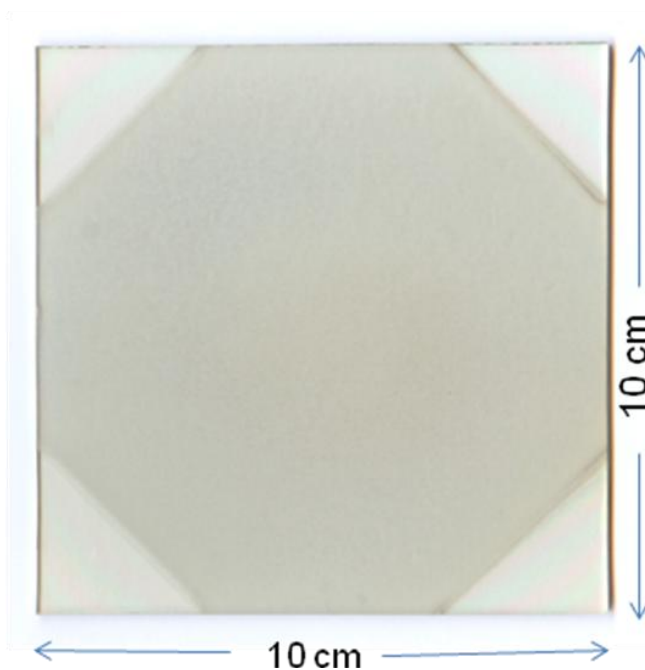
Figure 3.5. ZnO thin film on FTO coated glass

Pure and Ag:ZnO thin films have been deposited onto the ultrasonically cleaned glass substrates using zinc acetate as a precursor solution with the SPT. For growth of pure ZnO thin films, zinc acetate solution was used, while for growth of Ag:ZnO thin film, silver nitrate and zinc acetate precursors were used. An appropriate quantity of silver nitrate (0.2 M) solution was mixed into the zinc acetate solution to accomplish different doping concentrations (i.e. 1, 2, 3 and 4 At %) and subsequently the initial and deposited samples are denoted by ZnO_{pure}, $ZnOAg_1$, $ZnOAg_2$, $ZnOAg_3$, $ZnOAg_4$ respectively. The resulting solution was then pulverized pneumatically by means of a specially designed glass nozzle on to the preheated substrates. The sprayed droplets undergo evaporation, solute condensation and thermal decomposition, thereby resulting in the formation of ZnO thin films. During the synthesis, various preparative parameters like solution quantity (100 ml), solution spray rate (5 ml/min), nozzle to substrate distance (30 cm), carrier gas flow rate (2.5 kg cm^{-1}) etc. were kept at their optimized values. The deposition temperature was kept constant at 400 ^0C for the deposition of all samples.

3.3.3.3 Formation of Ag:ZnO

The precursor solution was sprayed onto the preheated corning glass and FTO coated glass substrates of size 0.125 cm × 2.5 cm × 7.5 cm held at optimized substrate temperature of 400 ^0C.

The resulting precursor solution with Ag doping concentration was sprayed onto the large area (100 cm^2) FTO coated corning glass by masking ~2 cm^2 area at the four corners. These four masked corners were used for making electrical contacts and application of bias. These developed large area ZnO electrodes were used in PEC detoxification reactor.

3.3.4 Preparation of Au:ZnO thin films

3.3.4.1 Substrate cleaning

Procedure, discussed in section 3.3.2.1 was used for substrate cleaning

3.3.4.2 Preparation of solutions

Au:ZnO thin films were deposited onto corning glass and FTO by spray pyrolysis technique. Initial ingredients used to deposit Au:ZnO thin films are as follows:

1. Zinc acetate (Zn(CH$_3$COO)$_2\cdot$2H$_2$O, Molecular weight = 219.18 g mol^{-1}) (ARgrade, 99 % pure), supplied by Thomas Baker Chem. Mumbai
2. Methanol (CH$_3$OH), (99 %), supplied by Thomas Baker Chem. Mumbai
3. Acetic Acid (99 %), supplied by Thomas Baker Chem. Mumbai
4. Auric Chloride (HAuCl$_4$), (99 %), supplied by Thomas Baker Chem. Mumbai

The precursor solution used for spray pyrolysis deposition was prepared by dissolving pure zinc acetate powder in methanol, distilled water and acetic acid. An appropriate quantity of Auric chloride (0.2 M) solution was mixed into the zinc acetate solution to accomplish different doping concentrations (i.e. 1, 2, 3, and 4 At %). A total 100 ml solution was used as a final solution for deposition of Au:ZnO thin films

3.3.4.3 Formation of Au:ZnO

The corning and FTO-coated glass were used as substrate for the spray pyrolytic deposition of Au:ZnO films. The optimized preparative parameters such as substrate temperature of 400 °C, the solution concentration 0.2 M and the quantity of spraying solution 100 ml were kept constant through the experiment. The compressed air (2.5 kg cm^{-2}) was used as carrier gas at a constant spray rate of 5 ml min^{-1}. The size of the FTO and corning glass substrates was 0.125 cm x 2.5 cm x 7 cm. Similar way, with optimized preparative parameters (substrate temperature of 400 ^{0}C, solution concentration 0.2M, quantity of solution 100 ml, Au doping concentration 3 at %) Au:ZnO thin films were coated onto the FTO coated corning glass of sixe 0.125 × 10 × 10 cm^3 by masking ~2 cm^2 area at the four corners. These four masked corners were used for making electrical

contacts and application of bias. These developed large area Au:ZnO electrodes were used in PEC detoxification reactor.

3.3.5 Preparation of ZnO/TiO$_2$ thin films

3.3.5.1 Substrate cleaning

Procedure, discussed in section 3.3.2.1 was used for substrate cleaning

3.3.5.2 Preparation of solutions

Using corning glass and conducting FTO, ZnO/TiO$_2$ thin films were deposited by spray pyrolysis technique. Initial ingredients used to deposit ZnO/TiO$_2$ thin films are as follows:

1. Zinc Acetate (Zn (CH$_3$COO)$_2 \cdot$ 2H$_2$O, Molecular weight = 219.18 g mol^{-1}) (AR grade, 99 % pure), supplied by Thomas Baker Chem. Bombay.
2. Methanol (CH$_3$OH) (99 %), supplied by Thomas Baker Chem. Bombay.
3. Acetic Acid (99 %), supplied by Thomas Baker Chem. Bombay.
4. Titanyl acetylacetonate powder (TiAcAc), (C$_{10}$H$_{14}$O$_5$Ti, molecular weight= 262.10 g mol-1), (AR grade, 99.9% pure, Merck made, Germany).

A required quantity of solution of zinc acetate was prepared as discussed in section 3.3.1.2 and that of TiO$_2$ solution in methanol by dissolving the required quantity of TiAcAc powder (yellowish in colour) in it. No additional additives or complexing agent is required to dissolves TiAcAc powder completely to form yellowish coloured solution.

3.3.5.3 Formation of ZnO/TiO$_2$

This corning glass and FTO were used as substrate for the spray pyrolytic deposition of TiO$_2$ films. The precursor solution consisted of titanyl acetylacetonate in methanol. The substrate temperature was 450 ^{0}C. The concentration of solution was 0.025 M. The quantity of the spraying solution was varied as 10, 20, 30, 40, 50, 60, 70, 80, 90 and 100 ml in order to obtain different thickness of TiO$_2$ layer on ZnO. The compressed air (2.5 kg cm^{-2}) was used as carrier gas at a constant spray rate of 5 ml min^{-1}. The size of the FTO substrates was 0.125 cm × 2.5 cm × 7 cm. ZnO/TiO$_2$ films were also coated on large area corning glass substrates of size 0.125 cm × 10 cm × 10 cm, leaving behind the four corners of the FTO undeposited. This was done keeping in mind the provision for bias by making the electrical contacts.

The ZnO/TiO$_2$ thin films were deposited onto FTO coated glass having size 0.125 cm × 10 cm × 10 cm, using the individual optimized deposition conditions for ZnO thin

films and that for TiO$_2$ thin films [2-7]. The first a thin layer (100 ml) of ZnO (at its optimized deposition conditions) was given on FTO coated glass, which was followed by a TiO$_2$ layer at its optimized deposition conditions (conc. = 0.025 M, Temp. = 450 ^{0}C and quantity = 90 ml). ZnO/TiO$_2$ thin films were deposited on large area corning glass substrates of size 0.125 cm × 10 cm × 10 cm, leaving behind the four corners of the F:SnO$_2$ undeposited for making the electrical contacts. These developed large area ZnO/TiO$_2$ electrodes were used in PEC detoxification reactor.

3.4 Photoelectrochemical (PEC) detoxification reactor
3.4.1 Working of PEC reactor

A way of increasing electron-hole separation and consequently enhancing quantum yield is the application of electrical bias, which is possible when the photocatalyst is deposited on an electrically conducting substrate [38-40].

The construction of photoelectrochemical cell reactor has described elsewhere [41]. An electrode (ZnO, Ag:ZnO, Au:ZnO and ZnO/TiO$_2$) coated on a FTO coated glass substrate was used as photoanode and a stainless steel plate at a distance of 0.1 cm, facing the photoanode, acted as cathode. The surface area of these electrodes in contact with the electrolyte was 64 cm^2 (identical to the illuminated area). The electrical bias between the electrodes was provided by a 1.5 V alkaline battery. Backside irradiation (through the transparent conducting substrate) was used, employing the UVA broadband lamp (18 W, 2mW/cm^2, center λ ∼ 365 nm), placed behind (∼ 1 cm) the photoelectrode. A fixed amount of electrolyte, the major part of it being contained in an external reservoir, was recirculated through the cell, with a constant flow rate of 12.2 lit/h (corresponding to a mean flow velocity of 4.24 cm /s across the photoelectrode) using a Gilson MINIPLUS peristaltic pump and silicon tubing. The ohmic electrical contacts to the photoelectrode are drawn as shown in fig. 3.6. All electrode potentials are quoted with respect to the steel counter electrode (steel disc).

Backside irradiation (through the transparent conducting substrate) was used, employing the UVA broadband lamp, placed parallel to the backside of photoelectrode at a distance of 2 to 5 cm as shown in fig. 3.7.

Fig. 3.6 shows respectively back side of reactor showing inlet, outlet & the four contacts for electrical bias and the front side of single cell photoelectrochemical reactor fitted to a Z-shaped stand under UVA illumination (fig.3.7).
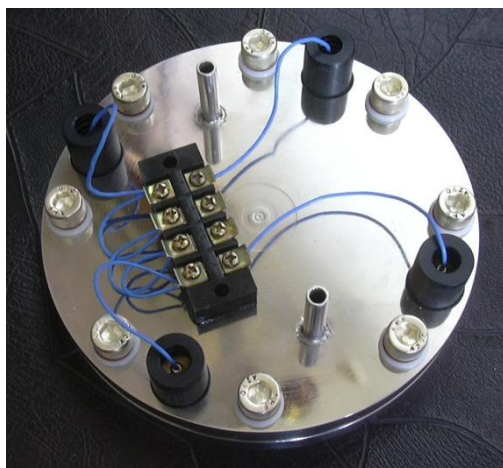
Figure 3.6. Backside view of single cell reactor showing electrical connections
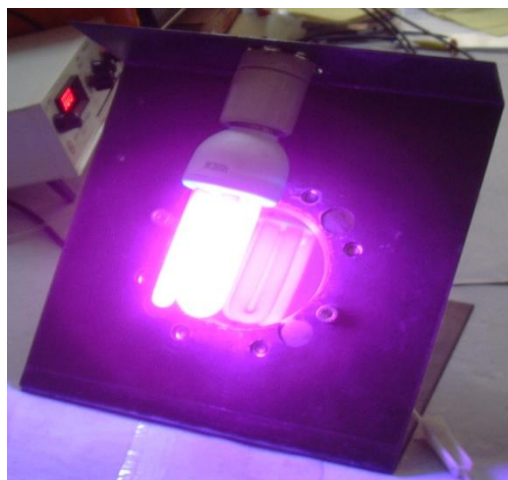
Figure 3.7 Front side of single cell reactor under UVA illumination

3.4.2 Photolectrochemical degradation of Methylene Blue (MB)

The single PEC cell reactor was used to test the performance of deposited photoelectrodes (ZnO, Ag:ZnO, Au:ZnO and ZnO/TiO$_2$) under UVA light illumination. The single cell reactor was fitted on Z shape stand. The electrolyte (0.1 M NaOH) was circulated through the reactor with constant flow rate with UVA illumination to measure i-E curve.

In order to understand the photoelectrocatalytic degradation of organic matter contained in water Methylene Blue (MB) used as model dye in the present work. 200ml solution of MB (1ppm) was circulated through the single cell reactor for degradation

study in the absence and presence of ZnO, Ag:ZnO, Au:ZnO and ZnO/TiO$_2$ photocatalyst under UVA illumination. The aliquots were withdrawn from the reaction mixture after some intervals (at 0, 30, 60, 90, 120, 150 and 180 min). The concentration of MB in the sample was determined by measuring the UV-Vis absorbance using Shimadzu UV- 1800 spectrometer. Degradation of MB was analyzed by HPLC, FTIR and COD measurement before and after the photoelectrocatalytic treatment.

3.4.3 Photoelectrochemical inactivation of *E.coli*

The *E.coli* Davis strain was obtained from NCL Pune and cultivated on a sterile agar medium, containing Tryptone 10g/l, Yeast extract 5 g/l, NaCl 5g/l and Agar –Agar 2.5 % at pH of 7.4 for at least 24 h. Well developed colonies having young *E.coli* cell were suspended into one liter of saline water and well stirred so that the cell count reached a minimum of 10^{10} CFU/ml before passing through reactor. A fixed amount of electrolyte, the major part of it being contained in an external reservoir, was recirculated through the PEC cell, with a constant flow rate of 12.2 lit/h (corresponding to a mean flow velocity of 4.24 cm/s across the photoelectrode) using a Gilson MINIPLUS peristaltic pump, France and silicon tubing. After each 30 min interval of time 1ml sample was taken out for measurement of total viable count of bacteria. Serially diluted 0.1 ml samples were spread over an Agar plate and kept at 37 ^{0}C for 48 hours for incubation. After incubation the plate count was measured. The experiment was repeated under only UV light, UV light + ZnO electrode and UV light + ZnO electrode + bias to study the performance of the ZnO electrode in the photocatalytic antibacterial process. The same set of experiment was carried out for Ag:ZnO, Au:ZnO and ZnO/TiO$_2$ photoelectrodes. Moreover, ZnO/TiO$_2$ photoelectrode has been used to study degradation of Methyl orange, Textile effluent and inactivation of water born gram positive and gram negative microorganisms such as *E.coli, Bacillus*, *Saphyleloccocous* and *salmonella.*

References:

[1]   K. Nomura, H. Ohta, A. Takagi, T. Kamiya, M. Hirano, H. Hosono, Nature, 432 (2004)488

[2]   Y. Liang, C. S. Enache, R. Krol, I. J. Photoenergy, 2008(2007) 1

[3]   M. Okuya, N. A. Prokudina, K. Mushika, S. Kaneko, J. European Ceramic Society, 19 (1999) 903

[4]   P.S. Shinde, C.H. Bhosale, J. Anal. Appl. Pyrolysis 82 (2008) 83

[5]   P.S. Shinde, S.B. Sadale, P.S. Patil, P.N. Bhosale, A. Bru¨ gerd, M. Neumann Spallart, C.H. Bhosale, Sol. Ener. Mater. Sol.Cells, 92 (2008) 283

[6]   L. Hadjeris, L. Herissi, M. B. Assouar, T.Easwarakhanthan, J. Bougdira, N. Attaf, M S. Aida, Semicond. Sci. Technol. 24 (2009) 035006

[7]   S. S. Shinde, P. S. Shinde, C. H. Bhosale, K. Y. Rajpure, J. Photochem. Photobio. B: Biology, 104 (2011) 425

[8]   D. Perednis ,L. Gauckler, Journal of Electroceramics, 14(2005)103

[9]   P. S. Patil, Materials Chemistry and Physics 59 (1999) 185

[10]   C. Gümüş, O. M. Ozkendir, H. Kavak, Y. Ufuktepe, J. Optoelectronics Advan. Mater., 8(2006)299

[11]   S. S. Shinde, C. H. Bhosale, K.Y. Rajpure, Journal of Molecular Structure, 1021(2012) 123

[12]   P. M. Kadam, N. L. Tarwal, P. S. Shinde, S. S. Mali, R. S. Patil, A. K. Bhosale, H. P. Deshmukh, P. S. Patil, Journal of Alloys and Compounds, 509(2011)1729

[13]   P. H. Ngan, N. Q. Tien, D. T. Dat, P.VanNh, Journal of the Korean Physical Society, 52(2008)1594-1597

[14]   B. C. Jiao, X. D. Zhang, C. C. Wei, J. Sun, Q. Huang, Y. Zhao, Thin Solid Films 520 (2011) 1323

[15]   R. Ayouchia, F. Martinb, D. Leinena, J.R. Ramos-Barrado, Journal of Crystal Growth 247 (2003) 497

[16]   S. H. Lim, S. Desu, A.C. Rastogi, J. Phys. Chem. Solids, 69 (2008) 2047

[17]   S. Tewar, A. Bhattacharjee,Pramana, J. Phys., 76 (2011) 153

[18]   C. H. Lee, L. Y. Lin, Applied Surface Science, 92 (1996) 163

[19]   M. Aguilar-Frutis, M. Garcia, C. Falcony, Appl. Phys. Lett., 72 (1998)1700

[20]   P. S. Patil, L. D. Kadam, Applied Surface Science, 199 (2002) 211

[21] V. R. Shinde, T. P. Gujar, C. D. Lokhande, Sensors and Actuators:B, 120 (2007) 551

[22] L. S. Daglas, C.J. Curtis, D. S Ginley,US Patent No. 6126740,3 Oct. 2000

[23] D. Y. Lee, J. Kim, J. Korean Physical Society, 57(2010)1600

[24] V. V. Killedar, C. D. Lokhande, C. H. Bhosale, Thin Solid Films 289 (1996) 14

[25] S. H. Pawar, A. J. Pawar, P. N. Bhosale, Bull. Mater. Sci., 8(1986) 423

[26] B. Godbole, N. Badera, S. B. Shrivastav, V. Ganesan, Jl. of Instrum. Soc. of India, 39(2009) 42

[27] S. P. S. Arya, H. E. Hintermann, Thin Solid Films. 193 (1990) 841

[28] D. F. Vaslow, G.H. Dieckmann, D. D. Elli, A. B. Ellis, D. S. Holmes, Appl. Phys. Lett. 53, (1988) 324

[29] M. Miki-Yoshida, E. Andrade, Thin Solid Films, 224 (1993) 87

[30] S. H. Pawar, P. N. Pawaskar, Materials Research Bulletin, 30, (1995)277

[31] C.H. Chen, A. A.J. Buysman, E. M. Kelder, J. Schoonman, Solid State Ionics, 80 (1995) 1

[32] W. Siepert, Thin Solid Films, 120 (1984) 261

[33] C. S. Huang, C. S. Tao, C. H. Lee, J. Electrochem. Soc., 144(1997)3556

[34] K. Krunks, O. Bijakina, V. Mikli, T. Varema, E. Mellikov, J. Physica Scripta.,T79 (1999) 209

[35] C. Viguie, J. Spitz, J. Electrochem. Soc., 122(1975)585

[36] O. Wilhelm, Ph.D thesis, Swiss Federal Institute of Technology Zurich, University of Tübingen, 2004

[37] M. de la L. Olvera, H. Gomez, A. Maldonado, Sol. Ener. Mater. & Sol. Cells, 91 (2007) 1449

[38] H. Selcuk, W. Zaltner, J.J. Sene, M. Bekbolet, M.A. Anderson, Journal of Applied Electrochemistry, 34(2004) 653

[39] T.A. Mcmurray, J.A. Byrne, P.S.M. Dunlop, E.T. Mcadams, Journal of Applied Electrochemistry, (2005) 35:723

[40] M. Uzunova-Bujnova a, R. Todorovska b, D. Dimitrov a, D. Todorovsky, Applied Surface Science, 254 (2008) 7296

[41] C. Bechinger, S. Ferrere, A. Zaban, J. Sprague, B. A. Gregg, Nature, 383 (1996) 608

4.1 Introduction

Photocatalysis is an efficient process for the degradation and complete mineralization of organic compounds. It plays an important role in the degradation of toxic organic compounds from air and water into components that are nontoxic and safe. The discharge of highly colored synthetic dye effluents from industries can result in serious environmental pollution problems [1]. Moreover wastewater is expected to contain high levels of microorganisms and organic compounds; therefore, water disinfection has been an important and essential technology in biological and biochemical industries [2].

Photocatalytic process using semiconductors appear to be a promising technology under UV radiation that has a number of applications toward air and water purification, water disinfections and hazardous waste remediation. Among the semiconductor-assisted photocatalysts, ZnO plays a vital role due to its high activity towards photocatalytic degradation and mineralization of environmental organic/inorganic pollutants [3-5].

In this chapter, deposited ZnO films are characterized for their structural, morphological, optical and photochemical properties in order to optimize the various preparative parameters such as substrate temperature, solution concentration, quantity of sprayed solution etc. Moreover large area (100 cm^2) ZnO thin film was used in photoelectrocatalytic reactor in order to study degradation of Methylene blue (MB) and inactivation of *E.coli.*

4.2   Experimental

4.2.1   **Preparation of ZnO film**: The preparation of ZnO thin films by SPT has been discussed in section 3.3.2

4.2.2   **Photoelectrocatalytic degradation of Methylene Blue**: The procedure for degradation of MB has been discussed in section 3.4.2

4.2.3   **Photoelectrocatalytic inactivation of *E.coli*:** The procedure for photoelectrocatalytic inactivation of *E.coli* has been discussed in section 3.4.3

4.2.4   **Characterization of ZnO thin films**

Spray deposited ZnO thin films were characterized for their photoelectrochemical, structural, morphological and optical properties by means of photoelectrochemical, X-ray diffraction, scanning electron microscopy and UV- vis spectroscopy techniques. The various deposition parameters such as substrate

temperature, solution concentration and solution quantity have been optimized in order to achieve good quality ZnO thin films.

4.2.4.1 Photoelectrochemical (PEC) characterization

Optimization of preparative parameters of photoactive semiconducting electrode by PEC method is new, reliable and unique technique in thin film technology [6-7]. An appropriate redox electrolyte is chosen and short – circuit current (I_{sc}) and open circuit voltage (V_{oc}) of PEC cell formed with photo-electrode is measured with respect to one of the deposition parameters by keeping others at their fixed values. PEC cell was fabricated using a two- electrode configuration, comprising ZnO thin film as photoanode and graphite as a counter electrode. The 0.1 M NaOH was used as electrolyte. The cell was illuminated with 25 W UV OMNILUX lamp for the measurement of short circuit current (I_{sc}) and open circuit voltage (V_{oc}).

4.2.4.2 X-ray diffraction (XRD)

Structural properties of ZnO thin films were studied by analyzing the X-ray diffraction patterns obtained using Philips X-ray diffractometer Model PW 3710 for λ = 1.05406 and 2.2897 A^0 for Cu- K_α and Cr-K_α radiation respectively.

4.2.4.3 Scanning electron microscopy

The morphological characterization of the thin films was studied with a JEOL JSM- 6360 Scanning Electron Microscope (SEM).

4.2.4.4. UV-Vis spectroscopy and thickness measurement

Optical absorption studies were carried out in the wavelength range of 300 – 1000 nm using Systronic UV-Vis spectrometer model -119, Bangalore, India. Thickness of the deposited films was calculated by inter- ferrometric method.

4.3 Results and Discussion

4.3.1 Optimization of substrate temperature

4.3.1.1 Photoelectrochemical (PEC) characterization

Figure 4.1 shows the variation of short circuit current (I_{sc}) and open voltage (V_{oc}) with respect to substrate temperature. Both I_{sc} and V_{oc} increases gradually with substrate temperature, attains maximum value (I_{sc} = 15 μA , V_{oc} = 0.47 V) at 400 ^{0}C substrate temperature and then decreases for higher temperatures. The lower values of I_{sc} and V_{oc} at low temperatures are due to partial decomposition of spraying solution. The decreases in I_{sc} and V_{oc} after 400 ^{o}C temperature is due to fast evaporation rate of spraying solution. Upon illumination of junction in PEC cell, the magnitude of V_{oc}

increases with negative polarity towards the ZnO thin film indicating cathodic behavior of photo voltage which confirms that the films are n-type. Thus 400 ^{0}C substrate temperature is optimized from photoelectrochemical studies.
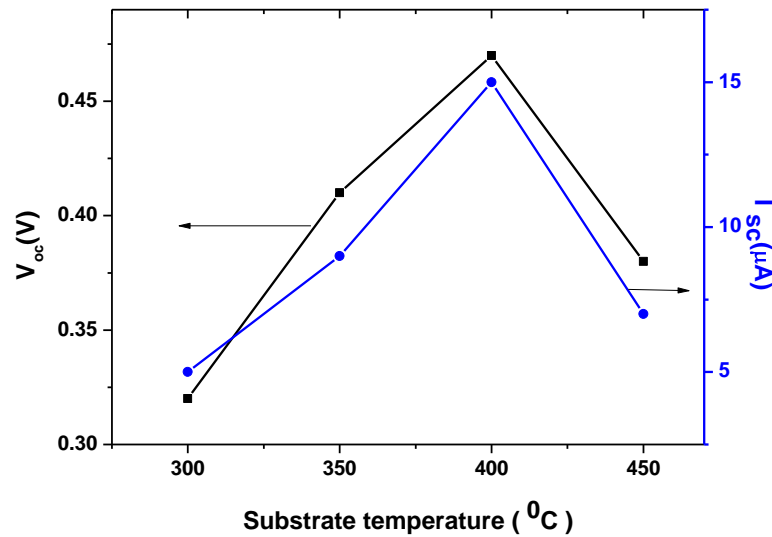
Figure 4.1 Variation of I$_{sc}$ and V$_{oc}$ against substrate temperature for ZnO thin films deposited onto FTO glass substrate.

4.3.1.2 Structural Analysis

XRD pattern of deposited ZnO thin films are shown in fig. 4.2. From XRD data, it is seen that the films exhibit hexagonal crystal structure with preferential growth along the (002) plane. The intensity of the (002) diffraction is relatively highest at the substrate temperature of 400 ^{0}C, indicating an improvement of the film crystallinity. The reason for relatively lower peak intensities is the lower film thickness.The analogous results were reported for spray deposited ZnO films, deposited through aqueous medium [8]. All the peaks in the diffraction pattern were indexed using JCPDS data card No. 05 – 0664. The crystallite size of the ZnO thin films was evaluated using Scherrer's formula,

$$D = \frac{0.94\lambda}{\beta\cos\theta}$$

(4.1)

where λ, θ and β are X-ray wavelength, Bragg diffraction angle and FWHM respectively. It is found that as substrate temperature increases, the crystallite size increases; it becomes maximum at 400 ^{0}C and then decreases further with in substrate

temperature. An increase in crystallinity with substrate temperature is due to the optimum rate of supply of thermal energy for crystallization with substrate temperature. The decrease in crystallite size above 400 ^{0}C may be due to the drying up of the droplets before reaching the substrate.
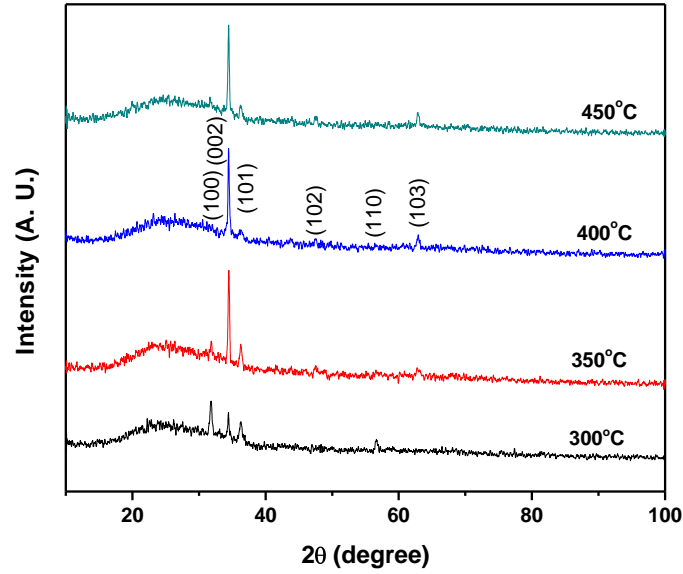
Figure 4.2 XRD patterns of ZnO thin films deposited onto glass substrates for different substrate temperatures

The dislocation density (δ) which represents the amount of defects in the film, was determined using the formula [9].

$$\delta = \frac{1}{D^2} \tag{4.2}$$

The dislocation density exhibit decreasing trend with increasing deposition temperature which leads decrease in lattice imperfections with deposition temperature.

Lattice constants a and c are calculated by using well known analytical method. Zn – O bond length L is given by formula [10]

$$L = \sqrt{\frac{a^3}{3} + \left(\frac{1}{2} - u\right)^2 c^2} \tag{4.3}$$

where the u parameter in the Wurtzite structure is given by,

$$u = \frac{a^2}{3c^2} + 0.25 \tag{4.4}$$

Zn- O bond lengths is given table 1. It is observed that bond length is minimum at 400 ^{0}C.

Table 1: Variation of structural properties with respect to temperature

Temperature (^{0}C)	Crystallite size(nm)	δ,(10^{-4}),(nm^{-2})	a/c	Zn- O bond length (A^0)	Film thickness(nm)
300	35	1.863	0.6296	1.9699	156
350	36	1.175	0.6223	1.9756	204
400	53	1.175	0.6294	1.9655	252
450	46	0.9032	0.6236	1.9725	205

Quantitative information concerning the preferential crystal orientation can be obtained from the texture coefficient, TC defined as,

$$TC(hkl) = \frac{\dfrac{I(hkl)}{I_0(hkl)}}{\dfrac{1}{n}\sum \dfrac{I(hkl)}{I_0(hkl)}}$$

(4.5)

where *TC (hkl)* is the texture coefficient, *I(hkl)* is the XRD intensity and n is number of diffraction peaks considered, *I$_0$ (hkl*) is the intensity of the XRD reference of randomly oriented grains [11].

As TC (hkl) increase, the preferential growth of the crystallites in the direction perpendicular to the (hkl) plane is the higher. The variation of TC (002) of films with respect to temperature is shown in Fig. 4.3. It can be seen that at 300 ^{0}C deposition temperature there is no orientation of grains along c – axis, as temperature increases c-axis orientation increases. TC (002) has its maximum value of about 4.5 at 400 ^{0}C.

After structural analysis, it has been found that the films prepared at 400 ^{0}C have relatively higher crystallinity than deposited at lower and higher temperatures. Thus 400 ^{0}C is fixed as the optimize temperature for further film depositions.
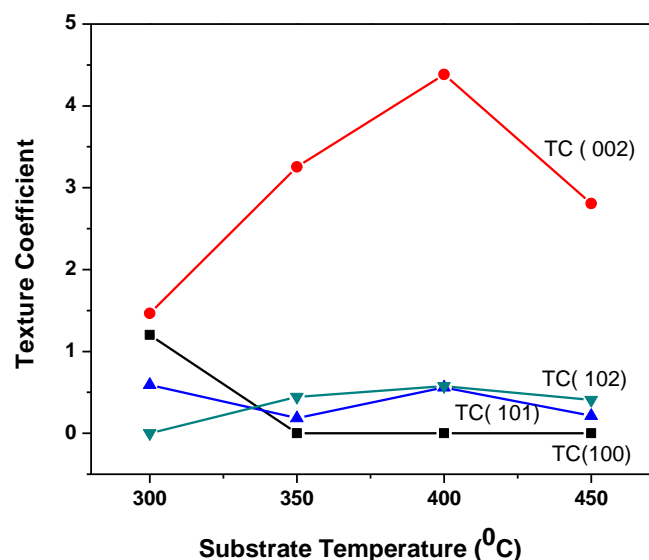
Fig 4.3 Texture coefficient of various planes at different substrate temperatures

4.3.1.3 Morphological properties

Scanning electron micrograph (SEM) images of zinc oxide thin films deposited at different substrate temperatures are shown in Fig. 4.4 (a-d). The micrographs show that substrate is well covered with compactly organized large number of grains.
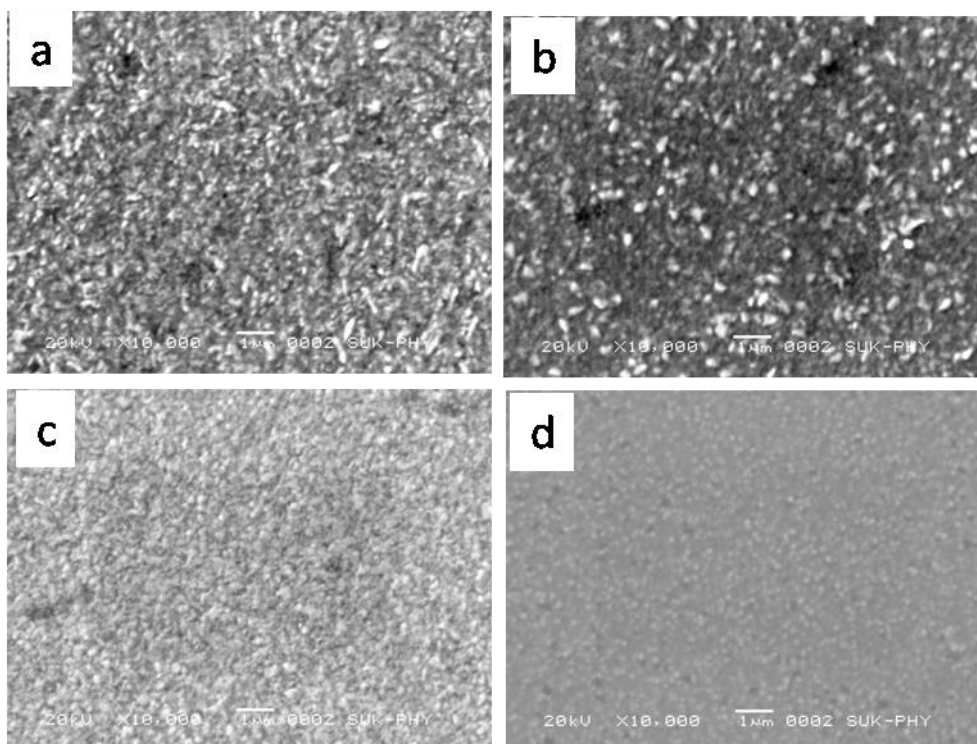
Figure 4.4 Scanning Electron micrographs of ZnO thin films deposited at a) 300, b) 350, c) 400, d) 450 ^{0}C substrate temperatures

As we increase temperature the overgrown particles disappears due to complete decomposition of precursor solution. At higher temperature (400 ^{o}C), films become more rough, loose and grains are randomly grown on surface of substrate. The film surface becomes relatively smooth, dense and mixtures of large and small platelets are seen in Fig. 4.4 (c) for film deposited at 400 ^{0}C temperature. It is observed that the grain size ($\sim$125-200 nm) observed by SEM images is larger than the value determined by XRD, which may be due to the discrepancy between the mean dimension of the crystallites perpendicular to diffracting planes by XRD and the observable aggregates in SEM images. For higher temperatures, these platelets are clustered forming large grains as seen in Fig 4.4 (d). Therefore, it can be concluded that the morphology of particles changes and their size reduces by increasing the substrate temperature [12].

4.3.1.4 Optical properties

Optical transmission spectra of ZnO thin films are shown in Fig.4.5. As temperature increases the transmittance goes no increasing attains maximum at 400 ^{0}C then decreases for further increase in temperature [8]. The films show moderate optical transmittance between 82 to 94 % at 550 nm. At lower temperatures, relatively lower transmission is due to the formation of whites milky films due to incomplete decomposition of the sprayed droplets. The amplitude of interference fringes decreased for higher temperatures indicated the loss in surface smoothness, leading to light scattering loss. These interferences fringes are used to determine to the film thickness by fitting observed and calculated transmittance data. It is seen that the film thickness increases with increasing substrate temperature attains maximum value at 400 ^{0}C ($\sim$252 nm), beyond which it decreases. This can be explained as follows: initially, at lower substrate temperature eg. 300 ^{0}C, the temperature may not be sufficient to decompose the sprayed droplets therefore, results in low thickness. At a particular substrate temperature of 400 ^{0}C, decomposition occurs at the optimum rate resulting maximum thickness. The decrease in film thickness at higher substrate temperature may be due to a higher evaporation rate of the   initial ingredients of the solution [13]. Similar kind of variation is already observed [14].
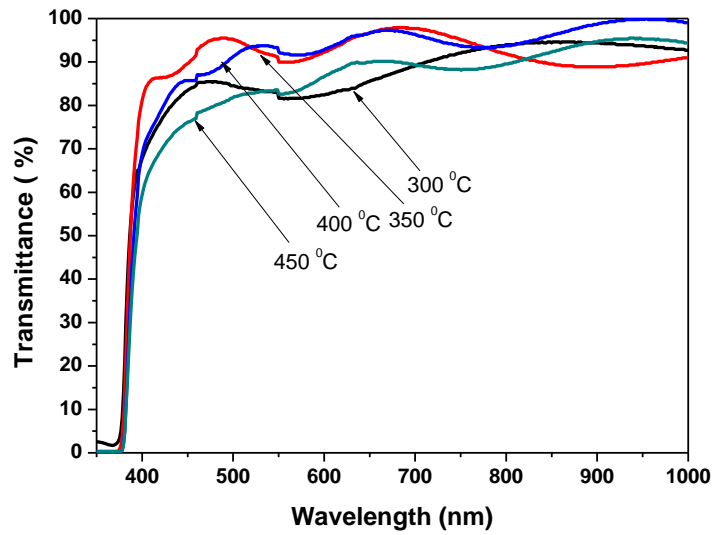
Figure 4.5 Transmittance spectra of ZnO thin films deposited at different temperatures
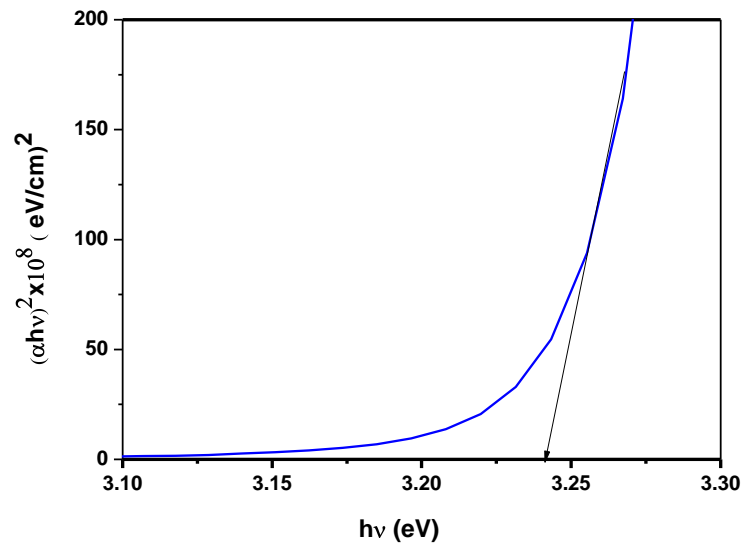
Figure 4.6 plot of (αhν)^2 vs hν for the typical ZnO thin film deposited at 400 ^{0}C

For the direct transition, the optical band gap energy of ZnO thin film was determined by using the equation,

$$\alpha = Const. \frac{\left(h\nu - E_g \right)^{\frac{1}{2}}}{h\nu} \tag{4.6}$$

where $h\nu$ is the photon energy and E_g is the optical band gap. By extrapolating the linear part of the plot of (αhν)^2 vs hν to α = 0, optical band gap was estimated. The

band gap value of films increases from 3.10 to 3.24 eV, up to 400 °C. The band gap energy decreases for higher substrate temperature due to the relaxation of the built in strain. It is well known that the ZnO band gap is particularly sensitive to small changes in carrier concentration, grain boundary configuration and film stress [15]. The decrease of band gap with the increase of substrate temperature is attributed to an increase of crystallite size and a modification of the grain boundary configuration during growth [16].

4.3.2 Optimization of solution concentration

4.3.2.1 Photoelectrochemical (PEC) characterization
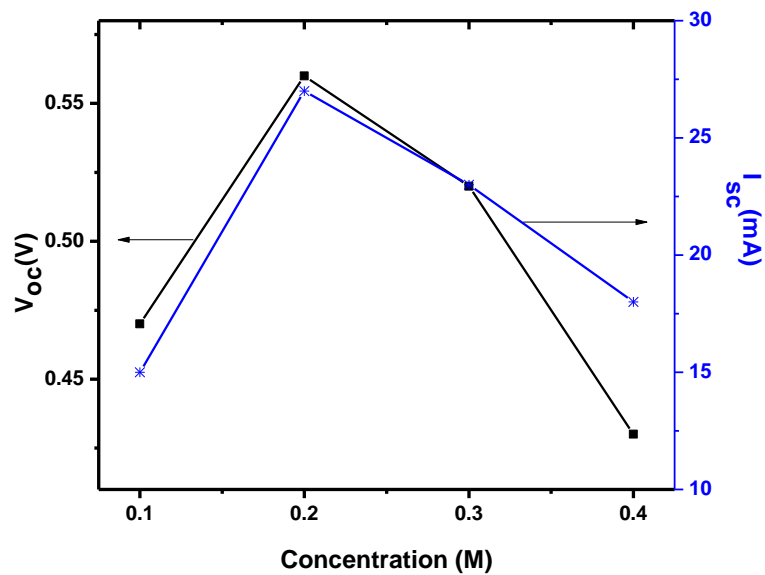
Figure 4.7 Variation of I_{sc} and V_{oc} against concentration for ZnO thin films deposited onto FTO glass substrate

The variation of short circuit current (I_{sc}) and open circuit voltage (V_{oc}) as a function of solution concentration is shown in fig. 4.7. It shows that I_{sc} and V_{oc} increases with increasing in solution concentration and attains maximum values (I_{sc} = 27 µA, V_{oc} = 0.56 V) for the films deposited at 0.2 M concentration. The lower values of I_{sc} and V_{oc} at low concentration are due to decreased absorption of incident light owing to low film thickness. The corresponding lower values for higher solution concentration are due to incomplete growth of compound and showing powdery nature of films [17-18].

4.3.2.2 Structural Analysis

Fig. 4.8 show x-ray diffraction patterns of ZnO thin films with different solution concentrations in spraying solution prepared at optimized substrate temperature of 400 ^{0}C. The crystallinity of the films increases up to 0.2 M concentration and then decreases for higher concentrations. A matching of observed and standard 'd' values of ZnO using JCPDS card No. 05-0664 confirms that the deposited films fit well with the hexagonal crystal structure having preferred orientation along (002) plane. As the solution concentration increases, the intensity of planes increases evidently up to 0.2 M and then decreases [19]. Some weak reflections such as (100), (101) and (110) have also been observed with smaller intensities.
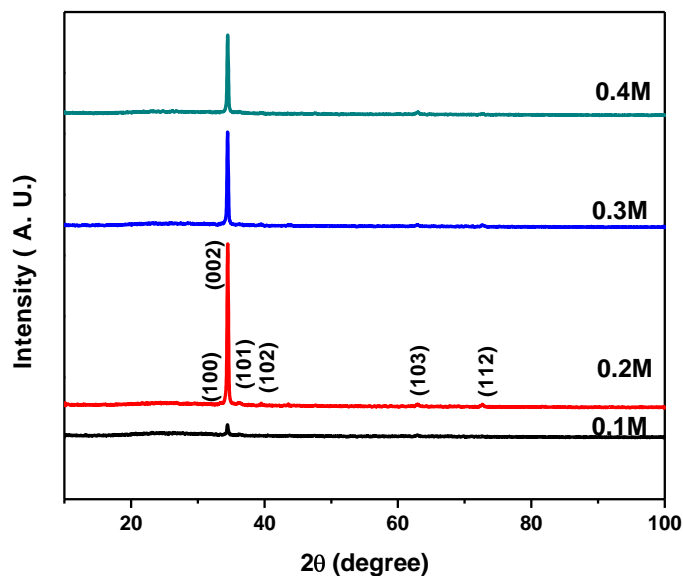
Figure 4.8 XRD patterns of ZnO thin films deposited at various solution concentrations

The variation of TC (002) of films with respect to concentration is shown in Fig. 4.9. As concentration increases intensity of (002) plane increases and other planes disappears which shows ZnO films are highly oriented along [002] direction at 0.2 M concentration.

The average crystallite size of ZnO thin films is calculated using the Scherrer's relation 4.1. The average crystallite size of the ZnO thin films increases up to 0.2 M concentration and then increases. Average crystallite varies from 42-55 nm.
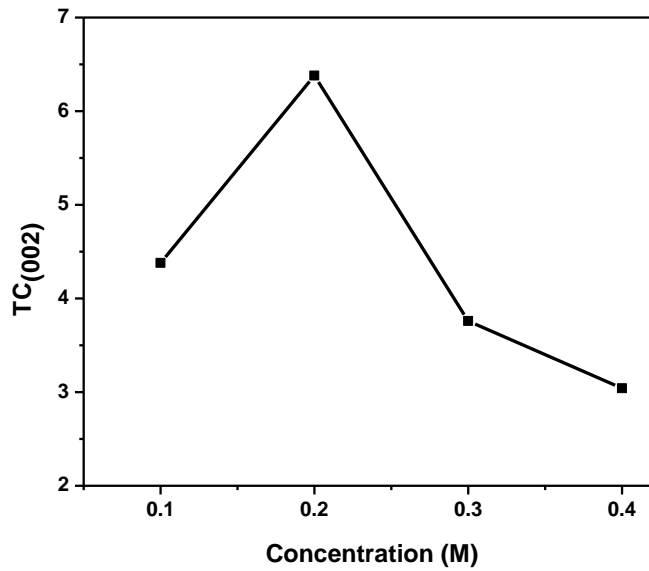
Figure 4.9 Variation of TC (002) with solution concentration

4.3.2.3 Morphological properties
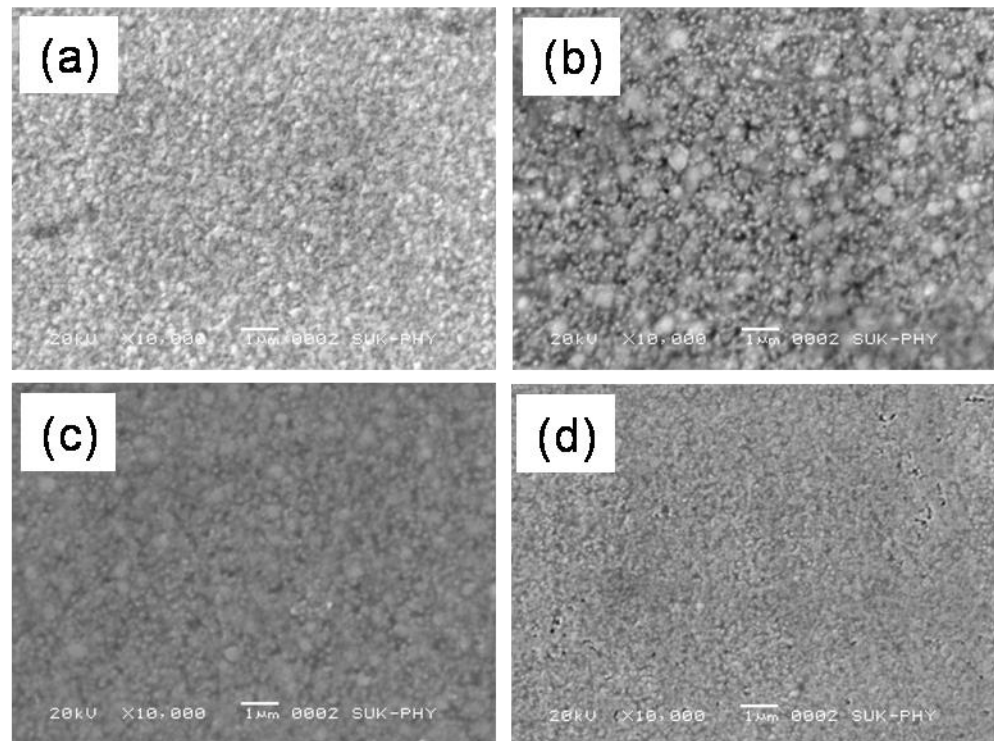
Figure 4.10 Scanning electron micrographs of ZnO thin films deposited at

(a) 0.1, (b) 0.2, (c) 0.3, (d) 0.4 M solution concentrations

Fig. 4.10(a-d) shows the scanning electron micrographs of ZnO thin films deposited at various solution concentrations. It is seen that films are uniform, smooth, compact, adherent, densely packed and well covered by large number small and big grains. As the

concentration increases the roughness and grain size increases without over growth up to 0.2 M concentration and then decreases for higher concentrations with over growth. Average grain size varies from 142-333 nm at different concentrations. Films deposited at 0.2 M concentration (Fig. 4.10 b) shows densely organized mixture of large small grains.

4.3.2.4 Optical properties

The optical transmission spectra of ZnO films over spectral range 350–1000 nm for all the films deposited at various solution concentrations are as shown in Fig. 4.11. As the concentration increases the transmittance goes on increasing attains maximum at 0.2 M, then decreases for further increase in concentration. The films show moderate optical transmittance between 74 and 94 % at 550 nm. The increase in transmittance might be attributed to uniform, adherent and well-crystallized films on surface of substrate. The well-developed interference pattern is observed for all deposited films showing specular to great extent. Thickness of the film varies from 252-850 nm, with 400 nm being optimum at 0.2 M concentration. Direct band gap (Fig. 4.12) of ZnO thin films decreases from 3.26-3.25 eV up to 0.2 M and further increases for higher solution concentrations.
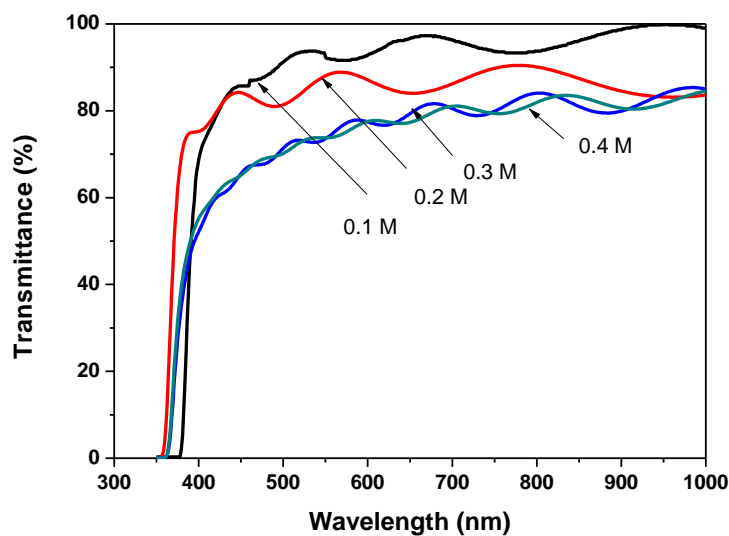
Figure 4.11 Transmittance spectra of ZnO thin films deposited at various solution concentrations
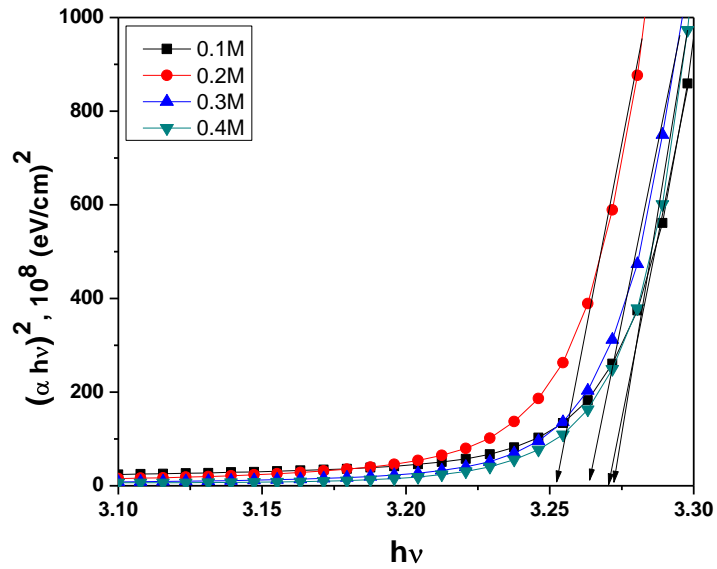
Figure 4.12 Plot of $(\alpha h\nu)^2$ vs $h\nu$ for ZnO thin films deposited at different concentrations

4.3.3 Optimization of quantity of sprayed solution

4.3.3.1 Photoelectrochemical (PEC) characterization
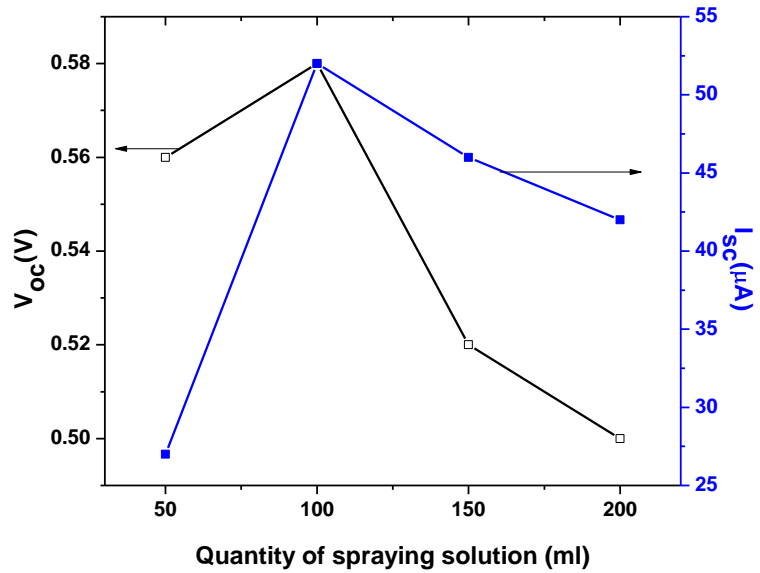
Figure 4.13 Variation of I_{sc} and V_{oc} against quantity of spraying solution for ZnO thin films deposited onto FTO glass substrate

The variation of short circuit current (I_{sc}) and open circuit voltage (V_{oc}) as a function of concentration has been shown in Fig. 4.13. It shows that I_{sc} and V_{oc} increases with increasing in solution quantity and attains maximum values   (I_{sc} = 52 µA, V_{oc} =

0.58 V) for the films deposited at 100 ml. The lower values of I_{sc} and V_{oc} at 50 ml solution quantity are due to decreased absorption of incident light owing to low film thickness. The corresponding lower values of I_{sc} and V_{oc} for the film deposited at › 100 ml solution quantity due to incomplete growth of compound.

4.3.3.2 Structural Analysis

The XRD patterns for the ZnO thin films grown on glass substrates a studied in the 2θ range of 10–100° are shown in Fig. 4.14. It is seen that the material deposited is polycrystalline irrespective to the quantity of spraying solution. It is found that, the film tends to grow in specific (002) crystallographic directions. However, as quantity of solution is increased, the intensity of (002) peak increases up to 100 ml spraying quantity and decreases for higher quantity. The variation of preferred orientation with respect to quantity of spraying solution may be attributed to the change in film thickness [20].

Above 100 ml, milky and powdery films are resulted. It is seen that the crystallite size increases with increase in spraying solution. The analysis reveals that the quantities of spraying solution strongly influence the crystallite size (38 – 63 nm) as well as thickness of the thin films (Fig. 4.15).
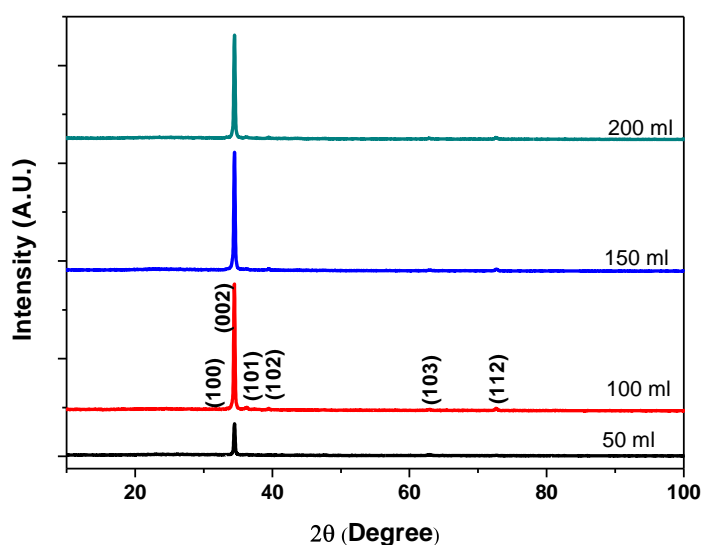
Figure 4.14 XRD patterns of ZnO thin films deposited at different quantities of spraying solution
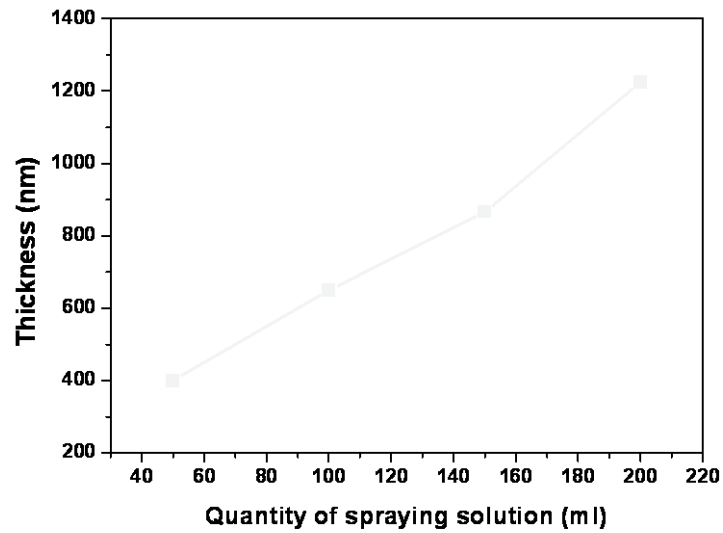
Figure 4.15 Variation of thickness with quantities of spraying solution

4.3.3.3 Morphological properties
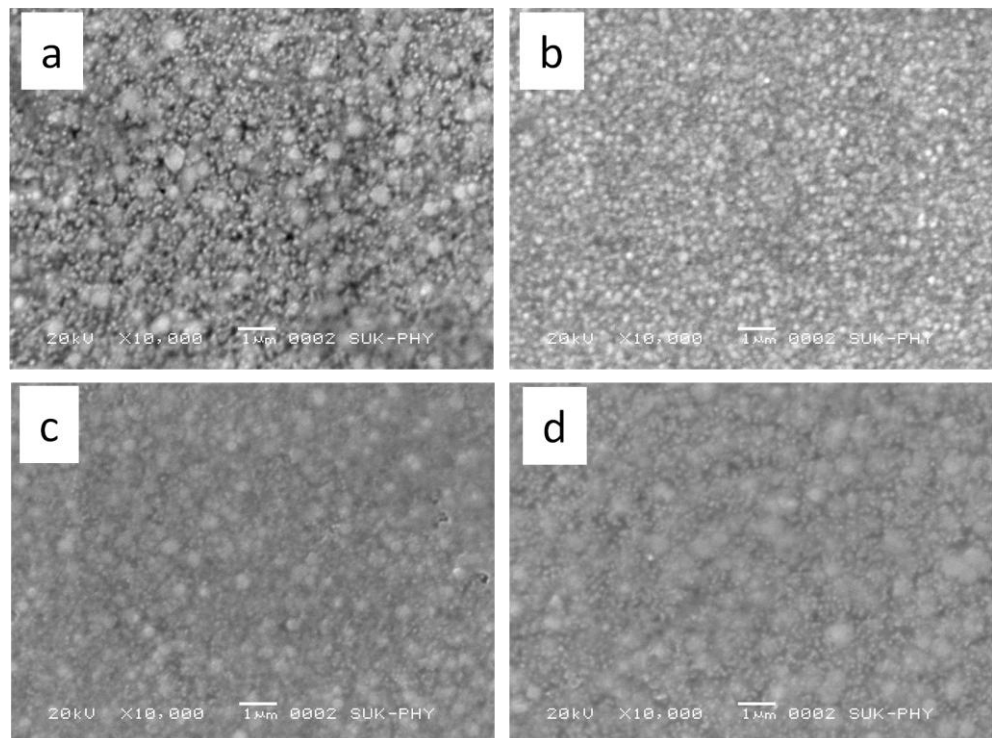
Figure 4.16 Scanning electron micrographs of ZnO thin films deposited at (a) 50 ml, (b) 100 ml , (c) 150 ml and (d) 200 ml quantities of spraying solution

Fig. 4.16(a-d) show SEM images of ZnO thin films deposited with different quantities of spraying solution. It is observed that the surface morphology of the films is strongly dependent upon the quantity of spraying solution. It is seen that films are uniform, smooth, compact, adherent, densely packed and well covered by large number small and big grains, at lower concentration the layers are made up of mixture of small grains and big grains. This is due to incomplete decomposition of initial ingredient of the solution. The average grain size varies from 266 – 540 nm.

4.3.3.4 Optical properties

Fig. 4.17 shows the spectral transmittance as a function of wavelength for ZnO thin films deposited with solution quantity between 50 ml to 200 ml at a fixed substrate temperature of $T_s=400$ °C. It is seen that transmittance decreases with increase in solution quantity.

The low transmittance is attributed to increase in thickness, which causes surface darkening. At higher solution quantity › 100 ml films prepared with this solution are thicker and consequently less transparent. At higher thickness, the films tend to be powdery in nature and whitish in appearance. However, there is a slight shift in the absorption band edge. The shift in the absorption edge can be accounted for the increase in carrier concentration and blocking of low energy transitions. Band gap energy decreases with increasing quantity of spraying solution from 3.25 to 3.20 eV due to increase in particle size.
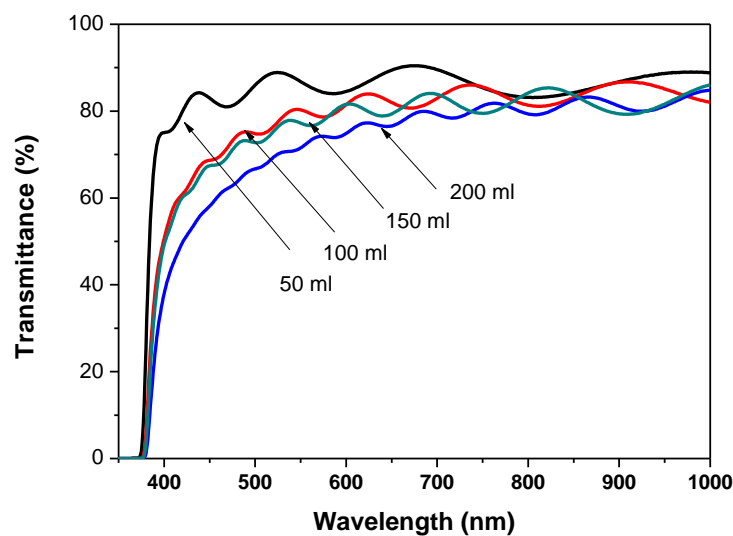
Figure 4.17 Transmittance spectra of films deposited at various solution quantities

4.4 Photoelectrocatalytic degradation of Methylene Blue (MB) by ZnO Photoelectrode

Photoelectrochemical studies of ZnO thin film

Especially the wavelength of 365 nm was selected in view of later application of the ZnO layers in water purification, as 365 nm are readily available, making photochemical processes convenient to be carried out. In Fig. 4.18, a typical current–potential curve in the dark and under illumination in 0.1N NaOH is shown for optimized ZnO film deposited on FTO. The plateau photocurrents reached a few millivolts above the photocurrent onset potential, showing the semiconducting properties of the n-ZnO [21].
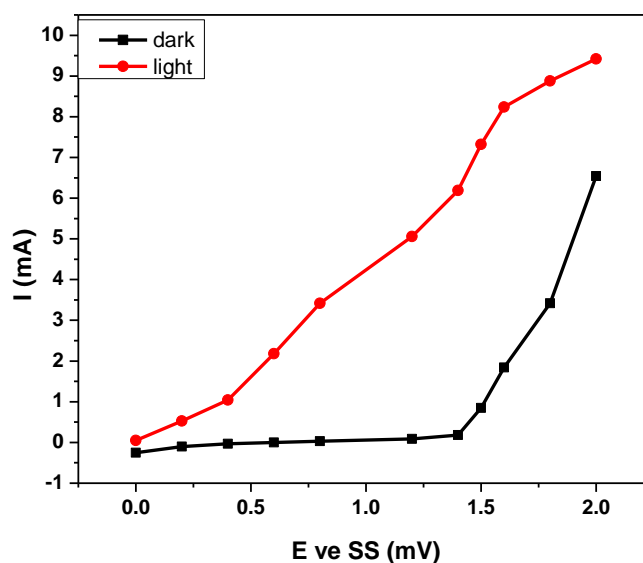
Figure 4.18. i–E curve for a glass/FTO/ZnO electrode; with electrolyte 0.1M NaOH under UVA illumination (Active area 64 cm^2)

Photoelectrocatalytic degradation of Methylene blue

Sulfur dyes are the most commonly used dyes manufactured for cotton in terms of volume. They are cheap, generally have good wash-fastness and are easy to apply. The dyes are absorbed by cotton from a bath containing sodium sulfide or sodium hydrosulfite and are made insoluble within the fiber by oxidation. In the present work, methylene blue is selected as a model of dye pollutant with which the degradation efficiency of the as-prepared ZnO thin film catalysts are to be investigated. Methylene blue (MB), $C_{16}H_{18}ClN_3S$, is a brightly blue in colour (Fig. 4.18). It has many uses in a

range of different fields such as biology and chemistry. At room temperature it appears as a solid, odorless, dark green powder, which yields a blue solution when dissolved in water [22].
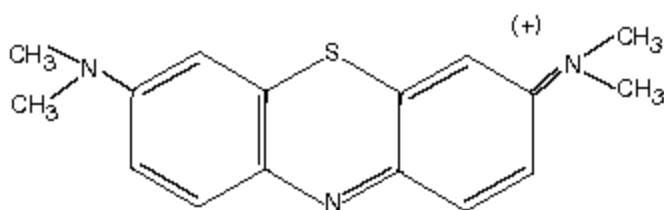
Figure 4.18 The structure of Methylene Blue C$_{16}$H$_{18}$ClN$_3$S (MW 319.85 gm)

During the course of the degradation experiments, the concentration of MB decreases due to decomposition (photoelectrochemical oxidation). Blank experiments (no light or no bias, not shown) showed the total absence of degradation. First, MB degradation was studied under broadband UVA illumination. A dilute solution of MB in 10 mM Na$_2$SO$_4$ was circulated at a flow rate of 12.2 l h^{-1} through the single electrochemical cell. After equal interval of time 4 ml MB solution was withdrawn with help by syringe for spectroscopic and COD analysis. The photocurrent at a fixed bias voltage of 1.5 V vs. steel was passed through the cell, the average photocurrent in 0.004 A.

Figure 4.19(a) shows the variation in the extinction spectra of MB collected at various intervals during its photocatalytic detoxification recorded in the wavelength range from 400 to 800 nm. During the course of the degradation experiments, the concentration of MB decreases due to its decomposition (photochemical oxidation). It is further used to plot variation in ln(C/C$_0$) as a function of reaction time as shown in figure 4.20 (b) that shows degradation kinetics (extinction taken at 665 nm). The linear integral transform ln(C/C$_0$) as a function of degradation time reveals the apparent first order reaction kinetics. The linear portion in this plot has a slope of rate constant (*-k*). As illustrated in Fig. 4.19 (b), the photocatalytic activities (kinetic fit for the degradation of MB) of nanocrystalline ZnO are investigated on the photodegradation of MB under UVA light illumination. Figure 4.19 (c) shows that 48 % reduction of COD values during degradation of MB.The decrease of photocurrent in later stages of the experiment is due oxidation of organic species as well as photocorrossion of ZnO photoelectrode.

In the lower part of Fig. 4.19(b) the variations in ln(C/C$_0$) as a function of illumination time are plotted. The linear section in this can be taken as the apparent first order rate constant of the degradation reaction:

$$\ln\left(\frac{C}{C_0}\right) = -kt \qquad (4.8)$$

where C is the concentration of MB remaining in the solution at time t and C_0 is the initial concentration at t = 0.

The rate constant in a batch reactor of given electrode size is inversely proportional to the volume. Moreover, k is proportional to the area of the electrode if a sufficiently well collimated light source is used and to its intensity and therefore to the photocurrent. In order to intangible from these external parameters and to make comparison of experimental data obtained under various conditions possible, it is useful to define,

$$k' = kV \qquad (4.9)$$

$$k'' = \frac{k'}{A} \qquad (4.10)$$

$$k''' = \frac{kVF}{i_{ph}} \qquad (4.11)$$

$$p = \frac{1}{k'''} \qquad (4.11)$$

where F is Faraday's constant (96,500 mol^{-1}), V the volume, A the area of electrode, k''' the rate constant or kinetic parameter, which is independent of total photocurrent (i_{ph}) and total volume of solution. The p reflects the efficiency of oxidative degradation of the solute (when extinction is used) or of the amount of oxidizable atoms in the solution (in the case of COD).
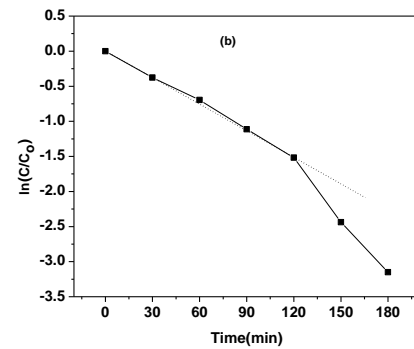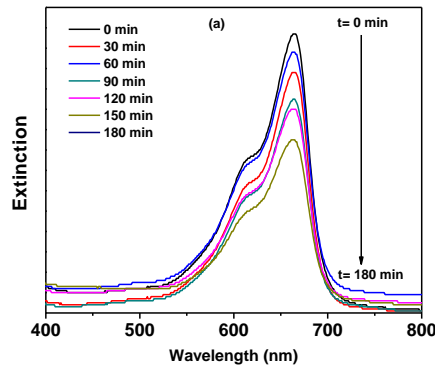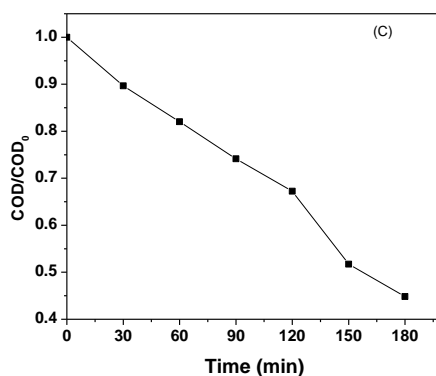
Figure 4.19 Detoxification of MB with ZnO under UVA light illumination a) extinction spectra with reaction time and b) kinetics of detoxification (extinction taken at 665 nm) c) normalized COD with reaction time

It is generally accepted that, when semiconductor photocatalyst are irradiated by light with energy higher than or equal to the band gap, an electron (e^-) in the valence band (VB) can be excited to the conduction band (CB) with the simultaneous generation of a hole (h^+) in the VB. The photoelectron can be easily trapped by electronic acceptors like adsorbed O_2, to produce a superoxide radical anion ($O_2^{\bullet}$), whereas the photo-induced holes can be easily trapped by electronic donors, such as organic pollutants, to oxidize organic pollutants [23]. However, if the photo-generated electrons recombined with the photo-induced holes, the photocatalytic activity would be decreased. In general, oxygen vacancies in ZnO catalyst can act as the active centers to capture photo-induced electrons and the recombination of photo-induced electrons and holes can be effectively inhibited, so that the photocatalytic activity can be greatly improved [24]. The values of the parameters k, k', k'', k''' and p are found to be1.2 $\times10^{-3}$ s^{-1} , 2.4 $\times10^{-3}$ cm^3.s^{-1}, 3.75$\times$ 10^{-5} cm.s^{-1} , 57900 M^{-1} and 1.72 x 10^{-5} M respectively. The unlikely higher values of k'' and k''' can be explained by an improvement of the photoanode surface by prolonged illumination and interfacial electron transfer. In this experiment, it is possible to degrade MB with a ZnO photocatalyst to about 56 % in 180 min. reaction time. Photocatalytic activity of ZnO is attributed to the donor states caused by the large number of defect sites such as oxygen vacancies and interstitial zinc atom and the acceptor states which arise from zinc vacancies and interstitial oxygen atoms [25].
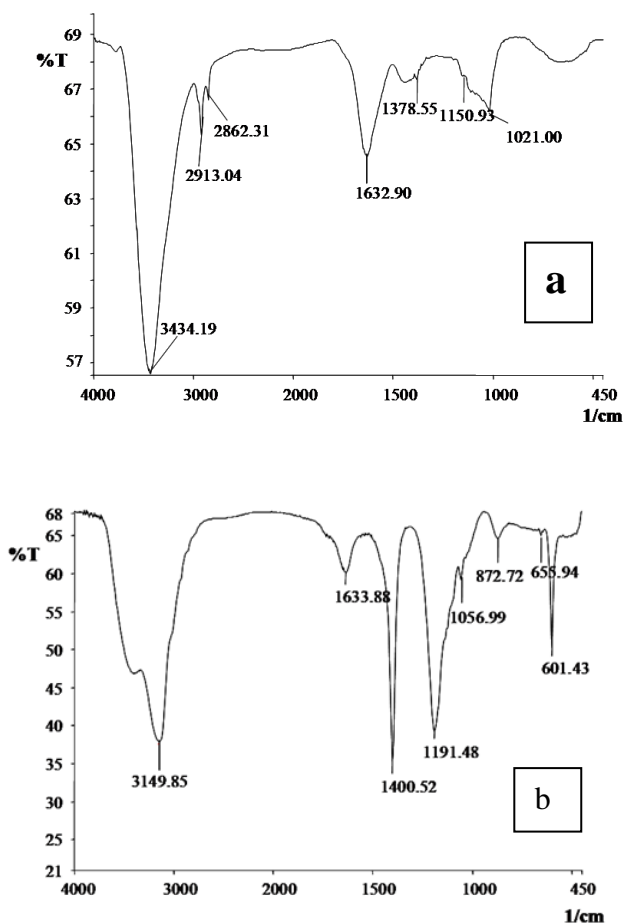
Figure 4.20 FTIR spectra of methylene blue (a) before and (b) after degradation

FTIR analysis of control MB showed presence of N-H stretch at 3433.19 cm^{-1}, alkanes at 2862.31-2913.04 cm^{-1}, presence of azo bond (N=N stretch) at 1632.90 cm^{-1}, aromatic ether at 1378.55 cm^{-1}, S=O stretch at 1150.93 cm^{-1} provides the evidence for sulfonated bond present in MB, primary alcohol (C-OH stretch) at 1021-cm^{-1} confirms the MB dye with phenolic group, (Fig. 4.20 a), whereas metabolite formed after degradation of MB showed N-H stretch at 3149 cm^{-1}, presence of azo bond (N=N stretch) at 1633.88 cm^{-1}, C-H deformation at 601.43 - 872.72 and 1400.52 cm^{-1} respectively, peak at 1191.48 cm^{-1} showed presence of aliphatic ether, a peak at 1056.99 cm^{-1} showed presence of C-OH stretch (Fig. 4.20 b). Absence of peak at 1150.93 cm^{-1} for sulfonated bond in formed metabolites obtained after degradation confirms the cleavage of sulfonated bond by photoelectrocatalytic degradation.

Photocorrossion of ZnO photoelectrode was examined by measuring zinc by atomic absorption spectroscopy in degraded sample. During the course of degradation of MB 24 % ZnO thin film was dissolve due to photocorrossion.

4.5 Photelectrocatalytic inactivation of *E.coli*

A number of mechanisms have been proposed to interpret the antibacterial behavior of metal oxides. Moos et al.[26] attributed the antibacterial behavior of MgO to several mechanisms including the production of active oxygen species, interaction between metal oxide particles and membrane cell walls, penetration of individual metal oxide particles into cells. Sawai et al. measured the active oxygen species generated in ZnO slurries by using chemiluminescence and oxygen electrochemical analysis and found that H_2O_2 was produced in ZnO slurries and the concentration of produced H_2O_2 was linearly proportional to the ZnO particle concentration. H_2O_2 was also detected by Matsunaga et al. [27] with a spectrophotofluorometer. Stevenson et al. [28] suggested that electrostatic interactions between the bacteria surface and nanoparticles could be involved. We shall start the discussion by looking at the structure of the cell envelope of *E. coli.*

E. coli is a Gram-negative bacterium and has a membrane structure as shown in Fig. 2.11. *E. coli* cells have a rod-like morphology with a length of approximately 1–3 μm and a diameter of 0.5–1 μm. The cell envelope of *E. coli* consists of an inner membrane (~8 nm thick), a periplasm containing the peptidoglycan (cell wall) and an outer membrane (~10–15 nm thick). The inner and other membranes have a lipid bilayer structure. The outer layer of the outer membrane (OM) bilayer consists of lipopolysaccharide (LPS) and the inner layer of the OM bilayer consists of phospholipids. The OM also contains proteins such as porins that act as passive diffusion channels for hydrophilic molecules. The inner membrane consists of ~ 40 % phospholipids and ~ 60 % protein.

In an inactivation of *E.coli* bacteria in this work, the initial population of *E.coli* count was around 10^{10} CFU/ml in 10 mM Na_2SO_4. In all experiments, the solution was circulated through the photoelectrochemical cell. Photocatalytic antibacterial activity of the ZnO films against *E. coli* was investigated under various conditions (Fig 4.21). Also it is observed that BOD reduction is 60 % during the inactivation of the *E.coli*.
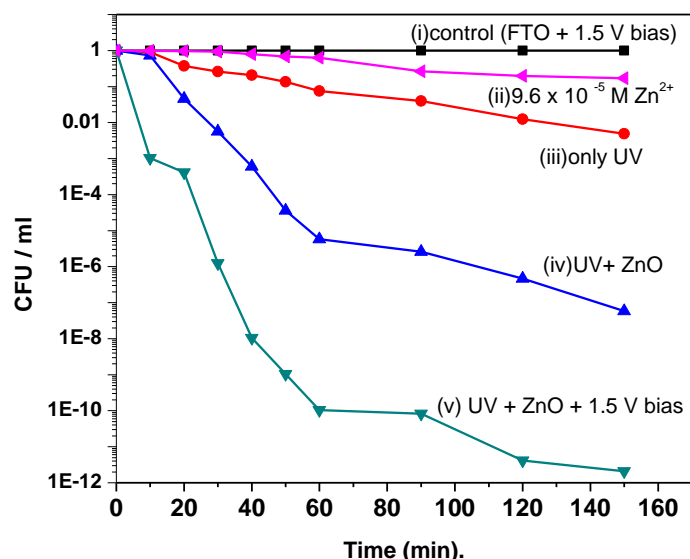
Figure 4.21 Normalized inactivation count of *E.coli* with reaction time

i.   In one of the blank experiments (no ZnO film present on the FTO substrate, application of 1.5 V to the cell) there was no noticeable decrease of bacterial count after 150 min.

ii.   In another blank experiment, the influence of the presence of Zn^{2+} ions was tested, by dispersing the bacteria in a solution of 0.096 mM Zn^{2+}, 10 mM Na_2SO_4. This is the zinc ion concentration, originating from photocorrosion, which was found in the middle of an experiment where a ZnO electrode was illuminated under a bias of 1.5 V for 2 h (Fig. 4.21). After the 150 min. degradation experiment, in the absence of light and electrical bias, the bacterial count was decreased by 1 %.

iii. In an experiment with direct UVA illumination, the bacterial count was decreased to less than 1 percent. In this experiment the ZnO covered glass/FTO plate was replaced by a glass plate.

iv.   A dramatic effect was noticed when a UVA illuminated ZnO electrode was used. This corresponds to the photoelectrochemical mode under open circuit. Direct absorption of UV light by the bacteria was excluded as light was almost entirely absorbed by the backside illuminated ZnO layer before entering the solution. In the open circuit mode, both light induced

charge carriers (e⁻, h⁺) are available at the surface of the semiconducting electrode but the rate of recombination is high. At the end of the experiment, the bacterial count was decreased by a factor of 10^7. Similar results on bacterial photokilling have been obtained earlier. A.G. Rincon et al. reported an *E.coli* count decrease from 10^7 to 10^3 CFU/ml due to only UV light after 4 h illumination and a decrease from 10^7 to 10 CFU/ml due to light and TiO_2 suspended particles after 1.25 h [29]. In another report the antibacterial activity of nanorods based ZnO thin films synthesized by a hydrothermal process against *E.coli* bacteria was investigated under UV irradiation and showed strong antibacterial activity with an apparent first order degradation rate constant of 0.0015 s^{-1} in a drop of 100 μl [30].

v. An even larger effect was noticed when the ZnO layer was electrically biased in order to suppress charge carrier recombination. In this case, conduction band electrons were not present at the interface and recombination is suppressed. As expected, the bacterial count was further reduced, killing practically all the bacteria initially present. From the initial slope, a first order rate constant of 0.0115 s^{-1} was found.

Such high rate constants cannot be explained on the basis of a single attack of a cell by a valence band hole or a surface bound $^{\bullet}$OH radical, based on the measured electrical currents during the reaction (around 4 mA). It is well known that dead bacterial cells and their contents, spilling out once the wall is damaged, is toxic for living cells. This effect and the accessibility of iron for the Fenton reaction, after wall destruction, may be responsible for the observed high rate constants. However, since the strongly oxidizing reactants (h⁺, $^{\bullet}$OH) and other potentially toxic intermediates ($^{\bullet}O_2^-$, H_2O_2) are only available at the electrode surface, reactions involving these species are confined to the electrode surfaces.

ZnO nanoparticles exhibit strong antibacterial activities on a broad spectrum of bacteria. The antibacterial mechanism of ZnO is still under investigation. The photocatalytic generation of hydrogen peroxide was suggested to be one of the primary mechanisms. In addition, penetration of the cell envelope and disorganization of the bacterial membrane upon contact with ZnO nanoparticles were also indicated to inhibit bacterial growth. However, in the photoelectrochemical mode, hydrogen peroxide is an

intermediary product of the electrode processes water oxidation / oxygen reduction and is therefore not present in the bulk of the solution. As to the role of Zn^{2+} ions released through photocorrosion, the binding of Zn^{2+} ions to the membranes may have some effect. In fact, prolongation of the lag phase of the microbial growth cycle has been suggested [31]. However, chemical interactions between ZnO and the components of the cell envelope (lipid bilayer, peptidoglycan, membrane proteins, lipopolysaccharides) and physical interactions between ZnO and the cell envelope structure causes to final death of the cell.

References

[1]   P. P. Vijaya and S. Sandhya, The Environmentalist, 23 (2003) 145.

[2]   H. L. Liu, C. K. T. Yang, Proc. Biochem., 39 (2003) 475.

[3]   K. I. Okamoto, Y. Yamamoto, H. Tanaka, M. Tanaka, Bull. Chem. Soc. Jpn. 58 (1985) 2015.

[4]   D. Li, H. Haneda, Chemosphere, 51(2003) 129.

[5]   B. Dindar, S. Icli, J. Photochem. Photobiol. A: Chem. 140 (2001) 263.

[6]   P. S. Shinde and C.H. Bhosale, J. Anal. Appl. Pyrol., 82 (2008) 83.

[7]   V. M. Nikale and C.H. Bhosale, Sol. Energy Mater. Solar Cells, 82 (2004) 3.

[8]   A. Djellou, K. Bouzid, F. Guerrab, Turk. J. Phys, 32 (2008) 49.

 [9]   X. S. Wang, Z. C. Wu, J. F. Webb, Z. G. Liu, Appl. Phys. A, 77 (2003) 561.

[10]   S. Ilican, Y. Caglar, M. Caglar, J. Optoelect. Adv. Mater., 10 (2010) 2578.

[11]   S. J. Kang, Y. H. Joung, H. H. Shin, Y. S. Yoon, J. Mater Sci: Mater. Electron., 19 (2008) 1073.

[12]   Z. Gong, Z. C. Niu, Z.D. Fang, Z.H. Miao, S.L. Feng, Appl. Phys. Lett., 86 (2005) 013104.

[13]   F. A. Mahmoud, G.Kiriakidis, J. Ovonic Res., 5 (2009) 15.

[14]   U. Ayer, Thin Solid Films, 515 (2007) 3448.

[15]   V. Srikant, D. R. Clarke, J. Mater. Res., 12 (1997) 1425.

[16]   K. S. Hwang, J. H. Jeong, Y. S. Jeon, K. O. Jeon, B. H. Kim, Ceramics International, 33 (2007) 505.

[17]   P. S. Shinde, P. S. Patil, P. N. Bhosale, C. H.   Bhosale, J. Am. Ceram. Soc., 91 (2008) 1266.

[18]   A. Wahl and J. Augustynski, J. Phys. Chem. B, 102 (1998) 7820.

[19]   K. S. Kim, T. S. Lee, J. H. Lee, B. K. Jeong, Y. J. Cheong, W. Baik, M. Kim, J. Appl. Phys. 100 (2006) 063701.

[20]   M.O. Abou-Helal, W.T. Seeber J. Non-Crystalline Solids, 218 (1997) 139.

[21]   P. S. Shinde, S. B. Sadale, P. S. Patil, P. N. Bhosale, A. Bru¨ ger, M. Neumann-Spallart, C.H. Bhosale, Sol. Ener. Mater. Sol. Cells, 92 (2008) 283.

[22]   A. K. Paul, M. Prabu, G.Madras, S. Natarajan, J. Chem. Sci., 122 (2010) 771.

[23]   X. P. Lin, T. Huang, F. Q. Huang, W. D. Wang, J. L. Shi, J. Phys. Chem. B, 110 (2006) 24629.

[24]   J. Liqiang, Q. Yichun, W. Baiqi, L. Shudan, J. Baijiang, Y. Libin, F. Wei, F. Honggang, S. Jiazhong, Sol. Energy Mater. Sol. Cells, 90 (2006) 1773.

[25]   F. Tuomisto, K. Saarinen, Phys. Rev., 72 (2005) 085206.

[26]   P. J. Moos, K. Chung, D. Woessner, M. Honeggar, N. S. Cutler, J. M. Veranth, Chem. Res. Toxicol., 23 (2010) 733.

[27]   Matsunaga, T., R. Tomoda, Y. Nakajima, N. Nakamura, T. Komine. Appl. Environ. Microbiol. 54 (1988) 1330.

[28]   M. Stevenson, K. Bullock, W. Y. Lin, K. Rajeshwar. Res. Chem. Intermed, 23 (1997) 311.

[29]   G. Rincon, C. Pulgarin, Appl. Catalysis B: Envirn. 49 (2004) 99.

[30]   O. Akhavan, M. Mehrabian, K. Mirabbaszadeh, R. Azimirad, J. Phys. D: Appl. Phys. 42 (2009) 225305.

[31]   J. J. Vora, S. K. Chauhan, K. C. Parmar, S. B. Vasava, S. Sharma, L. S. Bhutadyua, E-J. Chemistry, 6 (2009) 531.

5.1 Introduction

ZnO has been extensively investigated as one of the potential semiconductor photocatalyst used in water purification. However, a major limitation to achieve high photocatalytic efficiency in semiconductor nanoparticle systems is the quick recombination rate of photoinduced charge carriers [1-2]. To overcome this limitation, one efficient way is to dope noble metals, such as gold [3-4], platinum [5-6] and silver [7-8] in the ZnO semiconductors. On the other hand, strong antibacterial activities of both Ag and Ag^+ have been known for a long time [9-12]. ZnO is inorganic antibacterial agent, it can be expected that ZnO will be an excellent support for Ag atoms. In addition, these Ag:ZnO may inhibit the growth of bacteria synergistically due to the strong interaction between them. Keeping these views in mind, we planned to dope silver and gold in ZnO matrix, which not only inhibit photocorrossion of ZnO electrode but also enhance the degradation of methylene blue (MB) and inactivation rate of the bacteria.

This chapter contains synthesis and characterization of Ag and Au doped ZnO thin films. Influence of doping concentration onto PEC structural morphological, optical and luminescence properties has been investigated. Moreover large area (100 cm^2) Ag and Au doped ZnO thin films have been prepared on FTO coated glasses (10 – 15 Ω). Finally these films have been used for photoelectrocatalytic degradation of MB and inactivation of *E.coli*.

5.2 Experimental

 5.2.1 **Preparation of Ag:ZnO thin fims** : Preparation of Ag:ZnO thin fims has been discussed in 3.3.3

 5.2.2 **Preparation of Au:ZnO thin fims:** Preparation of Au:ZnO thin fims has been discussed in 3.3.3

 5.2.3 **Degradation of MB and inactivation of *E.coli*** : Degradation of MB and inactivation of *E.coli* has been in section 3.4.2 and 3.4.3 respectively

5.3 Results and discussion

A. Characterization of Ag:ZnO thin films

5.3. A.1 Photoelectrochemical (PEC) characterization

Fig. 5.1 shows variation of I_{sc} and V_{oc} values for different Ag doping concentrations. It is observed that with increasing Ag doping I_{sc} and V_{oc} values increase upto 3 atomic wt

% (At %) Ag doping and then decrease for higher concentrations. This consists with the presence of discrete Ag clusters leading to retarded recombination of the photoinduced electron–hole pair and enhanced absorption by surface plasmons resonance (SPR) phenomenon [13].
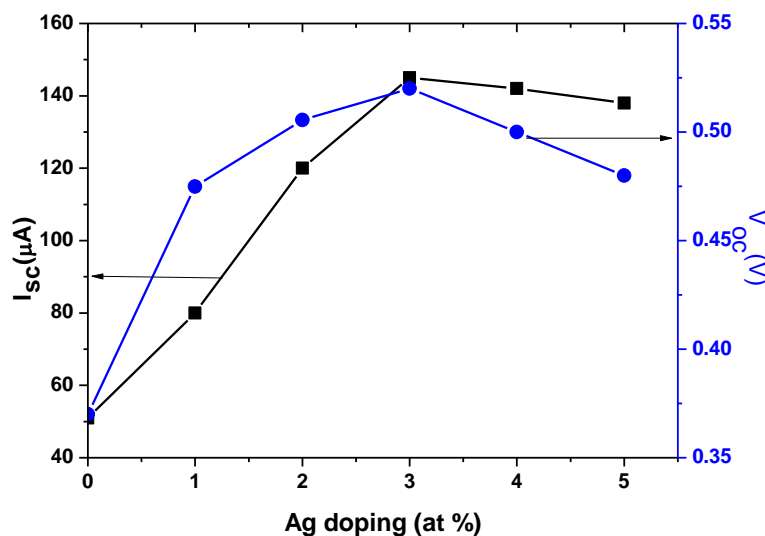

Figure 5.1 Variation of I_{sc} and V_{oc} for the PEC cell formed with Ag:ZnO thin film versus Ag doping

5.3. A.2 Structural analysis

The X-ray diffraction patterns (C_r K_α, λ= 2.2897 A°) of undoped and silver doped ZnO thin films are shown in Fig. 5.2. The spectrum of undoped ZnO thin film shows typical X-ray diffraction pattern of have hexagonal crystal structure (JCPDS No. 80-0074). Ag can be incorporated in ZnO system either by substitution of Zn^{2+} or by interstitial atom [14]. If the silver is substituted for $Zn^{2+,}$ a corresponding peak shift would be expected in XRD. Simultaneously, compared to the (002) diffraction peak of typical undoped ZnO film which located at 2θ = 52.13°, the (002) and that of 1 At % to 4 At % located at, 2θ = 52.15°, 52.17°, 52.18° and 52.23° respectively. Jeong et al. [15] reported that for 4 wt % silver doped ZnO, the position of (002) was shifted to lower 2θ (0.700°) with increasing Ag

dopant, in our case shift is small (0.100°). It is might be due to the segregation of Ag particles in the grain boundaries of ZnO crystallites rather than going into the lattice of ZnO or only an insufficient quantity may be going to substitutional Zn site.
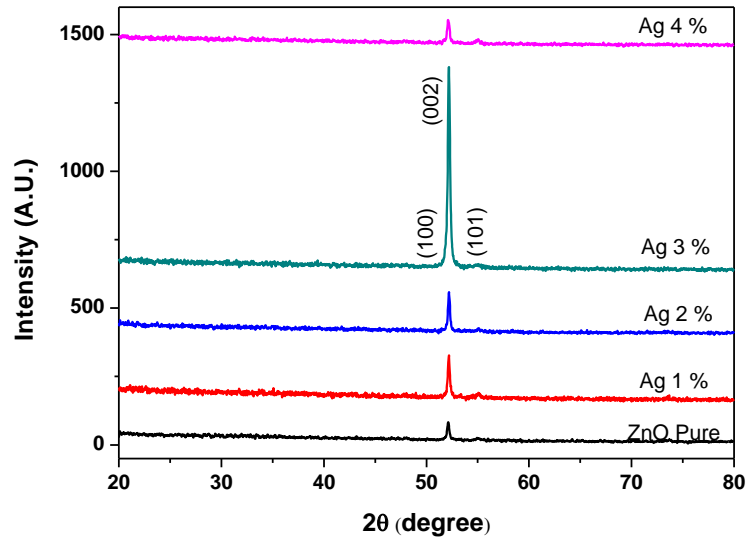
Figure 5.2 XRD patterns of undoped and doped ZnO thin films prepared by spray pyrolysis onto glass substrates

No peaks corresponds to either Ag metal or any of its oxide were observed in the patterns, which indicates that, within the limit of X–ray diffraction no additional phase is present in the Ag:ZnO films. It is evident from XRD analysis and previous reports, the Ag doped ZnO films have preferred orientation along (002) plane [16]. Because Ag^+ ions have larger ionic radius (0.122 nm) than Zn^{2+} (0.074 nm), they either substitute ions of Zn^{2+} leading to the distortion of unit cell or segregate at the grain boundaries of ZnO and hence induced considerable distortion and faster growth of ZnO grains [17]. Ag^+ would preferentially choose to site in the vicinity of grain boundaries due to its larger radius [18]. The intensity of the ZnO (002) plane increases with Ag until 3 At % and then decreases with further increase of the Ag which suggest that 3 At % Ag doping can enhance the ZnO (002) preferential orientation but excess Ag doping will deteriorate it. This may be due to the fact that 3 At % Ag quantity of Ag atoms exists an interstitial that share the oxygen with

Zn atoms and hence improve the (002) orientation. The excess Ag doping atoms can be energetically favorable to coalesce into metallic silver cluster and hence inhibit c – axis prepared growth of ZnO film.

5.3. A.3 Morphological properties
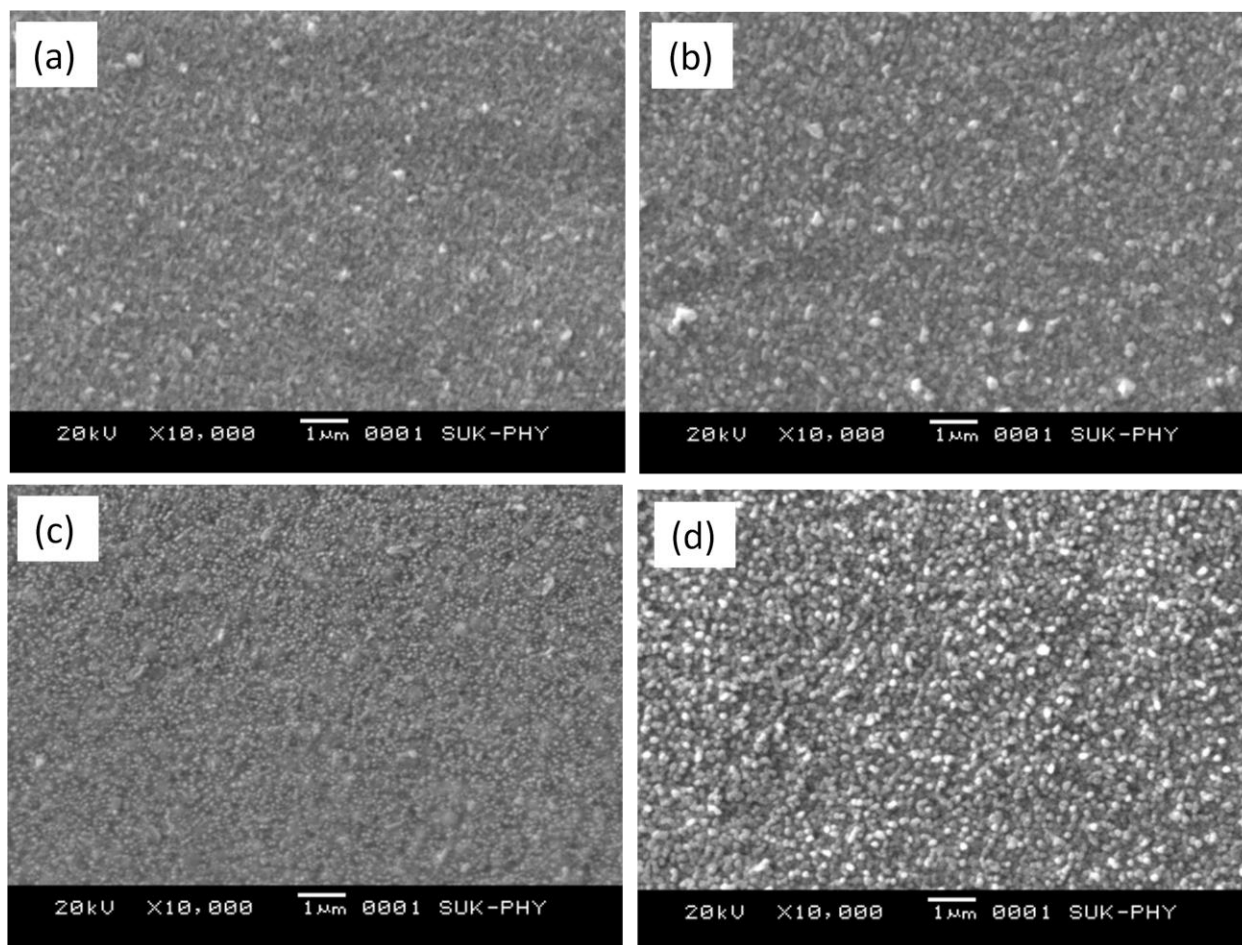
Figure 5.3 Scanning Electron micrographs of (a) ZnOAg$_1$, (b) ZnOAg$_2$, (c) ZnOAg$_3$, (d) ZnOAg$_4$,

The morphology of the ZnO thin films were examined by scanning electron microscopy. Fig. 5.3 (a-d) shows SEM images of 1 % - 4 % Ag doped ZnO thin films, respectively. The 3 % of Ag doped ZnO thin film shows the smooth surface covered with grains. The improvement in the grains was observed as Ag doping percentage increases.

Average grain size varies from 140 to 166 nm with Ag doping concentration. The surface of 3 At % Ag doping film was found to be hydrophobic [19].
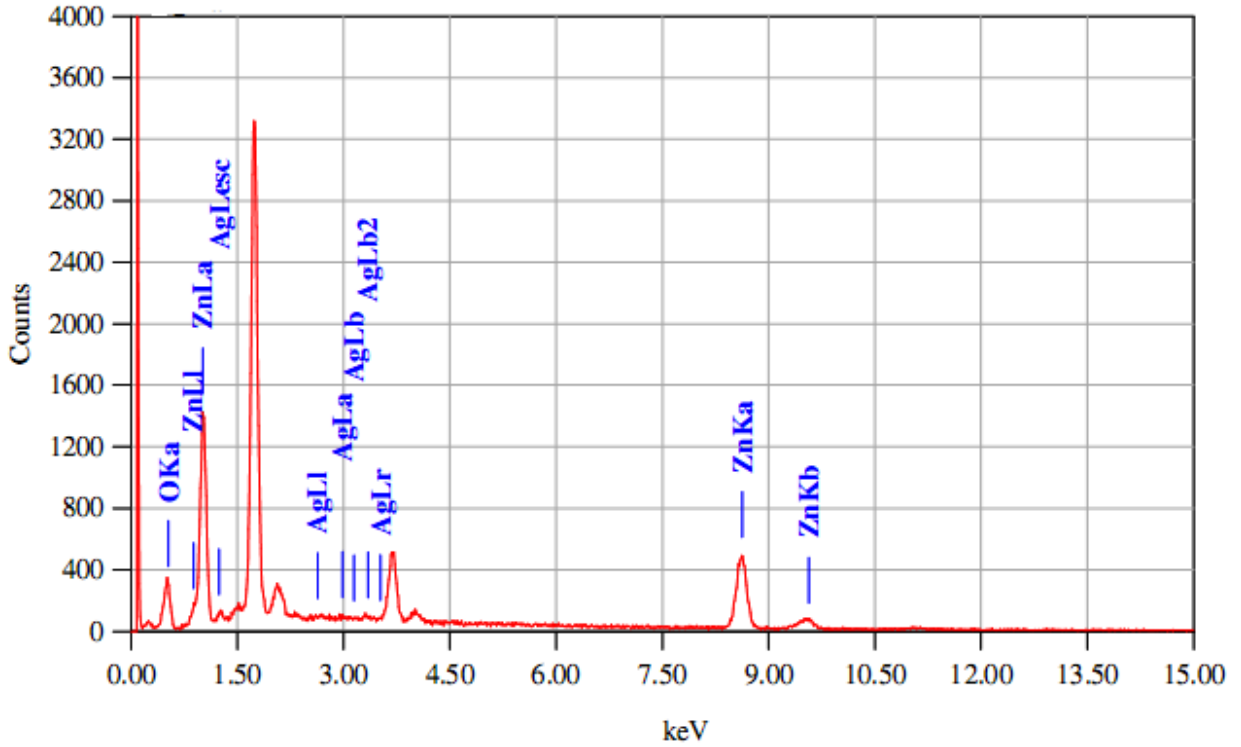
Figure 5.4 EDAX pattern of typical 3 At % Ag doped ZnO thin film

Table 5.1 EDAX data typical 3 At % Ag doped thin films

Element	(Mass %)	At %
O K	17.82	47.09
Zn K	81.27	52.55
Ag L	0.91	0.36
Total	100	100

The chemical composition is determined by the EDAX technique for the ZnO sample deposited at 3 At % Ag doping (Fig. 5.4). The values of atomic wt % and mass % of elements are listed in table 5.1. It has been observed that the atomic wt % of Ag in the film is less than that of starting solution.

5.3. A.4 Optical properties
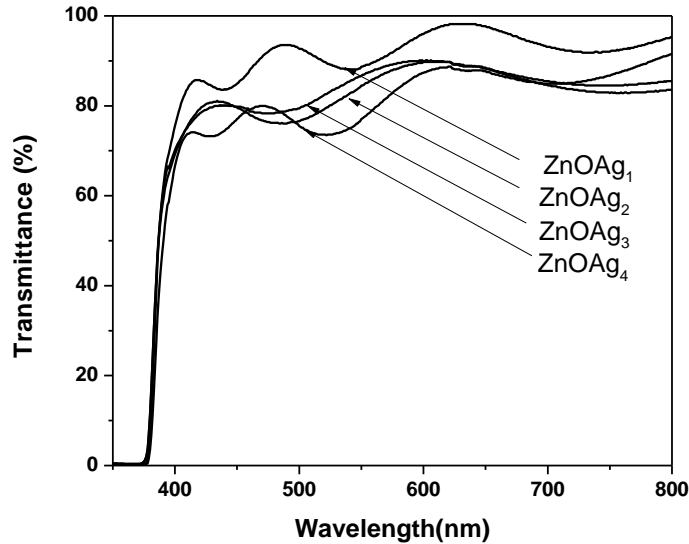
Figure 5.5 Optical transmittance spectra of ZnO thin films deposited at various silver doping concentrations

The optical transmittance spectra for the thin films recorded over wavelength range 300–800 nm at room temperature (Fig.5.5.). The sinusoidal nature of transmittance spectra is due to the light interference at the interface between the film and substrate materials. The transmittance of Ag:ZnO films in the visible region decreases from 89 to 74 % as the Ag doping percentage increases. This decrease in the transmittance value of the Ag–ZnO thin films are may be due to the grain boundary scattering. The optical band gap energy (E_g) is an intrinsic property of the semiconductor and is estimated from optical absorption measurement. The optical band gap energy is found to be 3.24 eV for pure ZnO thin films, which is comparable to the band gap energy reported by Natsume et al. [20] and for the Ag–ZnO thin films, it is found to be in the range of 3.23 eV. With increasing silver contents, the absorption edge shifted slightly to a longer wavelength region. The band gap also narrowed with increasing Ag contents. Similar results are also observed by Sahu [21].

Photoluminescence properties

The PL spectra of undoped and Ag doped ZnO thin films were recorded at room temperature (Fig. 5.6). Spectra reveal several bands, therefore deconvolution of the spectra

was performed assuming the emission peaks to be Gaussian. The deconvoluted spectrum of typical film $ZnOAg_3$ is shown in Fig.5.6 (b).

The UV band related deep- level emission peak, which is observed in ZnO thin films. The new emission peak at about 500 nm is due to Ag doping. The green band in visible region is generally explained by the radiative recombination of the photogenerated holes with electrons and structural defects in crystal. It might be due to oxygen vacancies and Zn interstitials. As Ag doping increases in ZnO lattice the excessive cation may generate more anion vacancies and make the concentration of the excitation increases. The Ag^+ ions are substituted for Zn^{2+} ions in the crystal, induced hybridization and charge transfer from a donar – derived impurity band to unoccupied 3d states at the ZnO Fermi level [22]. The valency of Ag could be assumed to be +1 or/and +2 in the Ag-doped ZnO films. The radius of Ag^+, Ag^{2+} and Zn^{2+} ions are 0.089, 0.072 and 0.122 nm, respectively. So, the Ag^+, Ag^{2+} substitute Zn^{2+} and the Ag^{2+} interstitial might be the main impurity in the Ag-doped ZnO films. The Ag^+ substitute was an accepter while the Ag^{2+} interstitial was a donor. When the amount of Ag less than 3 At % in the growth of Ag-doped ZnO films, the concentration of V_{Zn} and Z_{ni} might decrease, this resulted in the weakened blue band. With the increasing of Ag doping, the concentration of Ag^+ substitute and Ag^{2+} interstitial would increase and reach to the maximum, and then would decrease. Z_{ni} might increase with the increasing of the Ag+ substitute while Z_{ni} defects might increase with the increasing of the Ag^{2+} interstitial because ZnO was a self-assemble oxide compound. So the blue band became strong with the Ag increasing, and reached to the summit when Ag 3 At %, and then decreased [23].
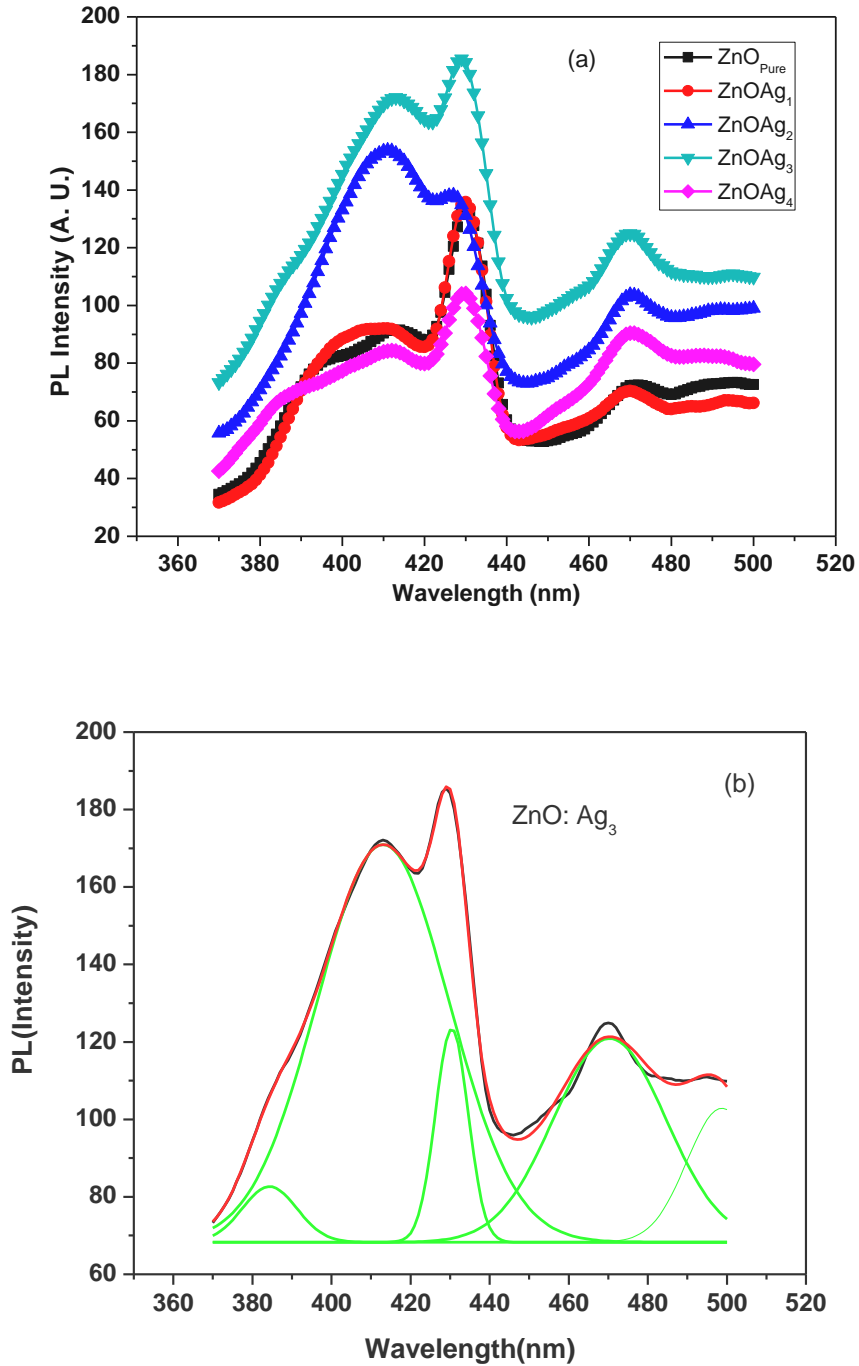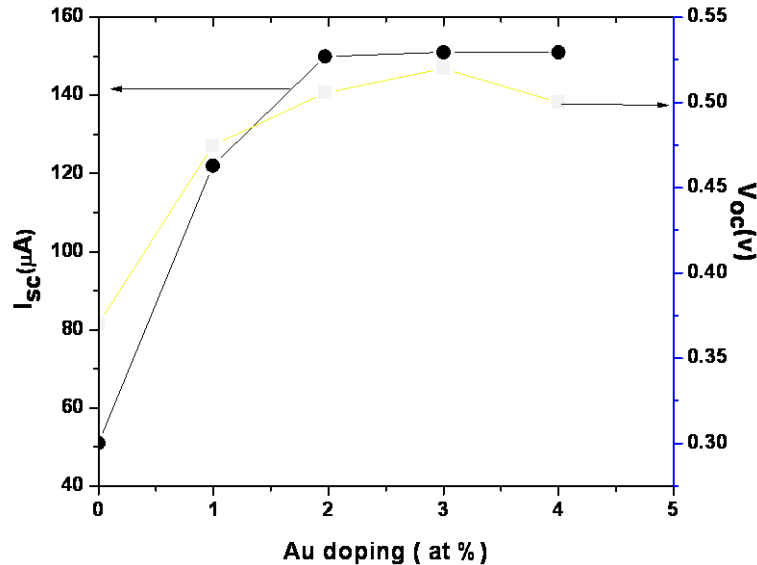
Figure 5.6 (a) PL spectra of Ag:ZnO thin films as a function of silver doping percentage (b) Deconvoluted spectrum of typical ZnO : Ag₃ film

B. Characterization of Au:ZnO thin films

5.3. B.1 Photoelectrochemical (PEC) characterization

Figure 5.7 Variation of I_{sc} and V_{oc} for the PEC cell formed with Au:ZnO thin films versus Au doping concentratin

From I-V measurement it seen that the I_{sc} and V_{oc} values increase as the Au percentage increases. This increment in the current values is related to the surface plasmons resonance (SPR) of Au nanoparticles. The variation in I_{sc} and V_{oc} values with concentration of Au is shown in Fig.5.7. The oscillation of high density free electrons occurs under the irradiation of light, which is called SPR. Under the irradiation of incident light having wavelength larger than the particle size, the high density electrons of the noble metal nanoparticles form an electron cloud and oscillate. When Au particles combining with ZnO, electrons are accumulate at the interface between Au and ZnO, which leads to the electron transfer from the Au particle to the ZnO side [24]. The reason is that the strong interaction coupling between Au and ZnO results in electron transfer from Au to ZnO during the formation of ZnO-Au nanoparticles [25].

5.3.B.2 Structural analysis
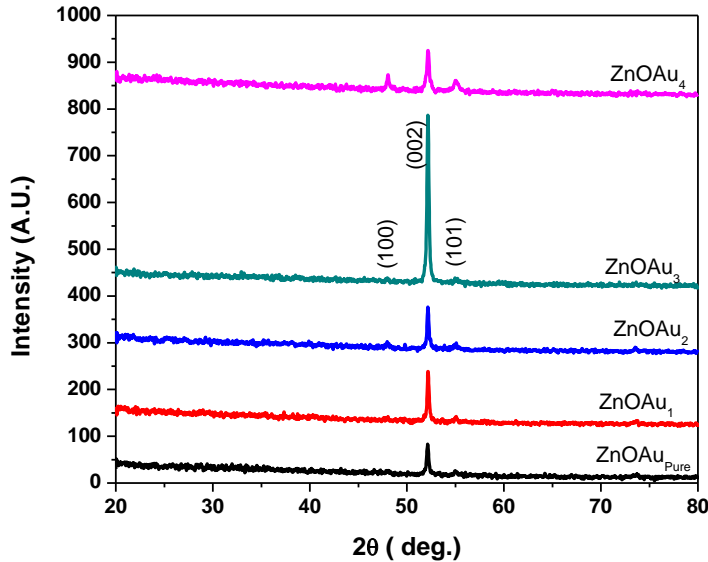
Figure 5.8 XRD patterns of undoped and Au:ZnO thin films prepared by spray pyrolysis technique onto glass substrates for different gold doping concentrations

The structural changes and identification of phases were studied with help of XRD technique. The diffraction angle (2θ) was varied between 20 to 80 ^{0}. Fig.5.8 shows XRD pattern of the Au:ZnO thin film for various Au doping concentrations. The XRD patterns reveal that all the films show polycrystalline in nature. The diffraction peaks are good agreement with JCPDS data card No. 80-0074. Upon increasing Au concentration, (002) plane of ZnO begins to improve up to 3 At % Au concentration and then decreases. The excess Au doping atoms can be energetically favorable to coalesce into metallic gold cluster and hence inhibit c – axis preferred growth of ZnO film [26-27].

5.3.B.3 Morphological properties

Fig. 5.9 (a-d) shows the SEM micrographs at different doping concentrations of gold. With increasing Au doping concentration in ZnO matrix, grain size increases. At 3 At % Au doping grains are spherical, uniform and compact and beyond 3 At % morphology looks like fish scales. The compositional analysis of typical 3 At % Au doped film is carried out by

EDAX technique (Fig. 5.10). It is observed that oxygen rich films were prepared by SPT technique. The oxygen contained is more due to environment oxygen. The elements and their mass % and atomic wt % are listed in table 5.2.
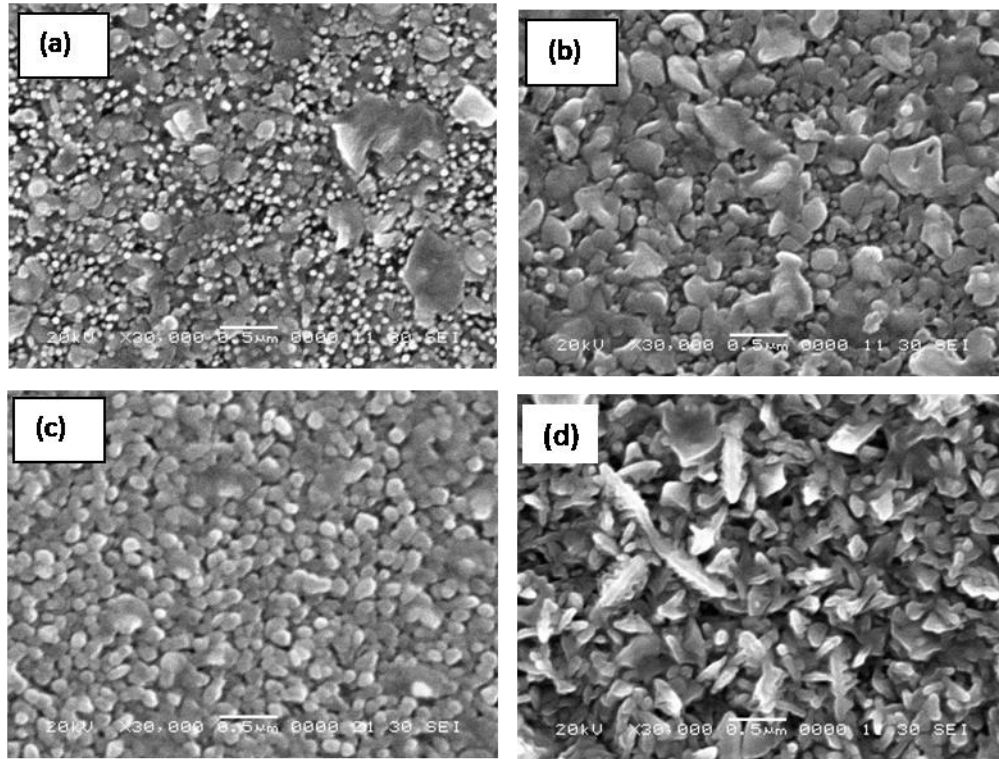
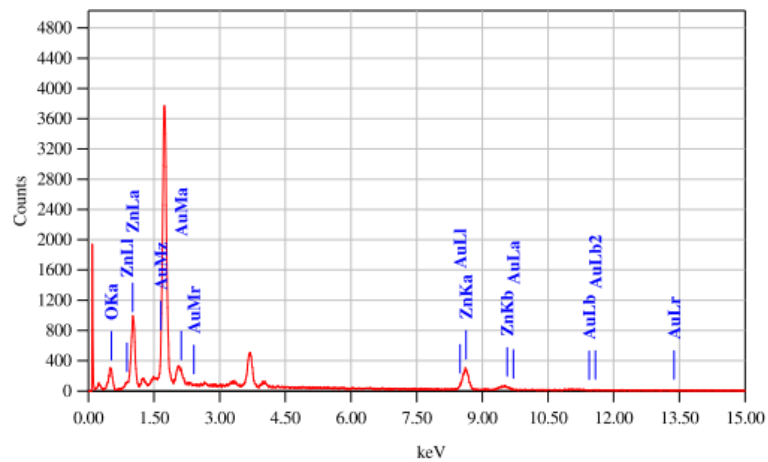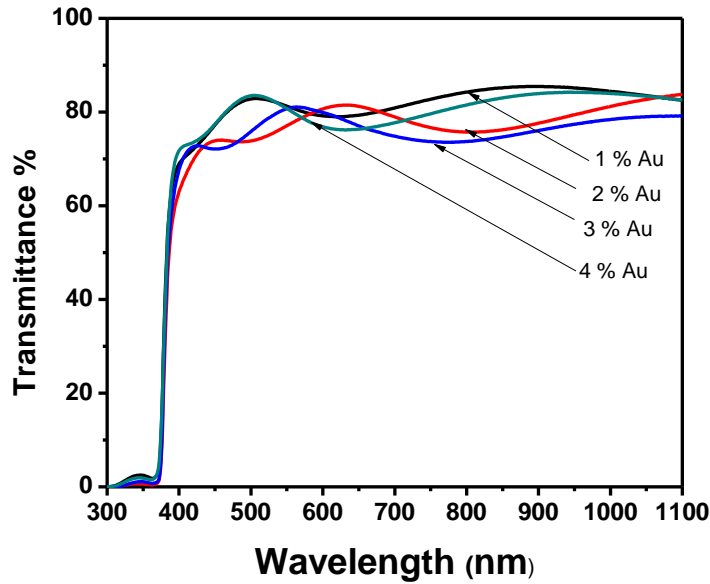**Figure 5.9 SEM of (a) ZnOAu$_1$, (b) ZnOAu$_2$, (c) ZnOAu$_3$, (d) ZnOAu$_4$,**

Figure 5.10 EDAX pattern of typical 3 At % Au-doped ZnO thin film

Table 5.2 EDAX data typical 3 At % Au doped thin films

Element	(Mass %)	At %
O K	24.47	57.83
Zn K	74.58	41.79
Au L	0.95	0.38
Total	100	100

5.3. B.4 Optical properties

Figure 5.11 Optical transmittance spectra of Au:ZnO thin films deposited at various gold doping concentrations

The transmittance spectra for Au:Zno thin films are shown in Fig. 5.11. The sinusoidal nature of transmittance spectra are due to the light interference between film and glass substrate [28]. The average transmittance is about 80 % in visible region. The reduction in transmittance may be attributed to strong scattering and absorption. The

strong scattering resulted from the existence of grain boundaries, the point defects and disorders in ZnO films.

Optical absorption spectra of Au:ZnO samples are shown in fig.5.12 and inset shows plot of $(\alpha h\nu)^2$ vs hν of typical film doped with 3 At % Au doping. The absorption edge is observed at 389 nm. The band gap energy for typical film doped with 3 At % Au is 3.26 eV. There is slight decrease in band gap energy with increase in Au concentration, confirms the progressive improvement of the structural quality of ZnO matrix [29].
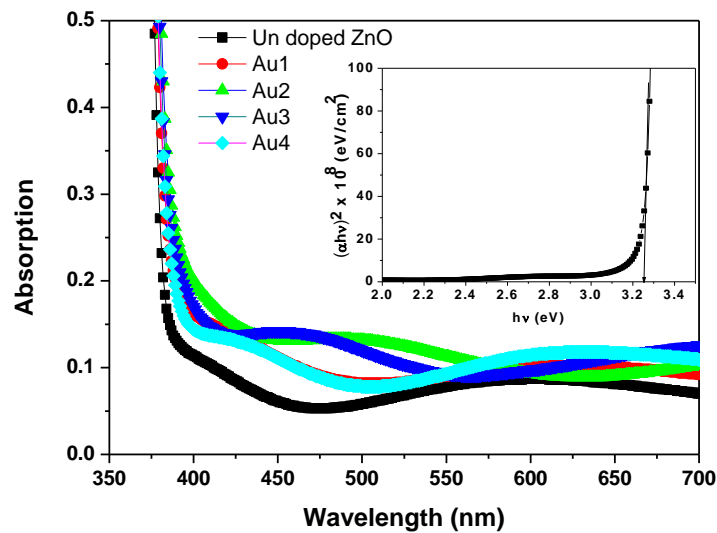
Figure 5.12 Optical absorption spectra of Au:ZnO thin films deposited at various gold doping concentrations

Photoluminescence properties

The PL measurements were performed at room temperature with an excitation wavelength 290 nm. Fig. 5.13(a) show PL spectra of the pure ZnO and 3 At % Au doped ZnO thin films and (b) shows deconvolatoion of undoped ZnO, (c) shows deconvoation of 3 At % Au:ZnO film. The. Pl spectra of pure ZnO show UV peak at 334 nm (weak), 360 nm (strong) and relatively weak visible peaks at 400, 420 and 440 nm. However, for 3 At % Au doped ZnO film we can observed UV emission at wavelength 337 (weak) and 360 nm (strong) and visible emission at wavelength 420 nm. The UV intensity of the Au doped ZnO

is increased by factor of 4.5 and visible emission intensity is increased by factor 2 compared with undoped ZnO film. Chen et al. found that the UV and visible emission intensities could be tailored by Au nanoparticles [30]. The significant changes in photoluminances (PL) of Au- ZnO composite nanoparticles were also reported by Lee et al. and Mishra et al. [31-32]. In the presence of Au particles, the enhancement of energy density of excitation source resulted in the improvement of excitation process and decay rate in emission process [33-34]. The visible emission at wavelength 440 nm and 400 nm are completely suppressed, while visible emission at wavelength 420 nm increases remarkably. Similar results are reported by Li et al. [35] and Sing et al. [36].
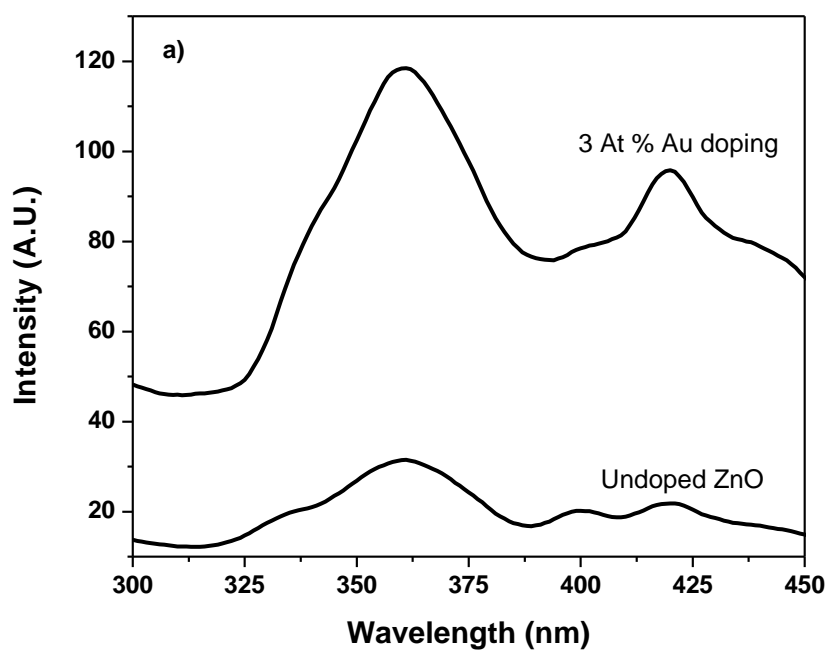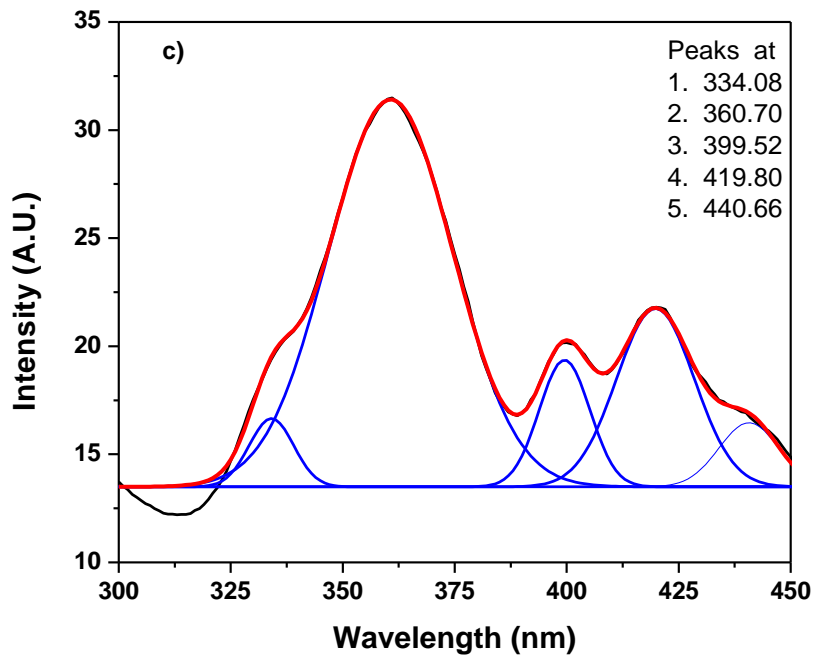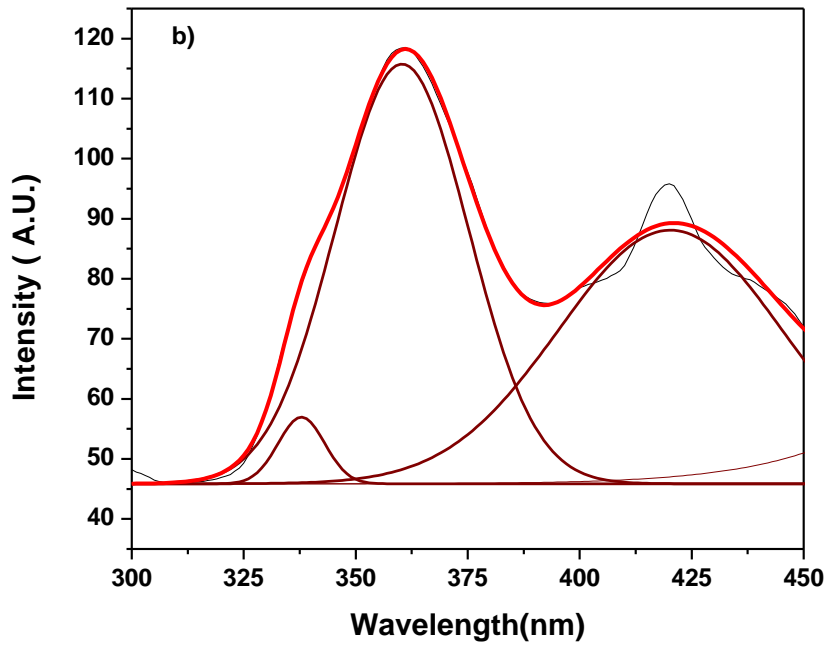
Figure 5.13 (a) Photoluminescence of undoped and 3 At % Au doped ZnO thin film
(b)deconvolation of undoped ZnO (c) deconvalation of 3 At % Au doped ZnO

C. Photoelectrocatalytic degradation of methylene blue (MB) and inactivation of *E.coli*

5.3. C.1 Photoelectrocatalytic degradation of MB

Effluents from the textile dyeing and finishing industries contain high levels of environmental contaminants, strong color, suspended solids, surfactants and some heavy metals. There are three methods for treatment of colored materials, including (1) physical methods employing precipitation, adsorption, and reverse osmosis; (2) chemical methods via oxidation (using air oxygen; ozone, NaOCl, and H_2O_2 as oxidants) and reduction (e.g., $Na_2S_2O_4$); and (3) biological methods including aerobic and anaerobic treatment [37]. The disadvantage of precipitation methods is sludge formation. The disadvantage of adsorption is that the adsorbent needs to be regularly regenerated. This is associated with additional costs and sometimes with very time-consuming procedures. Biological treatment is ineffective in cases where complicated aromatic compounds are present. Advanced oxidation processes (AOPs) provide a promising treatment option for textile wastewater compared to other treatment methods [38-40]. The advantage of R:ZnO/UVA (R= Ag, Au) photoelectrocatalytic processes is that they prevent any sludge formation during the treatment process. They can be carried out at ambient conditions with the possibility of completely mineralizing organic compound to CO_2 [41]. This study was undertaken to evaluate the effectiveness of the R:ZnO/UVA (R= Ag, Au) photoelectrocatalytic process in the decolorization of dye. Methylene blue (MB) was selected as a model dye for photocatalytic degradation using R:ZnO (R= Ag, Au) electrodes.
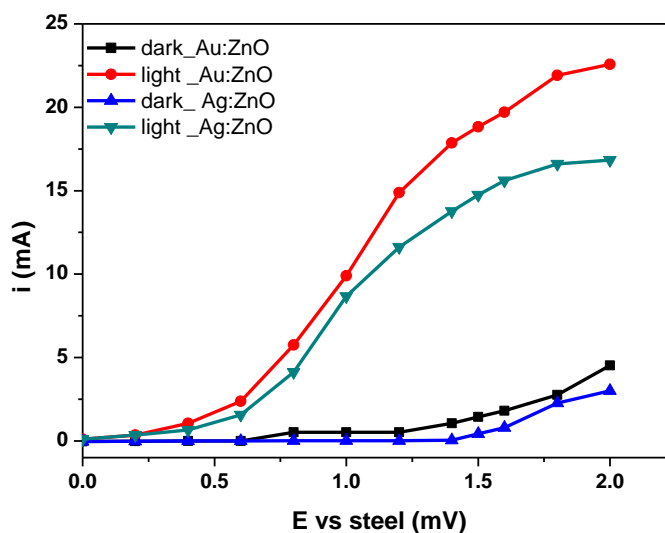
Figure 5.14 Dark and light current for Ag:ZnO and Au:ZnO electrodes (64 cm²) under UVA illumination for 0.1 M NaOH against applied voltage w.r.t. steel counter with a flow rate of 12.2 lh⁻¹

The testing of Ag:ZnO and Au:ZnO photocatalyst has been carried out by measuring i-E curve. An i-E curve of a 64 cm² Ag:ZnO and Au:ZnO catalyst in 0.1 M NaOH using a steel counter electrode at a distance of 1 mm under UVA illumination is shown in Fig. 5.14. The current reached to its saturation value of about 14.6 and 18.7 mA for Ag:ZnO and Au:ZnO respectively at bias voltage of 1.5 V. The average photocurrent during degradation of MB experiment is 14 and 18 mA for Ag:ZnO and Au:ZnO respectively. In last part of experiment there is slight decrease in photocurrent due to intermediates byproduct formed during photocatalytic reaction. Fig. 5.15 shows extinction of MB with reaction time for Au:ZnO film where as inset shows extinction for that of Ag:ZnO electrode. It is observed that initial degradation rate is very fast in case of both electrodes. Relatively rate of degradation of MB for Au:ZnO is high than that of Ag:ZnO film. The percentage of decolorization is calculated using formula,

$$Decolorization(\%) = \frac{A - A_0}{A_0} \times 100 \qquad (5.1)$$

where A_0 is absorbance at t= 0 and A is absorbance at time t.
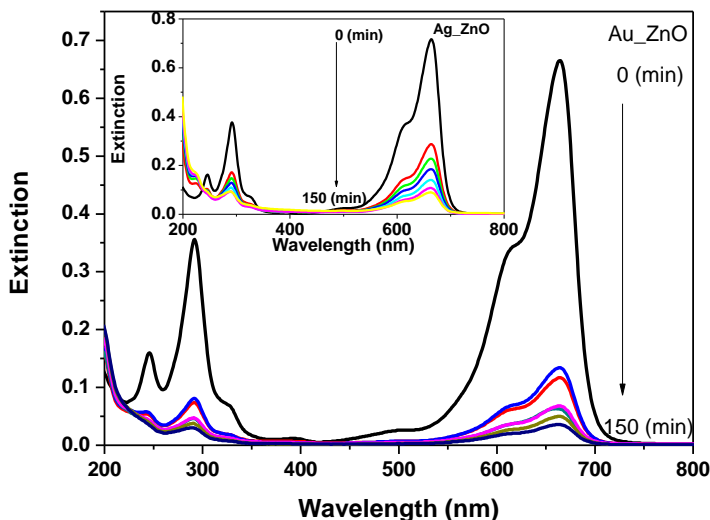
Figure 5.15 Extinction spectra of MB with Au:ZnO under UVA light illumination , inset Extinction spectra of MB with Ag:ZnO under UVA light illumination

It is found that percentage of decolorization for Au:ZnO is 94 % and that of Ag:ZnO is 87 %. Variation of $\ln(C/C_0)$ with reaction time and $\ln(COD/COD_0)$ of MB for Au:ZnO and Ag:ZnO catalyst are shown fig 5.16 (a) and (b) respectively. Slopes of these curves are used for further calculation of kinetic parameters such as k, k', k'',k''' and p using kinetic relations 4.9 to 4.11. These kinetic parameters for ZnO , Ag:ZnO and Au:ZnO are listed in table 5. 2.

The percentage of COD reduction is less than the percentage of decolorization which may be due to the formation of smaller organic compound as reduction of chemical oxygen demand reflects the extent of degradation or mineralization of organic species. Therefore, it requires more time to achieve complete mineralization of MB. From the kinetic parameters and degradation efficiency it is concluded that Au: ZnO photocatalyst gives better performance in degradation of MB.
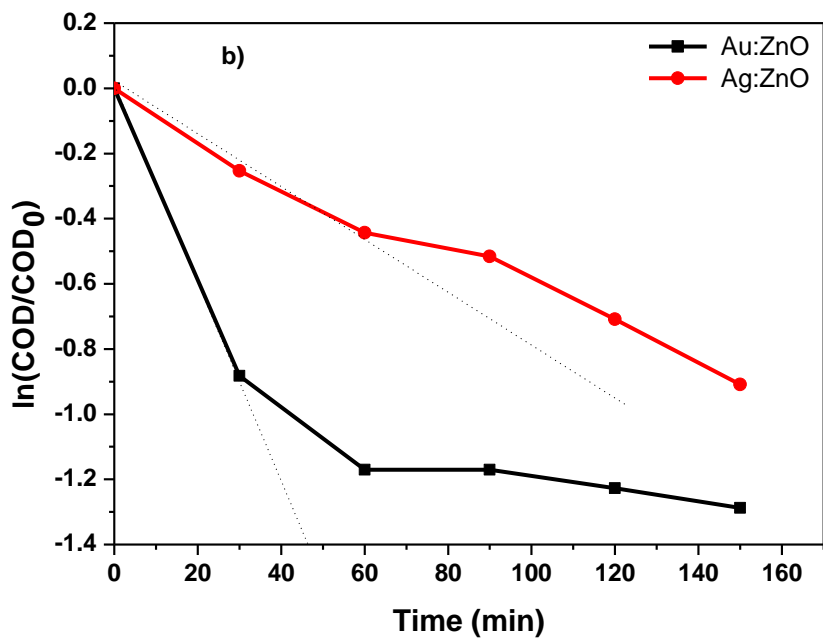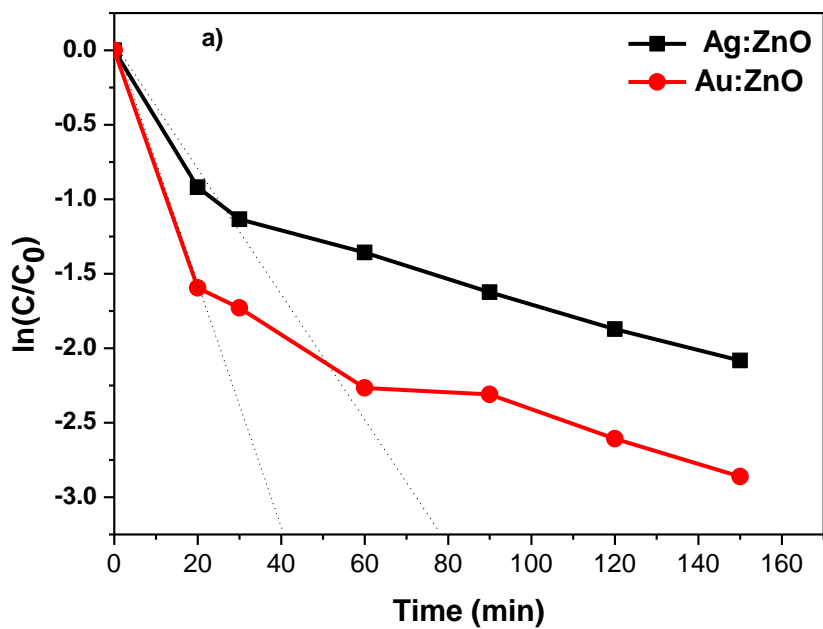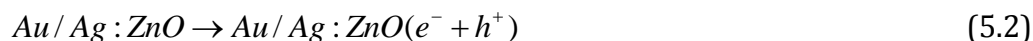
Figure 5.16 Detoxification of MB with Ag:ZnO and Au:ZnO UVA light illumination (a) kinetics of degradation (b) Variation of ln(COD/COD$_0$) with reaction time

Table 5.3 Kinetic parameters in photodegradation of BM with ZnO, Ag:ZnO and Au:ZnO films

Catalysts	K 10^{-3} **(s^{-1})**	K', 10^{-3} (cm^3.s^{-1})	K", 10^{-5} (cm/s)	K''' **(M^{-1})**	P= 1/k''' , 10^{-5} **(M)**	Efficiency %
ZnO	1.2	2.4	3.75	5790	0.172	48
Ag:ZnO	6.83	13.6	21.25	16470	6.07	80
Au:ZnO	13.5	27.0	42.18	15320	6.52	84

Based on the photocatalytic reaction the following mechanism has been proposed,

$$Au/Ag : ZnO \rightarrow Au/Ag : ZnO(e^- + h^+) \qquad (5.2)$$

$$h^+ + OH_{ad}^- \rightarrow {}^{\bullet}OH_{ad} \qquad (5.3)$$

$$h^+ + H_2O_{ad} \rightarrow {}^{\bullet}OH_{ad} + H^+ \qquad (5.4)$$

$$e^- + O_2 \rightarrow {}^{\bullet}O_2^- \qquad (5.5)$$

The photo generated holes at valance band migrates to the surface of semiconductor and combine with ${}^{\bullet}OH$ adsorbed on ZnO surface result into oxidation of MB. The electron in conduction band, combine with O_2 and forms ${}^{\bullet}O_2^-$ radical. Both these radicals are strong oxidizing agents which oxidize the organic molecules landed on the surface of the ZnO resulting the formation of intermediate organic species and subsequently complete oxidation of these species to water and carbon dioxide as,

$$Ag/Au : ZnO({}^{\bullet}O_2)or({}^{\bullet}OH) + MB \rightarrow Intermediates \rightarrow CO_2 + H_2O \qquad (5.6)$$

In the presence of Au on the surface of ZnO improves the photocatalytic activity of ZnO. The increase in photo-activity may be attributed to effect of Au in following way: Au increases absorbance in visible region, interacting in ZnO structure, electron scavenging by Au and the decrease in Fermi level to more negative side subsequently improvement in interfacial charge transfer process at ZnO interface by Au particle. Further regarding electron transfer process at the interface of ZnO and interfacial contact between Au on ZnO, so that the electron after excitation migrates to metal through conduction band driven by an external applied electric field as result the ultimate minimization of electron hole recombination and helps in improving the photo catalytic efficiency of Au:ZnO catalyst. So it combines effect of all these processes at the surface of film which results in overall increases in photo activity of Au:ZnO.

The Fu et al. and Gong et al. [42-43] gives degradation of pathways in which MB undergo a progressive degrading oxidation of one methyl group by an attack from $^{\bullet}OH$ radical, producing an alcohol, then an aldehyde, which is spontaneously oxidized into acid, decarboxylates into CO_2. However FTIR analysis of MB shows (Fig. 5.17) that azo bond present in the final intermediate formed after photoelectrocatalytic degradation.
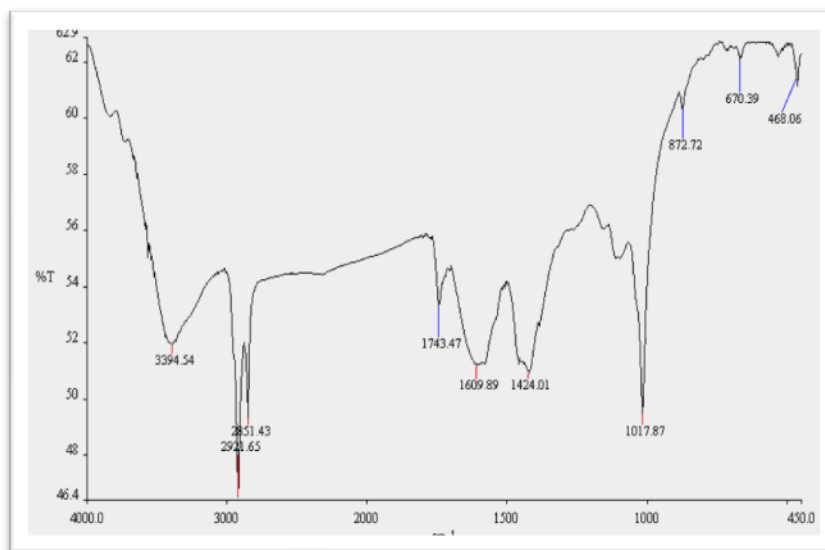
Figure 5.17 FTIR spectra of MB with Au:ZnO thin film after photoelectrocatalytic reaction
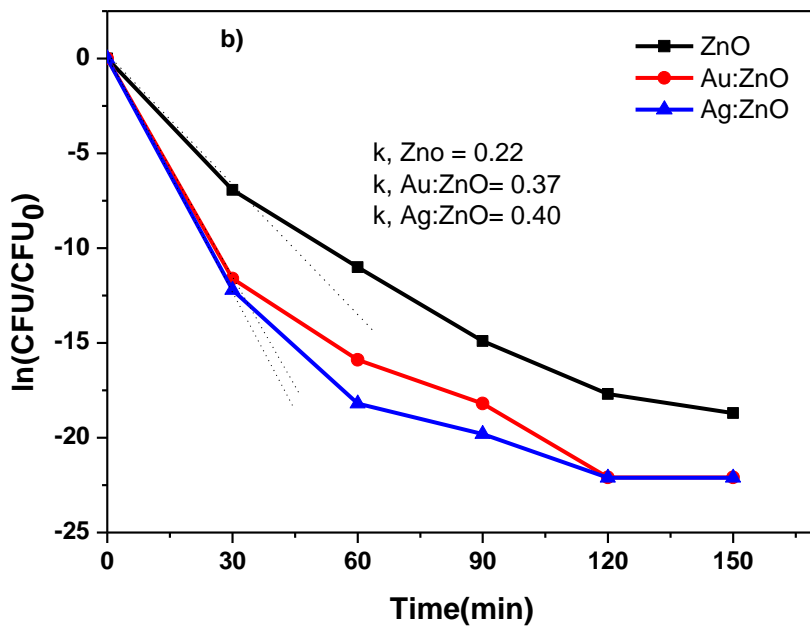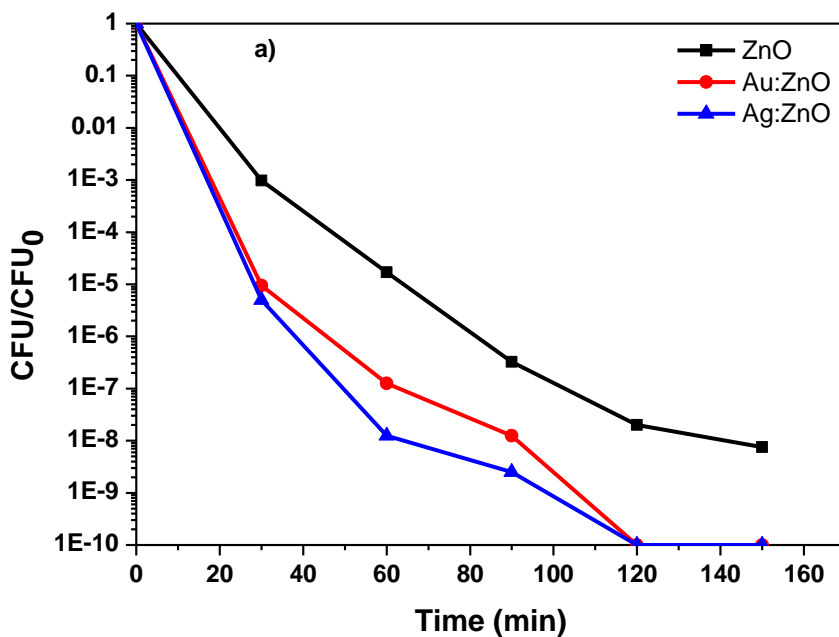
5.3. C.2 Photoelectrocatalytic inactivation of *E.coli*

Figure 5.19 Normalized viable count of *E.coli* (a) and its kinetics (b) for pure ZnO, Au:ZnO and Ag:ZnO

The well developed one loop (10^{10} CFU/ml) of *E.coli* suspended in 0.8 % Na_2SO_4 solution and circulated through the photoelectrocatalytic single cell using ZnO, Ag:ZnO and Au:ZnO in separate experiment setup. Fig 5.19 (a) shows CFU per ml with reaction time and (b) shows In (CFU/CFU$_0$) with inactivation reaction time. Inactivation rate constant for ZnO, Ag:ZnO and Au:ZnO are 0.22, 0.38 and 0.38 min^{-1}. It is observed that rate constant for Ag:ZnO is relatively high compared to ZnO and Au:ZnO. It is due to silver is more reactive for bactericidal activity than ZnO and Au:ZnO. 80 % BOD valued reduction is observed for Ag:ZnO and that of Au:ZnO is 75 %. It has been well documented that suspended nobel metal nanoparticles have strong antibacterial activity [44]. However, the open issue is that nobel metal nanoparticles can easily aggregate, which greatly decreases their antibacterial performance. To overcome this problem, in our study, Ag and Au particles have been doped in ZnO matrix. In addition, due to the strong interaction between Ag and ZnO and Ag:ZnO may undergo the antibacterial process synergistically. For comparison the antibacterial activity of pure ZnO, Ag:ZnO and Au:ZnO are also tested in separate experiment. The antibacterial activity against *E.coli* quantitatively has been determined. These results indicate that Ag:ZnO film has efficient antibacterial capability against *E.coli.*

From the practical and economical point of view, the Ag:ZnO films are more attractive compared to pure ZnO and Au:ZnO. This is due to silver is more reactive than gold to *E.coli* species. Also, Zeng et al. reported that, both Ag and ZnO show antibacterial activities, their antibacterial efficiency is different for Gram Negative (G−) and Gram positive (G+) bacteria. That is, Ag shows better antibacterial activity for G− bacteria than G+ bacteria, while ZnO shows better antibacterial activity for the G+ bacteria than G− bacteria. This phenomenon was also reported in the literature for Ag [45] and ZnO [46-47].

References:

[1]   M. R. Hoffmann, S. T. Martin, W. Y. Choi, D. W. Bahnemann, Chem. Rev., 95 (1995) 69.

[2]   A. L. Linsebigler, G. Q. Lu, J. T. Yates, Chem. Rev., 95 (1995) 735.

[3]   X. Z. Li and F. B. Li, Environ. Sci. Technol., 35 (2001) 2381.

[4]   V. Subramanian, E. Wolf, P. V. Kamat, J. Phys. Chem. :B., 105 (2001) 11439.

[5]   S. W. Lam, K . Chiang, T. M. Lim, R. Amal, G. K. C. Low, Appl. Catal. B: Environ., 72 (2007) 363.

[6]   F. B. Li and X. Z. Li, Chemosphere 48 (2002) 1103.

[7]   X. F. You, F. Chen, J. L. Zhang, M. Anpo, Catal. Lett., 102 (2005) 247.

[8]   V. Vamathevan, R. Amal, D. Beydoun, G. Low, S. McEvoy, J. Photochem. Photobiol. A, 148 (2002) 233.

[9]   F. Zeng, C. Hou S. Z. Wu, X. X. Liu, Z. Tong, S. N. Yu, Nanotechnol., 18 (2007) 055605.

[10]   S. Shrivastava, T. Bera, A. Roy, G. Singh, P. R. Rao, D. Dash, Nanotechnol. 18 (2007) 225103.

[11]   P. Gong, H. M. Li, X. X. He, K. M. Wang, J. B. Hu, W. H. Tan, S. C. Zhang , X. H. Yang, Nanotechnolo., 18 (2007) 285604.

[12]   V. A. Oyanedel-Craver and J. A. Smith, Environ. Sci. Technol., 42(2008) 927.

[13]   M. J. Height, S. E. Pratsinis, O. Mekasuwandumrong, P. Praserthdam, Appl. Catl.: B, Enviorn., 63 (2006) 305.

[14]   D. J. Blinks and R. W. Grimes, J. Am. Ceram. Soc., 76 (1999) 2370.

[15]   S. H. Jeong, D. G. Yoo, D. Y. Kim, N. E. Lee, J. H. Boo, Thin Solid Films, 516 (2008) 6598.

[16]   B. Kulyk, B. Sahraoui, V. Figa, B. Turko, V. Rudyk, V. Kapustianyk, J. Alloys. Compd, 481 (2009) 819.

[17]   S. T. Kuo, W. H. Tuan, J. Shieh, S. F. Wang, J. Eur. Ceram. Soc., 27 (2007) 4521.

[18]   Q. Wang, Z. Xiong, J. Dai, J. Rao, F. Jiang, Opt. Mater 30 (2008) 81.

[19]   D. P. Subedi, D. K. Madhup, A. Sharma, U. M. Joshi, A. Huczko, Int. Nano. Lett., 1(2011) 117.

[30]   Y. Natsume and H. Sakata, Mater. Chem. Phys. 78 (2002) 170.

[21]   D. R. Sahu, Microelectronics Journal 38 (2007) 1252.

[22]   Y. Jin, Q. Cui, K. Wang, J. Hao, Q. Wang, J. Zhang, J. App. Phys., 109 (2011) 053521.

[23]   F. K. Shan, G. X. Liu, W. J. Lee, B. C. Shin, J. Crystal Growth, 291 (2006) 328.

[24]   M. K. Lee, T. G Kim, W. Kim, Y. M. Sung, J. Phys. Chem.: C, 112 (2008) 10079.

[25]   X. Wang, K. Kong, Y. Yu, H. Zhang, J. Phys. Chem., C, 111(2007) 3836.

[26]   P. T. Gao, Y. Ding, W. Mai, W. L. Hughes, C. Lao, Z. L. Wang, Science, 309(2005)1700.

[27]   H. J. Wasserman, J. S. Vermaak, Surf. Sci, 22 (1970) 164.

[28]   Y. M. Lu, C. M. Chang, S. I. Tsai, T. S. Wey, Thin Solid Films, 56(2004)447.

[29]   X. Wang, J. Shi, S. Dai, Y. Yang, Thin Solid Films, 429(2003)102.

[30]   T. Chen, G. Z. Xing, Z. Zhang, H. Y. Chen, T. Wu, Nanotechnology,19(2008)435711.

[31]   M. K. Lee, T. G. Kim, W. Kim, Y. M. Sung, J. Phys. Chem.: C, 112 (2008) 10078.

 [32]   Y. K. Mishra, S. Mohapatra, R. Singhal, D. K. Avasthi, D.C. Agarwal, S. B. Ogle, Appl. Phys. Lett., 92 (2008)043107.

[33]   X. D. Zhang, P. Wu, Y. Y. Shen, L. H. Zhang, Y. H. Xue, F. Zhu, D. C. Zhang, C. L. Liu, Appl. Sur. Sci. 258 (2011) 151.

[34]   C. Sonnichsen, T. Franzl, T, Wilk, G. Vanplessen, J. Feldmann, Phys. Rev.Lett., 88 (2002) 07702.

[35]   X. Li, Y. Ren, Optics Express, 17 (2009) 8735.

[36]   T. Sing, D. K. Pandya, R. Singh, Thin solid Films, 2011, doi: 10.10191 j, t,sf. 2011.11.074.

[37]   S. Kurbus and L. Marechal, Dyes Pigments, 54(2002) 67.

[38]   C. Galindo and A. Kalt, Dyes Pigments, 40 (1998)27.

[39]   I. Arslan, I. Balciogtu, T. Tuhkanen, D. Bahnemann, J. Environ. Eng., 126 (2000)903.

[40]   C. Galindo, P. Jacques, A. Kalt, J. Photochem. Photobiol. A: Chem., 130 (2000) 35.

[41]   A. EI-Dein, J. Libra, U. Wiesmann, Chemosphere, 52 (2003) 1069.

[42]   A. Houas, H. Lachheb, M. Ksibi, Appl. Catal. B: Environ., 31(2001) 145.

[43]   P. Fu, Z. Zhuo, P. Peng, X. Dai, The Chinese Journal of Process Engineering, 8 (2008) 65.

[44]   P. Gong, H. M. Li, X. X. He, K. M. Wang, J. B. Hu, W. H. Tan, S. C. Zhang , X. H. Yang, Nanotechnology, 18 (2007) 285604.

[45]   F. Zeng, C. Hou, S. Z. Wu, X. X. Liu, Z. Tong, S. N. Yu Nanotechnology 18(2007) 055605.

[46]   O. Yamamoto, K. Nakakoshi, T. Sasamoto, H. Nakagawa, K. Miura, Carbon 39(2001)1643.

[47]   J. Sawai, J. Microbiol. Meth. 54(2003)177.

6.1 Introduction

The photocatalytic degradation of organic pollutants in water and air using semiconductors, such as TiO_2 and ZnO, has attracted extensive attention in the past two decades. Previous studies have proved that such semiconductors can degrade most kinds of persistent organic pollutants, such as detergents, dyes, pesticides and volatile organic compounds, under UV-irradiation [1]. Some studies have highlighted that ZnO exhibits better efficiency than TiO_2 for removing organic compounds in water and photo-electronic conversion [2]. However, ZnO undergoes photo-corrosion under UV light illumination, which results decrease in photocatalytic activity [3]. There are several ways to enhance photocatalytic ability. One way is the modification in shape, size and surface properties of ZnO [4-5], second way is to increase wavelength response range (i.e., excitation of wide band gap semiconductors by using visible light) and third way is to dope metals, non-metals and rare earth elements in host lattice [6-7].

The coupling of two semiconductors provides a novel approach to the enhancement in photocatalytic activity. Recent, studies have shown that binary oxides viz. TiO_2/SnO_2, TiO_2/ZrO_2, TiO_2/MoO_3, TiO_2/CdS, TiO_2/Fe_2O_3, TiO_2/WO_3, CdS/ZnO, CdS/AgI, ZnO/ZnS, $Fe_2O_3/ZnO/TiO_2$ and Fe_2O_3/TiO_2 etc. can provide a more efficient charge separation, increased lifetime of charge carriers and enhanced interfacial charge transfer to absorbed substrates [8-15]. However there is no detail study on ZnO/TiO_2 binary thin films.

The coupled ZnO/TiO_2 semiconductor photocatalysts may increase the photocatalytic efficiency by increasing the charge separation and extending the photo-responding range [18]. It is expected that in ZnO/TiO_2 binary oxide material used, not only to obtain higher efficiency but also to avoid the photo-corrosion of ZnO.

This chapter covers the fabrication and characterization of spray deposited coupled ZnO/TiO_2 thin films. These films were characterized for their structural, morphological, optical and photoelectrochemical properties. The photoelectrocatalytic degradation of MB dye, textile effluent and inactivation of bacteria has been investigated with coupled ZnO/TiO_2 film in the presence of UV illumination. Finally photo – bio coupled hybrid system has been developed to increase degradation efficiency.

6.2 Experimental

6.2.1 Prepearation and characterization of ZnO/TiO$_2$ thin film

The ZnO/TiO$_2$ thin films are prepared as per procedure given in section 3.3.4**.** The structural, optical, morphological, and Photoelectrochemical properties were studied. Large area (100 cm^2) electrodes were tested in a thin (1mm) flow-through photoelectrochemical detoxification reactor employing a stainless steel counter-electrode and broadband UVA light and used it in degradation experiments.

6.2.2 Photoelectrocatalytic decolorization of MB and textile effluent

Methylene Blue (MB) dye (200 ml, 1 ppm) was circulated through single cell photoelectrocatalytic reactor. Samples were collected using 10 ml plastic syringe at different time interval (0, 30, 60, 90, 120 minutes) until 180 minutes. The concentration of the dye was determined from the absorbance observed at its λ_{max} using UV-Vis spectrophotometer. Similar experiment was carried out for textile industry effluent obtained from Yashwant Textile Processing Industry, Ichalkaranji, India. Textile effluent was used without any further dilution. The decolorization of textile effluent was determined using American Dye Manufacturing Institute (ADMI) removal ratio [19]. The COD was estimated before and after the treatment using oxidation method.

6.2.3 Metabolite analysis

The photoelectrocatalytic degradation was monitored by using UV-vis spectroscopy analysis. The metabolites produced during degradation, were extracted with equal volumes of ethyl acetate; dried over anhydrous Na$_2$SO$_4$ and dissolved in HPLC grade methanol and directly used for HPLC study. FTIR (Perkin Elmer, US) was used for investigating the changes in surface functional groups of the samples, before and after decolorization. FTIR analysis was done in the mid IR region of 400-4000 cm-1 with 16 scan speed. The pellets were prepared using spectroscopic pure KBr (5:95) and fixed in the sample holder for the analyses. The by-products formed during degradation have been identified by GCMS technique.

6.2.4 Phytotoxicity analysis

Phytotoxicity of textile effluent was performed in order to assess the toxicity of textile industry effluent for common agricultural crop. The obtained byproduct was

dissolved in water to make a final concentration of 1000 ppm. Ten seeds of Sorghum vulgare and Phaseolus mungo plants were sowed into a plastic sand pot with daily watering of (5 ml) textile effluent (1000 ppm) and its degradation metabolites (1000 ppm) were obtained after degradation by photoelectrocatalytic ZnO/TiO_2. Control set was carried out using distilled water (daily 5 ml watering) at the same time. Germination (%) and length of shoot and root was recorded after seven days. The study was carried out at room temperature.

6.2.5 Photoelectrocatalytic inactivation of bacteria

The photoelectrocatalytic inactivation test was performed using serial dilution method [20]. In this work *E.coli, Bacillus*, *Salmonella*, and *Staphylococcus* were employed during the inactivation test. Well developed one loop of each bacteria suspended in 200 ml of 0.8 % Na_2SO_4 solution in four sterile bottles so that bacterial population reach to the order of 10^9 CFU/ml. This bacteria contained solution was circulated similarly as in case of MB degradation experiment. After equal interval of time 100 μL serial dilution of this suspension was placed onto agar agar medium. The plates were incubated at 37 ^{o}C for 48 hours. The colony forming units (CFU) count and inactivation rate was calculated.

6.2.6 Photo-bio coupled degradation of Methyl Red

This study is part of effort to develop new coupling method by using photoelectrocatalyst ZnO/TiO_2 and microbial agent *Galatoctomyces geotrichum* MTCC 1360 - *Brevibacillus laterosporus* MTCC 2298 (consortium GG-BL) for the treatment of textile azo dye Methyl Red (500 mg l^{-1}). Decolorization of Methyl Red at different experimental condition was carried out by using ZnO/TiO_2 , consortium GG-BL, consortium GG-BL- ZnO/TiO_2 system and ZnO/TiO_2 -consortium GG-BL system

6.3 Results and discussion

6.3.1Chacterization of ZnO/TiO_2 thin films

6.3.1.1 Photoelectrochemical (PEC) characterization

The Fig. 6.1 shows I–V characteristics of PEC cell prepared using ZnO, TiO_2 and ZnO/TiO_2 film electrodes, under UVA illumination. Both I_{sc} and V_{oc} values for ZnO, TiO_2 and ZnO/TiO_2 are 2.503×10^{-5} A/ cm^2 and 0.505 V, 1.4878×10^{-4} A/cm^2 and 0.585 V and

2.244 $\times 10^{-4}$ A/cm^2 and 0.675 V respectively. I$_{sc}$ has been enhanced for the TiO$_2$ /ZnO film relative to ZnO and TiO$_2$ film, Shaogui et al. [21] reported that photocurrent on ZnO/TiO$_2$ electrode is the relatively large among compared to Fe$_2$O$_3$/ZnO/TiO$_2$ and TiO$_2$ electrode.

The TiO$_2$/ ZnO/FTO film excited by photons with energy higher than the gap energy (E_g), a great number of electrons are promoted from valence band (VB) to the conduction band (CB) of ZnO and TiO$_2$, leading to the generation of electron/hole (e$^-$/h$^+$) pairs. The electron transfer from the CB of TiO$_2$ to the CB of ZnO, and conversely, the holes transfer from the VB of ZnO to the VB of TiO$_2$ give rise to decrease the pair's recombination rate (Fig. 6.2).
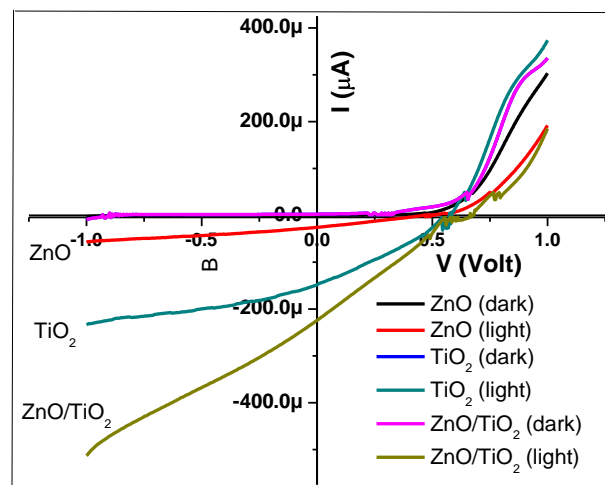
Figure 6.1 I-V characteristics of ZnO, TiO$_2$ and ZnO/TiO$_2$ thin films under dark and light

The charge transport in the ZnO/TiO$_2$ film is no doubt a key step for further increasing the photocatalytic efficiency. Though the ZnO possesses an energy band similar to that of TiO$_2$, it still plays an important role in electron transport. The energy level for electron injection is decreased after TiO$_2$ film cover the surface of ZnO film, which increases the driving force for electron injection and hence reduce recombination between electrons and holes. On the other hand, ZnO can increase concentration of free electrons in the CB of

TiO$_2$; this result implies that the charge recombination is reduced in the process of electron transport. All above of results increase the availability of the pairs on the surface of the photocatalyst and consequently an improvement of the occurrence of redox processes can be expected.
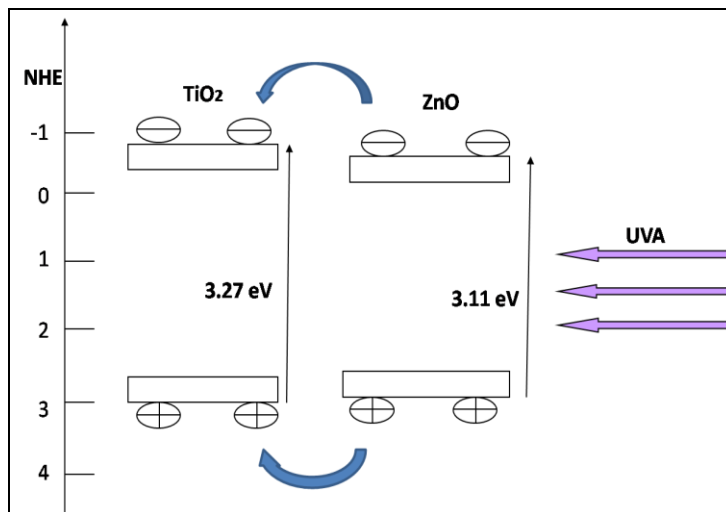
Figure 6.2 Schematics of band energy diagram of ZnO / TiO$_2$ film

6.3.1.2 Structural analysis

The x-ray diffraction patterns of ZnO, TiO$_2$ and coupled ZnO / TiO$_2$ photoelectrodes are shown in Fig. 6.3 . A comparison of observed and standard d values using JCPDS cards 80-0074 and 71-1119 for ZnO and TiO$_2$ respectively. It is seen that films are polycrystalline and having dominant orientation (002) and (101) for pure ZnO (hexagonal) and TiO$_2$ (tetragonal) thin films respectively while for coupled films it shows mixture of both phases. XRD depicts that required phases of respective materials has been achieved.

6.3.1.3 Morphological analysis

The Fig. 6.4 a) shows the cross-sectional and b) top surface SEM images of ZnO/TiO$_2$ thin film. It clearly demonstrates three layers of FTO, ZnO and TiO$_2$ photocatalysts respectively with properly conjugated layers. Thickness of FTO, ZnO and TiO$_2$ is about 1 μm, 150 and 125 nm respectively. Top view depicts, the surface of film consists of homogeneous spherical granules of TiO$_2$ layer.
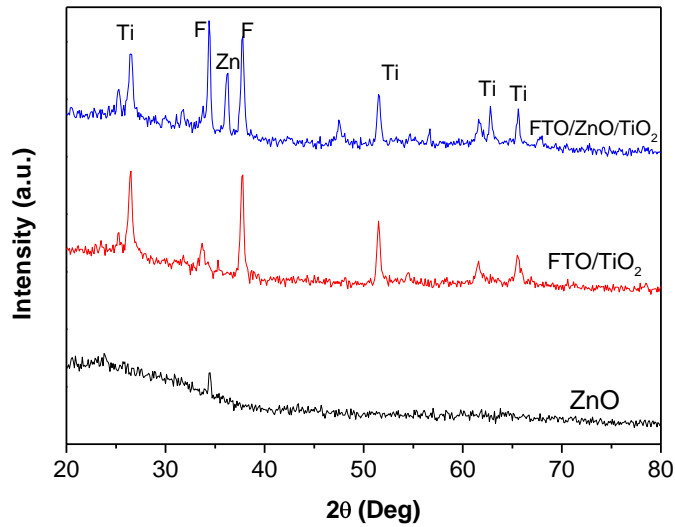
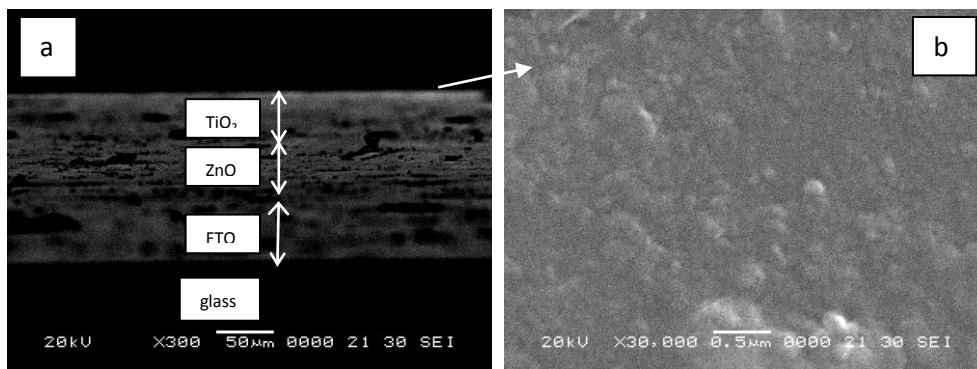**Figure 6.3 X-ray diffraction patterns of ZnO, TiO$_2$ and ZnO/TiO$_2$ thin films**

**Figure 6.4 SEM images of (a) cross sectional view and (b) top view of ZnO/TiO$_2$ film**

6.3.1.4 Optical properties

The absorption coefficient α of ZnO, TiO$_2$ and ZnO/TiO$_2$ films is determined from transmittance measurements. Since envelope method is not valid in strong absorption region, the calculation of absorption coefficient of the film in this region is calculated using the following expression:

$$\ln\left(\frac{1}{T}\right) = \alpha t \qquad (2)$$

where T is the normalized transmittance, t the film thickness. These absorption coefficient values are used to determine optical energy gap. Fig.6.5 inset shows the plot of $(\alpha h\nu)^2$ vs $h\nu$,

where α is the optical absorption coefficient and $h\nu$ is the energy of incident photon. The energy gap (E_g) is estimated by assuming a direct transition between valence and conduction band. The energy gap (E_g) is determined by extrapolating straight line portion of spectrum to α= 0.
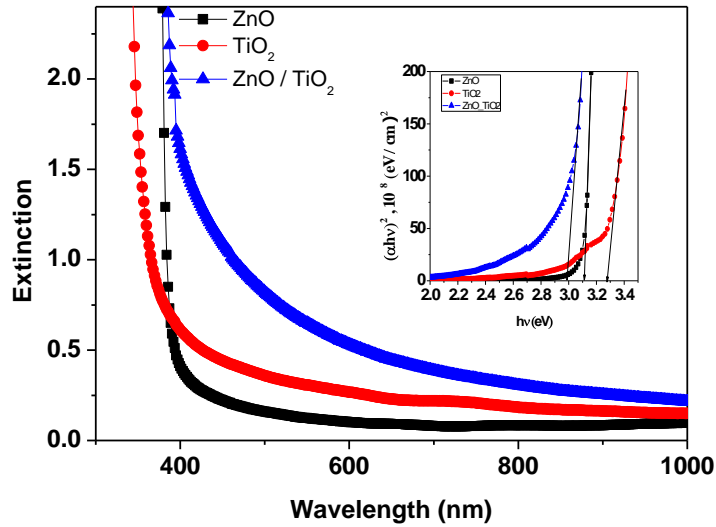
Figure 6.5 Optical absorbance of the ZnO, TiO₂ and ZnO/TiO₂ thin films; Inset shows the band gap energy plot
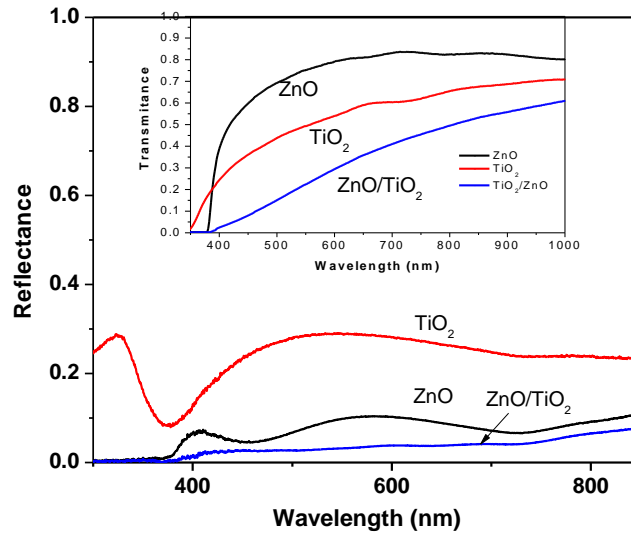

Figure 6. 6 Variation of transmittance and reflectance of ZnO, TiO₂ and ZnO/TiO₂ thin films

The optical energy gap, E_g = 3.11 eV, 3.27 eV, and 2.99 eV are deduced for ZnO, TiO$_2$ and ZnO/TiO$_2$ films respectively (inset Fig. 6.5). As shown in Fig 6.5, the absorption edge of TiO$_2$, ZnO and ZnO/TiO$_2$ films are at around 391, 398 and 414 nm, respectively and similar results are reported by Zhang et al [22]. The significant red-shift with lower band energy of ZnO/TiO$_2$ film comparing with the ZnO film and TiO$_2$ film may be owing to the differences in the surface state. The ZnO/TiO$_2$ film need lower energy to be excited than the ZnO film and TiO$_2$ film [23]. The reflectance of the films is shown in Fig.6.6 and inset shows transmittance. Transmittance is decreases from ZnO, TiO$_2$ to ZnO/TiO$_2$. The TiO$_2$, ZnO and ZnO/TiO$_2$ films shows about 30 %, 8 % and 2 % reflection respectively in visible region.

6.3.2 Photoelectrocatalytic degradation of Methylene Blue

This study is part of effort to fabricate the ZnO/TiO$_2$ heterojunction to prevent photocorrossion of ZnO. The semiconducting ZnO thin film deposited onto FTO by spray, and then the thin TiO$_2$ semiconducting layers with optimized thickness of approximately 89 nm are coated using a spray pyrolysis technique. For the case of thin layers TiO$_2$ on the ZnO films, the photocurrent and the resulting photoelectrocatalytic properties increases as the thickness of the thin layer increased. This result is understood in terms of the charge carrier lifetime. Charge carriers are unstable, i.e. easily recombined in the ZnO, while they are more stable in the TiO$_2$. Under applied bias of 1.5V, both of the photocurrent and the photodecomposition increased. In the case where only one TiO$_2$ layer is coated on ZnO films, photodecomposition of phenol has increased from 23.3% (bare ZnO film) to 27.2%. However, the photocatalytic decomposition increased with three times of TiO$_2$ coating on ZnO. Rusmidah Ali et al [24] showed that 0.015 g TiO$_2$ and 0.085 g ZnO (15: 85) is the optimum ratio of TiO$_2$ and ZnO mixture to degrade MB. Choi et al. [25] prepared a ZnO/TiO$_2$/ZnO multi-layer on quartz glass substrate via electron beam evaporation and optical and structural properties are investigated. The TiO$_2$ buffer layer is found to improve the crystallinity of the ZnO thin film.
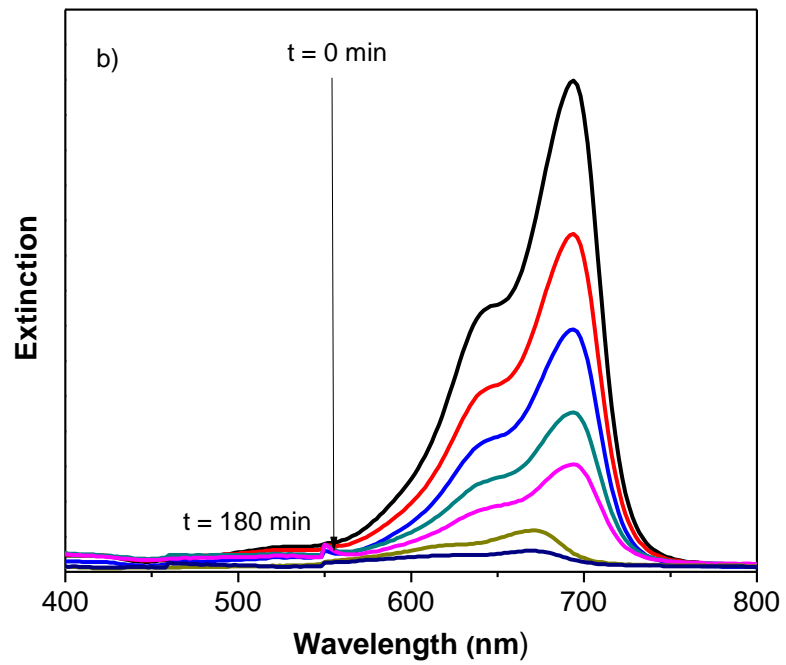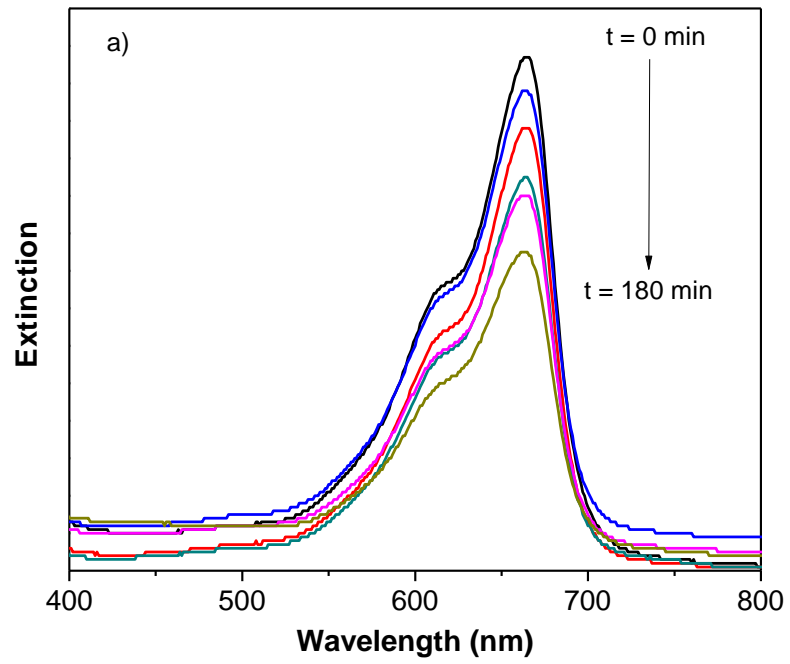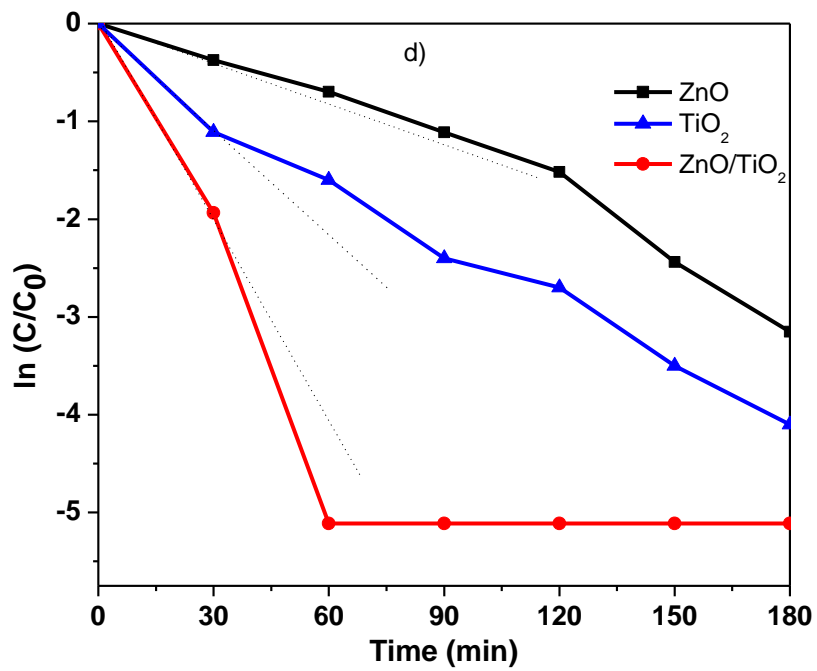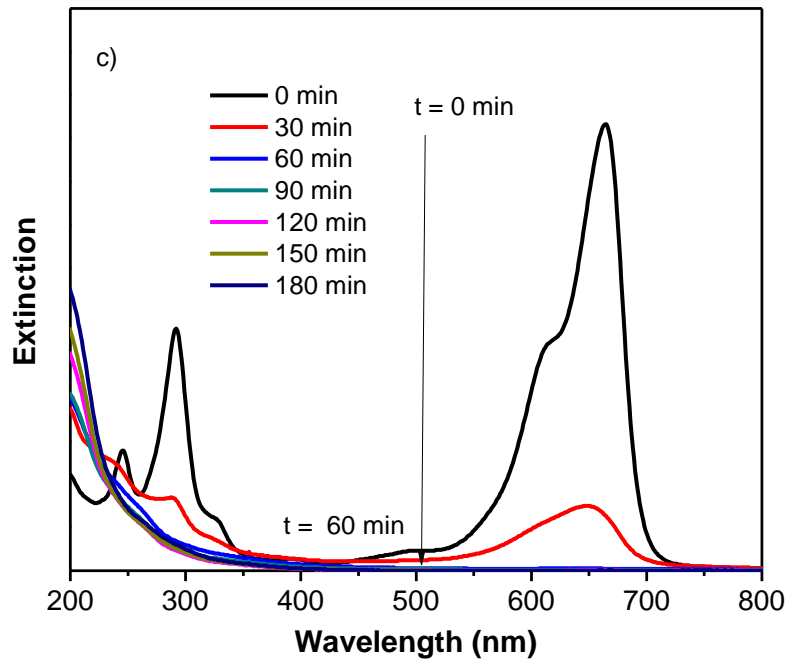
Fig.6.7 Extinction of MB with reaction time a) ZnO, b) TiO$_2$, c) ZnO/TiO$_2$ thin film and d) its kinetics

To evaluate the photo-stability of the ZnO thin film catalyst, Atomic Absorption spectra (AAS) is performed for detection of Zn in the final MB solution and it is found that 0.028 µg/lit, which shows 24 % ZnO film is dissolved during photoelectrocatalytic process. However zinc is not detected when ZnO/TiO$_2$ electrode used for degradation of MB. It is also conformed form figure 6.7 (a) that a significant decrease in photocatalytic activity for pure ZnO is found in which only 38.68 % of MB is degraded within 180 min, for TiO$_2$ (Figure 6.7 b) is 95.80 % and 99.41% of MB can be degraded with ZnO/TiO$_2$(Figure 6.7 c). The drastic decrease in photocatalytic activity for ZnO resulted from the photo-corrosion effect [26]. In this system, the presence of TiO$_2$ on the surface of ZnO suppressed the photo-corrosion phenomenon and enhanced the stability of the catalyst under UV irradiation. The plot of $\ln(C/C_o)$ against irradiation time for MB is suggesting that the photodegradation reaction approximately follows the first order kinetics. Rate constant (k) is estimated from figure 6.7 (d) and are found to be 0.01714, 0.0250, and 0.0852 min^{-1} for pure ZnO , TiO$_2$ and ZnO/TiO$_2$ catalysts respectively. The k (0.0852 min^{-1}) value for ZnO/TiO$_2$ catalysts which is higher than reported one (k = 0.0548 min^{-1}) [27]. Kanjwal et al. showed that the ZnO-TiO$_2$ hierarchical nanostructure can eliminate all the methyl red dye within 90 min and the rhodamine B dye within 105 min. However, pure ZnO and TiO$_2$ nanostructures could not totally remove any of the dyes, after 3h [28]. Similar results are found to Zhang et al, in which monomolecular-layer polyaniline (PANI) is dispersed on the surface of ZnO and formed the hybrid effect between ZnO and PANI [26]. Thus spray deposited ZnO/TiO$_2$ thin film showed dramatic photocatalytic activity for the degradation of the MB and the photo-corrosion of ZnO is successfully inhibited.

FTIR analysis of MB (Fig.6.8 a) shows presence of prominent bands for the C=N central ring stretching at 1632 cm^{-1}, the multiple ring stretching at 1378 cm^{-1}, the C-N (i.e., the bond between the side aromatic ring and the nitrogen atom) stretching at 1333 cm^{-1}, the N-CH$_3$ (i.e., the bond between CH$_3$ and the nitrogen atom) stretching at 1150 and 1021 cm^{-1}, the C-H asymmetric stretching of CH$_3$ at 2913 cm^{-1}, and the C-H symmetric stretching of CH$_3$ at 2862 cm^{-1} , whereas metabolite formed after degradation of MB(Fig.6.8 b) showed C- C stretch at 3149.85 cm^{-1}, alkanes observed in untreated MB are absent in metabolite formed, presence of C=O stretch at 1633.36 cm^{-1}, C-H deformation at 601, 655,

147

872.46 and 1400 cm^{-1} respectively, aromatic ether at 1119.32 cm^{-1}, peak at 1056.06 cm^{-1} shows presence of aliphatic ether, a peak at 1020.86 cm^{-1} showed presence of C-OH stretch. During the photoelectrocatalysis of MB, all of the constituent elements of MB can be converted to the final oxidation products including CO_2, H_2O, NH^{4+} and SO^4. Thus, it can be concluded that aniline, aldehydic species, $R-NH^{3+}$, carboxylate, and phenol observed during the MB degradation were the intermediate species that should be eventually converted to the final oxidation products.
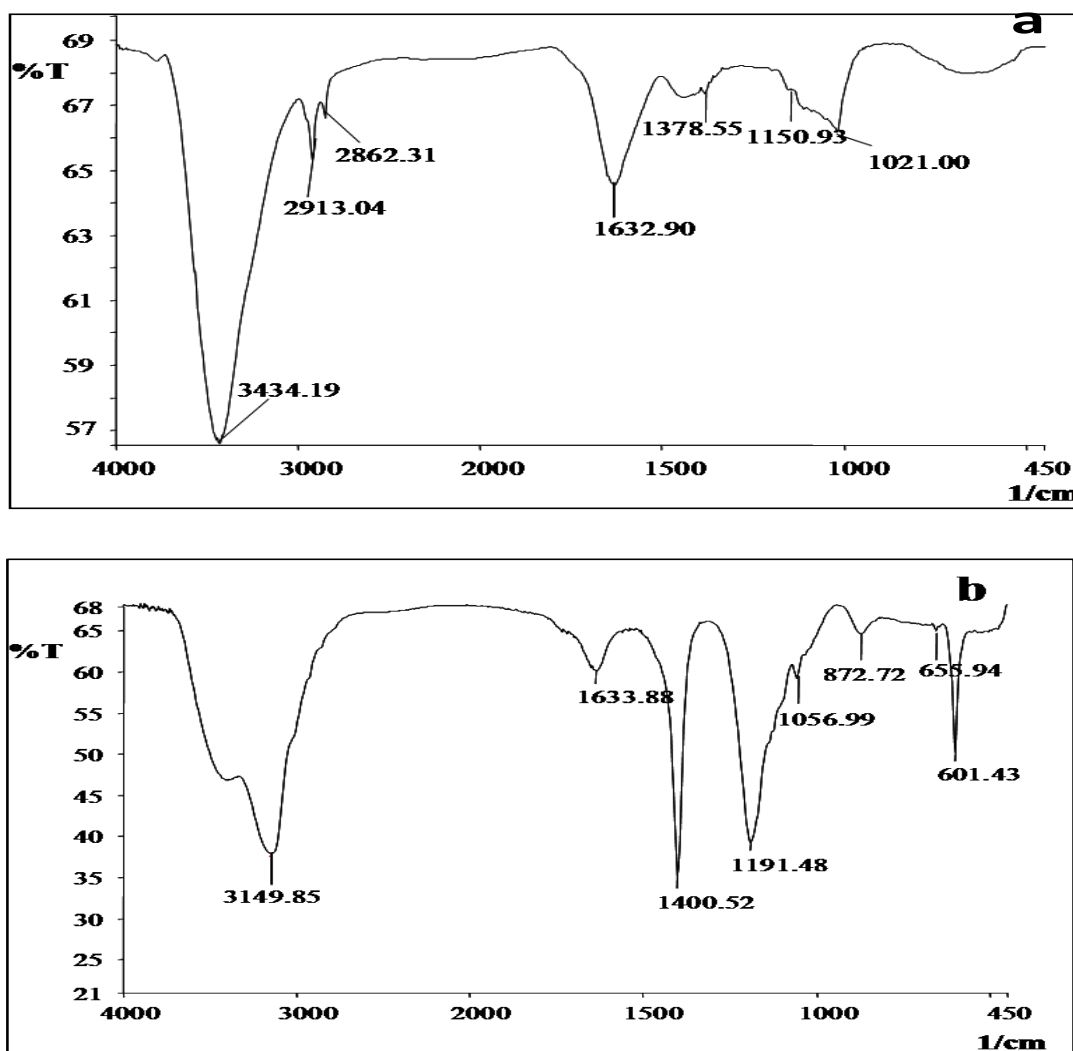
Figure 6.8 FTIR analysis of control dye methylene blue (a) and metabolites formed after degradation by photocatalyst (b)Identification of Intermediate Products and Reaction Pathway

.
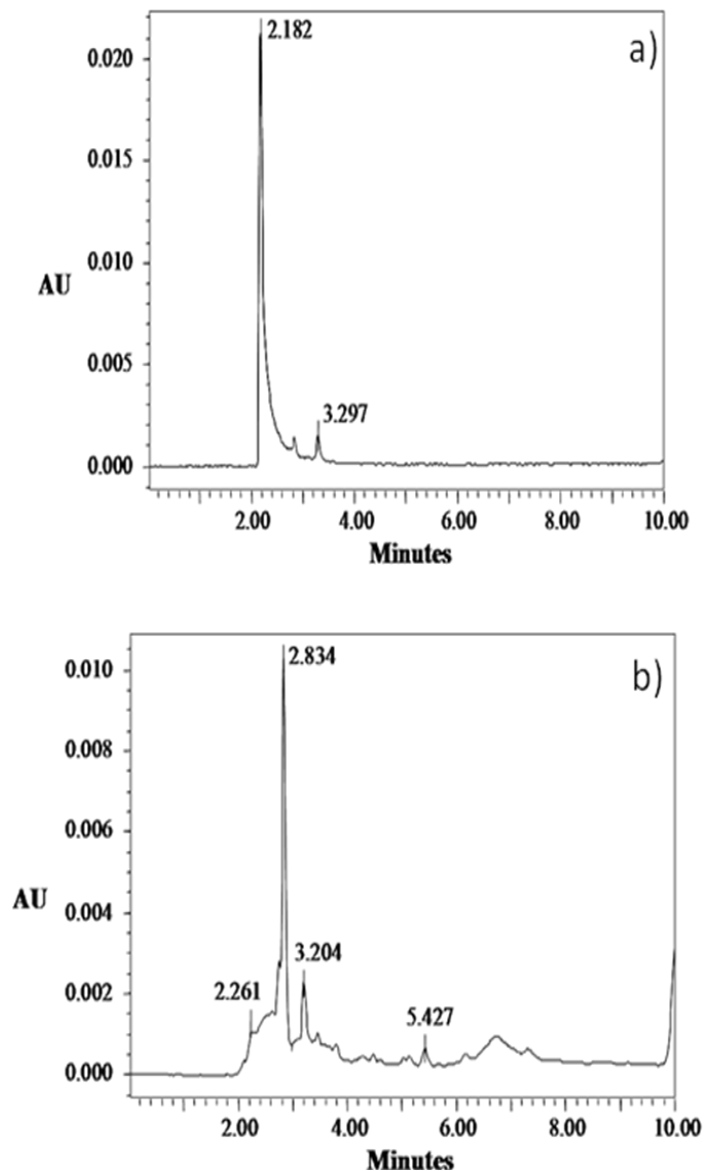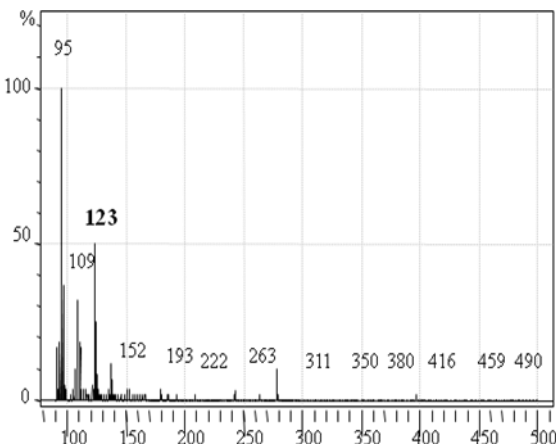
Figure 6.9 HPLC analysis of MB (a) its metabolites, (b) formed after degradation by photocatalyst

After 180 min of photoelectrocatalytic degradation process, we stopped the reaction to identify intermediate products by the HPLC-MS method [29]. The chromatograms in Fig.6.9 (a-b) shows a photocatalytic degradation of MB. The Fig.6.9 (a) shows main two peaks at retention times of 2.182 and 3.297 min. for MB. After photoelectrocatalysis main products are observed at retention times of 2.261, 2.843, 3.204 and 5.427 min. The two

products identified in HPLC=MS present peaks at 123 m = z. These can be assigned to the chemical structures I and II, as shown in table 6.1. On the basis of these results, we propose a general reaction pathway of the photoelectrocatalytic degradation of MB, as presented in Fig. 6.10. This reaction pathway has several stages: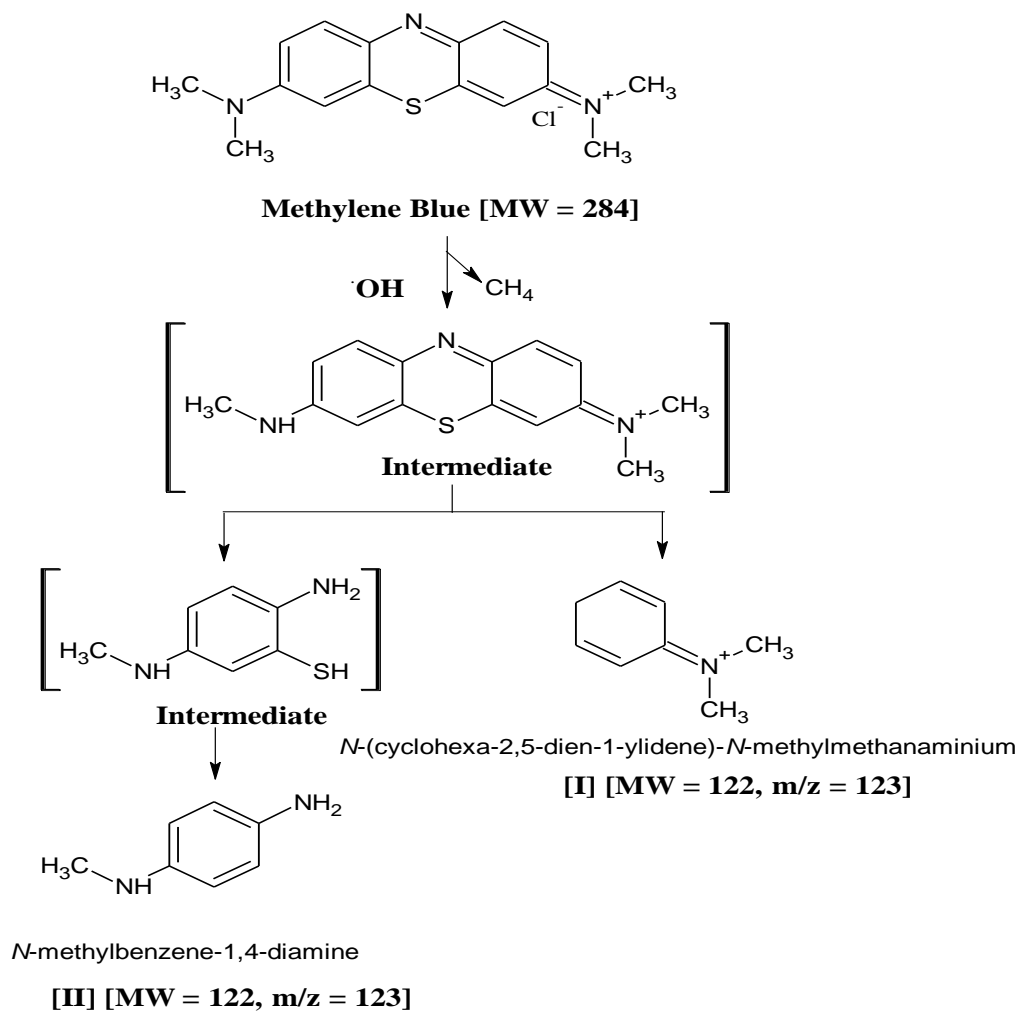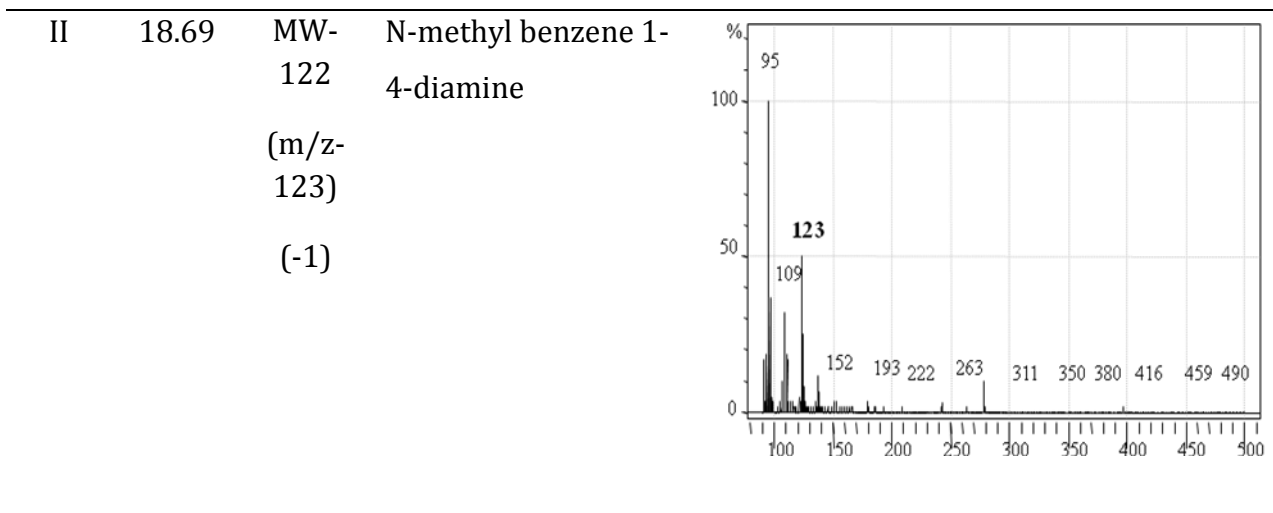 hydroxylation, desulfonation, deamination, desalkylation, and deshydroxylation. The two compounds viz. N-(Cyclohexa - 2, 5 dien -1-ylidene) – N- methylmethanaminium (Mw= 122) and N-Methyllbenzene-1, 4-diamine (Mw = 122) detected during the degradation of MB shows the complexity of the photocatalytic process and suggests the existence of various degradation routes, resulting in multistep and interconnected pathways

Table 6.1: The chemical structures I and II of metabolites of MB after degradation with ZnO/TiO₂ photocatalysts

Peak	Rt. time (min)	MW (m/z)	Name of metabolites	Mass peaks
I	18.93	MW-122 (m/z-123) (-1)	N-cyclohexa 2,5-dien 1-yliedene)-N-methylmethanaminium	

| II | 18.69 | MW-122 (m/z-123) (-1) | N-methyl benzene 1-4-diamine | |

Methylene Blue [MW = 284]

$^{\cdot}$**OH** $\quad$ CH$_4$

Intermediate

Intermediate

N-(cyclohexa-2,5-dien-1-ylidene)-*N*-methylmethanaminium

[I] [MW = 122, m/z = 123]

N-methylbenzene-1,4-diamine

[II] [MW = 122, m/z = 123]

Figure 6.10 Possible reaction pathway of MB degradation

6.3.3 Photoelectrocatalytic decolorization and degradation of textile effluent

It has been observed that the photoelectrocatalytic degradation technique has been found to be better for the degradation of Ponceau 6R dye [30]. Dyes of different structures are often used in the textile processing industry. The effluents from the industry are markedly variable in composition. Hence, photoelectrocatalytic degradation of textile industrial effluent was studied to enhance applicability of the process. Fig. 6.11(a) shows the changes in the extinction spectra of textile effluent collected at various intervals during its photoelectrochemical degradation using ZnO/TiO_2 recorded in the wavelength range from 200 to 400 nm. During the course of the degradation experiments, the textile effluent decolorize due to its decomposition. 93% decolorization was observed (ADMI removal) after 180 min.
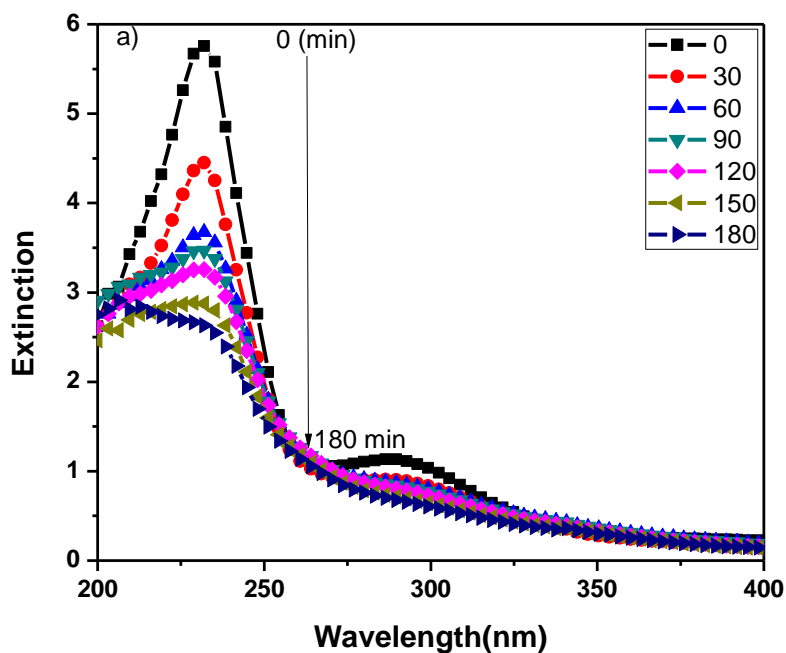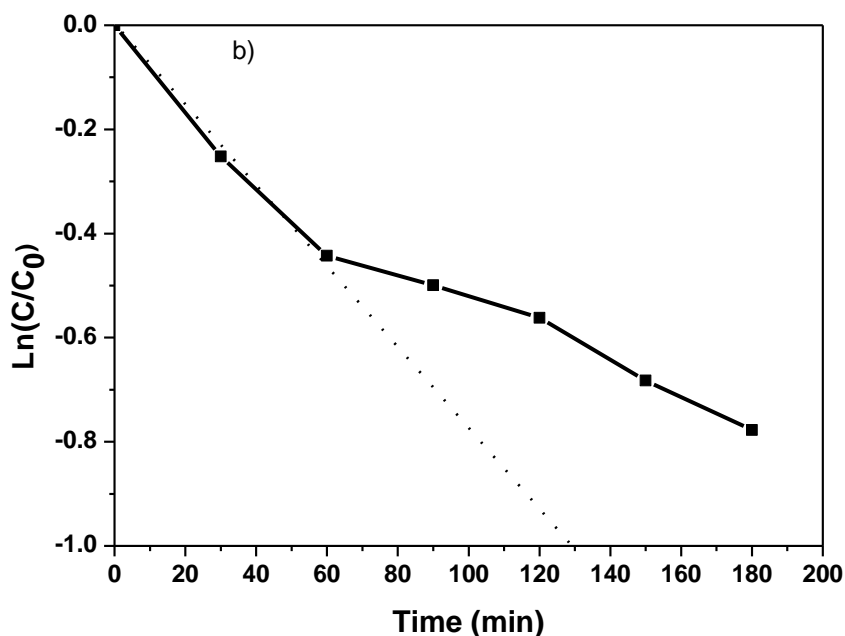
Fig 6.11 Extinction with reaction time for textile effluent a) and its kinetics b)

Figure 6.11 (a), is further used to plot variations in $\ln(C/C_0)$ as a function of reaction time shown in Fig. 6.11 (b). The integral linear transform, $\ln(C/C_0)$ as a function of degradation time revealed apparent first order reaction kinetics and slope gives rate constant (- k)[31]. Byrapaa et al synthesized ZnO by hydrothermal method and studided photocatalysis against rodamine B dye and textile effluent. For textile effluent COD reduction and photocatalytic efficiency were 83 % and 85.95 % respectively after 10 h of exposure [32]. However in our case ZnO/TiO$_2$ film shows 93 % decolorization of textile effluent within 3 h at room temperature with significant reduction in COD (69 %). The present investigation revealed that ZnO induced photoelectrocatalysis of textile influent as the first order kinetics with rate constant 7.81×10^{-3} (min^{-1}) [33-34].

Metabolite analysis of textile effluent

HPLC analysis of control textile effluent showed one major (3.083 min) and eight minor peaks at retention time of 2.154, 2.725, 2.880, 3.409, 3.721, 4.232, 4.786 and 5.786 min respectively (Fig. 6.12 a) which indicates textile effluent contains mixture of dyes, whereas metabolite formed after degradation showed one major (3.095 min) and six minor

peaks at retention time of 2.200, 2.470, 2.835, 3.250, 3.403 and 3.741 min respectively (Fig. 6.12 b). The HPLC analysis shows that one minor peak has been found at same retention time (3.4 min) in HPLC data of control and treated textile effluent. However all others have been observed at different retention time, which indicates parent compounds are degraded into its metabolites.

FTIR analysis (Fig.6.13 a) of control textile effluent showed presence of N-H stretch at 3433.84 cm^{-1}, alkanes at 2855.07-2923.29 cm^{-1}, presence of azo bond (N=N stretch) at 1627.60 cm^{-1} showed presence of azo dye in textile effluent, aromatic ether at 1244.87 cm^{-1}, S=O stretch at 1194.28 cm^{-1} provides the evidence for sulfonated dye present in textile effluent, primary alcohol (C-OH stretch) at 1017.24 cm^{-1} confirms the dye with phenolic group, C-H deformation at 829.37-872.26 cm^{-1}, whereas metabolites formed after degradation of textile effluent showed N-H stretch at 3436.46 cm^{-1}, alkanes at 2847.82-2922.68 cm^{-1}, presence of C=O stretch at 1633.36 cm^{-1}, C-H deformation at 800.46 and 1465.26 cm^{-1} respectively, multiple ring stretching at 1378.55 cm^{-1}, aromatic ether at 1259.32 cm^{-1}, peak at 1098.06 cm^{-1} showed presence of aliphatic ether, a peak at 1020.86 cm^{-1} showed presence of C-OH stretch (Fig. 6.13 b). Absence of peak at 1627.60 cm^{-1} for azo bond in formed metabolites obtained after degradation confirms the cleavage of azo bond by photoelectrocatalytic action [35].
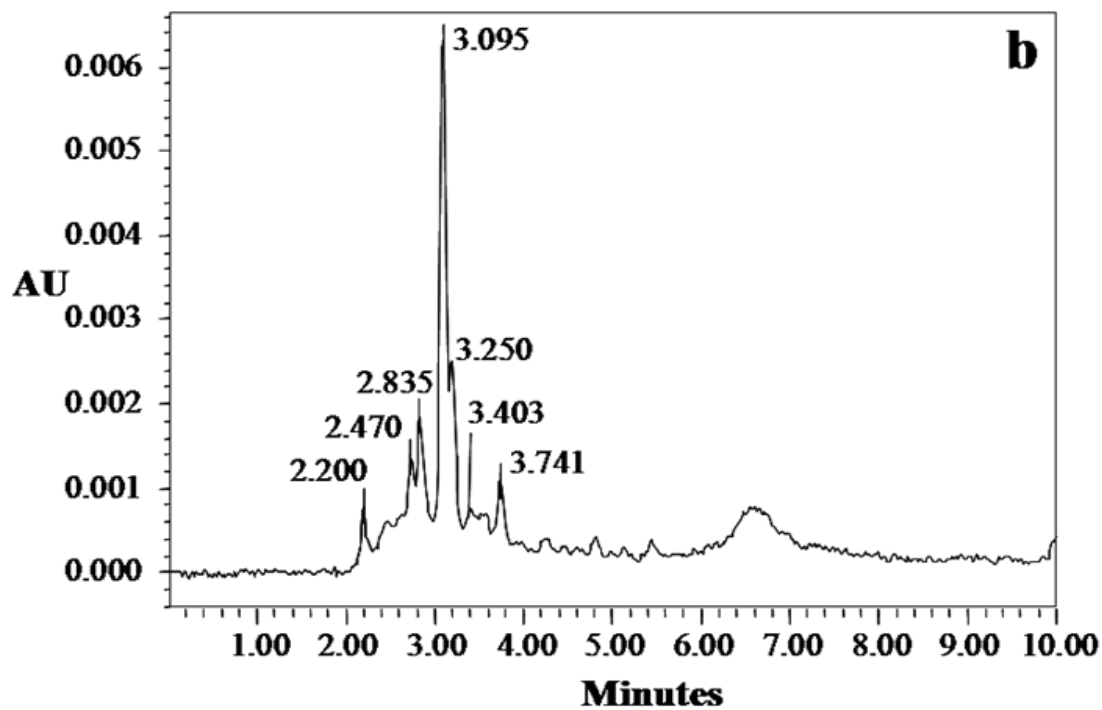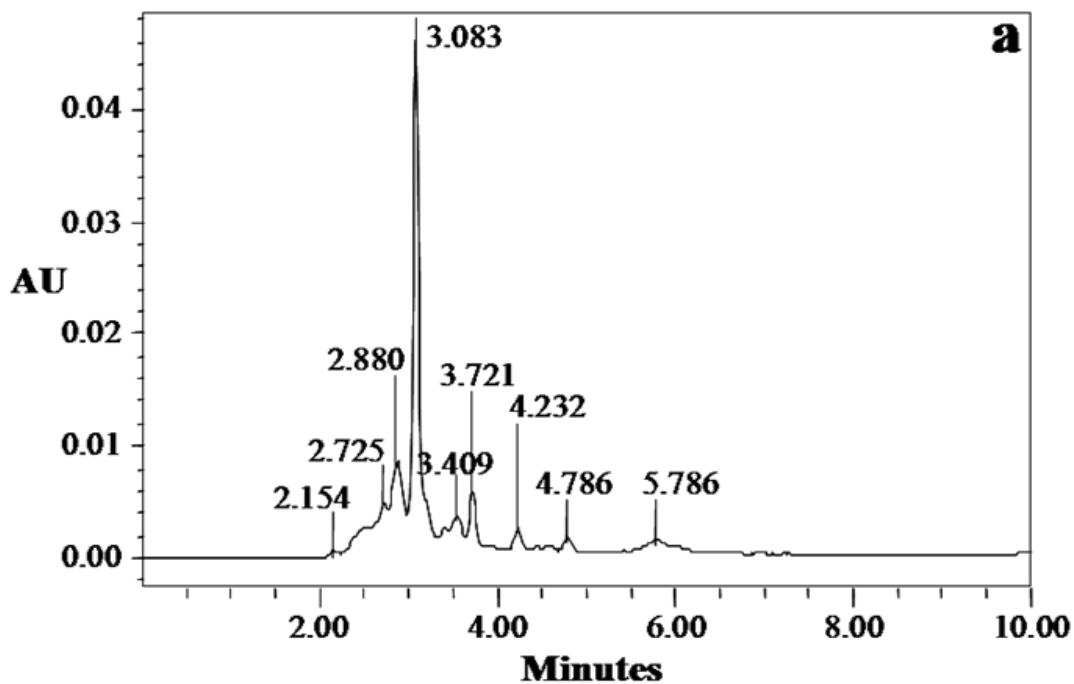
Figure 6.12 HPLC analysis of textile effluent (a) and its metabolites (b) formed after degradation by photocatalyst

155
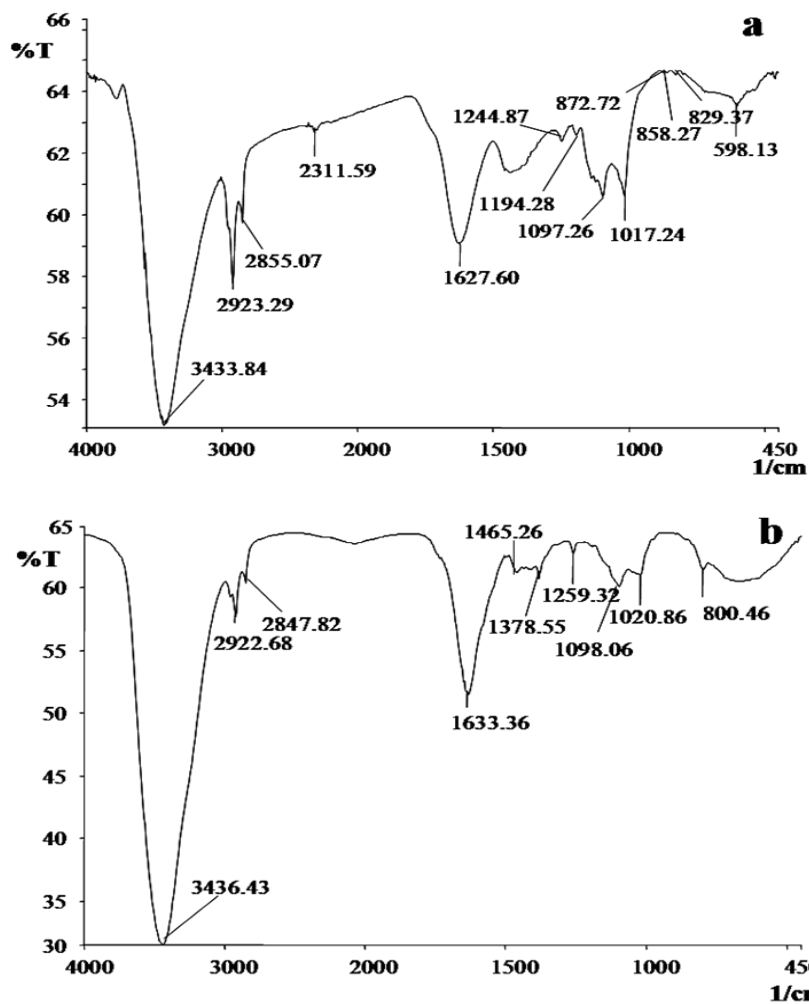
Figure 6.13 FTIR analysis of textile effluent (a) and its formed metabolites (b) obtained after photocatalytic degradation

Phytotoxicity analysis

The toxic nature of the textile effluent is mainly based on the chemical nature of the dyes present in textile effluent. Phytotoxicity study revealed the toxic nature of textile effluent to the P. mungo and S. vulgare plants. Germination (%) of these plants was less with textile effluent treatment as compared to the metabolites obtained after its decolorization and distilled water (Table 6.2). The textile effluent significantly affected the shoot and root growth than the metabolites obtained after its decolorization. This study revealed the less toxic nature of degraded metabolites as compared to the textile effluent.

Table 6.2: Phytotoxicity of textile effluent (1000 ppm) and its metabolites formed after degradation (1000 ppm) for the Phaseolus mungo and Sorghum vulgare (I-Seeds treated with plain distilled water; II-Seeds treated with textile effluent; III-Seeds treated with formed metabolite. Data was analyzed by one-way ANOVA Test and mentioned values are the mean of ten germinated seeds of three sets SEM (±). Seeds germinated in textile effluent are significantly different from the seeds germinated in plain water at *P < 0.001 and the seeds germinated in degradation products are significantly different from the seeds germinated in textile effluent at $P < 0.05, $$P < 0.001 when compared by Tukey Kramer Multiple Comparison Test)

Observation	*Phaseolus mungo*			*Sorghum vulgare*		
	I	II	III	I	II	II
Germination (%)	100	70	90	90	20	80
Shoot length (cm)	12.20 ± 0.30	9.58 ± 0.36	11.44 ± 0.49$	1.72 ± 0.12	1.06 ± 0.57**	2.14 ± 0.18$$
Root length (cm)	7.57 ± 0.32	2.56 ± 0.90**	4.50 ± 0.25$	3.47 ± 0.11	0.52 ± 0.06**	4.58 ± 0.26$$

6.3.4 Photoelectrocatalytic Inactivation of bacteria

The photocatalytic inactivation of bacteria is cell dependent therefore Gram positive (*Bacillus, Staphylococcus*) and Gram negative bacteria (*E.coli, Salmonella*) has been selected to study photoelectrocatalytic inactivation effect. The cell wall structure for Gram negative bacteria is relatively more complex than that of Gram positive cells (Fig. 6.14).
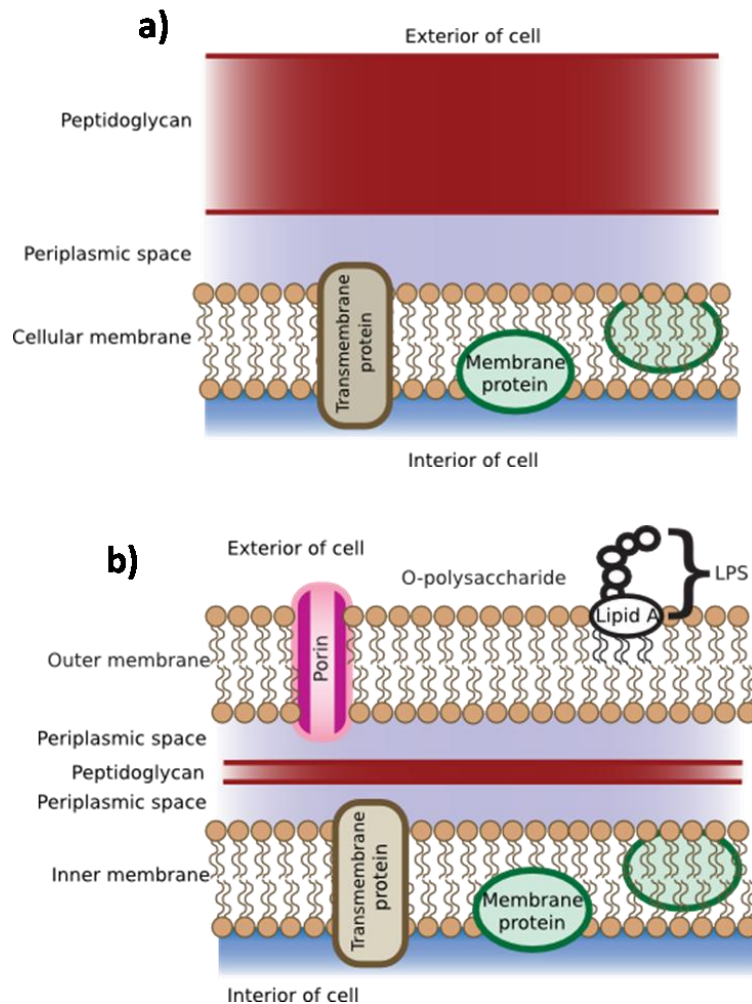
Figure 6.14 Schematic diagram of cell membrane (a) Gram-positive (b) Gram-negative bacteria.

The cell wall of Gram –positive bacteria consistance of many polymer layess of Peptidoglycan connected by amino acid bridges. The Peptidoglycan polymer is composed of an alternating sequence of N- actly glucosamine (NAG) and N- acetly – muraminic acid (NAMA). Each Peptidoglycan layer is connected or cross- linked, to the other by a bridge made of amino acides and aminoacid derivatives. The cell wall of Gram –negative bacteria is much thiner, being comprised of only 20 % Peptidoglycan. It also have two unique regions which surround the outer plasma membrane (The periplamic space and lipopolysaccharide layer). The periplasmic space separates the outer plasma membrane from the peptidoglycan layer. Therefore, a longer oxidation time or more photocatalyst would be required for inactivation of Gram negative cells if it is required that cell wall

158

destruction is necessary during photocatalytic inactivation [37]. However, the inactivation kinetics was seen to be more rapid for the Gram negative *E.coli* and *Salmonella* than that for the Gram positive Bacillus and Staphylococcus in this study. Thus result is in good agreement with the work by Bekbolet and Araz [38]. The mechanism of photocatalytical inactivation of bacteria is still ambiguous. Cell membrane damage has been observed either as loss of potassium ions, proteins and RNA from bacterial cells, or as an increase in intracellular calcium ions due to the greater permeability of cell membrane to calcium ions [39]. On the other hand, Wamer et al. [40], suggested that nucleic acids are the potential target for photooxidative destruction of the cell cycle stimulated by TiO_2, which induced the formation of free radicals under UV irradiation. From the results of the present study, we hypothesised that Gram positive and Gram negative cells may adapt different photocatalytical inactivation mechanisms. Further investigation should be addressed to elucidate this hypothesis. ZnO has also proved to be a good candidate to inactivate both Gram-negative and Grampositive bacteria photocatalytically in the present study. Many functions, such as semipermeability, respiration, and oxidative phosphorylation reactions, rely on an intact membrane structure [41]. As a result, normal functions associated with an intact membrane, such as respiratory activity, are lost. Fig.6.15 shows colony forming unit per ml (CFU/ml) for *E.coli* , Salmonella, *Bacillus,* and *Staphylococcus* with reaction time. All four bacteria s are totally inactivated within 30 min of reaction time. According to Gerischer and Heller [42] at the higher concentration of organic water contaminants and high light intensity the rate of oxidation by photogenerated holes is high. In another report Pin-Ching et al. reported that in presence of 0.1mg TiO_2 /ml and UV light about 92 to 98 % of the *E.coli* cell was killed when the initial cell concentration was about 10^8 CFU/ml [43].
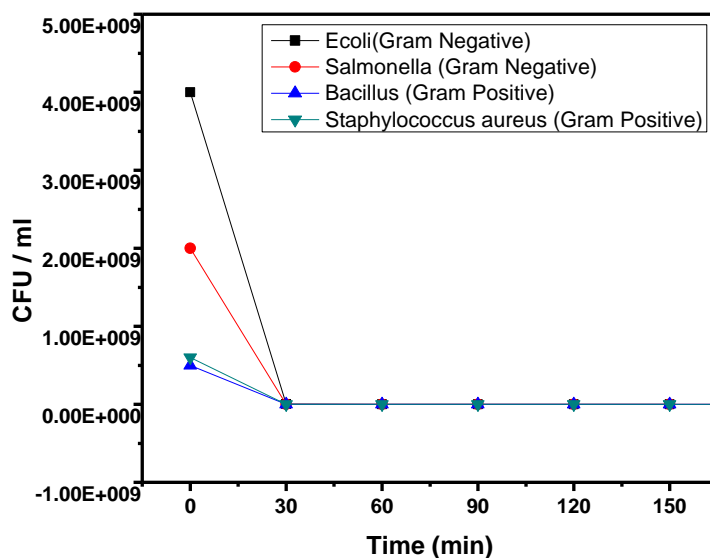
Figure 6.15 Viable count CFU/ml of different bacteria with time

It is generally accepted that hydroxyl radicals $OH^\bullet$ are the main oxidative species responsible for the bactericidal action of ZnO thin film. However there is also some evidence that other reactive oxygen species generated photocatalyticaly, such as suproxide radicals O^{-2}, perhydroxyl radicals HO_2 and hydrogen peroxide H_2O_2 also contributes to photocatalytic inactivation [44]. Cell membrane is the crucial site of attack for effective inactivation regardless the oxidative species involved in the process. It has been proposed that the cell wall is initially damaged; followed by a progressive damage of the cytoplasmic membrane and intracellular components, thus eventually leading to loss of essential cell functions. The compete oxidation of organic compounds and bacterial cells to carbon dioxide can be achieved. Furthermore, the solution contains species e.g. $OH^\bullet$, H^+, $^\bullet O^{-2}$, $^\bullet HO_2$, H_2O_2, and O^2, which are due to the ZnO/TiO_2 thin film light-water-oxygen interactions. These hydroxyl radicals can perform reactions with cell membrane as

Cell membrane + hydeoxyl radicals ($OH^\bullet$, H^+, $^\bullet O^{-2}$, $^\bullet HO_2$, H_2O_2, and O_2) $\rightarrow$ CO_2+ reduced organic compounds

Based on our findings, we propose that reactive oxygen species (ROS), are generated on the irradiated TiO_2 surface, operate in concert to attack polyunsaturated phospholipids in *E.coli*. The lipid peroxidation reaction that subsequently causes a breakdown of the cell

160

membrane structure and therefore its associated functions is the mechanism underlying cell death. All life forms have a cell membrane made up of a variety of lipids with various degrees of unsaturation and rely on their structures to carry out essential functions. Thus, the proposed killing mechanism is applicable to all cell types.

6.3.5 Photoelectro – Bio degradation of Methyl red

This study is part of effort to develop new coupling method by using photoelectrocatalytic ZnO/TiO_2 and microbial agent (combination GG-BL) for the treatment of textile azo dye Methyl Red (200 mg l^{-1}). Decolorization of Methyl Red at different experimental conditions was carried out by using ZnO/TiO_2, consortium GG-BL, consortium GG-BL-ZnO/TiO_2 system and ZnO/TiO_2-consortium GG-BL system (Table 6.3). The decolorization of Methyl Red (200 mg l^{-1}) using consortium GG-BL and ZnO/TiO_2 showed 63 % and 70 % decolorization with 38 and 40 % reduction of chemical oxygen demand (COD) within 2 h respectively. Whereas the consortium GGBL-ZnO/TiO_2 system showed 83 % decolorization of Methyl Red within 4 h for with 60% reduction in COD, while ZnO/TiO_2– consortium showed 100 % decolorization with 80 % reduction of COD. It means that ZnO/TiO_2-consortium GG-BL system was efficient for the successful and faster decolorization of Methyl Red. Previous study reported degradation of textile dye by photocatalysis and biological methods[45-49].

Table 6.3 Degradation parameters of Methyl red with and without coupling of photoelectrocatalytic and biological method

Degradation method	Decolorization %	COD reduction %	Reaction time (hrs)
ZnO/ TiO_2	70	40	2
GG-BL	63	38	2
GG –BL : ZnO/TiO_2	83	60	2 +2
ZnO/TiO_2 : GG –BL	100	80	2 +2

References

[1]   C. Wang, X. Wang, B.Q. Xu, J. Zhao, B. Mai, P. Peng, G. Sheng, J. Fu, J. Photochem.Photobiol. A: Chem., 168 (2004) 47.

[2]   C. C. Chen, J. Molecular Catalysis A: Chemical, 264 (2007) 82.

[3]   G. Kenanakis, Z. Giannakoudakis, D. Vernardou, C. Savvakis, N. Katsarakis,, Catal. Today, 151 (2010) 34.

[4]   V.V. Shvalagin, A.L. Stroyuk, S. Ya. Kuchmii, Theoretical and Experimental Chemistry, 40 (2004) 6.

[5]   L. Zhang, H. Cheng, R. Zong, Y. Zhu, J. Phys. Chem. C 113 (2009) 2368.

[6]   N.V. Kaneva, D.T. Dimitrov, C.D. Dushkin, Appl. Surf. Sci., 257 (2011) 8113.

[7]   H. Zhang, R. Zong, Y. Zho, J. Phys. Chem. C, 113 (2009) 4605.

[8]   C. Wang, J. Zhao, X. Wang, B. Mai, G. Sheng P. Peng, J. Fu. Appl. Catal. B: Environ., 39 (2002) 269.

[9]   D.L. Liao, C.A. Badour, B.Q. Liao. J. Photochem. Photobiol. A: Chem., 194 (2008) 11.

[10]   S. Liao, D. Huang, D. Yu, Y. Su, G. Yuan, J. Photochem. Photobiol. A: Chem., 168 (2004) 7.

[11]   Y. Shaogui, Q. Xie, L. Xinyong, L. Yazi, C. shuo, C. Guohu, Phys. Chem. Chem. Phys., 6 (2004) 659.

[12]   R. Ali, W. Azelee W.A. Bakar, L.K. Teck, Modern Appl. Sci., 4 (2010) 59.

[13]   D. L. Liao, C.A. Badour, B. Q. Liao, J. Photochem. Photobiol. A: Chem., 194 (2008) 11.

[14]   Q. Zhang, W. Fan, L. Gao, Appl. Catal. B: Environ., 76 (2007) 168.

[15]   M. A. Aramendía, V. Borau, J. C. Colmenares, A. Marinas, J. M. Marinas, J. A. Navío, F. J. Urbano, Appl. Catal. B: Environ., 80 (2008) 88.

[16]   Y. Abdollahi, A. H. Abdullah, Z. Zainal, N. A. Yusof, Inter. J. Appl. Sci. Technol., 1 (2011).

[17]   B. Neppolian, H. C. Choi, S. Sakthivel, B. Arabindoo, V. Murugesan, J. Haz. Mater. B89 (2002) 303.

[18]   Y. Li, W. Xie, X. Hu, G. Shen, X. Zhou, Y. Xiang, X. Zhao, P. Fang Langmuir, 26 (2010) 591.

[19]   T. R. Waghmode, M. B Kurade, S. P. Govindwar, Inter. Biodeter. Biodegrad. 65 (2011)

479.

[20]   M. Fang, J. F. Chen, X. L. Xu, R. H. Yang, H. F. Hildebrand, Int. J. Antimicrob. Agenccs, 27 (2006) 513.

[21]   Y. Shaogui, Q. Xie, L. Xinyong, L. Yazi, C. shuo, C. Guohu, Phys. Chem. Chem. Phys. 6 (2004) 659.

[22]   Z. Zhang, Y. Yuan, Y. Fang, L. Liang, H. Ding, L. Jin, Talanta 73 (2007) 523.

[23]   C. W. Zou, X. D. Yan, J. Han, R. Q. Chen, J. M. Bian, E. Haemmerle, W. Gao Chem. Phys. Lett. 476 (2009) 84.

[24]   R. Ali, W. Azelee, W. A. Bakar, L. K. Teck, Modern Appl. Sci., 4 (2010) 59.

[25]   W. S. Choi, E. J. Kim, S. G. Seong, Y. S. Kim, C. Park, S. H. Hahn, Vacuum, 83 (2009) 878.

[26]   H. Zhang, R. Zong, Y. Zho, J. Phys. Chem. C 113 (2009) 4605.

[27]   N. Daneshvar, J. Photochem. Photobiol. A: Chem., 162 (2004) 317.

[28]   M. A. Kanjwal, A. M. Nasser Barakat, F. A. Sheikh, S. J. Park, H. Y. Kim, Macro. Res., 18 (2010) 233.

[29]   M. A. Mottaleb, D. Littlejohn, Analytical Science, 17 (2001) 429.

[30]   A. A. El-Zomrawy, J. Saudi Chem. Soc. (2011), doi:10.1016/j.jscs.2011.05.003.

[31]   J. J. Vora, S. K. Chauhan, K. C.Parmar, S. B.Vasava, S. Sharma, L. S.Bhutadiya, E-J.Chemistry, 6 (2009) 531.

[32]   K. Byrappa, A. K. Subramani, S. Ananda, K. M. Lokanatha Raj, R. Dinesh, M. Yoshimura,   Bull. Mater. Sci., 29 (2006) 433.

[33]   A. M. de Freitas, C. Sirtori, P. Peralta-Zamora, Environ. Chem. Lett., 9 (2011) 97.

[34]   P. S. Shinde, P. S. Patil, P. N. Bhosale, A. Bru¨ger, Nauer, M. Neumann- Spallart, C. H. Bhosale, Appl. Catal. B: Environ., 89 (2009) 288.

[35]   Z. Yu and S. S. C. Chuang, J. Phys. Chem. C, 111 (2007) 13813.

[36]   P. C. Maness, S. Smolinski, D. D. Blake, Z. Huang, E. J. Wolfrum, W. A. Jacoby, Appl. Envion. Microbiol., 65(1999) 4094.

[37]   T. Saito, T, Iwase ,J. Horie,T. Morioka. J Photochem Photobiol B, 14 (1992) 369.

[38]   M. Bekbolet, C. V. Araz, Chemosphere, 32 (1996) 959.

[39]   T. Sakai, E. Ito,R. Cai, T. Yoshioka,Y. Kubota, K. Hashimoto, K, Fujishima Biochim Biophys Acta, `1201 (1994) 259.

[40]   W. G. Wamer, J. J. Yin,R. R. Wei, Free Radic Biol Med, 23 (1997) 851.

[41]   H. L.Liu, T. C.-K. Yang, Process Biochemistry ,39 (2003) 475.

[42]   H. Gerischer and A. Heller, J.Electrochem.Soc.,139 (1992) 113.

[43]   M. Cho, H. Chung, W. Choi, J. Yoon, Water Research, 38 (2004) 1077.

[44]   C. Sahoo, A. K. Gupta, A. Pal, Desalination, 181 (2005) 91.

[45]   U. U. Jadhav, V. V. Dawkar, G. S. Ghodake, S. P. Govindwar, J. Hazard. Mater., 158 (2008) 507.

[46]   P. Dhawal, M. Tamboli, B. Kurade, T. R. Waghmode, S. M. Joshi, S. P. Govindwar, J. Hazard. Materials, 182 (2010) 169.

[47]   S. Songa, L. Xua, Z. Hea, H. Ying, J. Chen, X. Xiao, B. Yan, J. Hazard. Mater., 152 (2008) 1301.

[48]   B.Y. Chen, K. W. Lin, Y. M. Wang, C. Y. Yen, J. Hazard. Mater., 166 (2009) 187.

[49]   K. C. Chen, J. Y. Wu, D. J. Liou, S. C. J. Hwang, J.Biotechnol., 101(2003) 57.

Water is one of the most indispensible source of life. It plays a crucial role in economic and social development processes. In today's life, environmental pollution has far reaching negative consequences in the lives of human beings. Increasing pollution levels deteriorate underground water reservoirs, rivers, lakes and oceans. Environmental problems associated with hazardous wastes and toxic water pollutants have attracted much attention. So, much efforts have been pursued to purify water without intensive use of chemicals or production of toxic byproducts relatively at lower costs and to re-use wastewater, all of which hold great promise for increasing water sources.

Advanced Oxidation Processes (AOPs) are modern chemical method for the treatment of water containing non- biodegradable/toxic substances and to decontaminated drinking water. AOPs degrading the organic pollutants in water with byproducts carbon dioxide and water. For disinfection of water AOPs are an alternative to conventional chlorination process, which leads to generate of toxic chlorinated byproducts in the presence of natural organic matter. Thus, in recent years, novel heterogeneous metal oxide semiconductors such as ZnO, Ag:ZnO, Au:ZnO and ZnO/ TiO_2 have been developed and they have attracted considerable attention owing to their photocatalytic ability in the degradation of various environmental pollutants.

The proposed work is divided into seven chapters.

Chapter I commences with general introduction followed by a brief literature survey on photoelectrochemical purification of water using ZnO, Ag:ZnO, Au:ZnO and ZnO /TiO_2 oxides. In light of the work done on water purification using semiconductor oxide thin films and scope for the studies, the purpose of present work is discussed in this chapter. The essential detailed information about different characterization techniques such as X-ray diffraction (XRD), Scanning electron microscopy (SEM), Energy dispersive X-ray analysis (EDAX), UV-Vis spectroscopy, photoelectrochemical (PEC) characterization, FTIR, HPLC, GCMS, COD and BOD analysis etc. are described.

Chapter II covers the theoretical background related with different some important terminologies associated with the present work. It covers the classification of photon/semiconductor systems. The energetics and redox power of semiconductors are described. The fundamental about photocatalysis and photoelectrocatalysis is followed by the mechanism and reaction kinetics, which is essential to understand the various

phenomena occurring at the site of water purification processes. Moreover it covers mechanism of inactivation of bacteria. Various parameters, such as light intensity, pH, initial solute concentration, electrode (photocatalyst) material, potential bias, temperature, effect of dopant and effect of heterojunction are responsible for photocatalytic process of water purification.

Chapter III opens with the introduction of one of the simplest and economical thin film deposition techniques; the spray pyrolysis. The essentials of spray pyrolysis technique, scheme of pyrolysis and formation of thin films and factors governing the spray pyrolysis technique are discussed in detail. This follows the experimental details about substrate cleaning, preparation of solution, and film formation for depositing fluorine doped tin oxide (F:SnO$_2$) coated glass substrates, ZnO, Ag:ZnO , Au:ZnO and ZnO/TiO$_2$ oxide thin films. It also contains procedure for degradation of Methylene blue (MB) and inactivation of *E.coli.*

Chapter IV includes synthesis, characterization of zinc oxide thin films and their photoelectrocatalytic activity in degradation of MB and inactivation of *E.coli.* The films have been characterized by XRD, SEM, UV-Vis spectroscopy. The preparative parameters such as substrate temperature and solution concentration and quantity of spraying solution of the films have been optimized by novel PEC technique.

The XRD patterns of ZnO thin films deposited at different substrate temperatures reveal that the films are polycrystalline and exhibit hexagonal (wurtzite) crystal structure with preferred orientation along (002) plane. SEM micrographs show the densely packed grains of size 370-425 nm. The optical transmission spectra of ZnO films show average visible transmittance of about ~ 80-90%.

XRD of ZnO thin films reveals increase in crystallinity with solution concentration and solution quantity. Densely organized mixture of large and small hexagonal platelets having voids has noticed in SEM micrographs. Film thickness 625 nm is optimized for the preparative parameters (400 ^{o}C, 0.2 M and 100 ml). From structural, morphological and PEC measurement it has been observed that optimized preparative parameters are temperature = 400 ^{o}C, solution concentration = 0.2 M and quantity of spraying solution = 100 ml. Also, this chapter explores the photoelectrocatalytic detoxification of MB and inactivation of *E.coli* using ZnO under UVA light illumination. The i-E curves have been

measured for ZnO photocatalyst to show maximum saturation current of 8 mA at 1.5 bias voltage.

The initial experiments confirmed that MB did not undergo any degradation under direct UVA illumination in the absence of catalyst. The plot of $\ln(C/C_0)$ as a function of reaction time illustrates first order kinetics of degradation of MB by taking extinction at 665 nm. FTIR analysis shows there is absence of azo bond in metabolites formed which confirms the cleavage of azo bond in MB dye. Photocorrossion of ZnO electrode is examined by measuring zinc by atomic absorption spectroscopy; during course of degradation of MB 24 % ZnO film is dissolved due to photocorrossion. Moreover inactivation of *E.coli* experiment is carried out which shows decrease of *E.coli* population from 10^9 CFU / ml to 3 CFU/ml in 180 min reaction time.

Chapter V deals with the synthesis and characterization of noble metal (Ag/Au) doped zinc oxide thin films. These films have been characterized for their PEC, structural, morphological, compositional and optical properties. The maximum value of I_{sc} and V_{oc} for 3 At % Ag:ZnO and Au:ZnO thin films confirms the optimization of doping percentage. Films are nanocrystalline and fit well with hexagonal crystal structure with no any extra phases of silver or gold or zinc compounds.

For degradation of MB and inactivation of E. coli both Ag:ZnO and Au:ZnO films are used as photoelectrode, it is observed that 80 % degradation due to Ag:ZnO and due to Au:Zno 84 % degradation of MB occurs in 150 min. For comparison the antibacterial activity of pure ZnO, Ag:ZnO and Au:ZnO are also tested in separate experiment. The antibacterial activity against *E.coli* indicates that Ag:ZnO film has efficient antibacterial capability*.* Photocorrossion of ZnO electrode is examined by measuring zinc by atomic absorption spectroscopy and no zinc was observed in AAS measurement.

The untreated textile effluent was circulated through photoelectrocatalytic reactor under UVA illumination for the decolorization and degradation. Textile effluent was decolorized to 93 % within 3 hrs at room temperature with significant reduction in COD (69 %). High performance liquid chromatography (HPLC) and Fourier transform infrared spectroscopy (FTIR) analysis of samples before and after decolorization confirmed the degradation of dye molecules from textile effluent into simpler oxidizable products. Phytotoxicity study revealed reduction in toxic nature of textile effluent after treatment.

In chapter VI, the nanocrystalline ZnO, TiO$_2$ and ZnO/TiO$_2$ films are deposited onto FTO-coated glass substrates by using spray pyrolysis technique. The structural, morphological, optical and photoelectrochemical properties of the ZnO, TiO$_2$ and ZnO/ TiO$_2$ are investigated by X-ray diffraction, scanning electron microscopy, UV–Vis spectroscopy and photoelectrochemical techniques. XRD analysis shows that films are polycrystalline and having hexagonal and tetragonal crystal structures for pure ZnO and TiO$_2$ respectively. The photocatalytic degradation of MB has been investigated with ZnO, TiO$_2$ and ZnO/TiO$_2$ photocatalysts. ZnO/TiO$_2$ thin films have proved quite effective mineralization of methylene blue, while pure ZnO and TiO$_2$ do not lead complete mineralization of methylene blue. The metabolites produced during degradation are analyzed by HPLC and Fourier transforms infrared spectroscopy. The by-products detected during degradation have been identified by GCMS technique namely N-methylbenzene-1,4-diamine and N-(cyclohexa-2,5-dien-1-ylidene)-N-methylmethanaminium. The achieved maximum degradation efficiency of about 99.41% for coupled ZnO/TiO$_2$ photocatalyst for MB without any photo-corrosion.

The untreated textile effluent was circulated through photoelectrocatalytic reactor under UVA illumination for the decolorization and degradation. Textile effluent was decolorized to 93 % within 3 hrs at room temperature with significant reduction in COD (69 %). HPLC and FTIR analysis of samples before and after decolorization confirmed the degradation of dye molecules from textile effluent into simpler oxidizable products. Phytotoxicity study revealed reduction in toxic nature of textile effluent after treatment. Recyclibility of the photocatalyst was also studied so as to make the process cost effective

To study inactivation of pathogens such as bacteria *E. coli Salmonella, Bacillus* and *Staphylococcus* are inactivated using ZnO/TiO$_2$ electrode. The inactivation kinetics has been seen to be more rapid for the Gram negative *E. coli* and *Salmonella* than that for the Gram positive *Bacillus* and *Staphylococcus*. Based on our findings, we propose that reactive oxygen species (ROS) such as   OH$^\bullet$, H$^+$, $^\bullet$O^{-2}, $^\bullet$HO$_2$, H$_2$O$_2$, and O$_2$ are generated on the irradiated ZnO/TiO$_2$ surface, operate in concert to attack polyunsaturated phospholipids in bacterial cell membrane. Finally we proposed inactivation of bacteria process is proposed as under:

Cell membrane + hydroxyl radicals (OH$^\bullet$, H$^+$, $^\bullet$O^{-2}, $^\bullet$HO$_2$, H$_2$O$_2$, and O$_2$) $\rightarrow$ CO$_2$+ reduced organic compounds

The new coupling method is developed by using photoelectrocatalytic ZnO/TiO$_2$ thin film and microbial agent (combination GG-BL) for the treatment of textile azo dye Methyl Red (200 mg l^{-1}). Decolorization of Methyl Red at different experimental conditions was carried out by using ZnO/TiO$_2$, consortium GG-BL, consortium GG-BL-ZnO/TiO$_2$ system and ZnO/TiO$_2$-consortium GG-BL system. The decolorization of Methyl Red (200 mg l^{-1}) using consortium GG-BL and ZnO/TiO$_2$ shows 63 % and 70 % decolorization with 38 and 40 % reduction of chemical oxygen demand (COD) within 2 hrs respectively. Whereas the consortium GGBL-ZnO/TiO$_2$ system showed 83 % decolorization of Methyl Red within 4 hrs for with 60 % reduction in COD, while ZnO/TiO$_2$ consortium showed 100 % decolorization with 80 % reduction of COD. It means that ZnO/TiO$_2$-consortium GG-BL system was efficient for the successful and faster decolorization of Methyl Red.

Thus ZnO/TiO$_2$ thin film is chemically stable with no photocorrossion occurring during photodegradation and can be used as user end application in water purification.